DEVELOPMENT OF NEW REUSABLE MATERIALS BASED ON Ru COMPLEXES WITH CATALYTIC ACTIVITY FOR OLEFIN EPOXIDATION AND NITRILE HYDRATION

Íngrid FERRER VALL-LLOSADA

Dipòsit legal: Gi. 1929-2015
http://hdl.handle.net/10803/322785

http://creativecommons.org/licenses/by/4.0/deed.ca

Aquesta obra està subjecta a una llicència Creative Commons Reconeixement

Esta obra está bajo una licencia Creative Commons Reconocimiento

This work is licensed under a Creative Commons Attribution licence

Doctoral thesis

DEVELOPMENT OF NEW REUSABLE MATERIALS BASED ON Ru COMPLEXES WITH CATALYTIC ACTIVITY FOR OLEFIN EPOXIDATION AND NITRILE HYDRATION

Íngrid Ferrer Vall-llosada

2015

Doctoral programme in Experimental Sciences and Sustainability

Supervised by: Dra. M. Isabel Romero García
Dra. Montserrat Rodríguez Pizarro

This manuscript has been presented to opt for the doctoral degree from the University of Girona

Departament de Química

Àrea de Química Inorgànica

Dra. M. Isabel Romero García and Dra. Montserrat Rodríguez Pizarro, from the Universitat de Girona,

WE DECLARE:

That the thesis entitled “Development of new reusable materials based on Ru complexes with catalytic activity for olefin epoxidation and nitrile hydration” presented by Íngrid Ferrer Vall-llosada to obtain a doctoral degree, has been completed under our supervision.

For all intents and purposes, we hereby sign this document.

Dra. M. Isabel Romero García Dra. Montserrat Rodríguez Pizarro

Girona, 1st June 2015

The work performed in the present doctoral thesis has been possible thanks to the funding of:

- Universitat de Girona through a BR predoctoral grant.
- Ministerio de Economía y Competitividad (MINECO) through projects: CTQ2007-60476/PPQ and CTQ2010-21532-C02-01.
- Generalitat de Catalunya through project: 2014/SGR/149.

Als meus avis

i a en Jordi

Agraïments

Després d'escriure tantes pàgines de la tesi i ara m'enfronto a les més complicades... És difícil plasmar per escrit l'agraïment a totes les persones que d'alguna manera han ajudat a fer realitat aquesta tesi.

Per començar voldria agrair a les meves directores de tesi Dra. Marisa Romero i Dra. Montse Rodríguez. Gràcies per donar-me l'oportunitat d'entrar en el món de la recerca inorgànica per fer el doctorat, quan ja pensava que no seria possible. Moltes gràcies per tot el què m'heu ensenyat durant aquests quasi 5 anys i per tot el suport que m'heu donat tant a nivell científic com personal.

També vull agrair a tots els col·laboradors que han fet possible aquesta tesi. A la Dra. Anna Roig de l'ICMAB per les mostres de sílice i l'ajuda. Als Serveis Tècnics de Recerca de la UdG: la Dra. Lluïsa Matas pels espectres de RMN, l'Anna Costa pels anàlisis elementals i masses, en Xavier Fontrodona per les estructures de Raigs X i en Joan Pere López pels anàlisis termogravimètrics. A L'Anna i la Judit dels Serveis de Microscòpia de l'ICMAB. I a la Dra. Mònica Iglesias per ajudar-me amb els anàlisis a l'ICP.

Un agraïment especial als companys de laboratori de quan vaig arribar al grup: Jordi i Mònica. Gràcies per ensenyar-me tot el funcionament d'un laboratori d'inorgànica i per totes les estones que vam passar tant al laboratori com al despatx! A la resta de companys de despatx: Plani i Pep A., per totes les estones de riure que vam passar i sobretot a tu, Pep A., amb qui més hores de despatx i més moments surrealistes he compartit!!! Les estones disteses al despatx també han estat gràcies a en Pep Duran i la Mª Angeles amb el seu bon humor.

També a tots els estudiants que heu anat passant pel grup: Ester, Alberto, Juan, Josep M., Adrià, Anna, Ming i Yoel, per fer més amenes totes les hores al laboratori. Ester, molta sort en la tesi!

Agrair també a la resta de becaris amb els que hem compartit incomptables dinars, sopars i alguna que altra sortida: Magda, Ewelina, Aida, Laia, Cristina, Iteng i Cristina C. A la Dolors per fer més distrets tots els trajectes compartits La Plana-Girona de l'últim any! Aida, Cris i Iteng, amb vosaltres he pogut compartir molts bons moments aquests últims anys, un plaer haver tornat a coincidir amb vosaltres i molts ànims en aquesta recta final!

A la Raquel, Mònica F i Mónica R. per fer que els inicis a Girona fossin més fàcils, vam compartir moltíssims moments durant la carrera i més de 10 anys després encara en compartim d'especials... espero poder continuar gaudint de la vostra amistat! Mònica F., a més, agrair-te tot el què hem conviscut durant els dos anys que hem viscut juntes i per estar al meu costat en moments difícils!

A l'Anna C., que des que vam coincidir al màster i malgrat la distància, m'has ajudat moltíssim en els moments més difícils! Als amics (Raquel, Rosa, Joan, Rafa, Ingrid i Laura) per fer dels caps de setmana grans moments de desconnexió!

Però tot això no hagués estat possible sense els meus avis, gràcies a vosaltres sóc qui sóc i he arribat fins aquí. No us podré agrair mai tot el què heu arribat a fer per mi, gràcies per estar sempre al meu costat! En aquest punt, també m'agradaria tenir un record per vosaltres: mama, tiet, perquè malgrat no ho heu pogut veure, sé que allà on sigueu, se us dibuixarà un somriure al veure fins a on he arribat. I també agrair a tota la meva família política per acollir-me com una més de la família.

I, finalment, a tu Jordi, que sense el teu suport i la teva insistència aquest últim tram hagués estat molt més dur. Gràcies per estar sempre al meu costat i per fer-me tan feliç!!

List of publications

Publications related to the thesis content

- *Ru(II) complexes containing dmso and pyrazolyl ligand as catalysts for nitrile hydration in environmentally friendly media.*

  Ferrer, I.; Rich, J.; Fontrodona, X.; Rodríguez, M.; Romero, I. *Dalton Trans.* **2013**, *42*, 13461-13469.

- *Ru(II)-dmso complexes containing azole-based ligands: Synthesis, linkage isomerism and catalytic behavior.*

  Ferrer, I.; Fernández, J.; Fontrodona, X.; Rodríguez, M.; Romero, I.

  To be submitted

- *New Ru complexes containing the trpy-$PO_3(Et)_2$ ligand as catalysts for epoxidation reactions.*

  Ferrer, I.; Fontrodona, X.; Rodríguez, M.; Romero, I.

  Manuscript in preparation

Abbreviations

Anal. Found (Calc.)	analysis found (analysis calculated)
bpy	2,2'-bibyridine
d	doublet
DFT	density functional theory
dmso	dimethyl sulfoxide
DPV	differential pulse voltammetry
Conv.	conversion
COSY	correlation spectroscopy
CV	cyclic voltammetry
d	doublet
dd	doublet of doublets
ddd	doublet of doublet of doublets
dt	doublet of triplets
ε	extinction coefficient
E	potential
$E_{1/2}$	half wave potential
E_{pa}	anodic peak potential
E_{pc}	cathodic peak potential
ESI-MS	electrospray ionization mass spectrometry
FTIR	Fourier transform infrared
GC	gas chromatography
HMBC	heteronuclear multiple bond correlation
HSQC	heteronuclear single-quantum correlation
ICP-AES	inductively coupled plasma atomic emission spectroscopy
IR	infrared
J	coupling constant
LMCT	ligand to metal charge transfer
m	multiplet

MLCT	metal to ligand charge transfer
MNPs	magnetic nanoparticles
MSP	magnetic silica particles
m/z	mass-to-charge ratio
NMR	nuclear magnetic resonance
NOESY	nuclear Overhauser effect spectroscopy
PCET	proton-coupled-electron transfer
ppm	parts per million
py	pyridine
pz	pyrazole
s	singlet
SCE	saturated calomel electrode
Select.	selectivity
SEM	scanning electron microscopy
SP	silica particles
T	temperature
t	triplet
TBAH	tetra(n-butyl)ammonium hexafluorophosphate
TGA	thermogravimetric analysis
TON	turnover number
trpy	2,2’:6’,2’’-terpyridine
trpy-P-Et	diethyl 2,2’:6’,2’’-terpyridine-4’-phosphonate
trpy-P-H	diethyl 2,2’:6’,2’’-terpyridine-4’-phosphonic acid
UV-Vis	ultraviolet-visible spectroscopy
ν	frequency
vs	versus
λ	wavelength

Electronic supporting information

The material listed below can be found in the attached CD:

- pdf file of the PhD dissertation
- pdf file of the publication
- cif files for each crystal structure presented within this thesis

Chapter	Crystal Structure	Code
Chapter 4	$[Ru^{II}Cl(trpy\text{-}P\text{-}Et)(pypz\text{-}Me)](PF_6)$	C3
Chapter 6	$[Ru^{II}Cl_2(pypz\text{-}H)(dmso)_2]$	933633
	$[Ru^{III}Cl_3(pypz\text{-}H)(dmso)]$	C5’’
	$[Ru^{II}Cl_2(pypz\text{-}Me)(dmso)_2]$	C6
	$[Ru^{II}Cl_2(pz\text{-}H)(dmso)_3]$	933634
	$[Ru^{II}Cl_2(CH_3\text{-}pz\text{-}H)(dmso)_3]$	C8
	$[Ru^{II}Cl_2(NO_2\text{-}pz\text{-}H)(dmso)_3]$	C9
	$[Ru^{II}Cl_2(CF_3\text{-}pz\text{-}H)(dmso)_3]$	C10
	$[Ru^{II}Cl_2(Br\text{-}Hind)(dmso)_3]$	C11

List of figures

Figure 1.1. Styrene transformations catalyzed by different Ru complexes......................4

Figure 1.2. Common polypyridyl ligands used in ruthenium coordination chemistry 5

Figure 1.3. Ru^{IV}=O schematic energy orbital diagram..7

Figure 1.4. Structure of cisplatin. 14

Figure 1.5. Structure of NAMI-A...15

Figure 1.6. Structure of KP1019 15

Figure 1.7. Possible transformations of alkenes with ruthenium catalysts. 22

Figure 1.8. Proposed mechanistic pathways for oxygen atom transfer process. 24

Figure 1.9. Proposed mechanism for the oxidation of aromatic olefins by ruthenium(IV) oxocomplexes. 25

Figure 1.10. Structure of the Parkins catalyst. 29

Figure 1.11. Structure of the hydrido-ruthenium complexes: tetranuclear cluster (a) and mononuclear complex (b). 33

Figure 1.12. Structure of the bis(acetylacetonate)-ruthenium(II) complexes. 34

Figure 1.13. Examples of arene-ruthenium(II) complexes. 36

Figure 1.14. Structure of water-soluble arene-ruthenium(II) complexes..................... 36

Figure 1.15. Schematic representation of different types of catalyst immobilization: adsorption (a), electrostatic immobilization (b), encapsulation (c), ionic liquid (d) and covalent binding (e). 40

Figure 1.16. General process for anchoring an homogeneous catalyst into a solid support. 42

Figure 1.17. Possible binding modes of a phosphonate unit to a metal oxide surface. 43

Figure 1.18. Structure of SiO_2-supported Ru catalyst. 46

Figure 1.19. Structure of biomimetic ruthenium complex. 46

Figure 1.20. Heterogenized molybdenumperoxo catalyst for olefin epoxidation on silica-coated MNPs. 47

Figure 1.21. Structure of $[Ru(BINAP\text{-}PO_3H_2)(DPEN)Cl_2]$. 48

Figure 1.22. Poly(N-vinyl-2-pyrrolidone) (PVP), a water-soluble polymer commonly used as a nanoparticle stabilizer. 49

Figure 1.23. Structure of the different ruthenium-based nanocatalysts.......................49

Figure 4.1. Ortep plot and labelling schemes for compounds *trans*-**C3** and *cis*-**C3**....... 77

Figure 4.2. ^{1}H-NMR spectrum of *trans* and *cis*-**C3**, 400 MHz, acetone-d_6. 79

Figure 4.3. UV-vis spectra of 0.03 mM of complexes **C3** (blue) and **C4** (red) in CH_2Cl_2. 79

Figure 4.4. Cyclic voltammogram of **C3** in CH_2Cl_2. 80

Figure 4.5. Cyclic Voltammogram of **C4** in water at pH =7. 81

Figure 4.6. Differential Pulse Voltammetry of **C4** in water at pH= 6.4. 82

Figure 4.7. Differential pulse voltammetries of **C4** in water at pH=2.6 (blue), 6.4 (red)83

Figure 4.8. Pourbaix diagram of *trans*-**C4**. The pH-potential regions of stability for the various oxidation states and their dominant proton compositions are indicated. 84

Figure 4.9. Pourbaix diagram of *cis*-**C4**. The pH-potential regions of stability for the various oxidation states and their dominant proton compositions are indicated. 84

Figure 5.1. SEM images of a) **SP1** b) **SP2** and c) **MSP** after the anchoring of the Ru complex. 98

Figure 5.2. Thermogravimetric profiles of **SP2** (blue), **SP1-C4** (red), **SP2-C4** (green), **MSP-C4** (grey). 99

Figure 5.3. IR spectra of **SP2** (red) and **SP2-C4** (blue). 100

Figure 5.4. UV-vis spectra for **SP2-C4** obtained through strategy 1b (red), 2 (blue) and homogeneous complex **C4** (dotted grey). 101

Figure 5.5. Differential Pulse Voltammetry of **SP2-C4** (red) and homogeneous complex **C4** (dotted grey) in water at pH=6.4. 102

Figure 5.6. Pourbaix diagram of **SP2-C4** obtained through strategy 1b. The pH-potential regions of stability for the various oxidation states and their dominant proton compositions are indicated. 103

Figure 5.7. Conversion and selectivity values obtained throughout a number of consecutive reuses of catalyst **SP2-C4** in the epoxidation of styrene: a) 6 h per run; b) 15 h per run. 106

Figure 5.8. Conversion and selectivity values obtained throughout a number of consecutive reuses of complex **SP2-C4** in the epoxidation of *cis*-β-methylstyrene. The number on the column of selectivity represents the percent of *cis* isomer obtained. 107

Figure 5.9. Conversion and selectivity values obtained throughout a number of consecutive reuses of complex **SP2-C4** in the epoxidation of 4-vinylcyclohexene...... 107

Figure 5.10. Conversion and selectivity values obtained throughout a number of consecutive reuses of complex **SP2-C4** in the epoxidation of 1-octene. 108

Figure 5.11. Conversion and selectivity values obtained throughout a number of consecutive reuses of catalyst **MSP-C4** in the epoxidation of styrene. 109

Figure 6.1. Ortep plot and labeling schemes for compounds **C5'** and **C6**................... 118

Figure 6.2. Ortep plots and labeling schemes for compounds **C7**-**C11**....................... 120

Figure 6.3. ^{1}H-NMR spectrum of **C5**, 400 MHz, CD_2Cl_2. 122

Figure 6.4. UV-visible spectra of 0.1 mM solutions of **C5** (red) and **C6** (grey) and a 1.1 mM solution of **C7** (blue), in CH_2Cl_2.. 124

Figure 6.5. Cyclic voltammogram of **C5** in CH_3CN. 126

Figure 6.6. Cyclic voltammetry for complex **C8** in CH_3CN starting the scanning at E_{init} = 0 V (blue) and at E_{init} = 1.8 V applying an equilibration time of 10 min (green). 128

Figure 6.7. Cyclic voltammograms of **C5** in CH_2Cl_2 (TBAH, 0.1M) vs Ag/AgCl starting from E_{init} = 0 V. Arrow indicates initial scan direction; scan rate: 0.20 - 8 V/s............ 130

Figure 6.8. Cyclic voltammograms of **C5** in CH_2Cl_2 (TBAH 0.1M) vs Ag/AgCl starting from E_{init} = 1.4 V. Arrow indicates initial scan direction; scan rates: 0.20 - 8 V/s................ 130

Figure 6.9. Cyclic voltammograms of **C8** in CH_2Cl_2 (TBAH, 0.1M) vs Ag/AgCl starting from 0 V. Arrow indicates initial scan direction; scan rate: 0.20 - 8 V/s.................... 131

Figure 6.10. Cyclic voltammograms of **C8** in CH2Cl2 (TBAH, 0.1M) vs Ag/AgCl starting from 1.7 V. Arrow indicates initial scan direction; scan rate: 0.20 - 8 V/s................. 131

Figure 6.11. UV-visible spectroscopy corresponding to the photochemical transformation of a 0.7 mM solution of **C5** into **C5'.** 136

Figure 6.12. Cyclic voltammograms of **C5** (1mM in 0.1M TBAH acetonitrile solution) after irradiation: t = 0, 21, 45, 70 and 85 minutes. 137

Figure 6.13. Ortep plot and labeling scheme for compound **C5''**.............................. 139

Figure 6.14. UV-visible spectra corresponding to the photochemical transformation of a 0.25 mM solution of **C5** into **C5''** in chloroform during 60 minutes. Isosbestic points are found at 328 and 352 nm. 140

Figure 6.15. DPV of a solution of complex **C8''** in dichloromethane, starting the scanning of potential at -0.2 V (a) and at 0.6 V (b). The equilibrium time applied in each case (0-180 s) is indicated. 142

Figure 6.16. Evolution of an aqueous solution of complex **C5** by warming at 60ºC for 2h. Isosbestic points are found at 280 and 302 nm. 144

Figure 7.1. UV-visible spectrum of 0.08 mM **C12** in methanol. 158

Figure 7.2. Cyclic voltammogram of **C12** in CH_2Cl_2. 159

Figure 7.3. UV-vis spectra for **SP2-C12** (blue) and homogeneous complex **C12** (dotted grey) in methanol. 162

Figure 7.4. Differential pulse voltammetry of **SP2-C12** in CH_2Cl_2. 163

List of tables

Table 1.1. Electrochemical parameters for aqua complexes of Ru 9

Table 1.2. Different mechanistic pathways for substrates oxidation by the oxocomplex *cis*-$[Ru(bpy)_2(py)O]^{2+}$..20

Table 1.3. Ligand effects on the epoxidation of *trans*-stilbene with Ru-aqua complexes 26

Table 1.4. Homogeneous *vs*. heterogeneous catalysis. Schematic comparison 39

Table 3.1. Parameters for all crystal structures 69

Table 4.1. pK_a and electrochemical data (pH = 7, $E_{1/2}$ in V vs SCE) for aqua complexes described in this chapter and others for purposes of comparison 85

Table 4.2. Catalytic epoxidation of *cis*-β-methylstyrene by Ru complexes using $PhI(OAc)_2$ as oxidant 87

Table 4.3. Ru-catalyzed hydration of nitriles to amides in water using aquacomplex $[Ru(trpy)(pypzMe)OH_2)]^{2+}$ as catalyst 88

Table 5.1. Physical parameters of the silica supports used 96

Table 5.2. Amount of Ru anchored in the different supports.......................................97

Table 5.3. Optimization of the reaction time on the catalytic oxidation of alkenes by **SP2-C4** using $PhI(OAc)_2$ as oxidant. 105

Table 6.1. UV-vis spectroscopic features in CH_2Cl_2 for complexes **C5**-**C11**..................123

Table 6.2. Electrochemical data (CH_3CN +0.1M TBAH *vs*. Ag/AgCl) for complexes **C5**-**C11** 125

Table 6.3. Thermodynamic and kinetic parameters for the linkage isomerization of **C5** and **C8** complexes, together with Ru-dmso complexes described in the literature.....133

Table 6.4. Ru-catalyzed hydration of nitriles to amides in water using complexes **C5** and **C7** as catalysts...146

Table 6.5. Ru-catalyzed hydration of nitriles to amides in water using complexes **C7**-**C11** as catalysts...148

Table 6.6. Consecutive reuses of catalysts **C5** and **C7** in the hydration of nitriles to amides in water and glycerol. 151

Table 7.1 UV-vis spectroscopic features for complexes **C5**, **C6** and **C12**. 158

Table 7.2. Electrochemical data (CH_2Cl_2 +0.1M TBAH *vs*. SCE) for complexes **C5**, **C6** and **C12** 160

Table 7.3. Ru-catalyzed hydration of nitriles to amides in water using complexes **C5**, **C6** and **C12** as catalyst. 164

Table 7.4. Ru-catalyzed hydration of benzonitrile to benzamide in water using the heterogeneous **SP2-C12** system as catalyst throughout three consecutive reuses. 165

Graphical abstracts

INTRODUCTION

CHAPTER 1. Introduction. (pages 1-50)

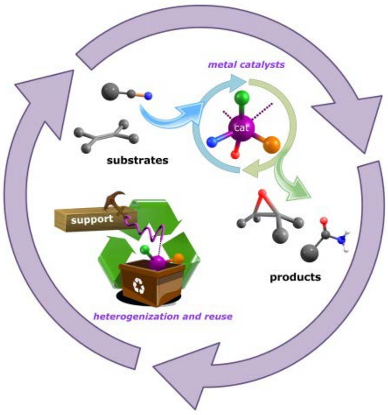
metal catalysts
cat
substrates
support
products
heterogenization and reuse

OBJECTIVES

CHAPTER 2. Objectives. (pages 51-56)

EXPERIMENTAL SECTION

CHAPTER 3. Experimental section. (pages 57-72)

RESULTS AND DISCUSSION

CHAPTER 4. Ru(II) complexes containing trpy-P-Et and pypz-Me ligands as catalysts for alkene epoxidation and nitrile hydration. (pages 73-90)

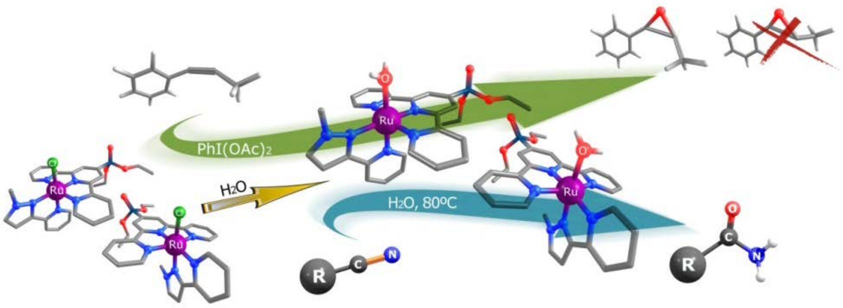
PhI(OAc)2
H2O
H2O, 80ºC
Ru
R
C
N

New ruthenium complexes with general formula $[Ru^{II}(trpy\text{-}P\text{-}Et)(pypz\text{-}Me)X]^{n+}$ (X = Cl, H_2O) have been synthesized. The complexes have been fully characterized through structural, analytical and spectroscopic techniques and the isomeric chlorido complexes have also been characterized in the solid state by monocrystal X-ray diffraction analysis. Redox properties of the Ru-OH_2 species together with its reactivity in alkene epoxidation and nitrile hydration have been studied.

CHAPTER 5. Heterogeneous catalytic systems based on [Ru(trpy-P)(pypz-Me)X]$^{n+}$ (X = Cl, H_2O) complexes. Evaluation of the catalytic activity in epoxidation and hydration reactions. (pages 91-112)

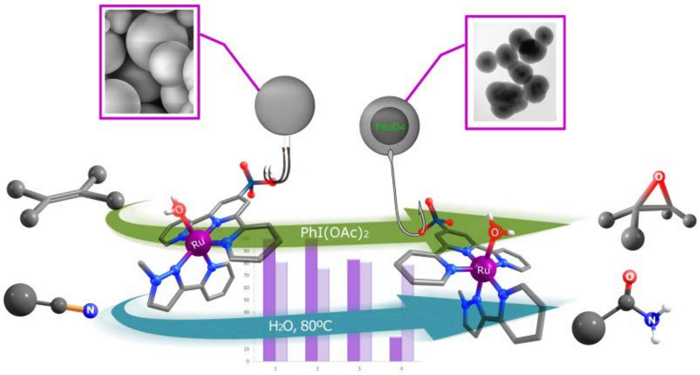

Phosphonated terpyridine complexes with general formula [Ru^{II}(trpy-P)(pypz-Me)X]$^{n+}$ (X = Cl, H_2O) have been anchored onto three different silica supports *via* covalent bonds. These new materials have been fully characterized by ICP-AES, SEM, TGA and spectroscopic techniques. The redox properties of heterogeneous Ru-OH_2 complexes together with their reactivity in alkene epoxidation and nitrile hydration have been studied. The results obtained have been compared with the analogous homogeneous systems.

CHAPTER 6. Ru(II) complexes containing dmso and pyrazolyl ligands as catalysts for nitrile hydration in environmentally friendly media. (pages 113-154)

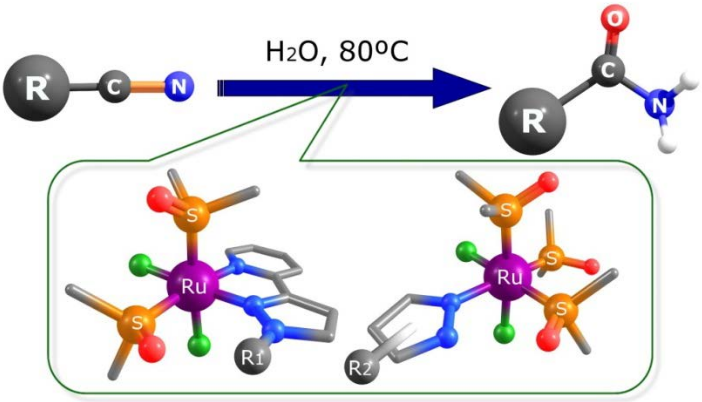

New efficient catalytic systems for nitrile hydrolysis to the corresponding amides in pure water or in glycerol as solvent are described. The catalysts employed are new ruthenium (II) complexes containing dmso and pyrazolyl ligands, which have been fully characterized through structural, analytical and spectroscopic techniques. Studies on linkage isomerization of dmso ligands and photoinduced substitution by solvent were carried out for some complexes. It is outstanding the conversion and selectivity obtained in the catalytic hydration of nitriles when using either aromatic or aliphatic substrates. The reuse of the catalysts has been explored for the first time in ruthenium-mediated nitrile hydration catalysis.

CHAPTER 7. Synthesis and heterogenization of complex [$RuCl_2$(pypz-Si)(dmso)$_2$] in SiO_2 support. Evaluation of the catalytic activity in hydration of nitriles. (pages 155-166)

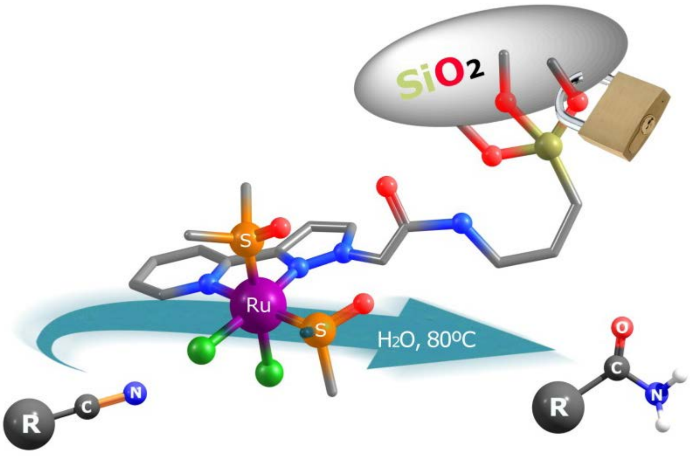

A ruthenium complex, [$RuCl_2$(pypz-Si)dmso$_2$], has been synthesized and has been anchored onto SiO_2 supports *via* covalent bonds. The complex and the functionalized silica supports have been characterized by spectroscopic and electrochemical techniques. Preliminary studies related to nitrile hydration catalysis in water were carried out with both homogeneous and heterogeneous catalytic systems.

CONCLUSIONS

CHAPTER 8. Conclusions. (pages 167-174)

REFERENCES

CHAPTER 9. References. (pages 175-200)

ANNEX

ANNEX. Supporting information. (pages 201-258)

Table of contents

Resum XXI

Resumen XXIII

Summary.. XXV

INTRODUCTION

CHAPTER 1. Introduction. (pages 1-50)

1.1. Generalities of ruthenium 3

1.2. Ruthenium polypyridyl aqua complexes 5

1.3. Ruthenium complexes with sulfoxide ligands 11

  1.3.1. Ru-dmso bond 11

    1.3.1.1. Ru-dmso coordination through sulphur 12

    1.3.1.2. Ru-dmso coordination through oxygen 12

  1.3.2. Applications of Ru-dmso complexes 12

    1.3.2.1. Anticancer activity of Ru-dmso..13

1.4. Ruthenium in catalysis 16

  1.4.1. Oxidation reactions 16

    1.4.1.1. Biomimetic oxidations 16

    1.4.1.2. Ru^{IV} as oxidation catalyst 19

    1.4.1.3. Epoxidation of alkenes catalyzed by Ru^{IV}=O complexes...................22

  1.4.2. Nitrile hydration reactions 26

    1.4.2.1. Ruthenium as nitrile hydration catalyst...30

1.5. Supported catalysts 37

  1.5.1. Homogeneous *vs.* heterogeneous systems...37

  1.5.2. Immobilization methods 40

  1.5.3. Supports 43

  1.5.4. Heterogenized catalysts for oxidation reactions 45

  1.5.5. Heterogenized catalysts for nitrile hydration 48

OBJECTIVES

CHAPTER 2. Objectives. (pages 51-56)

EXPERIMENTAL SECTION

CHAPTER 3. Experimental section. (pages 57-72)

3.1. Materials **59**
3.2. Preparations **59**
3.3. X-Ray structure determination **68**
3.4. Catalytic Studies **70**
    3.4.1. Epoxidation of alkenes 70
        3.4.1.1. Homogeneous phase 70
        3.4.1.2. Heterogeneous phase 70
    3.4.2. Hydration of nitriles 70
        3.4.2.1. Homogeneous phase 70
        3.4.2.2. Heterogeneous phase 71
3.5. Instrumentation and measurements **71**

RESULTS AND DISCUSSION

CHAPTER 4. Ru(II) complexes containing trpy-R and pypz-Me ligands as catalysts for alkene epoxidation and nitrile hydration. (pages 73-90)

4.1. Synthesis and crystal structures **75**
4.2. Spectroscopic properties **78**
4.3. Electrochemical properties **80**
4.4. Catalytic epoxidation of alkenes **86**
4.5. Catalytic hydration of nitriles **88**

CHAPTER 5. Heterogeneous catalytic systems based on [Ru(trpy-P)(pypz-Me)X]$^{n+}$ (X = Cl, H_2O) complexes. Evaluation of the catalytic activity in epoxidation and hydration reactions. (pages 91-112)

5.1. Strategies for the immobilization of Ru complexes 93
5.2. Characterization of supports 96
  5.2.1. Physical parameters of the silica supports used 96
  5.2.2. Atomic Emission Spectroscopy (ICP-AES)..96
  5.2.3. SEM images 97
  5.2.4. Thermal studies (TGA)...98
  5.2.5. Spectroscopic properties...99
  5.2.6. Electrochemical properties 101
5.3. Catalytic activity 104
  5.3.1. Catalytic epoxidation of alkenes 104
  5.3.2. Catalytic hydration of nitriles 110

CHAPTER 6. Ru(II) complexes containing dmso and pyrazolyl ligands as catalysts for nitrile hydration in environmentally friendly media. (pages 113-154)

6.1. Synthesis and crystal structures 115
6.2. Spectroscopic properties.. 121
6.3. Electrochemical properties and linkage isomerization 124
6.4. Photoinduced substitution reactions 135
  6.4.1. Photochemical study of [$RuCl_2$(pypz-H)$(dmso)_2$] (**C5**) and [$RuCl_2$(CH_3-pz-H)$(dmso)_3$] (**C8**) in acetonitrile and chloroform 135
  6.4.2. Photochemical study of [$RuCl_2$(pypz-H)$(dmso)_2$] (**C5**) in water 143
6.5. Catalytic hydration of nitriles 145

CHAPTER 7. Synthesis and heterogenization of complex [RuCl$_2$(pypz-Si)(dmso)$_2$] on SiO$_2$ support. Evaluation of the catalytic activity in hydration of nitriles. (pages 155-166)

7.1. Synthesis of [RuCl$_2$(pypz-Si)dmso$_2$] 157
7.2. Spectroscopic and electrochemical properties 158
7.3. Strategies for the immobilization of the Ru complex 160
7.4. Characterization of the functionalized supports 161
7.5. Catalytic activity in hydration of nitriles 163

CONCLUSIONS

CHAPTER 8. Conclusions. (pages 167-174)

REFERENCES

CHAPTER 9. References. (pages 175-200)

ANNEX

ANNEX. Supporting information. (pages 201-258)

Resum

En base a l'experiència del grup de recerca en la síntesi de complexos que contenen lligands N-donors i la seva posterior aplicació en catàlisi, en aquesta tesi es presenta la síntesi i caracterització de diferents tipus de complexos de ruteni amb la idea d'estudiar la seva química de coordinació, així com l'activitat catalítica dels complexos sintetitzats en l'epoxidació d'olefines i la hidròlisi de nitrils. Per altra banda, tenint en compte la importància i els avantatges de la catàlisi heterogènia, s'ha dut a terme la immobilització d'alguns d'aquests complexos sobre suports tipus sílice amb la finalitat d'aplicar-los en els mateixos processos catalítics en fase heterogènia i avaluar-ne l'activitat al llarg de successives reutilitzacions.

Al capítol 4 es descriu la síntesi, estructura i propietats espectroscòpiques i redox de nous complexos Ru-Cl i Ru-OH_2 que contenen el lligand neutre meridional trpy-P-Et i el lligand no-simètric didentat pypz-Me. Es descriu la influència de les propietats electròniques i geomètriques dels lligands sobre el pK_a i el comportament electroquímic d'aquests compostos i es porta a terme una comparació amb complexos anàlegs prèviament sintetitzats al nostre grup. Es descriu l'activitat catalítica de la mescla d'isòmers Ru-OH_2 en l'epoxidació d'olefines (utilitzant iodobenzè com a oxidant) i s'utilitza el complex anàleg contenint el lligand trpy per a avaluar la hidròlisi de nitrils en aigua. En epoxidació, el *cis*-β-metilestirè s'utilitza com a substrat de prova obtenint alts valors de conversió i estereoselectivitat en consonància amb el procés (IV/II) a dos electrons que té lloc en els complexos isòmerics Ru-OH_2. En hidròlisi de nitrils s'obtenen conversions moderades i altes selectivitats en la majoria dels casos. Al capítol 5 es mostra l'ancoratge dels complexos mencionats anteriorment en suports de partícules de sílice (SPs) i de partícules magnètiques recobertes de sílice (MNPs), sense modificar ni la coordinació ni les propietats del complex original. Igual que pels complexos homogenis, s'estudia l'activitat catalítica heterogènia en l'epoxidació d'olefines i en la hidròlisi de nitrils en aigua i el seu comportament es compara amb el dels catalitzadors homogenis anàlegs. Aquests sistemes permeten la reutilització del catalitzador durant 3-4 reusos en l'epoxidació de *cis*-β-metilestirè i 4-vinilciclohexè mantenint els valors de selectivitat. En la hidròlisi de nitrils, s'han obtingut uns

rendiments significativament més baixos que els obtinguts amb els sistemes homogenis tot i que es manté una selectivitat excel·lent per l’amida.

La segona família de complexos sintetitzats es basa en complexos de tipus Ru-Cl que contenen lligands dmso i derivats de pirazole Al capítol 6 es descriu la síntesi, estructura i propietats espectroscòpiques i redox de tres nous complexos amb lligands pirazòlics didentats i cinc complexos amb lligands pirazòlics monodentats. S’estudia la isomerització d’enllaç induïda per transferència electrònica en els complexos $[Ru^{II}Cl_2(CH_3\text{-pz-H})(dmso)_3]$ i $[Ru^{II}Cl_2(pypz\text{-H})(dmso)_2]$ i es calculen les velocitats d’isomerització d’enllaç i les propietats termodinàmiques d’ambdós. Els complexos tris-dmso mostren una isomerització d'enllaç Ru-S→Ru-O quantitativa d'un lligand dmso en paral·lel amb l'oxidació de l'espècie Ru^{II}(dmso-S) a Ru^{III}(dmso-O), mentre que el complex bis-dmso relacionat experimenta un cert grau d'isomerització. També es descriu la reactivitat dels complexos sota irradiació de llum en $CHCl_3$, CH_3CN i aigua, on té lloc la substitució d'un lligand dmso pel dissolvent (o per un lligand clorur en el cas de $CHCl_3$) en tots els casos. L'activitat catalítica en hidròlisi de nitrils s’estudia per tots els complexos en aigua i glicerol mostrant valors de selectivitat altament remarcables per l’amida així com una reutilització moderada en dissolució. Finament, al capítol 7, es duen a terme estudis preliminars d’heterogeneïtzació del complex $Ru^{II}Cl_2(pypz\text{-Si})(dmso)_2$ així com del seu comportament en la catàlisi heterogènia d'hidròlisi de nitrils.

Resumen

Basándonos en la experiencia del grupo de investigación en la síntesis de compuestos con ligandos N-donores y su posterior aplicación en catálisis, en esta tesis se presenta la síntesis y caracterización de diferentes tipos de complejos de rutenio con la idea de estudiar su química de coordinación, así como la actividad de los complejos sintetizados en la epoxidación de alquenos y en la hidrólisis de nitrilos. Por otro lado, teniendo en cuenta la importancia y las ventajas de la catálisis heterogénea, se ha llevado a cabo la inmovilización de algunos de estos complejos en soportes tipo sílice con la finalidad de aplicarlos en los mismos procesos catalíticos en fase heterogénea y evaluar su actividad a lo largo de sucesivas reutilizaciones.

En el capítulo 4 se describe la síntesis, estructura y propiedades espectroscópicas y redox de nuevos complejos Ru-Cl y Ru-OH_2 que contienen el ligando neutro meridional trpy-P-Et y el ligando no-simétrico didentado pypz-Me. Se describe la influencia de las propiedades electrónicas y geométricas de los ligandos sobre el pK_a y el comportamiento electroquímico de estos compuestos y se lleva a cabo una comparación con los complejos análogos previamente sintetizados en nuestro grupo. Se describe la actividad catalítica de la mezcla de isómeros Ru-OH_2 en la epoxidación de alquenos (utilizando iodobenzeno com oxidante) y se utiliza el complejo análogo conteniendo el ligando trpy para evaluar la hidrólisis de nitrilos en agua. En la epoxidación, el *cis*-β-metilestireno se utiliza como sustrato de prueba obteniendo elevados valores de conversión y estereoselectividad en consonancia con el proceso (IV/II) a dos electrones que tiene lugar en los complejos isoméricos Ru-OH_2. En la hidrólisis de nitrilos, los complejos muestran conversiones moderadas y elevadas selectividades en la mayoría de los casos. En el capítulo 5 se muestra el anclaje de los complejos mencionados anteriormente en soportes de partículas de sílice (SPs) y de partículas magnéticas recubiertas de sílice (MSPs), sin modificar ni la coordinación ni las propiedades del complejo original. Igual que para los complejos homogéneos, se estudia la actividad catalítica heterogénea en la epoxidación de alquenos y en la hidrólisis de nitrilos en agua y su comportamiento se compara con el de los catalizadores homogéneos análogos. Estos sistemas permiten la reutilización del

catalizador durante 3-4 reúsos en la epoxidación de *cis*-β-metilestireno y 4-vinilciclohexeno manteniendo los valores de selectividad. En la hidrólisis de nitrilos, se han obtenido unos rendimientos significativamente inferiores a los obtenidos con los sistemas homogéneos aunque se mantiene una excelente selectividad por la amida.

La segunda familia de complejos sintetizados se basa en complejos Ru-Cl que contienen ligandos dmso y derivados de pirazola. En el capítulo 6 se describe la síntesis, estructura y propiedades espectroscópicas y redox de tres nuevos complejos con ligandos pirazólicos bidentados y cinco complejos con ligandos pirazólicos monodentados. Se estudia la isomerización de enlace inducida por transferencia electrónica en los complejos $[Ru^{II}Cl_2(CH_3\text{-pz-H})(dmso)_3]$ y $[Ru^{II}Cl_2(pypz\text{-H})(dmso)_2]$ y se calculan las velocidades de isomerización de enlace y las propiedades termodinámicas de ambos. Los complejos tris-dmso muestran una isomerización de enlace Ru-S→Ru-O cuantitativa de un ligando dmso en paralelo con la oxidación de la especie Ru^{II}(dmso-S) a Ru^{III}(dmso-O), mientras que el complejo bis-dmso relacionado experimenta un cierto grado de isomerización. También se describe la reactividad de los complejos al someterlos a irradiación de luz en $CHCl_3$, CH_3CN y agua, donde tiene lugar la substitución de un ligando dmso por el disolvente (o por un ligando cloruro en el caso de $CHCl_3$) en todos los casos. La actividad catalítica en hidrólisis de nitrilos se estudia para todos los complejos en agua y glicerol mostrando valores de selectividad altamente remarcables para la amida así como una reutilización moderada en disolución. Finalmente, en el capítulo 7 se llevan a cabo estudios preliminares de heterogeneización del complejo $Ru^{II}Cl_2(pypz\text{-Si})(dmso)_2$ así como su comportamiento en la catálisis heterogénea de hidrólisis de nitrilos.

Summary

Based on the experience of the group in the synthesis of complexes containing N-donor ligands and their subsequent application in catalysis, in this thesis we present the synthesis and characterization of different types of ruthenium complexes with the idea of studying their coordination chemistry, as well as the performance of the complexes synthesized in alkene epoxidation and nitrile hydration reactions. On the other hand, taking into account the importance and advantages of the heterogeneous catalysis, we carry out the immobilization of some of these complexes on silica-type supports with the idea of applying them in the corresponding heterogeneous processes and evaluate their activity throughout successive reuses.

In Chapter 4, we describe the synthesis, structure, spectroscopy and redox properties of new Ru-Cl and Ru-OH_2 complexes containing the neutral meridional trpy-P-Et and the non-symmetric didentate pypz-Me ligands. We also discuss the influence of electronic and geometrical effects of the ligands over the pK_a and electrochemical behavior of these compounds and a comparison with the analogous complexes previously synthesized in our group is also done. We describe the catalytic performance of the Ru-OH_2 isomeric mixture with regard to the alkene epoxidation (using iodobenzene as the oxidant) and the analogous complex which contains trpy ligands was evaluated in nitrile hydration in water. For alkene epoxidation, the *cis*-β-methylstyrene was used as a test substrate obtaining high levels of conversion and stereoselectivity in accordance with the occurrence of a two-electron (IV/II) redox process in the two isomeric Ru-aqua compounds. In nitrile hydration, moderate conversion and high selectivity values are obtained in most cases. In Chapter 5, we illustrate the anchoring of the above mentioned complexes on silica particles (SPs) and silica-coated magnetic particles (MNPs) supports, without modifying the coordination and electronic properties of the original complex. As for homogenous complexes, we study the heterogeneous catalytic activity with regard to the alkene epoxidation and hydration of nitriles in water and the behavior of these heterogeneous systems are compared with the analogous homogenous catalysts. These systems permit recycling

the catalyst for 3-4 runs in the epoxidation of *cis*-β-methylstyrene and 4-vinylcyclohexene well-maintaining the selectivity values. For the catalytic hydration of nitriles significantly lower performance was obtained compared to the homogeneous system though with excellent selectivity for the amide product.

The second family of complexes synthesized is based on Ru-Cl complexes containing dmso and pyrazolyl ligands. In Chapter 6, we describe the synthesis, structure, spectroscopy and redox properties of three new complexes containing didentate pyrazolic ligands and five compounds containing monodentate pyrazolic ligands. We study the electron-transfer-induced linkage isomerization of the dmso ligands in compounds $[Ru^{II}Cl_2(CH_3\text{-pz-H})(dmso)_3]$ and $[Ru^{II}Cl_2(pypz\text{-H})(dmso)_2]$ and the linkage isomerization rates and some thermodynamic properties have been also calculated. Tris-dmso complexes show a quantitative Ru-S→Ru-O linkage isomerization process of a dmso ligand in parallel with the oxidation of Ru^{II}(dmso-S) species to Ru^{III}(dmso-O), whereas the related bis-dmso compound displays a certain degree of linkage isomerization. We also report the reactivity of the compounds upon light irradiation in $CHCl_3$, CH_3CN and water where the substitution of one dmso ligand for solvent (or for a chlorido ligand in the case of $CHCl_3$) takes place in all cases. The catalytic activity of all the complexes in nitrile hydration is evaluated in water and glycerol showing highly remarkable selectivity for the amide products as well as moderate recyclability in solution. Finally, in Chapter 7, preliminary studies on the heterogenization of one of the dmso complexes as well as its behavior in heterogeneous nitrile hydration reaction are presented.

INTRODUCTION

Chapter 1

Introduction

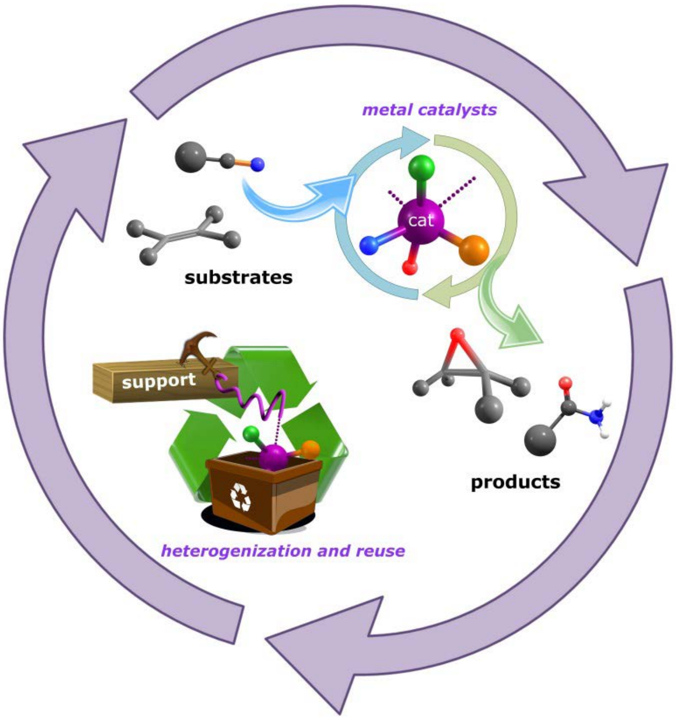
metal catalysts
cat
substrates
products
support
heterogenization and reuse

1.1. Generalities of ruthenium

Ruthenium is a metal situated in the d group of the periodic table whose electronic configuration is [Kr] $4d^7 5s^1$. Ruthenium is the unique among all the elements of the periodic table, together with osmium, that covers the widest range of accessible oxidation states, from -2 as in $[Ru(CO)_2]^{2-}$ to +8 as in RuO_4 (each with different coordination geometries), corresponding to the complete range of 11 oxidation states theoretically possible for a transition metal (from d^0 to d^{10}).[1,2] No less important is the fact that ruthenium is much less expensive than other platinum group metals such as palladium, platinum, rhodium and iridium.

The kinetic stability of ruthenium complexes in different oxidation states, the often reversible nature of the redox pairs and the synthetic relative simplicity make these complexes particularly interesting. Other general characteristics of ruthenium coordination compounds are their high electron transfer capacity[3-5] and their ability to stabilize reactive species like oxo-metals[6-8] and metal-carbene complexes.[9]

Ruthenium complexes are widely used and studied in different chemical fields. The properties, and therefore the applications, of ruthenium complexes are clearly correlated with the nature of the ligands coordinated to the central metal ion. Ruthenium complexes with π-conjugate ligands or systems that enable electronic delocalization have shown specific properties in nonlinear optics,[10-13] magnetism,[14-17] molecular sensors[18-20] and liquid crystals.[21,22] On the other hand, sulfoxide complexes have been extensively studied, as it will be seen in section 1.3.2, due to their relevant usefulness in chemotherapy.[23-25] Ruthenium complexes with heterocyclic N-donor ligands are the most employed due to their interesting spectroscopic, photophysical and electrochemical properties,[26,27] which lead to potential applications in diverse areas such as photosensitizers for photoactive conversion of solar energy,[28-32] molecular electronic devices[33-36] and photoactive DNA cleavage agents for therapeutic purposes.[37-42]

In the present work, catalysis is the most important application of the prepared ruthenium complexes. Synthetic versatility, easily available high oxidation states and a robust character of their coordination sphere make ruthenium complexes particularly useful for catalytic transformations, such as cyclopropanation,[43,44] isomerization,[45,46] metal-promoted radical reactivity,[47] oxidation,[48-50] addition,[51] hydrogen generation,[52,53] hydrogenation,[54-57] C-H and C-halogen bond activation[58,59] and olefin metathesis.[60-62] The effect of the ligands is crucial in determining the type of the catalytic reaction; in consequence the same metal can transform the same substrate into different products by changing the ligands coordinated to the metal. To illustrate it, in Figure **1.1** is shown how styrene can be transformed into multiple products using different ruthenium complexes.[63]

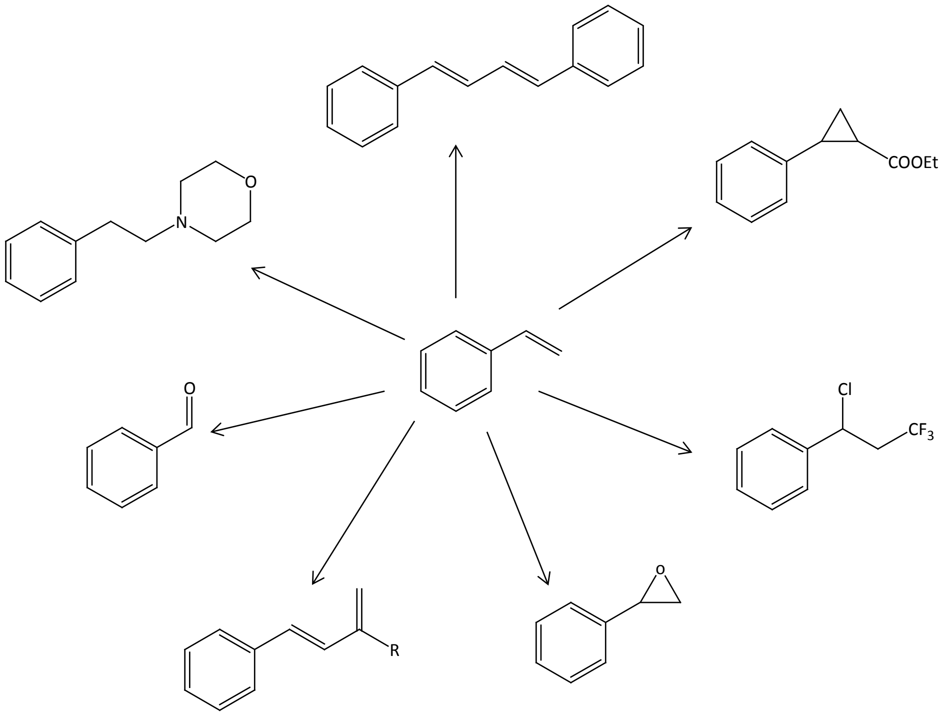

Figure 1.1. Styrene transformations catalyzed by different Ru complexes

Due to the importance of the ligand environment, numerous studies have been focused on the understanding of their electronic and geometric properties and how these properties influence the metal reactivity.

1.2. Ruthenium polypyridyl aqua complexes

The contributions of the Australian coordination chemist Frances P. Dwyer and co-workers during 1940s to 1960s can be considered as the beginning of the synthetic chemistry of polypyridyl complexes of ruthenium and osmium.[64,65] The synthetic procedures firstly described in these initial publications have been expanded and improved considerably. An example are Thomas J. Meyer and collaborators who began a systematic study of their relevant reactive properties based on their accessibility to long-lived excited states and oxidation states varying from M(II) to M(VI).[6,66,] It is important to notice that it is possible to create families of related complexes in which these redox properties can be varied by changing the ancillary ligands.[68]

Extensive coordination chemistry about hexacoordinated complexes containing polypyridyl ligands has been reported, due to these ligands stability against oxidation and their great coordinative capacity, increased by their quelating effect (Figure **1.2**). These properties give a great stability to the formed complex.

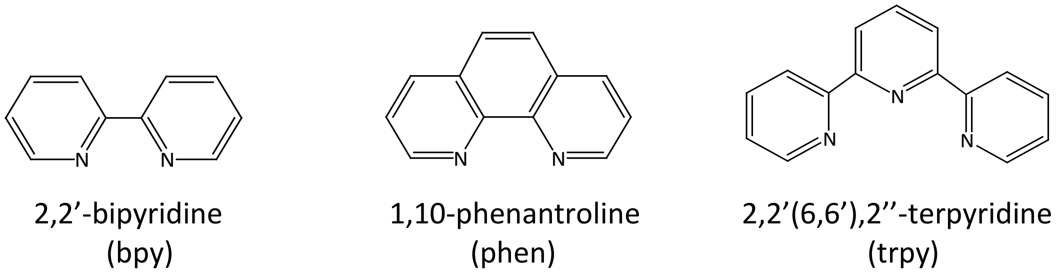

Figure 1.2. Common polypyridyl ligands used in ruthenium coordination chemistry.

The redox properties of these complexes become especially interesting when an aqua ligand is directly bound to the metal center. In this case, a proton-coupled-electron transfer (PCET) is possible, making the high oxidation states fairly accessible.[69]

As shown in Scheme **1.1**, the successive oxidation from Ru(II) to Ru(IV) are accompanied by a sequential loss of protons favored by the enhanced acidity of the bonded aqua ligand. Therefore, the initial $Ru^{II}-OH_2$ is oxidized to $Ru^{IV}=O$, passing through a $Ru^{III}-OH$ species.

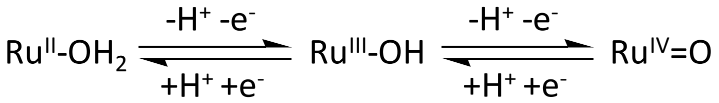

$$\mathrm{Ru^{II}\text{-}OH_2} \underset{+H^+ +e^-}{\overset{-H^+ -e^-}{\rightleftharpoons}} \mathrm{Ru^{III}\text{-}OH} \underset{+H^+ +e^-}{\overset{-H^+ -e^-}{\rightleftharpoons}} \mathrm{Ru^{IV}{=}O}$$

Scheme 1.1. PCET oxidation process characteristic of Ru-aqua complexes.

As a consequence of this behavior, the redox potentials of the aqua complexes are directly correlated with the pH of the medium in such a way that, if pH increases, the Ru(III/II) and Ru(IV/III) couples are shifted to lower potentials. The Nernst equation (Equation **1.1**) correlates pH with redox potential in such a way that, for a monoprotic and monoelectronic transfer, the redox potential diminishes in 59 mV by every pH unit increased.

$$E_{1/2} = E^0_{1/2} - 0.059\ (m/n)\ pH$$

$E_{1/2}$= half wave redox potential at a given pH, $E^0_{1/2}$= half wave redox potential at standard conditions, m= number of transferred protons, n= number of transferred electrons.

Equation 1.1. Relation between potential and pH in the Nernst equation.

The graphical representation of this pH dependence in front of the redox potential is known as Pourbaix diagram. This diagram combines the redox equilibria with the acid-base equilibria of all the thermodynamically stable species involved and represents the dependence of the half wave redox potential, $E_{1/2}$, with respect to the complete pH range.

In order to illustrate the trends of these ruthenium aqua complexes, Scheme **1.2** shows the Latimer diagrams for two different polypyridylic ruthenium complexes: (a) *cis*-$[Ru(bpy)_2(Cl)_2]$ and (b) *cis*-$[Ru(bpy)_2(py)(H_2O)]^{2+}$. In compound (b), two anionic chlorido ligands are replaced by neutral pyridine and aquo ligands. In this scheme, the electronic configurations ware pointed out due to their importance in redox processes where electrons are gained and lost from dπ levels.

$$\underset{(d\pi^4)}{cis\text{-}[Ru^{IV}(bpy)_2(Cl)_2]^{2+}} \xrightleftharpoons{1.7\text{ V}} \underset{(d\pi^5)}{cis\text{-}[Ru^{III}(bpy)_2(Cl)_2]^{+}} \xrightleftharpoons{0\text{ V}} \underset{(d\pi^6)}{cis\text{-}[Ru^{II}(bpy)_2(Cl)_2]} \quad (a)$$

$$\underset{(d\pi^4)}{cis\text{-}[Ru^{IV}(bpy)_2(py)(O)]^{2+}} \xrightleftharpoons{0.78\text{ V}} \underset{(d\pi^5)}{cis\text{-}[Ru^{III}(bpy)_2(py)(OH)]^{2+}} \xrightleftharpoons{0.67\text{ V}} \underset{(d\pi^6)}{cis\text{-}[Ru^{II}(bpy)_2(py)(H_2O)]^{2+}} \quad (b)$$

(V versus NHE, M=0.1 at pH=7)

Scheme 1.2. Latimer diagrams of Ru polypyridyl complexes (a) non-containing and (b) containing a coordinated water molecule.

The example shown in Scheme **1.2a** is the typical redox behavior observed in ruthenium chlorido polypyridyl complexes. For these compounds, the Ru(III/II) oxidation takes place at relatively low potentials (0 V) but an increase in charge and oxidation state shifts the Ru (IV/III) oxidation to highly positive potentials (1.7 V).[70] In the couples shown in Scheme **1.2b**, where the anionic chlorido ligands are replaced by neutral pyridine and water ligands, the increase in charge and the changes in bonding increase the Ru^{III}-OH/Ru^{II}-OH_2 potential (from 0 to 0.67 V) compared to the analogous couple in Scheme **1.2a**.[71-73] When comparing both equations it is surprising to observe a much smaller difference between the Ru(IV/(III) and Ru(III/II) couples in Scheme **1.2b**. These data point out to a clear stabilization of the Ru^{IV} species when the aqua ligand coordinates the metal centre.

This stabilization is promoted by the successive deprotonation and subsequent electronic stabilization of the higher oxidation states by the oxocomplex formation. As shown in Figure **1.3**, the energy orbital diagram of $d\pi_{Ru}$-$2p_{\pi,O}$ multiple bond interaction is the key factor favoring the stabilization of Ru(IV).

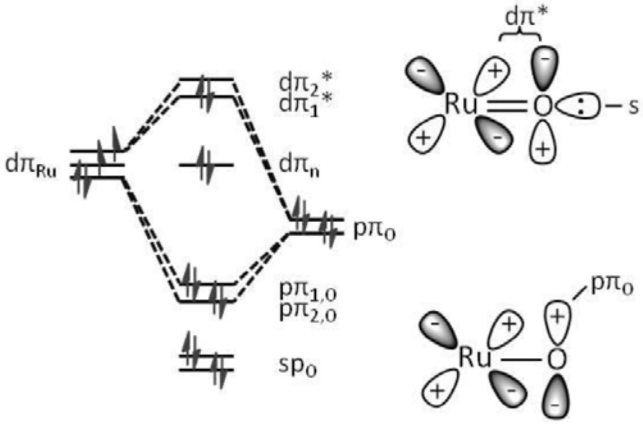

Figure 1.3. Ru^{IV}=O schematic energy orbital diagram.

The LUMO is dπ* character and provides a site for initial orbital interaction with electron donors, while the species is available for electron pair donation and initial coordination expansion. The sp^2 and $p_{\pi,O}$ electron pairs are available for electron donation and orbital interactions with electron acceptors. The final result of this process is the near overlap of the Ru(IV/III) and Ru(III/II) potentials. There is an important reactivity implications in this closeness of the redox potentials; thermodynamically, at pH=7, the Ru(IV) species can behave with almost the same efficiency as two-electron or one-electron oxidants.[74-76]

The reactivity of the ruthenium oxocomplexes depends on several factors which affect the values of half-wave potential, $E_{1/2}$, and the stability of the complex. One of the most studied factors is the effect of modifying the accompanying ligands. The possibility of modulate the complexes reactivity by tuning their redox potentials, in addition to the need of obtain selective catalysts, has resulted in a large number of systematic studies on the redox properties of these complexes, containing a large variety of ligands with different electronic and geometric nature.[77-80]

Table **1.1** shows the strong ligand effect over the Ru(IV/III) and Ru(III/II) redox couples potentials in different families of ruthenium complexes with N-containing ligands.[68]

In general, the Ru(III/II) and Ru(IV/III) couples are influenced by the ligands, as it can be observed in Table **1.1**. Ru(II) is stabilized by dπ-π*(L) back-bonding in the presence of ligands such as PPh_3, which has low-lying acceptor levels comparing with the presence of the py ligand (entries 10 and 20). However, Ru(III) oxidation state is clearly stabilized by σ-donor ligands as acetyl acetonate (acac) or oxalate, $C_2O_4^{2-}$ (entries 2 and 3).

On the other hand, Ru(IV/III) couples are, in general, less sensitive to ligand variations than Ru(III/II). This phenomena can be observed by comparing the complexes in entries 2 and 11 or 3 and 9, where changes in the accompanying ligands produce only a slight modification in the potential of the Ru(IV/III) couple whereas the Ru(III/II) couple is strongly influenced. This behavior is due to the control of the π-binding exerted by the oxo ligand through a $d\pi_{Ru}$-p_o interaction in the Ru(IV) species.

Table 1.1. Electrochemical parameters for aqua complexes of Ru (table extracted from ref.68)[a].

Entry	**Compound**	**$E_{1/2}$ (V)**[b]			**$\Delta E_{1/2}$**[c]
		$Ru^{III/II}$	**$Ru^{IV/III}$**	**$Ru^{IV/II}$**	
1	$[Ru(NH_3)(OH_2)]^{2+}$	-0.33	0.35	0.01	0.68
2	$[Ru(trpy)(acac)(H_2O)]^+$	0.19	0.56	0.38	0.37
3	$[Ru(trpy)(C_2O_4)(H_2O)]$	0.16	0.45	0.31	0.29
4	$[Ru(trpy)(H_2O)_3]^{2+}$ [c]	0.35	0.64	0.50	0.29
5	*trans*-$[Ru(trpy)(pic)(H_2O)]^+$	0.21	0.45	0.33	0.24
6	*cis*-$[Ru(trpy)(pic)(H_2O)]^+$	0.38	0.56	0.47	0.22
7	*cis*-$[Ru(6,6'\text{-}Me_2\text{-}bpy)(H_2O)_2]^{2+}$ [d]	0.57	0.73	0.65	0.16
8	$[Ru(trpy)(tmen)(H_2O)]^{2+}$	0.36	0.59	0.48	0.13
9	$[Ru(trpy)(phen)(H_2O)]^{2+}$	0.50	0.60	0.55	0.10
10	*cis*-$[Ru(bpy)_2(py)(H_2O)]^{2+}$	0.42	0.53	0.48	0.11
11	$[Ru(trpy)(bpy)(H_2O)]^{2+}$	0.49	0.62	0.56	0.13
12	$[Ru(trpy)(4,4'\text{-}((CO_2Et)_2bpy)(H_2O)]^{2+}$	0.66	0.80	0.73	0.13
13	$[Ru(trpy)(4,4'\text{-}Me_2\text{-}bpy)(H_2O)]^{2+}$	0.47	0.61	0.54	0.14
14	*cis*-$[Ru(bpy)_2(AsPh_3)(H_2O)]^{2+}$	0.50	0.67	0.59	0.17
15	*cis*-$[Ru(bpy)(biq)(PEt_3)(H_2O)]^{2+}$	0.45	0.63	0.54	0.18
16	$[Ru(tpm)(4,4'\text{-}((NO_2)_2\text{-}bpy)(H_2O)]^{2+}$	0.56	0.75	0.66	0.19
17	*cis*-$[Ru(bpy)_2(PEt_3)(H_2O)]^{2+}$	0.46	0.67	0.57	0.21
18	*cis*-$[Ru(bpy)(biq)(PPh_3)(H_2O)]^{2+}$	0.48	0.70	0.59	0.22
19	*cis*-$[Ru(bpy)_2(P(i\text{-}Pr)_3)(H_2O)]^{2+}$	0.45	0.68	0.57	0.23
20	*cis*-$[Ru(bpy)_2(PPh_3)(H_2O)]^{2+}$	0.50	0.76	0.63	0.26
21	*cis*-$[Ru(bpy)_2(SbPh_3)(H_2O)]^{2+}$	0.52	0.80	0.66	0.28
22	$[Ru(trpy)(dppene)(H_2O)]^{2+}$ [e]	1.17	1.53	1.35	0.36

[a] In H_2O at pH=7.0, T=22±2 °C, I=0.1M *vs* SSCE. [b] $E_{1/2}$ values for $Ru^{III}\text{-}OH/Ru^{II}\text{-}OH_2$, $Ru^{IV}{=}O/Ru^{III}\text{-}OH$ and $Ru^{IV}{=}O/Ru^{II}\text{-}OH_2$ couples. [c] $\Delta E_{1/2}=E_{1/2}(Ru(IV/III))-E_{1/2}(Ru(III/II))$. [d] pH=4.0. [e] In CH_2Cl_2/H_2O (3:1). Abbreviations: acac= acetyl acetonate; pic= picolinate anion; tmen= N,N,N,N-tetramethylethylenediamine; py= pyridine; biq= 1,1'-biquinoline; tpm= tris(pyrazolyl)methane; dppene= *cis*-1,2-bis(diphenylphosphino)ethylene.

The difference in potentials for the Ru(IV/III) and Ru(III/II) couples may have relevance to mechanism. Because of the accessibility of both Ru^{III} and Ru^{II}, Ru^{IV} can function as a one- or two-electron oxidant. In the middle part of Table **1.1**, the potential of the two-electron process is nearly the same as for the one-electron process. For entries 9 and 10, the driving force for Ru(IV) as a two-electron oxidant is only 50 mV lower than the driving force as a one-electron oxidant.

To obtain oxocomplexes with a two-electron process is important because this type of catalyst leads to concerted reactions avoiding a radical mechanism which may promote undesirable side reactions.[74,81]

Few examples of Ru complexes presenting bielectronic character can be found in the literature. In 1995, Reedijk *et al.* showed that the complex $[Ru(trpy)(pbz)(OH_2)]^{2+}$ (where bpz = 2,2'-bipyrazine) has a two-electron redox process and it was confirmed by electrochemical measurements and redox spectrophotometric assays in presence of Ce(IV) as oxidant.[82] More recently, other complexes were reported to show bielectronic processes, such as *trans*-$[Ru(CNC)(nBu\text{-}CN)(OH_2)]^{2+}$ (where CNC = 2,6-bis(butylimidazol-2-ylidene)pyridine; *n*Bu-CN= *N*-Butyl-*N'*-2-pyridylimidazolium), which shows a unique wave from values of pH = 2 to 14,[75,83] or $[Ru(trpy)(bpm)(OH_2)]^{2+}$ (where bpm = 2,2′-bipyrimidine), which shows a single wave in all range of pH and at high potential it can be possible to observe the wave corresponding to the Ru(V/IV) redox pair,[84] or *trans*, *fac*-$[Ru(bpea\text{-}pyr)(CN\text{-}Me)(H_2O)]^{2+}$ (where bpea-pyr = N,N-bis(pyridin-2-ylmethyl)-3-(1H-pyrrol-1-yl)-propan-1-amine; CN-Me = 3-methyl-1-(pyridin-2-yl)-1H-imidazol-3-ium-2-ide), which displays a unique redox wave throughout a wide pH range.[85]

Due to these properties, polypyridyl ruthenium complexes with aqua ligands have been extensively employed in oxidation reactions of organic and inorganic substrates, C-H insertion and proton-coupled electron transfer as it will be seen in section 1.4.1.2.

1.3. Ruthenium complexes with sulfoxide ligands

After the first transition metal complexes with sulfoxide ligands were reported in the 1960s,[86-89] the chemistry of these complexes has been quickly expanded. The interest of these compounds is centered on their use as precursors for the synthesis of a large variety of compounds[90-93] and they are applied in a wide number of catalytic processes.[94-100] Nevertheless, the most remarkable applications of these complexes are their utility in medicinal chemistry as antitumor compounds[91,101-105] and antimetastatic agents.[106-110] Finally, the ambidentate behavior of sulfoxide ligand, responsible for the bond isomerization observed in these type of complexes, makes them interesting from an academic point of view for their basic coordination chemistry[111-113] and their applications as molecular memories.[114-116]

Therefore, the properties of this kind of complexes are closely associated with the nature of the metal-sulfoxide bond. For this reason, the understanding of the factors which affects the bond mode is important for the study of these complexes.

1.3.1. Ru-dmso bond

Dimethyl sulfoxide (dmso) presents a selective affinity for different electronic population in Ru–dmso complexes. It acts as a S-bonded molecule (S–dmso) for Ru^{II} d^6 low spin configuration and an O-bonded molecule (O–dmso) for Ru^{III} d^5 low spin configuration.[117-120] Consequently, it must be taken into account that Ru-dmso complexes can suffer a linkage isomerization process. There are some factors that can provoke the isomerization:

- Coordination of π-acceptor ligands (such as CO or NO) in *trans* to S-dmso ligand provokes the isomerization to O-dmso.[121]
- Changes in metal oxidation state: $[Ru^{II}(NH_3)_5(S\text{-dmso})]^{2+}$ or $[Ru^{III}(NH_3)_5(O\text{-dmso})]^{3+}$.
- External factors such as temperature or photochemistry.

1.3.1.1. Ru-dmso coordination through sulphur

According to Pearson acid-base theory,[122] diffuse orbitals from metallic ions are well overlapped with donor orbitals from S which are also diffuse. Ru-S linkage is favored when a π-retrodonation from metal to dmso orbitals happes due to the π-acceptor properties of this ligand. This is the case of Ru(II) which stabilizes Ru-S linkage yielding π electronic density to empty orbitals of dmso ligand. The Ru(II)-dmso bond has some double bond character due to the π-retrodonation and, for this reason, it can be observed that the average Ru-S distance is lower than the sum of the covalent radius. When Ru(II) is oxidated to Ru(III), the π-retrodonation decrease and the Ru-S distance increase.

In complexes with two dmso ligands coordinated in *trans*, a high increase of the Ru-S bond distance is observed. This fact suggests a bond order reduction due to the competition for the π electronic density between the two dmso ligands. This effect can be observed in reactions between Ru(II)-dmso and π-acceptor ligands such as CO or NO, in these cases a isomerization of dmso bond is observed.

1.3.1.2. Ru-dmso coordination through oxygen

When a bond isomerization of the dmso ligand happens (from Ru-S to Ru-O) there is a decrease of the bond order in the S-O linkage so the bond distance increases from 1.47 Å (Ru-S) to 1.52 Å (Ru-O). For hard metallic ions the linkage through O is the favorite whereas in the case of soft metallic ion this linkage is possible for avoiding the *trans* disposition of two S-dmso or in presence of π-acceptor ligands (CO, NO).

1.3.2. Applications of Ru-dmso complexes

Since the introduction of $[Ru(Cl)_2(dmso)_4]$ by Wilkinson *et al.* in 1973,[90] a huge number of ruthenium compounds containing dmso ligands combined with a variety of auxiliary ligands have been described. Dmso ligand is classified as a versatile molecule for the development of Ru-based initiators for a variety of catalytic reactions because of its ambidentate behavior. Some of these catalytic reactions such as hydrogen-atom transfer,[96,97,123] hydrogenation,[94] R-alkylation of ketones,[124] oxidation of alcohols,[125] oxidation of aliphatic ethers to esters[126] or isomerization of alcohols[95] are important for the industry.

Some Ru(II) complexes with general formula [RuX_2(dmso)$_4$] (where X = Cl or Br) are good catalysts in the selective oxidation of aryl sulfides with molecular oxygen.[127] However, there are other complexes which are active in this type of catalysis such as [(dmso)$_2$H][*trans*-$RuCl_4$(dmso)$_2$], *mer*-[$RuCl_3$(dmso)$_3$], *mer*-[$RuCl_3$(dmso)$_2$(MePhSMe)] and *mer*-[$RuCl_3$(dmso)(MePhSMe)$_2$].[128]

Additionally, the catalytic activity of [RuCl(CO)$_2$(L)(X)]$^+$ complexes (where X = dmso or dmf and L = 2-phenylpyridine, benzoquinoline, 1-phenylpyrazole or azobenzene) has been demonstrated in reduction with molecular hydrogen of nitrocompounds, aliphatic and aromatic nitriles, aliphatic ketones and Schiff bases, to their saturated products.[129] Catalytic activity in oxygen transfer reactions in complexes such as [Ru(babp)(dmso)(L)] (where H_2babp = 6,6'-bis(benzoylamino)-2,2'-bipyridine and L = dmso, imidazole or pyridine derivatives) was also demonstrated.[130]

More recently, Wang *et al.* reported a family of complexes with general formula [Ru(k^3-bda)(dmso)L_2] (where k^3-bda= 2,2'-bipyridine-6,6'-dicarboxylate and L= imidazole, *N*-methylimidazole, 5-methylimidazole and 5-bromo-*N*-methylimidazole) which show high efficiency for water oxidation in homogeneous systems using Ce^{IV} as the oxidant.[99]

1.3.2.1. Anticancer activity of Ru-dmso

Cancer is one of the principal causes of death in developed countries although many treatment options exist including surgery, chemotherapy or radiation therapy. Despite the advances in this topic, there is no therapeutic treatment for majority of cancers and for this reason it is important the research of new chemotherapeutic agents.

cis-diamminedichloroplatinum(II) more known as cisplatin (Figure **1.4**) is among the chemotherapeutic agents most used during years despite its secondary effects and that lots of tumors present resistance to this treatment. These limitations encourages more studies with other transition metals.

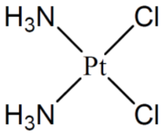

Figure 1.4. Structure of cisplatin.

In that sense, it is important to remark Ru-dmso complexes which are interesting for their antineoplastic capacity similar to cisplatin in some malign tumor in animals and their less toxic secondary effects.

The presence of dmso as ligand is a key point in the synthesis of these ruthenium compounds for these reasons:

- dmso is a polar molecule which is able to cross cellular membranes. Therefore, when it is coordinated to a metal center, the solubility of this complex could be better in water and the capacity to cross the biologic membranes could increase.
- dmso has a quite strong *trans* effect when dmso is coordinated through S, which could generate free coordination positions in the metal center.

Furthermore, Ru(III) complexes with S-dmso ligands in their coordination sphere present another characteristic: due to π-acceptor properties of S-dmso their reduction potential is especially high and their reduction *in vivo* to Ru(II) is favorable which makes them more labile and consequently more active.

Specifically, *trans*-imidazoledimethylsulfoxide-tetraclhororuthenate, known as NAMI-A (Figure **1.5**), is active against solid tumor metastases either in experimental mouse tumors or against human xenografts.[107,131-133] NAMI-A has a unique mechanism of activity which is not fully understood yet. Its high antimetastatic properties are accompanied with low antitumor effect for primary tumors in vivo and no cytotoxic effect in vitro. [134,135]

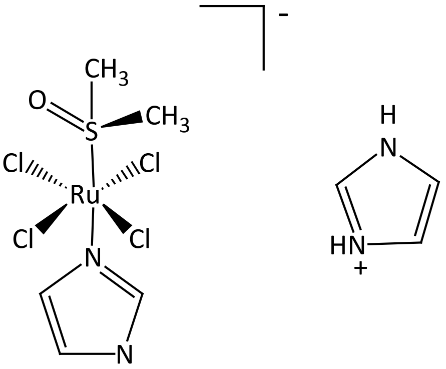
CH3
O
S
CH3
Cl
Cl
Ru
Cl
Cl
N
N
H
N
HN
+
-

Figure 1.5. Structure of NAMI-A

Due to their characteristics, different monomeric and dimeric Ru(II) complexes similar to NAMI-A have been synthesized.[136- 140] Preclinical studies with indazolium bis-indazoletetrachlororuthenate, known as KP1019 (Figure **1.6**) showed promising activity against colorectal tumours and the phase I study seems to support this.[141]

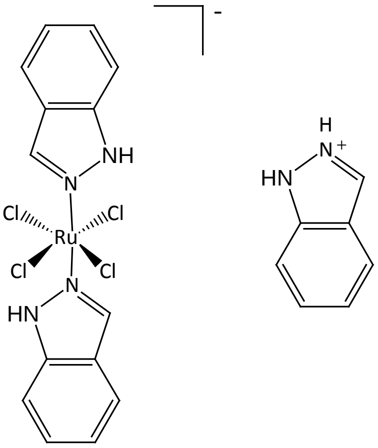
NH
N
Cl
Cl
Ru
Cl
Cl
N
HN
H
N+
HN
-

Figure 1.6. Structure of KP1019

1.4. Ruthenium in catalysis

The term catalysis was coined by Berzelius more than 150 years ago and the current definition is: “A catalyst is a substance that increases the rate of approach to thermodynamic equilibrium of a chemical reaction without being consumed”.

As can be seen in previous sections, ruthenium complexes can catalyze a variety of reactions and in this section we will focus on two kinds of processes: oxidation and nitrile hydration.

1.4.1. Oxidation reactions

1.4.1.1. Biomimetic oxidations

Nowadays a lot of studies are focused to mimic natural systems that carry out chemical transformations with excellent effectiveness in terms of selectivity and energy consumption. Concretely, the oxidation of organic substrates has received a special interest.[142- 146]

Selective oxidation of raw materials is an important area for the chemical industry, due to the necessity to produce oxygen-containing chemicals from fossil hydrocarbons avoiding the complete conversion to carbon dioxide. Selective oxidation is often a difficulty during the preparation of fine chemicals, since it is still challenging to cleanly introduce an alcohol function at the desired position of a drug precursor in the same manner as enzymes do.

Many enzymes are present in nature acting as “biological catalysts” capable of catalyzing oxidation reactions in living organisms.[147] Metals in enzymes participate in complex biochemical reactions and highly specialized biological functions thanks to their ability to exist in multiple oxidation states and different geometries.

Although biomimetic catalysts of iron[148- 150] or manganese[151- 153] are widely studied, different studies with ruthenium have been published.[154- 158] The development of artificial models of cytochrome P450 in oxidation reactions of organic substrates has received special attention.[143,154,159] Nature is able to efficiently perform monooxygenation reactions by introducing one oxygen atom of molecular oxygen into a defined substrate, while the second oxygen atom of O_2 is eliminated as a water molecule with the associated consumption of two electrons provided by NAD(P)H (Scheme **1.3**).

$$\text{R-H} + O_2 + 2e^- + 2H^+ \xrightarrow[\text{(e. g. Cytochrome P450)}]{\text{Monooxygenase}} \text{R-OH} + H_2O$$

Scheme 1.3. Monooxygenation reaction.

Although many artificial systems based on molecular oxygen together with an electron source have been reported to catalyze hydroxylation and epoxidation reactions, it has been observed the formation of water as the main product instead of the expected alcohol or epoxide, via the $2e^-$ reduction of the intermediate metal-oxo species.[160] An alternative way to avoid this difficulty is to use peroxides or single oxygen atom donors such as hydrogen peroxide (H_2O_2), alkylperoxides (ROOH), iodosylbenzene (PhIO), hypochlorite (NaOCl), monopersulfate ($KHSO_5$) or peracids.[161-163] The use of oxygen atom donors to generate the oxidized species is known as the “peroxide shunt” (Scheme **1.4**).[164,165] In particular hydrogen peroxide is the suitable “green” oxidant since the only side product after an oxidation reaction is water. However, peroxides have a weak and rather symmetrical O-O bond. The low dissociation energy leads to spontaneous homolytic cleavage and the formation of hydroxyl radicals HO•. Alkylhydroperoxides ROOH can be easily cleaved by transition metal complexes and the resulting alkoxyl radicals RO• are able to efficiently abstract hydrogen atoms from alkanes leading to a mixture of alcohols and ketones as in autoxidation reactions.[166]

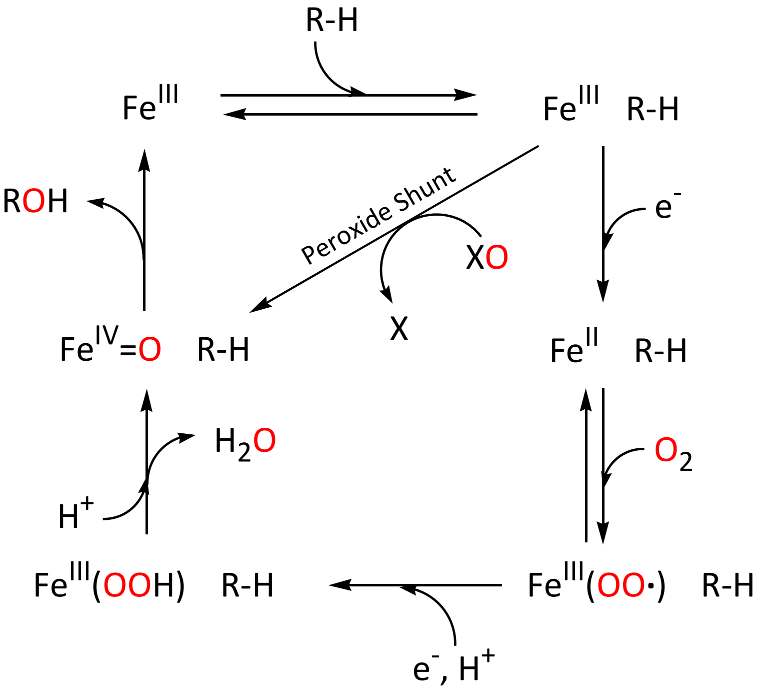

Scheme 1.4. Catalytic cycle for oxygen activation and transfer by cytochrome P450.

Effective monooxygenase models are able to perform both hydroxylation of alkanes and epoxidation of olefins, since the active species is an electrophilic high-valent metal-oxo entity like in the corresponding metalloenzymes. The metal center is able to activate the oxidant and then to control the oxygen atom transfer from the metal-oxo species to the substrate (the oxygen rebound mechanism involves an organic radical intermediate controlled by the metal center, without formation of free radicals). All the different studies on the modeling of oxygenases clearly confirm that the coordination of olefins to the metal-oxo center is not necessary to produce epoxides.

All the biomimetic oxidations have largely contributed to the development of methods for the characterization of high-valent metal-oxo species[167-169] and to the understanding of their chemical reactivity with respect to organic substrates,[170-173] although new studies are required to deepen in the processes and mechanisms.

1.4.1.2. Ru^{IV} as oxidation catalyst

The Ru^{IV}=O complexes are able to act as efficient oxidants for a wide range of substrates.[174] Firstly, as mentioned above, the oxo groups stabilize high oxidation states and make them accessible at fairly low potentials. In addition, from the mechanistic point of view, its ability to accept two electrons can avoid radicalary reaction pathways of high energy and reactivity.[74,75,81] Finally, the robust character of its first coordination sphere makes possible the easy exchange between Ru(II) and Ru(IV) without any dramatic changes in the catalyst structure, the oxo group being the only that modifies its composition.

Among the oxidation reactions promoted by Ru^{IV}=O complexes, the oxidation of alkenes, the epoxidation of alkenes, the cleavage of double bonds, the oxidation of alcohols and ethers and the oxidation of amines and amides can be pointed out. The orbital and energetic properties of Ru^{IV}=O promote different mechanistic pathways, including outer-sphere electron transfer, proton-coupled electron transfer, electrophilic ring attack, oxo transfer, hydride transfer and C-H insertion.

In Table **1.2** it can be seen a summary of different oxidative pathways for *cis*-[Ru^{IV}(bpy)$_2$(py)O]$^{2+}$ which is the most paradigmatic and studied complex inside this family. The mechanisms mentioned in this table are the result of a lengthy and exhaustive series of mechanistic studies through UV-Visible and infrared spectroscopy data, isotopic labeling, observation of intermediates and kinetic isotope effect.

Table 1.2. Different mechanistic pathways for substrates oxidation by the oxocomplex *cis*-$[Ru(bpy)_2(py)O]^{2+}$.

Reduced Form	Oxidized Form	Pathway	Ref.
$[Os^{II}(bpy)_3]^{2+}$	$[Os^{III}(bpy)_3]^{3+}$	Outer-sphere e$^-$ transfer	175
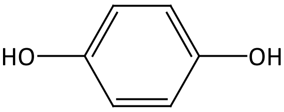 Hydroquinone	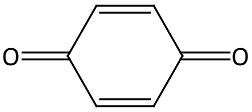 Benzonquinone	Proton-coupled e$^-$ transfer	176
H_2O_2	O_2	Proton-coupled e$^-$ transfer	177, 178
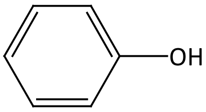 Phenol	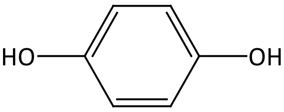 Hydroquinone[a]	Electrophilic ring attak	179
$(CH_3)_2SO$	$(CH_3)S_2O$	O transfer	180
$(CH_3)_2SO$	$(CH_3)SO_2$	O transfer	181
PPh_3	$O{=}PPh_3$	O transfer	182
PhHC=CHPh *cis-,trans*-stilbene	*cis-,trans-* 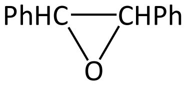	O transfer	183
$PhCH_2OH$	PhCHO	H$^-$ transfer	184
HCO_2^-	CO_2	H$^-$ transfer	185
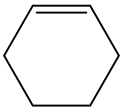	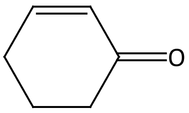	C-H insertion	186

[a] Followed by rapid oxidation to the quinone.

Among different oxidation agents used in the catalysis with oxocomplexes, should be mentioned oxygen donors such as sodium periodate,[187,188] iodosylbenzene (PhIO) or (diacetoxyiodo)benzene ($PhI(OAc)_2$),[189,190] hypochlorite,[191,192] pyridine *N*-oxide,[193,194] hydrogen peroxide,[183,195] t-butyl hydroperoxide[196,197] and molecular oxygen.[198,199] From the economic point of view and for reasons related to the preservation of the environment, the last three co-oxidants are considered ideal oxidation agents. However, PhIO and $PhI(OAc)_2$, two electrons oxidation agents, remain the most effective in the oxidation of organic substrates in the presence of ruthenium complexes.[200]

The catalytically active Ru=O species act as excellent catalysts for the oxidation of different organic substrates following the catalytic cycle shown in Scheme **1.5**. In this cycle the catalytic oxidation of the substrate is simultaneously accompanied by the reduction of ruthenium complex from oxidation state +IV to + II.

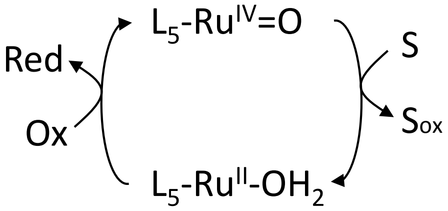

Scheme 1.5. Scheme of a catalytic cycle of oxidation of a substrate (S) with Ru^{IV}=O species.

With regard to substrates, alkenes are useful raw materials for both commodities and fine chemicals because of the high reactivity of the double bond.[201] However, an inherent difficulty in the oxidation of olefins is caused by different competing modes of oxidation, for example, epoxidation, allylic oxidation and double-bond cleavage. An overview of the different oxidation reactions of alkenes catalyzed by ruthenium is shown in Figure **1.7**.

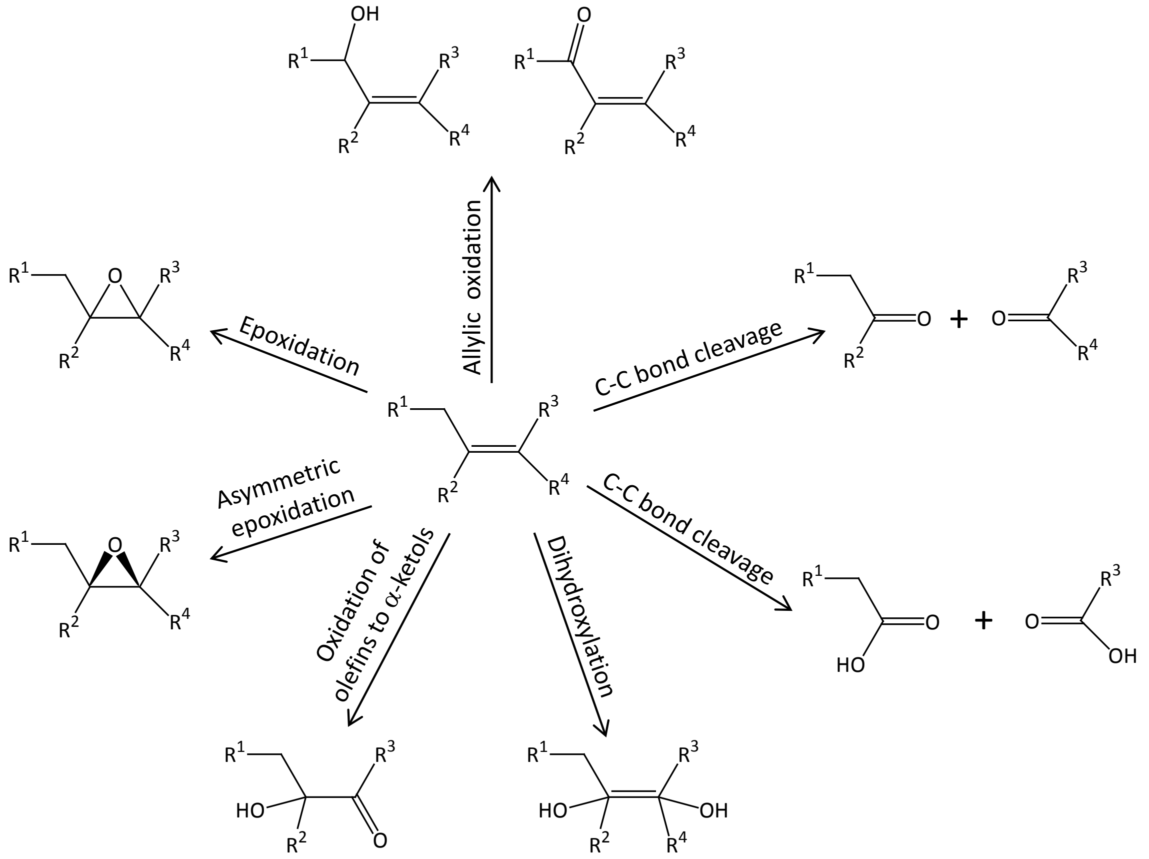
Allylic oxidation
Epoxidation
C-C bond cleavage
Asymmetric epoxidation
Oxidation of olefins to α-ketols
Dihydroxylation
C-C bond cleavage
R1
R2
R3
R4
OH
O
HO

Figure 1.7. Possible transformations of alkenes with ruthenium catalysts.

1.4.1.3. Epoxidation of alkenes catalyzed by Ru^{IV}=O complexes

The catalytic epoxidation of alkenes has received considerable interest from both academics and industry.[202,203] Olefin epoxidation has a great interest due to epoxides are useful intermediates in organic chemistry. By opening their ring, they can be easily transformed to functionalized compounds.[204] Epoxides are used in the synthesis of many industrial products. For example, the fine chemical Medrol, which is an anti-inflammatory and anti-allergic corticosteroid, is synthesized from an epoxide.[205] Epoxy polymers are widely used in the marine, automotive, aerospace and building industries.

Ruthenium complexes have proved efficient in the epoxidation of different olefins with relatively high selectivities.[206] Generally, epoxide yields depend on several factors such as the nature of the substrates, catalysts and reaction conditions. In the literature can be found a great variety of ruthenium oxocomplexes with different co-oxidants which can lead to the formation of the oxirane ring by transfer of their oxygen.[207] One of the first examples of the epoxidation by oxocomplexes was described by Griffith *et al.* The effectiveness of complex $[Ru(O)_2(bpy)\{IO_3(OH)_3\}]$ has been proved in the presence of $NaIO_4$ and the oxide *N*-methylmorpholine *N*-oxide (NMO) as a co-oxidant for the oxidation of different epoxide olefins with yields depending on the substrate.[188] Che *et al.* showed that the complex $[Ru^{IV}(ppz)(bpy)O](ClO_4)_2$ (ppz=2,6-bis[(4*S*,7*R*)-7,8,8-trimethyl-4,5,6,7-tetrahydro-4,7-methaneindazol-2-yl]pyridine) is capable of oxidizing, stoichiometrically, different aromatic olefins.[208]

It is believed that the oxygen atom transfer involves a side-on approach of the olefin to the Ru^{IV} active site. This kind of approach explains the lower enantioselectivities generally observed for *trans*-olefins compared to *cis*-olefins, both with porphyrin-based complexes and Jacobsen type manganese salen ligands, since the approach of *trans*-olefins is clearly more hindered.

Different mechanisms, concerted and non-concerted, have been proposed as possible pathways for oxygen atom transfer (Figure **1.8**). An oxygen atom can be transferred directly through a concerted oxene insertion (pathway a); through the formation of a 4 membered ring where both Ru and O atoms are respectively bonded to the $C\alpha$ and $C\beta$ of the olefin (pathway b); through a single electron transfer with the formation of a radical cation (pathway c); or through the formation of a benzylic radical intermediate (pathway d).[208]

Clean second-order kinetics for the oxidation of styrene and *cis*-β-methylstyrene was observed, being in concordance with a simple bimolecular kinetic scheme. For the oxidation of *cis* and *trans*-stilbene more complicated kinetics were observed and a direct oxygen atom insertion was proposed.[182]

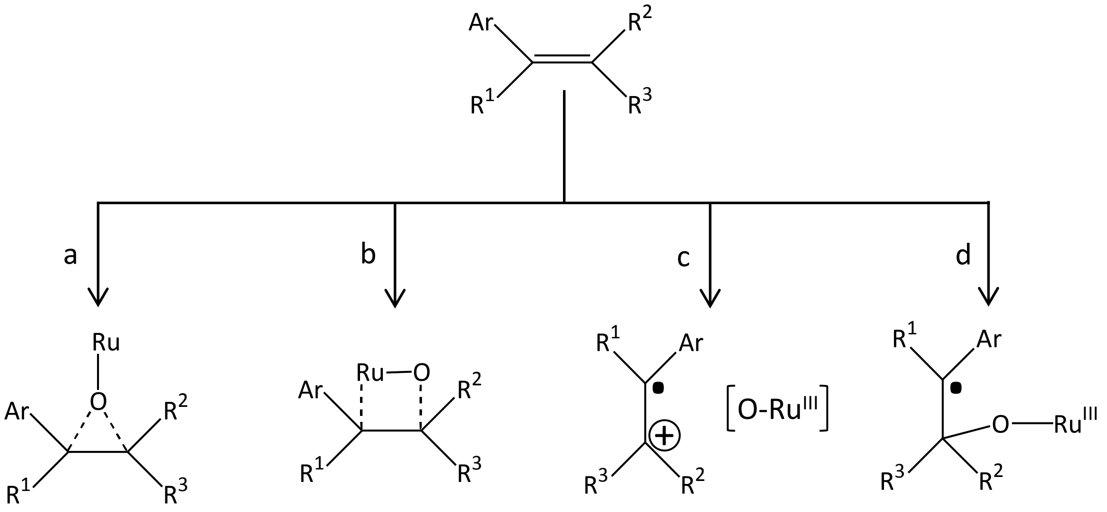

Figure 1.8. Proposed mechanistic pathways for oxygen atom transfer process.

The use of *cis*-alkenes, such as *cis*-β-methylstyrene, is known to be useful for determining whether a concerted or non-concerted pathway takes place.[209-212] If the epoxidation of the *cis*-alkene involves a breakage of the C=C π bond resulting in the formation of an acyclic intermediate (pathways **c** and **d**, Figure **1.8**), isomerization by the rotation of the C-C bond can take place, leading to the corresponding *trans*-epoxide. In consequence, the formation of mixtures of *cis* and *trans*-epoxides in the oxidation of *cis*-alkenes can be considered as an indication of a non-concerted pathway.

Stereoselectivities for *cis*-alkene epoxidations vary with both *cis*-alkenes and ruthenium oxidants. In the epoxidation of *cis*-β-methylstyrene mixtures of *cis* and *trans*-epoxides were observed (*cis*:*trans* ratios varying from 2:1 to 5:1). This loss of stereospecificity could not be explained with a concerted insertion of Ru^{IV}=O into the C=C bond (path a, Figure **1.8**) and, hence, a non-concerted pathway was proposed. Figure **1.9** shows the radical mechanism of epoxidaton reaction.

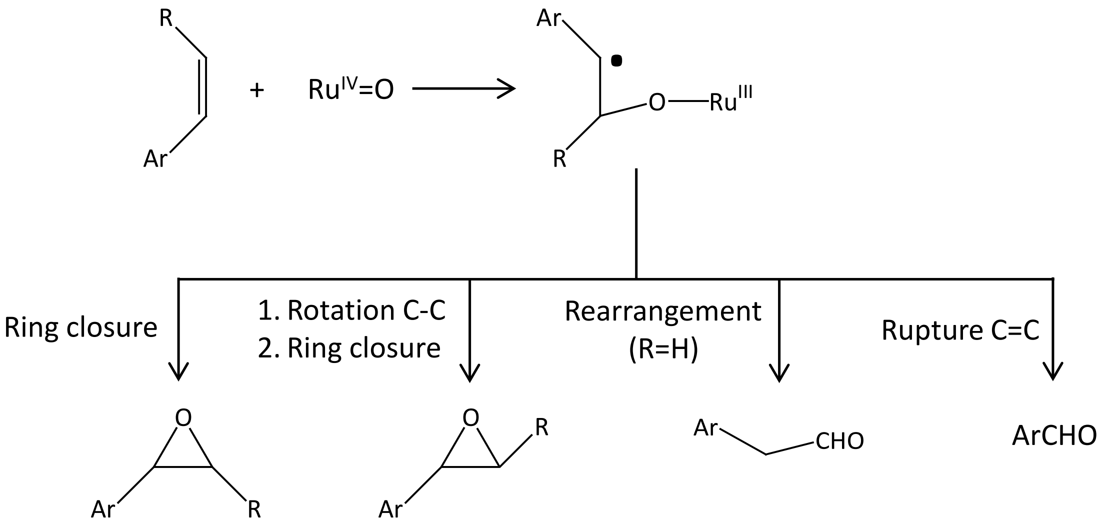

Figure 1.9. Proposed mechanism for the oxidation of aromatic olefins by ruthenium(IV) oxocomplexes.

Recently, Chatterjee has shown that for Ru-aqua complexes with general formula [Ru(T)(D)OH_2] (T=tridentate ligand and D=bidentate ligand), the geometry of the tridentate ligand and the electronic nature of the bidentate ligand play a key role in the catalytic performance of complexes in the epoxidation reactions. Indeed, the facial coordination of a tridentate ligand can make stereochemically easy the contact between the organic substrate and the catalytic species. The electrophilic character of ruthenium can be modulated by the auxiliary didentate ligand. Thus, a good π-acceptor bidentate ligand would make electron deficient the ruthenium center, while a good σ-donor ligand could increase the electron density. This reduces the tendency of the metal center to have a reduction via electron transfer through the external sphere, which allows the ruthenium acting as epoxidation catalyst instead of hydroxylation.[197]

In Table **1.3** examples of the effects of ligands on the reactivity of the ruthenium complexes in the case of epoxidation of *trans*-stilbene are shown.

Table 1.3. Ligand effects on the epoxidation of *trans*-stilbene with Ru-aqua complexes.

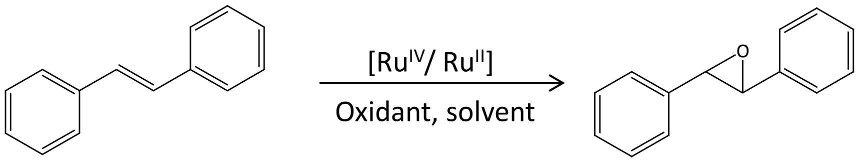

Entry	Complex	Oxidant	Yiel (% *trans*-stilbene)	Ref.
1	$[Ru^{II}(trpy)(bpy)OH_2]^{2+}$	NaOCl	7	187
2	$[Ru^{II}(trpy)(pic)OH_2]^{+}$	*t*-BuOOH	55	213
3	$[Ru^{II}(trpy)(phbox\text{-}i\text{Pr})OH_2]^{2+}$	$PhI(OAc)_2$	37,4	214
4	$[Ru^{II}(trpy)(box\text{-}C)OH_2]^{2+}$	$PhI(OAc)_2$	13,5	215
5	$[Ru^{II}(tpm)(box\text{-}C)OH_2]^{2+}$	$PhI(OAc)_2$	61	215

Abbreviations: pic = picolinate; phbox-*i*Pr = 1,2-bis[4'-alkyl-4',5'-dihydro-2'-oxazolyl]benzene; box-C = 4,4’-dibenzyl-4,4’,5,5’-tetrahydro-2,2’-bioxazole.

The substitution of a neutral ligand bpy (entry 1) by a stronger σ-donor pic ligand (entry 2) leads to improve the epoxide performance from 7 to 55%. This could be explained by the fact that the ruthenium electron density increases due to the important donor effect of the anionic pic ligand, which facilitates the attack of ruthenium to the substrate, while the π-acceptor nature of the phbox-*i*Pr ligand makes electron deficient the metal center and provokes a yield reduction (entry 3).

The change in the geometry of the tridentate ligand also could have an important influence on reactivity. Thus facial disposition of tpm ligand, unlike the meridional disposition of trpy ligand, promotes contact between the substrate and the active group Ru=O which leads to an increased yield (61%) (entries 4 and 5).

1.4.2. Nitrile hydration reactions

The hydration of nitriles to generate the corresponding amides is an important transformation from both academic and industrial points of view.[216] The amide bond is one of the most important functional groups in contemporary chemistry since amides not only constitute versatile building blocks in synthetic organic chemistry,[217,218] but also exhibit a wide range of industrial applications and pharmacological interest.[219,220] This reaction is also of biotechnological interest since nitrile hydratases, a family of non-heme iron enzymes,[221,222] are used in the industrial preparation of relevant amides, such as acrylamide, nicotinamide and 5-cyanovaleramide.[219,223-226] In addition, amides can be reduced to the corresponding amines under remarkably milder conditions, making the catalytic hydration of nitriles also interesting from this point of view.[227-229]

Accordingly, the development of atom-efficient catalytic methods for amide formation is currently an extremely active are of research.[230] Amides are commonly prepared by the reaction of activated carboxylic acid derivatives (acid chlorides, anhydrides and esters) with amines including ammonia,[231-233] or by direct union of the acids with the amines assisted by coupling reagents, such as carbodiimides or 1H-benzotriazole derivatives.[234] However, despite being of great applicability, these methods suffer from a low atom economy and are associated to the generation of large quantities of waste products, making their environmental profile unfavorable. For these reasons, increasing attention is being devoted to the development of more efficient and sustainable synthetic routes that allow access to this important class of compounds.[235,236]

In this context, one of the simplest methods of synthesizing primary amides is the catalytic hydration of nitriles (Scheme **1.6**). Conventionally, amides have been synthesized by the hydration or nitriles, catalyzed by strong acids[237] and bases.[238,239] These conventional methods suffer several drawbacks, such as the formation of undesired by-products, such as carboxylic acids (Scheme **1.6**) by hydrolysis of the amides. The formation of a large amount of salts after neutralization is another problem associated with these classical methodologies. Moreover, many sensitive functional groups do not endure such harsh conditions, which consequently decrease the selectivity of the reaction. Therefore, the development of efficient procedures for the synthesis of amides that circumvent the use of stoichiometric reagents and/or acidic and basic media is highly desirable.

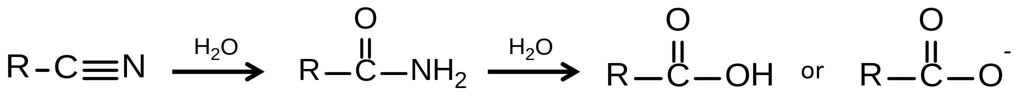

$$R\text{-}C\equiv N \xrightarrow{H_2O} R-\overset{\overset{O}{\|}}{C}-NH_2 \xrightarrow{H_2O} R-\overset{\overset{O}{\|}}{C}-OH \text{ or } R-\overset{\overset{O}{\|}}{C}-O^-$$

Scheme 1.6. The nitrile hydration and amide hydrolysis reactions.

To overcome these drawbacks, considerable efforts have been expended in the search of alternative methods for the nitrile hydration process. In this context, nitrile hydratases (NHases), a family of enzymes containing non-heme low spin Fe(III) or non corrinoid low-spin Co(III) active centers, have demonstrated great potential to promote the selective transformation of nitriles into amides under mild conditions.[240-242] In fact, these types of biocatalysts have found application in commercial production of some relevant amides, such as levetiracetam, an antiepileptic drug marketed under the trade name Keppra® (Scheme **1.7**).[243]

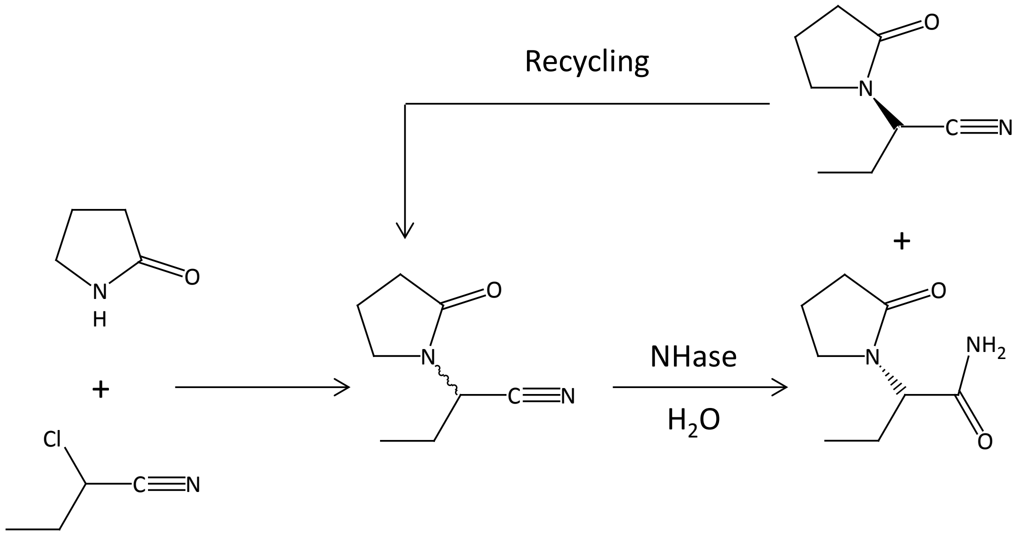

Scheme 1.7. Synthetic route of levetiracetam employing a nitrile hydratase.

Quite recently, in an attempt of mimicking the active sites of the iron-containing NHase enzymes, Grapperhaus and co-workers have also described the catalytic hydration of benzonitrile using octahedral ruthenium(II) complexes.[244] These complexes were able to operate in neat substrate/water mixtures, without the requirement of added base or buffer, generating benzamide in a selective manner albeit in very low yields.

Enzymatic catalysis offers cleaner and more selective protocols for the conversion of nitriles to amides, but despite the advances achieved in the field and its commercial success, the necessity of special procedures to handle microorganisms, their high cost and the narrow substrate specificity of the presently available enzymes severely limit their use.[222,223,225,240,241,245]

Metal ions are able to favor nitrile hydration by activating the nitrile substrate, the water nucleophile, or both upon coordination. Accordingly, methods based on homogeneous[246] or heterogeneous[247] metal based catalyst, where extreme acidity and basicity can be avoided, represent more attractive and powerful alternatives. For synthetic purposes, given their greater substrate scope and easier handling, these methods based on metal catalysts are much more appealing than the enzymatic ones.

A variety of transition-metal complexes (mainly of groups 8-12) have been investigated.[246,248] Concerning the homogeneous ones, the hydridoplatinum(II) complex [PtH(PMe$_2$OH){(PMe$_2$O)$_2$H}] developed by Parkins and co-workers achieved a extraordinary success (Figure **1.10**). [249-251]

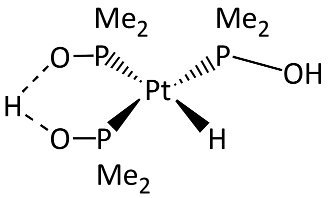

Figure 1.10. Structure of the Parkins catalyst.

This Pt system is able to catalyze the selective hydration of a wide range of nitriles, including very bulky nitriles, unsaturated nitriles (such as acrylonitrile) and nitriles containing acid and base-sensitive functional groups, under relatively mild (70-100°C) and neutral reaction conditions. All these properties, along with its exquisite functional group tolerance, has allowed the implementation of $[PtH(PMe_2OH)\{(PMe_2O)_2H\}]$ in the synthesis of a large number of complex organic molecules and natural products.[252- 255] The remarkable activity shown by the rhodium(I)-based systems $[\{Rh\text{-}(\mu\text{-}OMe)(cod)\}_2]/PCy_3$ (cod = 1,5-cyclooctadiene)[256] under ambient conditions deserve to be also highlighted.

1.4.2.1. Ruthenium as nitrile hydration catalyst

The application of a ruthenium complex to promote the selective hydration of nitriles to primary amides was described for the first time by Taube and co-workers in the 1970's.[257] Thus, using a stoichiometric amount of $[RuCl(NH_3)_5]Cl_2$ in combination with Ag_2O, trifluoroacetic acid and zinc amalgam, they were able to transform in high yields several aromatic, aliphatic and α,β-unsaturated organonitriles into the corresponding amides in dichloromethane. However, despite this early discovery, it was not until 1992 that the first truly catalytic system could be developed by Murahashi and co-workers employing the ruthenium dihydride complex $[RuH_2(PPh_3)_4]$ as catalyst. [258- 261] The Murahashi's ruthenium dihydride represents prototypical example of highly active and selective catalyst in 1,2-dimethoxyethane (DME) under neutral conditions, showing excellent functional group tolerance and applicability in the syntheses of complex organic molecules and natural products. A reaction pathway involving the intermolecular nucleophilic addition of water to the coordinated nitrile, to give an iminolate complex, was proposed (Scheme **1.8**). Reductive elimination, isomerization of the iminol to the amide and subsequent dissociation regenerates the catalytically active ruthenium species.[260]

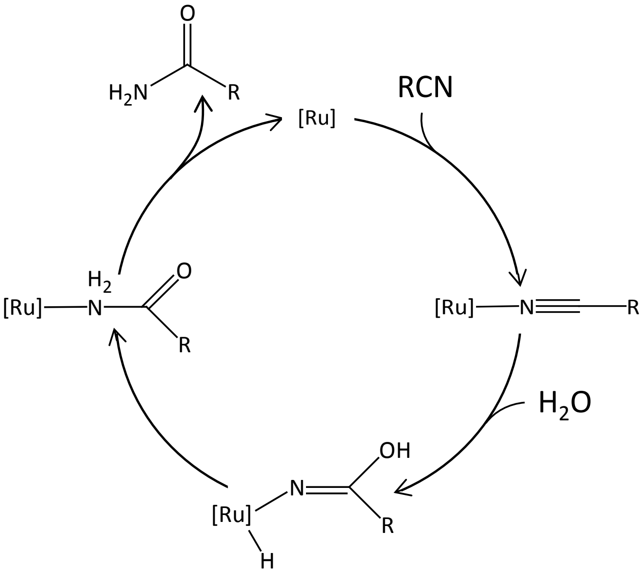

Scheme 1.8. Catalytic hydration of nitriles by means of complex $[RuH_2(PPh_3)_4]$.

The half-sandwich hydrido-ruthenium(II) complex $[RuH(\eta^5-C_9H_7)(dppm)]$ (dppm = bis(diphenylphosphino)methane; C_9H_7 = indenyl) revealed also as a quite effective catalyst for the selective conversion of nitriles to amides in water.[262,263] Worthy of note, its chlorido counterpart $[RuCl(\eta^5-C_9H_7)(dppm)]$ was found to be completely ineffective, suggesting that the hydride ligand plays a key role during the catalytic event. To clarify this point, Density Functional Theory (DFT) calculations were performed, pointing out an unusual promoting effect of the hydride (Scheme **1.9**). Hydride ligand activates the incoming water molecule through a Ru-H···H-OH dihydrogen-bonding interaction, favoring the nucleophilic attack of water on the coordinated nitrile. In this rate-determining step an iminol intermediate is produced, which quickly tautomerizes to the amide upon dissociation. Remarkably, despite the known tendency of the indenyl ligand to undergo $\eta^5 \rightarrow \eta^3$ ring slippage,[264-266] the DFT calculations indicated that coordination of the nitrile to ruthenium takes place by dissociation of one arm of the diphosphine dppm.

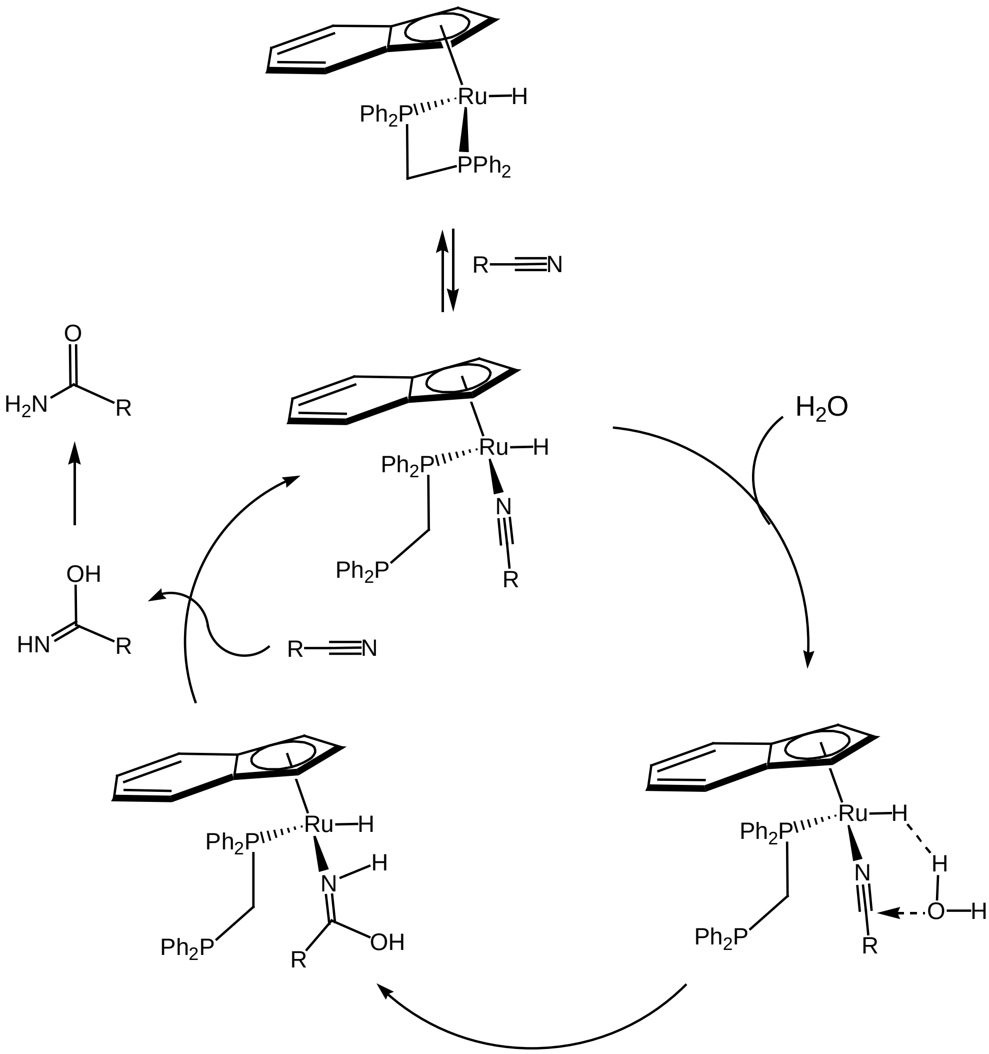

Scheme 1.9. Promoting effect of the hydride ligand of [RuH(η^5-C_9H_7)(dppm)] complex during the catalytic hydration of nitriles.

From the mechanistic point of view, although several reaction pathways have been proposed for these metal-catalyzed transformations, coordination of the nitrile to the metal is a common prerequisite for most of them. In this way, the CN bond is activated towards the nucleophilic addition of water, or the hydroxyl group if basic conditions are used, thus enhancing the rate of the hydration step versus the hydrolysis.[267-270]

The same promoting effect of the hydride ligand, via Ru-H···H-OH dihydrogen-bonding, was evidenced by means of DFT calculations in the reaction of the isoelectronic hydro(trispyrazolyl)borate complex [RuH(Tp)(PPh_3)(NCMe)] with water.[271] Both complexes are able to promote the selective conversion of several organonitriles to the corresponding primary amides in 1,4-dioxane/water mixtures. However, modest results in terms of activity were in general obtained.

The tetranuclear cluster and the mononuclear derivative shown in Figure **1.11** are additional examples of hydrido-ruthenium complexes able to promote the selective hydration of CN bonds employing ^{i}PrOH, THF, acetone or DME as solvent and 10-20 equivalents of water. The amides were obtained in all the cases in excellent yields in the case of tetranuclear cluster whereas for the mononuclear complex remarkably lower activity was obtained.

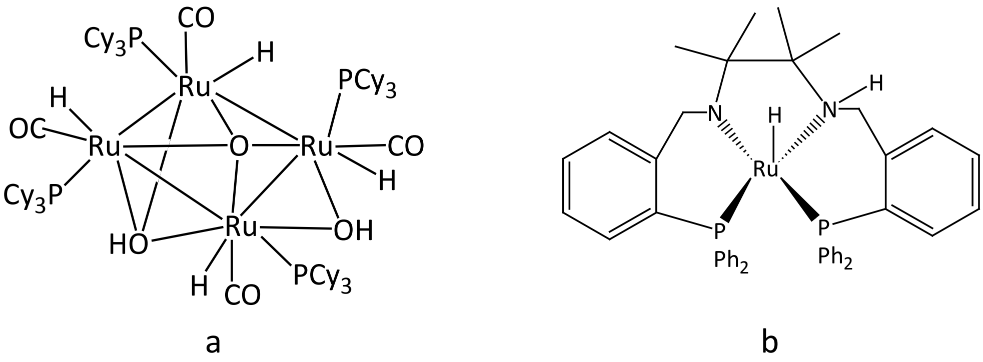

Figure 1.11. Structure of the hydrido-ruthenium complexes: tetranuclear cluster (a) and mononuclear complex (b).

The key role played by the auxiliary ligands in this catalytic transformation was clearly evidenced by Oshiki and co-workers using the octahedral ruthenium(II) derivative *cis*-[Ru(acac)$_2$(PPh$_2$py)$_2$].[272-274] This complex was able to hydrolize efficiently a large number of nitriles employing DME as solvent and 4 equivalents of water. Mediocre results were obtained with complexes *cis*-[Ru(acac)$_2$(PPh$_3$)$_2$], *cis*-[Ru(acac)$_2$(PMe$_3$)$_2$] and *cis*-[Ru(acac)$_2$(PBu$_3$)$_2$] containing non-cooperative phosphine ligands.[273] Such a cooperative effect of the PPh$_2$py ligand is a clear example of the so-called “bifunctional catalysis”, in which the substrates are activated by the combined action of the metal, which acts as a Lewis acid, and the ligand, which acts as a Lewis base. Such a concept has been largely exploited in homogeneous catalysis during the last years.[275-278]

Inspired by the works of Oshiki and co-workers, Šmejkal and Breit described the preparation and catalytic behavior of the bis(acetylacetonate)-ruthenium(II) complexes bearing the potentially cooperative P-donor ligands 6-diphenylphosphino-*N*-pivaloyl-2-aminopyridine and 3-diphenylphosphinoisoquinolone (Figure **1.12**).[279] All of them were able to promote the selective conversion of the model substrate 4-methylbenzonitrile. However, under the same reaction conditions their effectiveness was comparatively lower to that shown by complex *cis*-[Ru(acac)$_2$(PPh$_2$py)$_2$].

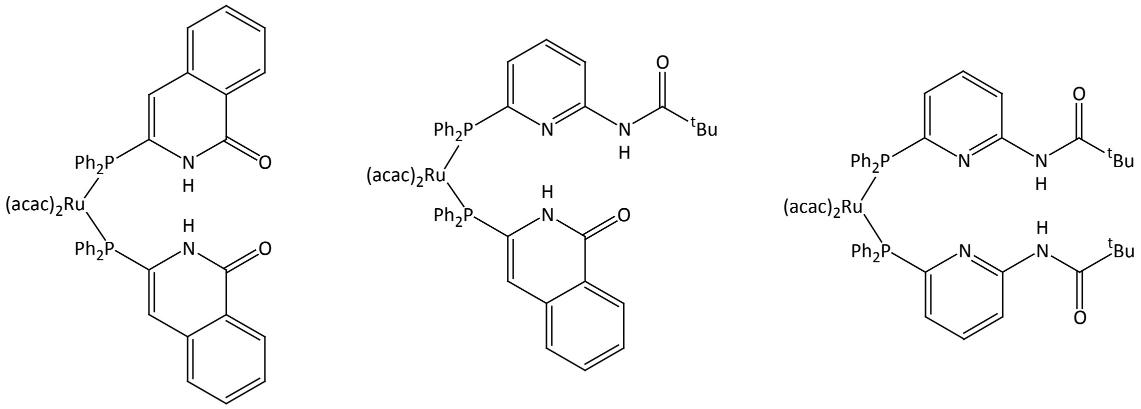

Figure 1.12. Structure of the bis(acetylacetonate)-ruthenium(II) complexes.

Most of the known homogeneous catalysts for nitrile hydration, including the examples commented above, operate in organic media in the presence of only small amounts of water.

Chemical transformations, as well as other industrial productive processes, are experiencing a profound transformation to meet sustainability criteria, moving from old methods to new ones developed in agreement with green chemistry principles.[280-284] Substitution of harmful and hazardous chemicals with others more compatible with human health and the environment is mandatory, and among these the solvent replacement is especially important since amounts of solvents are usually much larger than those of reagents and products.

Water has been much under-investigated as a solvent for chemical transformations basically because of poor solubility of organic molecules; however, water is the "ideal solvent"[285- 290] being economic, non-toxic, non-inflammable and compatible with the environment. Substitution of organic solvents by water is desirable, but it becomes especially suited for those chemical transformations in which water is one of the reagents.

In the search for cooperative effects of the ligands and being environmentally concerned, the catalytic behavior of different arene-ruthenium(II) complexes with potentially H-bond accepting amino-aryl-phosphines was also explored by Crochet, Cadierno and co-workers.[291] All these complexes (5 mol%) were able to hydrolize the model benzonitrile substrate in pure water as solvent.

In order to facilitate the solubility of the catalysts in water, remarkable efforts have been devoted in recent years to the study of ruthenium complexes bearing water-soluble phosphines. In this context, a possible cooperative effect of the "cage-like" phosphines 1,3,4-Triaza-7-phosphaadamantane (PTA), 1-benzyl-1-azonia-3,5-diaza-7-phosphaadamantyl (PTA-Bn), 3,7-Diacetyl-1,3,7-triaza-5-phosphabicyclo[3.3.1]nonane (DAPTA), 2,4,10-trimethyl-1,2,4,5,7,10-hexaaza-3-phosphatricyclo[3.3.1.1(3,7)]decane (THPA) and 2,3,5,6,7,8-hexamethyl-2,3,5,6,7,8-hexaaza-1,4-diphosphabicyclo[2.2.2] octane (THDP),[292- 295] via H-bonding of the nucleophilic water molecule with the nitrogen atoms present in their structures, has been proposed to explain the remarkably high effectiveness shown by the arene-ruthenium(II) (Figure **1.13**) and bis(allyl)-ruthenium(IV) complexes. [296- 299] All of them operate in pure water without the assistance of any acidic or basic additive, showing a wide substrate scope and high tolerance to common functional groups. In addition, after selective crystallization of the final amide, recycling of the aqueous phase containing the active species could also be demonstrated for $[RuCl_2(\eta^6\text{-}C_6Me_6)(PTA\text{-}Bn)]$.[296]

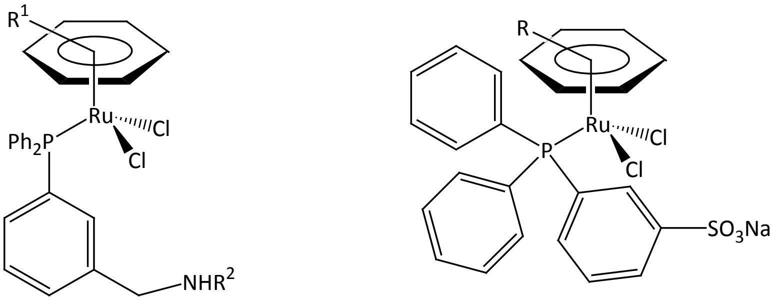

Figure 1.13. Examples of arene-ruthenium(II) complexes.

More recently, Cadierno *et al.*[300] developed a new class of water-soluble phosphine ligands, consisting of *N*-protonated thiazolyl-phosphine salts (Figure **1.14**). One of them turned out to be an excellent auxiliary ligand in the ruthenium-catalyzed selective hydration of nitriles to primary amides in environmentally friendly aqueous medium. In addition, the high solubility of complex in water allowed a facile amide product separation (by selective crystallization), and the effective reuse of the remaining aqueous solution containing the catalyst.

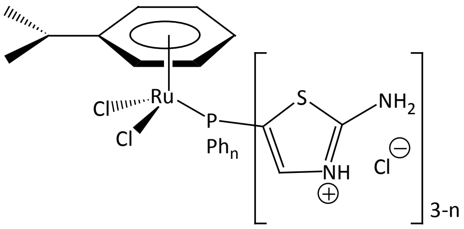

Figure 1.14. Structure of water-soluble arene-ruthenium(II) complexes

To the best of our knowledge, no report of complexes with N- or S-donor ligands applied to hydration of nitriles can be found in the literature.

On the other hand, catalyst recovery is an important topic in chemistry and, in this context, solvents are of prime importance. For homogeneous catalysts with high solubility in water, an efficient method for recycling the catalyst can be based on the higher solubility of the catalyst in the aqueous phase than in the extraction organic solvents.[301] Recently, glycerol appeared as a valuable green solvent[302- 306] and has also been described as a possible solvent for the immobilization of homogeneous catalysts in a similar way.[307,308]

1.5. Supported catalysts

An immobilized catalyst is the result of the transformation of a homogeneous catalyst to a heterogeneous one. The simplest process to perform this task is by supporting a soluble active molecule on the surface of an insoluble solid.

1.5.1. Homogeneous *vs.* heterogeneous systems

The main focus of catalysis research in the past was to enhance catalytic activity and selectivity. Recovery of the catalyst was not really a serious concern. However, in "green chemistry" approaches for catalytic reactions, the recovery and reuse of catalysts becomes an important factor because of stringent ecological and economical demands for sustainability.[309-311]

In general, catalysis is divided into homogeneous[312] and heterogeneous[313,314] catalysis; the former applies when the catalyst and the substrate are in the same phase and the later when they are not. Table **1.4** summarizes the principal differences between homogeneous and heterogeneous catalysis.[315]

Homogeneous catalysts have the advantage that they are well defined on a molecular level with well-defined active sites and readily soluble in the reaction medium. Such single-site catalysts are highly accessible to the substrates and often show high catalytic activity and selectivity, even under mild conditions. Consequently, there is a constant energetic interaction between each active site and the substrate. However, removing them from the reaction mixture to avoid contamination of the product requires expensive and tedious purification steps.

Moreover, the catalyst often consists of a high-priced noble metal and/or ligand. Thus, despite their intrinsic advantages, homogeneous catalysts are used in less than 20% of the industrially relevant processes.[316,317]

In contrast, heterogeneous catalysts allow easy product/catalyst separation and recovery from the reaction medium, easy handling and potential catalyst recycling. However, they often lack of good characterization at the molecular level, thus difficulting mechanistic studies. The preparation procedures are concerted and consequently not always easy to reproduce.[318,319] In addition, the fact that active sites are placed in a microporous environment often causes diffusion control of the catalyzed reaction and reduces the activity and the selectivity.

Table 1.4. Homogeneous *vs*. heterogeneous catalysis. Schematic comparison.

Features	Homogeneous catalyst	Heterogeneous catalyst
Form	Metal complex	Solid, often metal or metal oxide
Active centers	Well defined	Not defined
Activity	High	Variable
Selectivity	High	Variable
Reaction conditions	Mild	Drastic
Average time of life	Variable	Long
Sensitivity to poisons	Low	High
Problems of diffusion	None	Possible
Recycling	Difficult and expensive	Easy
Separation from products	Difficult	Easy
Variation of steric and electronic features	Possible	Difficult
Mechanism studies	Possible	Difficult

Recycling of homogeneous catalysts is thus an important issue in the sustainable and large-scale production of fine chemicals. It is of special importance for enantioselective transformations, in which the cost of sophisticated ligands often exceeds that of the noble metal employed.[320,321]

On the other hand, there are often different catalytically active sites with differing activities and selectivities in the bulk material of a heterogeneous catalyst, which are challenging to probe on a molecular level.

Therefore, the development of new catalyst that combines the best features of both kinds of systems is an interesting and growing area in catalysis. These hybrid catalysts are named immobilized heterogeneous catalyst or supported catalysts.[322-324]

1.5.2. Immobilization methods

The aim of supported catalysts is to combine the mentioned advantages of both homogenous and heterogeneous catalysis such as: (1) high activity, selectivity and reaction rates (homogeneous catalysis), (2) easy catalyst recovery and preparation of multifunctional catalysts (heterogeneous catalysis). Among the different techniques described to immobilize catalysts into solid supports, the most common methods used are (Figure **1.15**): adsorption,[325] electrostatic immobilization,[293,326] encapsulation,[327-330] ionic liquid [331-333] and covalent binding (anchoring).[334-337]

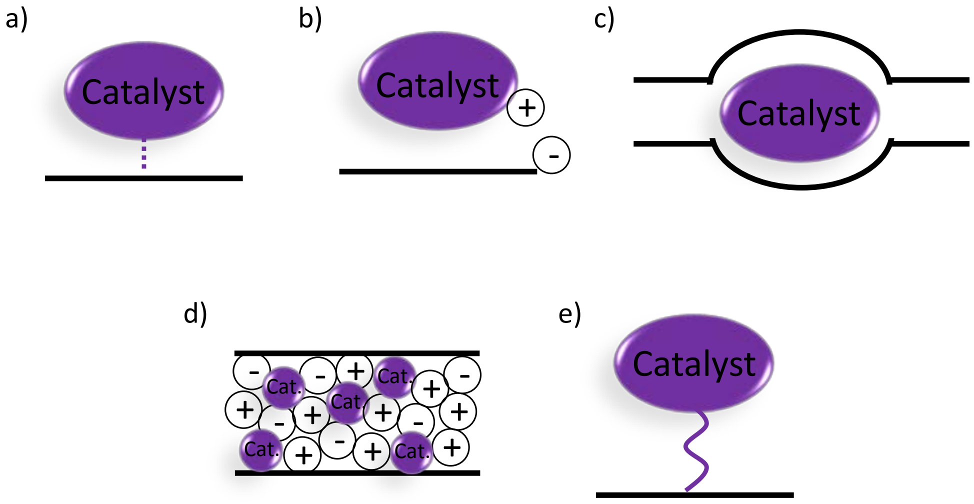

Figure 1.15. Schematic representation of different types of catalyst immobilization: adsorption (a), electrostatic immobilization (b), encapsulation (c), ionic liquid (d) and covalent binding (e).

a) Adsorption

The adsorption is usually established by Van der Waals interactions between groups such as aromatic systems and by hydrogen bonds (Figure **1.15a**). This method is one of the most time- and cost-effective procedures. However, the scope of this technique is quite limited taking into account that the surface of most supports is polar (limiting the application to the immobilization of polar catalysts) and that the adsorptive interactions are rather weak and can be disrupted by solvent effects or competition from oxidation products or polar oxidants. The range of supports that are used with this methodology is broad, including both amorphous and crystalline materials, such as silica and zeolites.

b) Electrostatic immobilization

The immobilization by electrostatic interactions is a simple and fast approach to the fabrication of heterogenized catalytic systems. However, an obvious limitation it that only charged catalyst can be immobilized in this manner (Figure **1.15b**). When using this method, possible interactions between the support and ionic substrates or oxidants that could compete with the catalyst must be considered. The charged supports used are ion-exchange resins, zeolites, clays, layered double-hydroxides, etc.

c) Encapsulation

This technique is based on the encapsulation of the catalyst inside the pores of the support (Figure **1.15c**). Encapsulation presents the advantage that the homogeneous catalyst does not suffer any change in its structure and chemical properties when being immobilized. Another advantage is the impossibility of deactivation by oligomerization, since each molecule, and just one, is encased in a well-defined cage, without being possible the interaction with neighbouring molecules. The range of application of this method is limited to complexes with a well-defined size and possible diffusion limitations of the substrate through the pores should be considered. This technique is very useful for the immobilization of complexes with bulky ligands such as porphyrins, phtalocyanines, bipyridines, tetradentate Schiff bases, etc. The supports used are often crystalline and contain cages, such as zeolites, mesoporous silica and coordination polymers.

d) Ionic liquid

Over the last decade, growing attention has been devoted to the use of ionic liquids (ILs) as solvents for organic synthesis. The strong interest in ILs for catalyzed reactions is due to the expected immobilization of the catalyst in the IL that would allow the recycling of the tandem catalyst/solvent (Figure **1.15d**). Furthermore, ILs have a rate acceleration effect on some catalytic reactions, and they are often considered as green alternatives to volatile organic solvents although their toxicity and biodegradability are yet to be fully determined.

Ionic liquids are in general defined as liquid electrolytes composed entirely of ions. Generally, ionic liquids include liquid compounds which involve organic compounds and organominerals. Those ionic liquids based on quaternary ammonium or phosphonium salts, usually named room temperature ionic liquids (RTILs), exhibit interesting physicochemical properties.[338,339] The use of the ionic liquid solvent allowed an easy catalyst recycling without the need of any catalyst modification.[340,341]

e) Covalent binding (anchoring)

This type of immobilization is the one that gives a stronger interaction between catalyst and support (Figure **1.15e**). This immobilization method has been used to support a wide variety of active homogeneous catalysts. One of its advantages is that the chemical surrounding of the metal centre is maintained as in the homogeneous parent precursor, but with all the heterogeneous advantages.[342] The general covalent immobilization process for an active homogeneous catalyst is represented in Figure **1.16**.

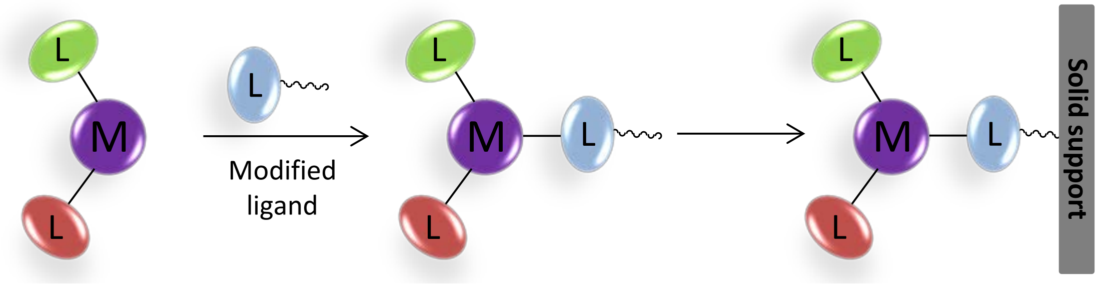

Figure 1.16. General process for anchoring an homogeneous catalyst into a solid support.

Following this methodology the catalyst must be modified by adding a linking group that attaches to the solid support. The most common linking groups used are organosilanes, of general formula R_nSiX_{3-n} (Cl, alkoxy), and organophosphorus acids resulting in the formation of a M-O-Si or M-O-P bond between the inorganic support

(M) and the linker. In the case of a phosphonic acid up to three M-O-P bonds can be formed with the metal oxide surfaces, as represented in Figure **1.17**.[334]

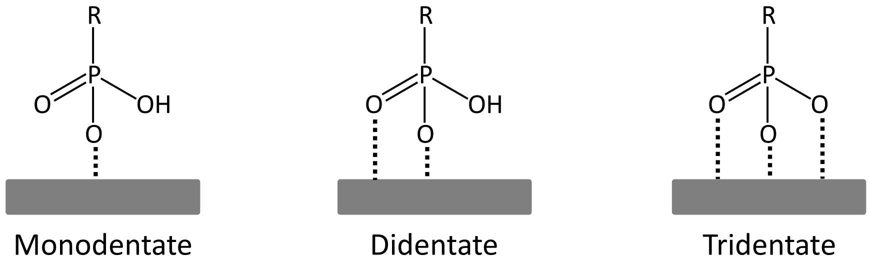

Figure 1.17. Possible binding modes of a phosphonate unit to a metal oxide surface.

1.5.3. Supports

When choosing a support for the immobilization of a catalyst, two main aspects must be taken into account. First, the metal complex must be well dispersed through the surface of the support in order to achieve proper activities and good diffusion conditions. For this reason, parameters such as surface charge, polarity and particle and pore size must be considered. Secondly, the system must be chemically and physically stable in the catalytic reaction conditions.

The supports can be organic[343] (such as polymers with a polystyrene, polypyrrole or polyacrylate backbone), inorganic[344,345] (such as silica, alumina, titania, zeolites, metallic nanoparticles) or metal-organic frameworks[346] (MOFs). Among these supports, some of them will be explained.

a) Polypyrrole

A wide diversity of modified electrodes has been described, which have been used as heterogeneous catalysts for a variety of chemical reactions.[347-349] Polypyrrole has become the most studied conducting polymer in the last few decades due to its stability and high electrical conductivity.[85,350,351]

b) Titanium dioxide

Structural modifications of titanium dioxide (TiO_2) can affect its band gap energy allowing it to absorb light in the visible zone, that being of interest in the solar cells research field. These modifications can be carried out by synthesizing new TiO_2-based composite materials,[352,353] through n-doping or by surface immobilization of sensitizing dyes.[30,354] The last approach is especially interesting because by introducing adequate functional groups in the organic framework of the ligands, a complex can be easily anchored onto the TiO_2 surface.[355]

c) Metal phosphates

Recently, some phosphates were used in heterogeneous solid / liquid catalysis. This was possible due to their structure, the presence of acid and basic Brønsted and Lewis sites and their ability to ion exchange with a wide variety of metals.[356-358]

d) $AlPO_4$ materials

The original family of silica-based zeolites and aluminosilicates (SiAlPOs) has been greatly extended in recent decades, including aluminophosphates (AlPOs), which constitute a wide family of new materials among the most studied, and most frequently employed, as catalysts as well as supports, in several organic reactions. [359,360] In general, they all exhibit high thermal and mechanical stability, and can be deeply modified throughout synthesis by hydrothermal and sol-gel methods, thus obtaining a large amount of crystalline materials ranging from microporous to mesoporous structures.[361]

e) Nanoparticles

Nanoparticles (NPs) can be defined as microscopic particles with a diameter of 1-100 nm. They are considered as a bridge between molecular structures and bulk materials or, in catalytic terms, a bridge between homogeneous and heterogeneous catalysis, these systems are often referred to as "quasihomogeneous" (or soluble heterogeneous) systems.[362] Iron oxide nanoparticles (MNPs) have attracted extensive interest due to their superparamagnetic properties and their potential applications in many fields.[363,364] There are three common iron oxides: iron (II) oxide (FeO), iron (III) oxide (Fe_2O_3) and iron (II,III) oxide (Fe_3O_4). Among these, γ-Fe_2O_3 (maghemite) and Fe_3O_4 (magnetite) have received more attention in catalysis.

In many cases silica-coated nanoparticles are used,[365,366] in this case each nanoparticle is formed by a well-defined magnetic nucleus. The magnetic nucleus is surrounded by a microporous silica shell ensuring the system's biocompatibility.[367]

1.5.4. Heterogenized catalysts for oxidation reactions

Oxidation catalysis usually involves the use or formation of oxometal complexes and other metal-oxygen bonds and, for this reason, the inhibition of undesired interactions between catalyst molecules will lead to the enhancement of their stability. In consequence, the heterogenization of the catalyst prevents its deactivation, either by ligand oxidative degradation or by formation of μ-oxo-bridged dimers or other oligonuclear species.

Heterogenized catalysts have been active in oxidation of alcohols,[344,368] olefins,[369] organic sulfides,[370,371] phenol[372] and aromatic C–H.[373] They also show activity in allylic oxidation[374] and dihydroxylation.[375]

A SiO_2-supported unsaturated Ru-monomer complex (Figure **1.18**) was reported by Iwasawa and co-workers,[376] exhibiting high values of selectivity for aldehyde oxidation and alkene epoxidation at ambient temperature.

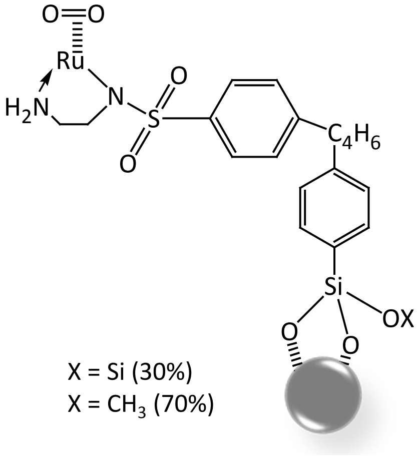

Figure 1.18. Structure of SiO_2-supported Ru catalyst.

Louloudi *et al.*[158] reported a biomimetic ruthenium complex covalently attached to silica surface (Figure **1.19**). The complex was efficient in alkene oxidation and, in some cases, it showed increased activity compared to the homogeneous ruthenium complex.

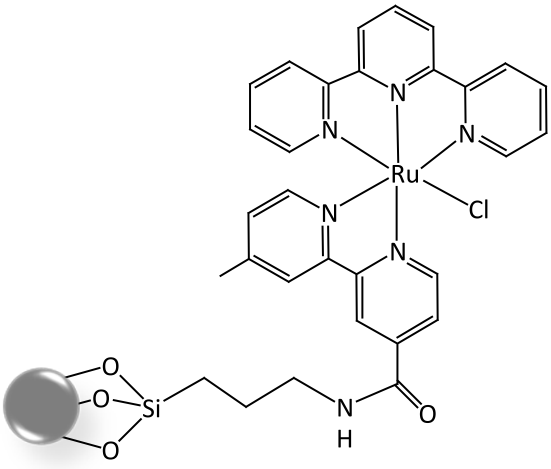

Figure 1.19. Structure of biomimetic ruthenium complex.

The range of immobilized catalysts used to perform the epoxidation of olefins is broad. Among the metals used we can find manganese,[377-380] iron,[380,381-383] titanium,[384,385] cobalt,[386] molybdenum,[387-389] vanadium,[390] tungsten[391-394] and ruthenium.[395-397]

Magnetic nanoparticles (MNPs) have been used for the oxidation of alcohols, olefins and amines as well as for the epoxidation of alkenes.[364,398-401] Mizuno and co-workers investigated the aerobic oxidation of alcohols and amines by using ruthenium hydroxide supported on magnetite ($Ru(OH)_x/Fe_3O_4$).[402] Organic-inorganic hybrid nanocatalysts obtained by covalently anchoring [(L-L)$MoO(O_2)_2$] (L-L = (3-triethoxysilylpropyl)[3-(pyridyl)-1-pyrazolyl]acetamide) (Figure **1.20**) on silica-coated MNPs were reported by Thiel and co-workers to be robust magnetically separable epoxidation catalysts.[403,404]

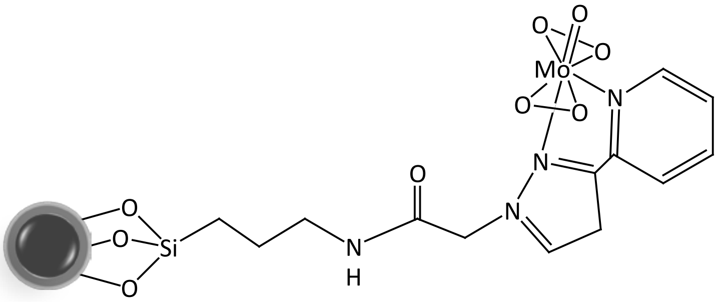

Figure 1.20. Heterogenized molybdenumperoxo catalyst for olefin epoxidation on silica-coated MNPs.

Magnetite nanoparticles were used, for Lin et co-workers,[405] to immobilize the ruthenium (II) complex with phosphonic acid-substituted BINAP [Ru(BINAP-PO_3H_2)(DPEN)Cl_2] (where BINAP = 2,2'-bis(diphenylphosphino)-1,1'-binaphthyl and DPEN = 1,2-Diphenyl-1,2-ethylenediamine) (Figure **1.21**). This complex was used for the hydrogenation of aromatic ketones presenting high reactivity and enantioselectivity.

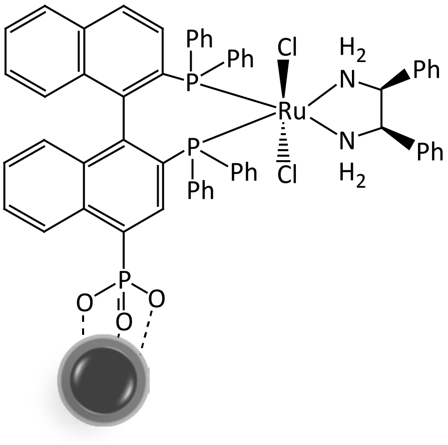

Figure 1.21. Structure of [Ru(BINAP-PO_3H_2)(DPEN)Cl_2].

1.5.5. Heterogenized catalysts for nitrile hydration

Despite the enormous interest for industry of heterogeneous catalysts due to their easier handling, higher stability, easier recovery and reusability, heterogeneous ruthenium-based systems for nitrile hydration reactions have been comparatively much less developed than the homogeneous ones.

In this context, the use of ruthenium supported on carbon (Ru/C)[406] and alumina (Ru/Al_2O_3),[407] as well as ruthenium nanoparticles combined with oxygen-containing copper compounds,[408] have been described in a series of Japanese patents. All of them were active and selective towards amide formation. Efficient and selective hydration of a number of organonitriles in water was described by Mizuno and co-workers employing ruthenium hydroxide supported on alumina ($Ru(OH)_x/Al_2O_3$) as catalyst.[409,410]

The first reported example of nitrile hydration by a nanoparticle catalyst was in a short letter published by Oshiki and co-workers.[411] They prepared water soluble palladium and platinum nanoparticles stabilized by a water-soluble polymer, poly(N-vinyl-2-pyrrolidone) (PVP; Figure **1.22**).

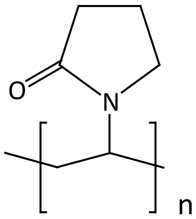

Figure 1.22. Poly(N-vinyl-2-pyrrolidone) (PVP), a water-soluble polymer commonly used as a nanoparticle stabilizer.

After this first heterogeneous catalyst, other metals such as nickel,[412] silver,[413-415] gold[416] and ruthenium[417] were reported as nitrile hydration catalysts.

Magnetic nanoparticles have also been used in hydration catalysts by means of ruthenium hydroxide supported on dopamine-functionalized Fe_3O_4 nanoparticles (Figure **1.23a**),[418,419] $Ru(OH)_x$[366] or Ag[420] or Mo_xO_y[421] nanoparticles (Figure **1.23b**) and a bifunctional ruthenium(II) complex[365] supported on silica-coated Fe_3O_4 nanoparticles (Figure **1.23c**). All these nanocatalysts showed excellent activities and selectivities for a broad range of activated and inactivated benzonitriles, as well as heteroaromatic, aliphatic and α,β-unsaturated nitriles. Because the super-paramagnetic nature of the Fe_3O_4 support, all these nanocatalysts could be easily separated from the reaction products with the help of an external magnet.[422]

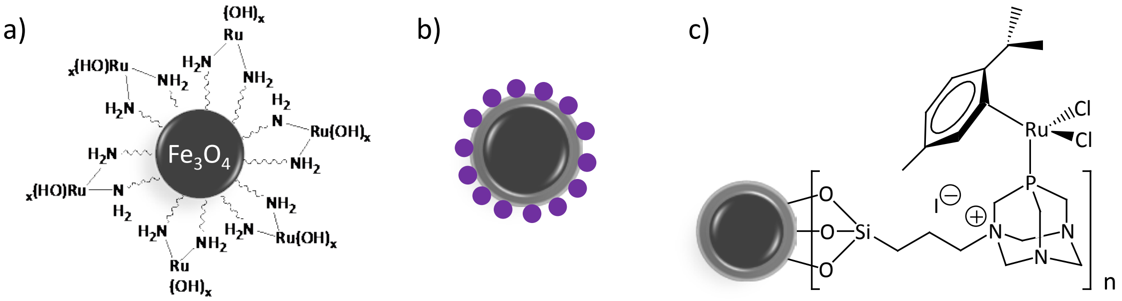

Figure 1.23. Structure of the different ruthenium-based nanocatalysts.

OBJECTIVES

Chapter 2

Objectives

As it has been seen in the introduction, catalytic epoxidation of alkenes and hydration of nitriles are important transformations from both academic and industrial points of view and, for this reason, a variety of transition-metal complexes have been investigated for both catalytic reactions. The structures of the catalysts are of paramount importance to understand and optimize their performance in these kinds of reactions. In this context, electronic and geometrical effects of the ligands coordinated to the metal are important in the understanding of the properties and behavior of these systems. Transition-metal complexes with ligands containing nitrogen as donor atom constitute an important class of coordination compounds that are able to perform a wide range of transformations. Nitrogen-based ligands have well-known advantages such as chemical robustness or rich coordination chemistry.

On the other hand, a huge number of ruthenium compounds containing dmso ligands combined with a variety of auxiliary ligands have been described as potent antitumor compounds or as precursors for the synthesis of a large variety of compounds but, although catalytic applications for Ru-dmso complexes are known, they have never been used as mediator complexes in nitrile hydration.

As described also in the introduction, heterogenization and reuse of catalysts are fields of unquestionable importance especially towards their application in large-scale processes but, to the best of our knowledge, there are not many examples in the literature that involve the use of well-defined molecular Ru compounds supported onto silica and magnetic nanoparticles (MNPs) to be applied as recyclable catalysts in epoxidation and hydration of nitriles.

For this purpose, the objectives of this thesis were the design of new families of ruthenium complexes with different types of N-donor and dmso ligands and their subsequent evaluation in catalytic oxidation and nitrile hydration reactions, together with the immobilization of some catalytic systems on the surface of silica supports and magnetic silica particles (MSPs).

Prior to this thesis, new ruthenium complexes with N-donor ligands were synthesized in our group, among which $[Ru(trpy)(pypz\text{-}Me)OH_2)]^{2+}$, whose catalytic activity for epoxidation of olefins was studied. Taking advantage of the group's experience with N-donor ligands, and with the above considerations related to the heterogenization of ruthenium complexes in mind, the specific objectives of this work were:

- The synthesis of two new ruthenium Ru-Cl and Ru-OH_2 complexes containing the modified tridentate (trpy-P-Et) and the bidentate (pypz-Me) ligands (Chart **2.1**) as well as their full characterization through elemental analysis, structural, spectroscopic (NMR, IR, UV-visible) and electrochemical techniques.

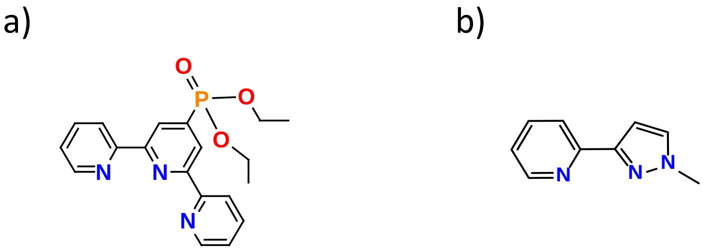

Chart 2.1. trpy-P-Et (a) and pypz-Me (b) ligands.

- The study of the Ru-aquo reactivity with regard to the epoxidation of alkenes using iodobenzene as the oxidant and the evaluation of its performance with regard to the hydration of some aromatic and aliphatic nitriles in water, rationalizing when possible the influence of electronic and geometrical effects of the ligands over the reactivity of these compounds and establishing a comparison with the analogous complexes previously synthesized in our group.

- The heterogenization of the trpy-P-Et Ru-Cl and Ru-aquo complexes onto different supports, silica and MSPs, and the full characterization of the functionalized supports through ICP-AES, SEM images, thermogravimetric analysis and spectroscopic (IR, UV-visible) and electrochemical techniques. As well as with homogeneous complex, we were also interested in the study of the reactivity and reutilization of these compounds as catalysts in the epoxidation of alkenes using iodobenzene as the oxidant, along with the hydration of nitriles in water.

- The synthesis of a new family of ruthenium complexes bearing the dmso ligand and different pyrazolic ligands (Chart **2.2**) as well as their full characterization through elemental analysis, structural, spectroscopic (NMR, IR, UV-visible) and electrochemical techniques.

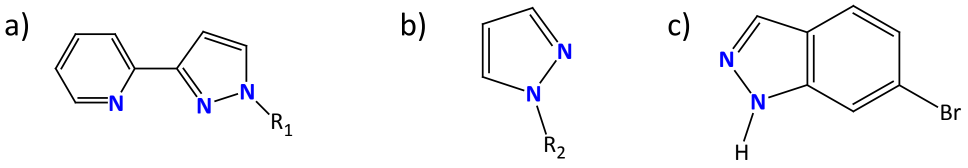

R_1 = H, CH_3 or Si R_2 = H, CH_3, NO_2 or CF_3

Chart 2.2. Pyrazolic ligands used.

- The study of the electron-transfer-induced linkage isomerization of the dmso ligands in representative compounds as $Ru^{II}Cl_2(CH_3\text{-pz-H})(dmso)_3$ and the bis-dmso complex $Ru^{II}Cl_2(pypz\text{-H})(dmso)_2$, and the study of the reactivity of the compounds towards light irradiation in $CHCl_3$, CH_3CN and water. The thermodynamic and kinetic parameters for the S- to O-bound dmso exchange will be also calculated.

- The study of the Ru-dmso complexes reactivity with regard to the hydration of some aromatic and aliphatic nitriles in water and glycerol and the reutilization of some systems in these media, together with the heterogenization of some of the compounds onto silica supports, including their full characterization through ICP-AES, UV-visible and electrochemical techniques.

EXPERIMENTAL
SECTION

Chapter 3

Experimental section

3.1. Materials

All commercial reagents and silica particles mesoporous (**SP2**) were purchased from Sigma-Aldrich and were directly used without further purification. Reagent grade organic solvents were obtained from SDS and Scharlab and high purity de-ionized water was obtained by passing distilled water through a nano-pure Mili-Q water purification system. Diethyl 2,2':6',2''-terpyridine-4'-phosphonate (trpy-P-Et, **L1**) and diethyl 2,2':6',2''-terpyridine-4'-phosphonic acid (trpy-P-H, **L2**) ligands were supplied by HetCat and were directly used without further purification. $RuCl_3{\cdot}2.38H_2O$ was purchased from Johnson and Matthey Ltd. and was used as received. Silica aerogel particles (**SP1**) and magnetic silica particles (**MSP**) were prepared in Dr. Anna Roig's group in ICMAB.

3.2. Preparations

$[Ru^{II}Cl_3(trpy\text{-}P\text{-}Et)]$[315] (**C1**) and $[RuCl_2(dmso)_4]$[90] (**C2**) complexes and the 2-(3-pyrazolyl)pyridine[423] (pypz-H, **L3**), (2-(1-alquil-3-pyrazolyl)pyridine)[424] (pypz-Me, **L4**) and (3-triethoxysilylpropyl)[3-(2-pyridyl)-1-pyrazolyl]acetic amide[424,425] (pypz-Si, **L5**) ligands were prepared according to literature procedures. Electrochemical experiments were performed under N_2 atmosphere with degassed solvents. All spectroscopic, electrochemical and synthetic experiments were performed in the absence of light unless explicitly mentioned.

trans and ***cis*-$[Ru^{II}Cl(trpy\text{-}P\text{-}Et)(pypz\text{-}Me)](PF_6)$, *trans-*** and ***cis*-C3.** A sample of **C1** (0.15 g, 0.26 mmol) was added to a 100 mL round bottomed flask containing a solution of LiCl (0.022 g, 0.52 mmol) dissolved in 40 mL of $EtOH/H_2O$ (3:1) under magnetic stirring. Then, NEt_3 (0.06 mL, 0.52 mmol) was added and the reaction mixture was stirred at room temperature for 30 min. Afterwards, pypz-Me, **L4**, (0.041 g, 0.26 mmol) was added and the mixture was heated at reflux for 3h. The hot solution was then filtered off in a frit and the volume was reduced in a rotary evaporator. After addition of a saturated aqueous solution of NH_4PF_6 a precipitate formed which was filtered off and washed with water. The solid obtained in this manner was a mixture approximately 1:1

of complexes *trans*-**C3** and *cis*-**C3**. Yield: 111 mg (61%). Anal. Found (Calc.) for **$C3 \cdot H_2O$**: C, 40.5 (40.6); H, 3.32 (3.77); N, 9.81 (10.1). IR (ν_{max}, cm^{-1}): 3050 (ν (=C-H)), 1598 (ν (C=C)), 1439 (ν (C=N)), 1243 (ν (P=O)), 1015 (ν (P-O-C)), 840-752 (ν (P-C)). $E_{1/2}$ (CH_2Cl_2 + 0.1M TBAH) = 0.93 V vs. SCE. UV-Vis (CH_2Cl_2) [λ_{max}, nm (ε, M^{-1} cm^{-1})]: 282 (28207), 324 (23103), 394 (7658), 512 (8615).

For *trans*-**C3**, ^{1}H-NMR (acetone-d_6, 400 MHz): δ 1.42 (t, 3H, H17, J_{17-16} = 7 Hz), 1.44 (t, 3H, H19, J_{19-18} = 7 Hz), 3.02 (s, 3H, H28), 4.34 (m, 4H, H16, H18), 7.24 (d, 1H, H26, J_{26-27} = 2.8 Hz), 7.51 (ddd, 2H, H2, H14, J_{2-1} = J_{14-15} = 5.6 Hz; J_{2-3} = J_{14-13} = 7.5 Hz; J_{2-4} = J_{14-12} = 1.1 Hz), 7.58 (d, 1H, H27, J_{27-26} = 2.8 Hz), 7.85 (d, 2H, H1, H15, J_{1-2} = J_{15-14} = 5.6 Hz), 7.91 (ddd, 1H, H21, J_{21-20} = 5.6 Hz; J_{21-22} = 7.2 Hz; J_{21-23} = 1.3Hz), 8.06 (ddd, 2H, H3, H13, J_{3-2} = J_{13-14} = 7.7 Hz; J_{3-4} = J_{13-12} = 5.2 Hz; J_{3-1} = 1.4 Hz), 8.35 (dt, 1H, H22, J_{22-21} = J_{22-23} = 7.2 Hz; J_{22-20} = 1.5 Hz), 8.53 (d, 1H, H23, J_{23-22} = 7.2 Hz), 8.84 (d, 1H, H4, J_{4-3} = 5.2 Hz), 8.86 (d, 1H, H12, J_{12-13} = 5.2 Hz), 8.87 (s, 1H, H7), 8.90 (s, 1H, H9), 10.16 (d, 1H, H20, J_{20-21}= 5.6 Hz). ^{13}C-NMR (acetone-d_6): δ 16.8 (C17, C19), 38.3 (C28), 63.9 (C16, C18), 105.6 (C26), 123.1 (C23), 124.5 (C4, C7), 124.6 (C9), 125.1 (C12), 125.6 (C21), 128.8 (C2, C14), 137.2 (C27), 137.9 (C3, C13), 138.3 (C8, C22), 153.4 (C1, C15), 153.8 (C24, C25), 153.9 (C20), 159.7 (C5), 160.6 (C11), 160.8 (C6), 161.6 (C10).

For *cis*-**C3**, ^{1}H-NMR (acetone-d_6, 400 MHz): δ 1.42 (t, 3H, H17, J_{17-16} = 7.1 Hz), 1.44 (t, 3H, H19, J_{19-18} = 7.1 Hz), 4.34 (m, 4H, H16, H18), 4.73 (s, 3H, H28), 6.91 (ddd, 1H, H22, J_{22-21} = 7.8 Hz; J_{22-23} = 5.8 Hz; J_{22-20} = 1.3 Hz), 7.37 (d, 1H, H23, J_{23-22} = 5.8 Hz), 7.53 (ddd, 2H, H2, H14, J_{2-1} = J_{14-15} = 6.1 Hz; J_{2-3} = J_{14-13} = 8 Hz; J_{2-4} = J_{14-12} = 1.1 Hz), 7.61 (d, 1H, H26, J_{26-27} = 2.8 Hz), 7.72 (dt, 1H, H21, J_{21-20} = J_{21-22} = 7.8 Hz; J_{21-23} = 1.3Hz), 8.03 (ddd, 2H, H3, H13, J_{3-2} = J_{13-14} = 8 Hz; J_{3-4} = J_{13-12} = 5.2 Hz; J_{3-1} = 1.4 Hz), 8.10 (d, 2H, H1, H15, J_{1-2} = J_{15-14} = 6.1 Hz), 8.17 (d, 1H, H20, J_{20-21}= 7.8 Hz)' 8.47 (d, 1H, H27) J_{27-26} = 2.8 Hz, 8.81 (s, 1H, H7), 8.82 (d, 1H, H4, J_{4-3} = 5.2 Hz), 8.83 (d, 1H, H12, J_{12-13} = 5.2 Hz), 8.85 (s, 1H, H9). ^{13}C-NMR (acetone-d_6): δ 16.8 (C17, C19), 42.0 (C28), 63.9 (C16, C18), 106.2 (C26), 122.6 (C20), 124.4 (C7), 124.5 (C4), 125.0 (C12, C22), 125.1 (C9), 128.8 (C2, C14), 137.0 (C21), 138.0 (C3, C13), 138.1 (C8, C27), 151.2 (C24), 152.7 (C23, C25), 154.3 (C1, C15), 159.5 (C5), 159.5 (C11), 161.4 (C6), 161.5 (C10).

For the NMR assignments we use the same labeling scheme as for the X-ray structures (Figure **4.1**).

trans and ***cis*-[Ru^{II}(trpy-P-Et)(pypz-Me)OH$_2$](PF$_6$)$_2$, *trans*-** and ***cis*-C4.** A 0.03 g (0.036 mmol) sample of *trans* and *cis*-**C3** was dissolved in 40 ml of water, the resulting solution was heated at reflux for 18h. After reduction of the volume in a rotary evaporator a saturated aqueous solution of NH_4PF_6 was added. The precipitate formed was filtered off and washed several times with cold water. The solid obtained in this manner was a mixture of complexes *trans*-**C4** and *cis*-**C4**. Yield: 16 mg (42%). Anal. Found (Calc.) for **C4·1.5($(C_2H_5)_2O$)**: C, 39.1 (38.9); H, 4.1 (4.4); N, 8.0 (8.0). IR (ν_{max}, cm^{-1}): 3081 (ν (=C-H)), 2918 (ν (O-H)), 1602 (ν (C=C)), 1441 (ν (C=N)), 1227 (ν (P=O)), 1015 (ν (P-O-C)), 840-753 (ν (P-C)). UV-Vis (CH_2Cl_2) [λ_{max},nm (ε, M^{-1} cm^{-1})]: 278 (45478), 320 (36314), 382 (7540), 480 (10418).

For *trans*-**C4**, ^{1}H-NMR (acetone-d$_6$, 400 MHz): δ 1.45 (m, 6H, H17, H19), 3.08 (s, 3H, H28), 4.39 (m, 4H, H16, H18), 7.28 (d, 1H, H26), 7.65 (m, 3H, H2, H14, H27), 8.03 (ddd, 1H, H21), 8.07 (d, 2H, H1, H15), 8.19 (m, 2H, H3, H13), 8.46 (dt, 1H, H22), 8.64 (d, 1H, H23), 8.96 (m, H4), 8.99 (dd, 1H, H12), 9.03 (s, 1H, H7), 9.06 (s, 1H, H9), 9.68 (d, 1H, H20). $E_{1/2}$ (IV/II), phosphate buffer pH = 7.12: 0.42 V vs. SCE.

For *cis*-**C4**, ^{1}H-NMR (acetone-d$_6$, 400 MHz): δ 1.45 (m, 6H, H17, H19), 4.39 (m, 4H, H16, H18), 4.64 (s, 3H, H28), 6.94 (ddd, 1H, H22), 7.40 (d, 1H, H23), 7.65 (m, 3H, H2, H14, H26), 7.76 (dt, 1H, H21), 8.19 (m, 4H, H1, H3, H13, H15), 8.29 (ddd, 1H, H20), 8.56 (d, 1H, H27), 8.95 (dd, 1H, H4), 8.96 (m, H12), 8.97 (s, 1H, H7), 9.00 (s, 1H, H9). $E_{1/2}$ (IV/II), phosphate buffer pH = 7.12: 0.52 V vs. SCE.

For the NMR assignments we use the same labeling scheme as for the X-ray structures of complex **C3** (Figure **4.1**).

Preparation of the heterogeneous systems SP1-C4, SP2-C4 and MSP-C4.

In order to obtain **C4** anchored onto different types of particles, we have followed two synthetic strategies.

Strategy I

I.1) *Preparation of ligand-functionalized silica.*

For ligand **L1**: a sample of **SP2** (0.1 g) was added to a solution of trpy-P-Et, **L1**, (0.05 g, 0.14 mmol) in toluene (10 ml) and the suspension was refluxed overnight. The resulting **SP2-**(trpy-P) modified silica was centrifuged, washed with acetone (2 x 10 ml) and dried in a hot air oven at 110°.

For ligand **L2**: A sample of **SP1** or **MSP** (0.1 g) was added to a solution of trpy-P-H, **L2**, (0.05 g, 0.16 mmol) in water (10 ml). The suspension was stirred overnight. The resulting **SP1-**(trpy-P) or **MSP-**(trpy-P) modified silica was centrifuged, washed with water (2 x 10 ml) and dried in a hot air oven at 110°.

I.2) *Coordination of ruthenium to the ligand-functionalized silica.*

A 0.1 g sample of organically modified silica (**SP1-**(trpy-P), **SP2-**(trpy-P) or **MSP-**(trpy-P) was added to a solution of $RuCl_3·3H_2O$ (0.042 g, 0.16 mmol) in methanol. The mixture was stirred overnight. The resulting solid (**SP2-**(trpy-P)$RuCl_3$, **SP1-**(trpy-P)$RuCl_3$ or **MSP-**(trpy-P)$RuCl_3$) was centrifuged, washed with methanol (2 x 10 ml) and dried in a hot air oven at 110°C.

I.3) *Preparation of **C4**-functionalized silica.*

A 0.1 g sample of ruthenium-functionalized silica (**SP1-**(trpy-P)$RuCl_3$, **SP2-**(trpy-P)$RuCl_3$ or **MSP-**(trpy-P)$RuCl_3$) was placed in a round-bottomed flask together with 6 ml of methanol. Then, LiCl (0.014 g, 0.32 mmol) and triethylamine (44.6 μl, 0.32 mmol) were added under nitrogen atmosphere and the mixture was stirred at room temperature for 30 min. After this time, pypz-Me (**L4**) ligand (0.026 g, 0.16 mmol) dissolved in 4 ml of methanol was added and the mixture was heated at reflux for 2 h. The resulting modified silica (**SP1-**[Ru(trpy-P)(pypz-Me)(H_2O)], **SP1-C4**, **SP2-**[Ru(trpy-P)(pypz-Me)(H_2O)], **SP2-C4**, or **MSP-**[Ru(trpy-P)(pypz-Me)(H_2O)], **MSP-C4**) was centrifuged, washed with methanol (2 x 10 ml) and dried in a hot air oven at 110°C. For **SP1-C4**: Ru

ICP-AES analysis [% (mmol·g^{-1})]: 0.023% (2.27·10^{-3} mmol·g^{-1}). For **SP2-C4**: Ru ICP-AES analysis [% (mmol·g^{-1})]: 1.05% (0.1 mmol·g^{-1}). $E_{1/2}$ (III/II), phosphate buffer pH = 6.4: 0.56 V vs SCE. UV-Vis (CH_2Cl_2) [λ_{max}, nm]: 276, 316, 378, 484. For **MSP-C4**: Ru ICP-AES analysis [% (mmol·g^{-1})]: 0.73% (0.08 mmol g^{-1}). $E_{1/2}$ (III/II), phosphate buffer pH = 6.4: 0.64 V vs SCE.

Strategy II

SP2 (0.1 g) was added to a solution of **C3** (0.05 g, 0.06 mmol) in 9 ml of toluene. The mixture was stirred and heated at reflux for 4 h. Afterwards, 1 ml of acetone was added and the solution was refluxed for 20h. The resulting product was centrifuged, washed with acetone (2 x 10 ml) and dried in a hot air oven at 110°C. $E_{1/2}$(III/II), phosphate buffer pH = 7.1: 0.55 V vs. SCE. UV-Vis (CH_2Cl_2) [λmax, nm]: 280, 328, 386, 490.

***cis*, *cis*-[Ru^{II}Cl$_2$(pypz-H)(dmso)$_2$], C5**. A 0.045 g (0.31 mmol) sample of pypz-H and 0.15 g (0.31 mmol) of **C2** were dissolved in 20 ml of ethanol and the resulting solution was refluxed for 2h. A light orange solid was formed and was filtered on a frit, washed with ether and vacuum-dried. Yield: 58 mg (40%). Anal. Found (Calc.) for **C5**: C, 30.6 (30.45); H, 3.98 (4.04); N, 8.62 (8.87); S, 13.54 (13.54). ^{1}H-NMR (CD_2Cl_2, 400 MHz): δ 2.00 (s, 3H, H12), 3.02 (s, 3H, H11), 3.52 (s, 3H, H9), 3.54 (s, 3H, H10), 6.99 (d, 1H, H7, $J_{7,8}$=2.8Hz), 7.54 (ddd, 1H, H2, $J_{2,1}$=6.8Hz; $J_{2,3}$=7.4Hz; $J_{2,4}$=1.5Hz), 7.79 (d, 1H, H8, $J_{8,7}$=2.8Hz), 7.95 (ddd, 1H, H4, $J_{4,3}$=7.4Hz; $J_{4,2}$=1.5Hz; $J_{4,1}$=0.9Hz), 8.02 (t, 1H, H3, $J_{3,2}$=$J_{3,4}$=7.4Hz; $J_{3,1}$=1.5Hz), 9.43 (ddd, 1H, H1, $J_{1,2}$=6.8Hz; $J_{1,3}$=1.5Hz; $J_{1,4}$=0.9Hz), 13.10 (s, 1H, H2B).^{13}C-NMR ($CDCl_3$): δ 44.2, 45.1 (C11, C12), 45.6, 46.1 (C9, C10), 105.5 (C7), 122.1 (C4), 125.2 (C2), 132.1 (C8), 139.1 (C3), 151.3 (C6), 152.5 (C1, C5). For the NMR assignments we use the same labeling scheme as for the X-ray structure (Figure **6.1a**). IR (ν_{max}, cm^{-1}): 3107 (ν (N-H)), 3052 (ν (=C-H)), 3025 (ν (-C-H)), 1609 (ν (C=C)), 1438 (ν (C=N)), 1093-967 (ν (S=O)), 781-681 (ν (=C-H)). $E_{1/2}$ (CH_3CN + 0.1M TBAH): 0.98 V *vs*. SCE; (CH_2Cl_2): 1.09 V *vs*. Ag/AgCl. UV-Vis (CH_3CN) [λ_{max}, nm (ε, M^{-1} cm^{-1})]: 330 (2030), 400 (1058); (CH_2Cl_2): 264 (27904), 320 (4150), 408 (1914). ESI-MS (m/z): 438 [M-Cl]$^+$.

***mer*-[Ru^{III}Cl$_3$(pypz-H)(dmso)], C5''**. A solution of **C5** in CHCl$_3$ was irradiated overnight with a 200W Tungsten lamp. The volume of the solution was reduced and a precipitated was formed after addition of Et$_2$O in quantitative yield. Anal. Found (Calc.) for **C5''**: C, 28.0 (27.8); H, 3.4 (3.0); N, 9.5 (9.7). E$_{1/2}$(CH$_2$Cl$_2$+0.1M TBAH): 0.05 V vs. Ag/AgCl. UV-Vis (CH$_2$Cl$_2$) [λmax, nm]: 276 (15112), 318 (5336), 360 (4464), 406 (9782).

[Ru^{II}Cl$_2$(pypz-Me)(dmso)$_2$], C6. A 0.049 g (0.31 mmol) sample of pypz-Me and 0.15 g (0.31 mmol) of **C2** were dissolved in 20 ml of ethanol and the resulting solution was refluxed for 2h. The volume was reduced in a rotary evaporator, and an orange-yellow solid, corresponding to a mixture of isomers was precipitated by addition of diethyl. Yield: 59 mg (39%). A single isomer, *cis*-Cl *trans*-dmso, was obtained after evaporation of the mother liquor as a yellow solid that was washed with pentane. Anal. Found (Calc.) for *cis*-Cl *trans*-dmso-**C6·2(dmso)**: C, 31.7 (31.5); H, 5.2 (5.2); N, 6.5 (6.1). ^{1}H-NMR (CD$_2$Cl$_2$, 400 MHz) δ 2.93 (s, 6H, H10, H12), 3.10 (s, 6H, H11, H13), 4.28 (s, 3H, H9), 6.89 (d, 1H, H7, $J_{7,8}$=3.1Hz), 7.34 (ddd, 1H, H2, $J_{2,1}$=5.77Hz; $J_{2,3}$=7.5Hz; $J_{2,4}$=1.5Hz), 7.57 (d, 1H, H8, $J_{8,7}$=3.1Hz), 7.77 (ddd, 1H, H4, $J_{4,3}$=8Hz; $J_{4,2}$=1.5Hz; $J_{4,1}$=0.75Hz), 7.86 (t, 1H, H3, $J_{3,2}$=7.5Hz; $J_{3,4}$=8Hz; $J_{3,1}$=1.5Hz), 9.50 (ddd, 1H, H1, $J_{1,2}$=5.77Hz; $J_{1,3}$=1.5Hz; $J_{1,4}$=0.75Hz).^{13}C-NMR (CD$_2$Cl$_2$): δ 41.6 (C9), 41.8 (C10, C12), 43.1 (C11, C13), 105.1 (C7), 121.3 (C4), 124.1 (C2), 135.9 (C8), 137.1 (C3), 153.6 (C6), 154.6 (C1), 156.4 (C5). For the NMR assignments we use the same labeling scheme as for the X-ray structure (Figure **6.1b**). IR (ν_{max}, cm^{-1}): 3098 (ν (N-H)), 3002 (ν (-C-H)), 1611 (ν (C=C)), 1447 (ν (C=N)), 1080-1000 (ν (S=O)), 790-676 (ν (=C-H)). $E_{1/2}$ (CH$_2$Cl$_2$ + 0.1M TBAH) = 0.92 V vs. SCE. UV-Vis (CH$_2$Cl$_2$) [λ_{max}, nm (ε, M^{-1} cm^{-1})]: 270 (21913), 366 (5669). ESI-MS (m/z): 373.9 [M-dmso-Cl]$^+$.

***cis, fac*-[Ru^{II}Cl$_2$(pz-H)(dmso)$_3$], C7.** This complex was prepared through a modification of the method previously described in the literature.[426]

A 0.017 g (0.25 mmol) sample of pz-H (**L6**) and 0.12 g (0.25 mmol) of **C2** were dissolved in 10 ml of methanol and the resulting solution was refluxed for 2h. A pale yellow solid was formed and was filtered on a frit, washed with methanol and vacuum-dried. Yield: 78 mg (65%). Anal. Found (Calc.) for **C7**: C, 23.1 (23.0); H, 3.9 (3.9); N, 5.9 (6.0). ^{1}H-NMR (CD$_2$Cl$_2$, 400 MHz): δ 3.12 (s, 6H, H4, H8), 3.41 (s, 6H, H5, H9), 3.46 (s, 6H, H6, H7), 6.42

(dd, 1H, H2, $J_{2,3}$=3.02Hz; $J_{2,1}$=3.78Hz), 7.72 (dd, 1H, H1, $J_{1,2}$=3.78Hz; $J_{1,3}$=0.9Hz;), 8.48 (dd, 1H, H3, $J_{3,2}$=3.02Hz; $J_{3,1}$=0.9Hz), 14.01 (s, 1H, H2D).^{13}C-NMR (CD_2Cl_2, 400 MHz): δ 46.0 (C6, C7), 47.2 (C4, C5), 47.7 (C8, C9), 107.4 (C2), 131.2 (C1), 142.3 (C3). For the NMR assignments we use the same labeling scheme as for the X-ray structure (Figure **6.2a**). IR (ν_{max}, cm^{-1}): 3102 (ν (N-H)), 3004 (ν (=C-H)), 2916 (ν (-C-H)), 1531 (ν (C=C)), 1407 (ν (C=N)), 1091-934 (ν (S=O)), 771-674 (ν (=C-H)). $E_{1/2}$ (CH_3CN + 0.1M TBAH): 1.60 V vs. Ag/AgCl. UV-Vis (CH_3CN) [λ_{max}, nm (ε, M^{-1} cm^{-1})]: 354 (450); (CH_2Cl_2): 356 (463).

***cis, fac*-[Ru^{II}Cl$_2$(CH$_3$-pz-H)(dmso)$_3$], C8.** A 0.034 g (0.41 mmol) sample of fomepizole (**L7**) ligand and **C2** (0.2 g, 0.41 mmol) were dissolved in 10 ml of CH_2Cl_2 and the resulting solution was refluxed for 1 h at 60°C. After this time, the mixture was allowed to cool to room temperature and the volume was reduced; a yellow-orange precipitate was formed and was collected on a frit, washed with ether and vacuum-dried. Yield: 144.9 mg (71.84%). Anal. Found (Calc.) for **C8**: C, 24.61 (24.6); H, 4.94 (4.9); N, 5.69 (5.7). ^{1}H-NMR (CD_2Cl_2, 400MHz): δ 2.09 (s, 3H, H4), 3.12 (s, 6H, H6, H9), 3.40 (s, 6H, H5, H10), 3.45 (s, 6H, H7, H8), 7.48 (s, 1H, H1), 8.25 (s, 1H, H3), 13.71 (s, 1H, H2). ^{13}C-NMR (CD_2Cl_2, 400 MHz): 9.8 (C4), 46.8 (C7, C8), 47.2 (C6, C9), 47.7 (C5, C10), 118.0 (C2), 130.1 (C1), 142.1 (C3). For the NMR assignments we use the same labeling scheme as for the X-ray structure (Figure **6.2b**). IR (ν_{max}, cm^{-1}): 3133 (ν (N-H)), 3016 (ν (=C-H)), 2925 (ν (-C-H)), 1570 (ν (C=C)), 1497 (ν (C=N)), 1410-1301 (ν (C-N)), 1091-925 (ν (S=O)), 797-612 (ν (=C-H)). E_{pa} (CH_3CN + 0.1M TBAH): 1.49 V vs Ag/AgCl. UV-Vis (CH_2Cl_2) [λmax, nm (ε, M^{-1}·cm^{-1})]: 359 (574).

***cis, fac*-[Ru^{II}Cl$_2$(NO$_2$-pz-H)(dmso)$_3$], C9.**This compound was prepared following a method analogous to that described for **C8** starting from compound **C2** (0.2 g, 0.41 mmol) and 4-nitro-1H-pyrazole (**L8**) ligand (0.046 g, 0.41 mmol). Yield: 122mg (56.89%). Anal. Found (Calc.) for **C9**: C, 20.7 (20.8); H, 3.9 (4.04); N, 7.9 (8.1). ^{1}H-NMR (CD_2Cl_2, 400MHz): δ 3.20 (s, 6H, H5, H9), 3.45 (s, 6H, H4, H8), 3.47 (s, 6H, H6, H7), 8.38 (s, 1H, H1), 9.14 (s, 1H, H3), 15.1 (s, 1H, H2). ^{13}C (CD_2Cl_2, 400MHz): δ 46.2 (C6, C7), 47.2 (C4, C8), 47.6 (C6, C7), 19.8 (C1), 139.3 (C3). For the NMR assignments we use the same labeling scheme as for the X-ray structure (Figure **6.2c**). IR (ν_{max}, cm^{-1}): 3150 (ν

(N-H)), , 1515 (ν (C=C)), 1405-1335 (ν (C-N)), 1109-919 (ν (S=O)), 881 (ν (NO_2)), 819-673 (ν (=C-H)). E_{pa} (CH_3CN + 0.1M TBAH): 1.60 V vs Ag/AgCl. UV-Vis (CH_2Cl_2) [λmax, nm (ε, $M^{-1}\cdot cm^{-1}$)]: 310 (329).

***cis, fac*-[Ru^{II}Cl$_2$(CF$_3$-pz-H)(dmso)$_3$], C10.** This compound was prepared following a method analogous to that described for **C8** starting from compound **C2** (0.1 g, 0.21 mmol) and 3-trifluoromethyl-pyrazole (**L9**) (0.028 g, 0.21 mmol). Yield: 34.66 mg (30.95%). Anal. Found (Calc.) for **C10**: C, 21.1 (22.1); H, 3.3 (3.8); N, 4.5 (5.1). ^{1}H-NMR (CD_2Cl_2, 400MHz): δ 3.15 (s, 6H, H6, H10), 3.43 (s, 6H, H5, H9), 3.47 (s, 6H, H7, H8), 6.74 (s, 1H, H2A), 8.59 (s, 1H, H3), 15.33 (s, 1H, H2). ^{13}C (CD_2Cl_2, 400MHz): δ 46.0 (C9, C10), 47.1 (C7, C8), 47.6 (C5, C6), 107.4 (C2), 134.7 (C1), 135.1 (C4), 143.7 (C3). For the NMR assignments we use the same labeling scheme as for the X-ray structure (Figure **6.2d**). IR (ν_{max}, cm^{-1}): 3115 (ν (N-H)), 3010 (ν (=C-H)), 2925 (ν (-C-H)), 1458-1350 (ν (C-N)), 1267 (ν (C-F)), 1100-919 (ν (-C-H)), 742-718 (ν (CF_3)). E_{pa} (CH_3CN +0.1M TBAH): 1.73 V vs Ag/AgCl. UV-Vis (CH_2Cl_2) [λmax, nm (ε, $M^{-1}\cdot cm^{-1}$)]: 356 (560).

***cis, fac*-[Ru^{II}Cl$_2$(Br-Hind)(dmso)$_3$], C11.** This compound was prepared following a method analogous to that described for **C8** starting from compound **C2** (0.2 g, 0.41 mmol) and 6-bromo-1H-indazole (**L10**) (0.08 g, 0.41 mmol) except that the reflux was maintained for 20 min. Yield: 154.1mg (61.89%). Anal. Found (Calc.) for **C11**: C, 23.9 (25.1); H, 3.4 (3.8); N, 4.3 (4.04). ^{1}H-NMR (CD_2Cl_2, 400MHz): δ 3.17 (s, 6H, H9, H12), 3.45 (s, 6H, H8, H13), 3.49 (s, 6H, H10, H11), 7.32 (d, 1H, H4, $J_{4,5}$=8.6Hz), 7.62 (s, 1H, H5, $J_{5,4}$=8.6Hz), 7.76 (s, 1H, H2A), 9.10 (s, 1H, H7), 14.18 (s, 1H, H2B). ^{13}C (CD_2Cl_2, 400MHz): δ 46.1 (C10, C11), 47.3 (C12, C13), 47.8 (C8, C9), 113.8 (C2), 122.1 (C6), 122.8 (C3), 123.3 (C5), 126.2 (C4), 139.0 (C7), 141.4 (C1). For the NMR assignments we use the same labeling scheme as for the X-ray structure (Figure **6.2e**). IR (ν_{max}, cm^{-1}): 3528 (ν (N-H)), 3020 (ν (=C-H)), 2916 (ν (-C-H)), 1625 (ν (C=C)), 1413-1348 (ν (C-N)), 1097 (ν (C-H)), 1057 (ν (C-Br)), 1006-951 (ν (C-H)), 590 (ν (C-Br)). E_{pa} (CH_3CN + 0.1M TBAH): 1.66 V vs Ag/AgCl. UV-Vis (CH_2Cl_2) [λmax, nm (ε, $M^{-1}\cdot cm^{-1}$)]: 280 (10931), 343 (532).

[Ru^{II}Cl$_2$(pypz-Si)(dmso)$_2$], C12. A 0.2 g (0.41 mmol) sample of **L5** and 0.2 g (0.41 mmol) of **C2** were dissolved in 20 ml of ethanol and the resulting solution refluxed for 2h. The mixture was cooled and the volume was reduced in a rotary evaporator to dryness. Afterwards, the orange solid was washed with chloroform and pentane and was dried under vacuum. Yield: 31 mg (11%). Anal. Found (Calc.) for **C12·2H$_2$O**: C, 29.95 (29.74); H, 4.95 (4.8); N, 6.8 (5.55). $E_{1/2}$ (CH_2Cl_2 + 0.1M TBAH) = 1.21 V vs. SCE. UV-Vis (MeOH) [λ_{max}, nm (ε, M^{-1} cm^{-1})]: 282 (23184), 374 (4340). ESI-MS (m/z): 701.4 $[M-Cl]^+$.

Preparation of C12 anchored onto silica particles, SP2-C12.

In order to obtain **C12** anchored onto silica particles, we have followed two synthetic strategies.

Strategy I

I.1) *Preparation of (pypz-Si)-functionalized silica.*

SP2 (0.2 g) was added to a solution of pypz-Si, **L5**, (0.2 g, 0.5 mmol) in toluene (15 ml) and the mixture was refluxed overnight. The resulting **SP2-L5** modified silica was centrifuged, washed with acetone (2 x 10 ml) and dried in a hot air oven at 110°.

I.2) *Preparation of **C12**-functionalized silica.*

A mixture of **SP2-L5** (0.13 g) and [RuCl$_2$(dmso)$_4$], **C2** (0.1 g, 0.21 mmol) in ethanol (20 ml) were stirred under nitrogen atmosphere at room temperature for 2 h. After this time, the resulting **SP2-C12** modified silica was centrifuged, washed with methanol (2 x 10 ml) and dried in a hot air oven at 110°C. Ru ICP-AES analysis [% (mmol·g^{-1})]: 3.5% (0.35 mmol·g^{-1}).

Strategy II

SP2 (0.02 g) was added to a solution of **C12** (0.02 mg, 0.05 mmol) in 10 ml of toluene. The mixture was stirred and heated at reflux for 24 h. The resulting **SP2-C12** modified silica was centrifuged, washed with methanol (2 x 10 ml) and dried in a hot air oven at 110^o. Ru ICP-AES analysis [% (mmol·g^{-1})]: 4.5% (0.44 mmol·g^{-1}). $E_{1/2}$ (CH_2Cl_2 + 0.1M TBAH): 0.68 V vs. SCE. UV-Vis (MeOH) [λ_{max}, nm]: 270, 378.

3.3. X-Ray structure determination

The measurements were carried out on a *BRUKER SMART APEX CCD* diffractometer using graphite-monochromated Mo $K\alpha$ radiation (λ = 0.71073 Å) from an x-Ray Tube. Programs used: data collection, Smart;[427] data reduction, Saint+;[428] absorption correction, SADABS.[429,430] Structure solution and refinement was done using SHELXTL.[431,432] The structure was solved by direct methods and refined by full-matrix least-squares methods on F^2. In all complexes the non-hydrogen atoms were refined anisotropically. For complexes **C3**, **C6**, **C8**, **C10** and **C11**, all the H-atoms were placed in geometrically optimized positions and forced to ride on the atom to which they are attached, whereas for complexes **C5**, **C8**, **C10** and **C11** some particular treatments were applied as described next. For complex **C5**, N-H and O-H hydrogen atoms were located in the difference Fourier Map. The N-H hydrogen was refined freely while the O-H bond distance was constrained to 0.85(1) Å. For complex **C8**, the N-H hydrogen was located in the difference Fourier map and refined freely. For complex **C10**, the N-H and OH_2 hydrogens were located from the difference Fourier map. The N-H hydrogen was refined freely. The O-H hydrogens were refined as riding contributions with isotropic displacement parameters 1.5 times those of the attached atom. For complex **C11**, the hydrogen atoms associated with the solvent waters could not be located and so are omitted from the final refinement and structure factor calculations. They are, however, included in the reported chemical formula and derived values (e.g. formula weight, F(000), etc).

Complex **C3** is a co-crystal consistent of an equimolar mixture of two isomeric molecules. However, the quality of the data only allows its refinement as a single molecule with disordered positions at the area of atoms C20-C28.

The refinement parameters for all the crystal structures solved are gathered in Table **3.1**.

Table 3.1. Parameters for all crystal structures.

Complex	Color	Solvent of crystallization	T (K)	θ range	Data collection	Number of reflections	Unique reflections [R(int)]
C3	black	diethyl ether/CH_2Cl_2	100(2)	1.432-27.491°	hemi-sphere, ω and ϕ scans	9874	7286 [0.0458]
C5	n.d.	CH_2Cl_2	300(2)	1.96-28.30°	full-sphere, ω and ϕ scans	28194	4562 [0.0207]
C6	orange	diethyl ether/CH_2Cl_2	293(2)	2.643-28.404°	full-sphere, ω and ϕ scans	53905	4898 [0.0704]
C7	n.d.	methanol	300(2)	2.55-28.79°	full-sphere, ω and ϕ scans	8492	3561 [0.0229]
C8	yellow	CH_2Cl_2	298(2)	2.35-28.25°	full-sphere, ω and ϕ scans	30077	4791 [0.0319]
C9	yellow	CH_2Cl_2	298(2)	1.96-28.80°	full-sphere, ω and ϕ scans	26979	4651 [0.0430]
C10	yellow	CH_2Cl_2	298(2)	1.75-28.34°	full-sphere, ω and ϕ scans	20988	5340 [0.0314]
C11	yellow	CH_2Cl_2	298(2)	2.14-28.33°	full-sphere, ω and ϕ scans	33944	5402 [0.0382]

Crystallographic data in CIF format can be found in the electronic supporting information.

3.4. Catalytic Studies

3.4.1. Epoxidation of alkenes

3.4.1.1. Homogeneous phase

The ruthenium catalyst (1.25 μmol), alkene (125 μmol) and $PhI(OAc)_2$ (250 μmol) were stirred at room temperature in CH_2Cl_2 (2.5 ml) for 24 h. After addition of an internal standard, the sample was filtered through a basic alumina plug and quantified by gas chromatographic (GC) analysis based on calibration curves for each substrate and epoxide.

3.4.1.2. Heterogeneous phase

Alkene (125 μmol) and $PhI(OAc)_2$ (250 μmol) were dissolved in 2.5 ml of CH_2Cl_2 together with 1.25 μmol of SP or MSP-supported ruthenium catalyst. The amount of heterogenized catalyst was calculated taking into account the functionalization of SPs and MSPs (mmol $Ru \cdot g^{-1}$) in each case. For experiments using SP2-based system, the resulting solution was centrifuged while for MSP-based system a magnet was used for the separation of the catalytic material from the reaction medium. The catalytic heterogeneous systems were washed with CH_2Cl_2 and were used in a subsequent catalytic run.

For leaching calculations, the resulting solution after several reuses was centrifuged and filtered through celite in order to avoid particles in the ICP analysis.

3.4.2. Hydration of nitriles

3.4.2.1. Homogeneous phase

The ruthenium catalyst (0.01 mmol), water (3 ml) and the corresponding nitrile (1 mmol) were introduced into a sealed tube and the reaction mixture was stirred at 80-90°C for 20 h. The nitrile was extracted with chloroform and quantified by GC, whereas the identity of the resulting amides was assessed by ^1H-NMR.

The catalytic reactions with glycerol as solvent were carried out under the same experimental conditions as described in water except for the extraction step, where CH_2Cl_2 instead of chloroform was used.

For the recycling procedure, a new load of the corresponding nitrile was added to the solution after the extraction with chloroform or CH_2Cl_2.

3.4.2.2. Heterogeneous phase

Nitrile substrate (1 mmol) was placed in a sealed tube together with 3 ml of water and 1 mmol of **SP2**-supported ruthenium catalyst. The amount of heterogenized catalyst was calculated taking into account the functionalization of **SP2** (mmol $Ru \cdot g^{-1}$). For the recycling experiments, after 20 h of reaction, acetone was added to the solution mixture to fully solubilize nitrile and amide products. The resulting solution was centrifuged for the separation of the catalytic material from the reaction medium. The catalytic heterogeneous system was washed with acetone and was used in a subsequent catalytic run.

3.5. Instrumentation and measurements

FT-IR spectra were taken in a Mattson-Galaxy Satellite FT-IR spectrophotometer containing a MKII Golden Gate Single Reflection ATR System.

UV-Vis spectroscopy was performed on a Cary 50 Scan (Varian) UV-Vis spectrophotometer with 1 cm quartz cells.

Cyclic voltammetric (CV) and *differential pulse voltammetry* (DPV) experiments were performed in an IJ-Cambria IH-660 potentiostat using a three electrode cell. Glassy carbon electrode (3 mm diameter) from BAS was used as working electrode, platinum wire as auxiliary and SSCE as the reference electrode. All cyclic voltammograms presented in this work were recorded under nitrogen atmosphere unless explicitly mentioned. The complexes were dissolved in solvents containing the necessary amount of $n\text{-}Bu_4NH^+PF_6^-$ (TBAH) as supporting electrolyte to yield a 0.1 M ionic strength solution. All $E_{1/2}$ values reported in this work were estimated from cyclic voltammetric experiments as the average of the oxidative and reductive peak potentials ($(E_{p,a}+E_{p,c})/2$), or directly from the DPV peak. Unless explicitly mentioned the concentration of the complexes was approximately 1mM.

Elemental analyses were performed using a CHNS-O Elemental Analyser EA-1108 from Fisons.

ESI-MS experiments were performed on a Navigator LC/MS chromatograph from Thermo Quest Finnigan, using acetonitrile as a mobile phase.

Monochromatic irradiations were carried out by using a 80 W lamp source from Phillips on complex solutions, typically 1mM.

SEM images were recorded using a SEM QUANTA FEI 200FEG-ESEM.

For *metal content determination* a sequential inductively coupled plasma atomic emission spectrometer (ICP-AES, Liberty Series II, Varian, Australia) in radial configuration and a quadrupole-based inductively coupled plasma mass spectrometer system (ICP-MS, Agilent 7500c, Agilent Technologies, Tokyo, Japan) were used. This latest instrument is equipped with an octapole collision reaction cell. However, in this work, the collision reaction cell acts only as an ion focusing lens because it was not filled with any pressurized gas. Prior to measurements, samples were digested with $HCl:HNO_3$.

Thermogravimetric analysis (TGA) was performed under N_2 atmosphere with a 10^{o}C min^{-1} heating rate from 30^{o}C to 700^{o}C.

The *BET specific surface area* (S_a) was determined by N_2 adsorption-desorption measurements at 77 K using an ASAP 2000 (Micrometrics Instrument Corporation, USA) after degasification at 120^{o}C under vacuum for 24h.

NMR spectra were recorded on a 300 MHz and 400 MHz NMR spectrometer from Bruker. Chemical Shifts (δ) for ^{1}H and ^{13}C were referred to internal solvent resonances.

Catalytic experiments analyses were performed in a GC-2010 Gas Chromatograph from Shimadzu, equipped with an Astec CHIRALDEX G-TA Column (30 m x 0.25 mm diameter) incorporating a FID detector. All the product analyses in the catalytic experiments were performed based on calibration curves using biphenyl as internal standard.

RESULTS AND DISCUSSION

Chapter 4

Ru(II) complexes containing trpy-P-Et and pypz-Me ligands as catalysts for alkene epoxidation and nitrile hydration.

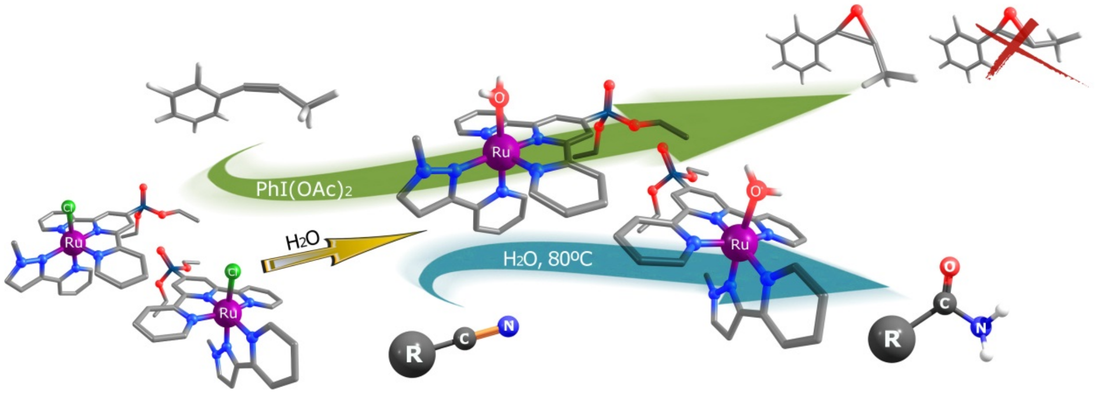

New ruthenium complexes with general formula $[Ru^{II}(trpy\text{-}P\text{-}Et)(pypz\text{-}Me)X]^{n+}$ (X = Cl, H_2O) have been synthesized. The complexes have been fully characterized through structural, analytical and spectroscopic techniques and the isomeric chlorido complexes have also been characterized in the solid state by monocrystal X-ray diffraction analysis. Redox properties of the Ru-OH_2 species together with its reactivity in alkene epoxidation and nitrile hydration have been studied.

4.1. Synthesis and crystal structures

The synthetic strategy followed for the preparation of Ru^{II} complexes **C3** and **C4** is outlined in Scheme **1.1**.

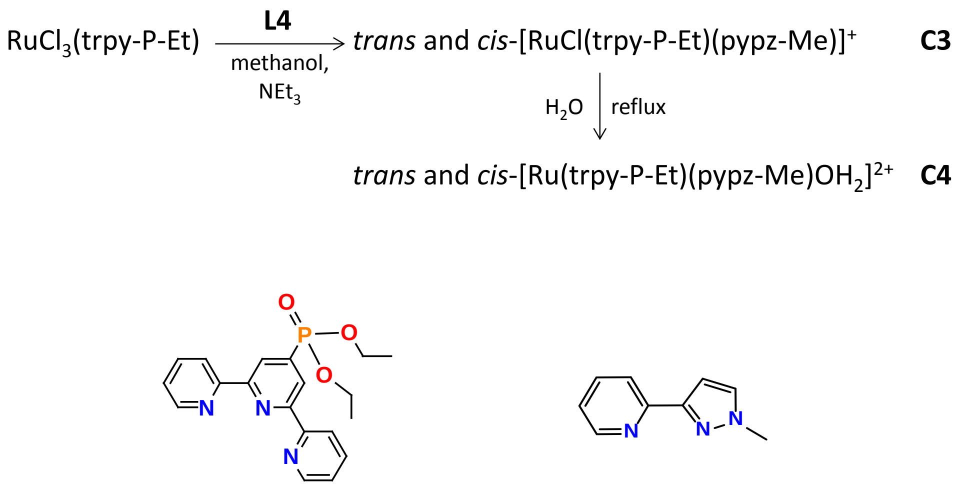

$$\text{RuCl}_3(\text{trpy-P-Et}) \xrightarrow[\text{methanol, NEt}_3]{\textbf{L4}} \textit{trans}\text{ and }\textit{cis}\text{-[RuCl(trpy-P-Et)(pypz-Me)]}^+ \quad \textbf{C3}$$

$$\downarrow \text{H}_2\text{O} \mid \text{reflux}$$

$$\textit{trans}\text{ and }\textit{cis}\text{-[Ru(trpy-P-Et)(pypz-Me)OH}_2]^{2+} \quad \textbf{C4}$$

trpy-P-Et, **L1**

pypz-Me, **L4**

Scheme 1.1. Synthetic strategy for the synthesis of complexes **C3** and **C4**, and ligands used.

In the complexes, the nomenclature *cis* or *trans* refers to the relative position of the monodentate ligand (Cl or H_2O) with regard to the pyrazole ring of the ligand pypz-Me.

Reaction of equimolar amounts of $RuCl_3{\cdot}3H_2O$ and the trpy-P-Et ligand, **L1**, in dry methanol at reflux for 3 h produces the trichlorido Ru complex $[Ru^{III}Cl_3(\text{trpy-P-Et})]$,[315] **C1**, which is used as starting material. After the reduction of Ru(III) to Ru(II) with NEt_3, the didentate ligand, pypz-Me, was added producing the substitution of two chlorido ligands at the starting complex. After addition of a saturated aqueous solution of NH_4PF_6 the precipitate formed, corresponding to complex **C3** (see Scheme **1.1**), was obtained as a 1:1 mixture of *trans* and *cis* isomers, due to the nonsymmetric nature of the pypz-Me ligand. Further addition of saturated aqueous solution of NH_4PF_6 to the mother liquor lead to the precipitation of a little fraction of the almost isomerically pure *cis*-$[Ru^{II}Cl(\text{trpy-P-Et})(\text{pypz-Me})](PF_6)$ complex.

The ruthenium aqua complex [Ru^{II}(trpy-P-Et)(pypz-Me)OH$_2$](PF$_6$)$_2$, **C4**, is easily obtained dissolving complex **C3** in water under reflux, where the chloride ligand is substituted by aqua ligand, and it is also isolated as a mixture of *cis*-and *trans*- isomers. It is worth mentioning here that this behavior is different to that shown by the analogous complex [Ru(trpy)(pypz-Me)OH$_2$)]$^{2+}$ [190] where addition of AgNO$_3$ is necessary to produce the exchange of chlorido by aqua ligand. Probably, the presence of the phosphonate group on the trpy ligand in complex **C4** produces different electronic effects that make Cl ligand more labile, as can be found in the literature for other substituted trpy ligands.[433]

The crystal structures of complexes *trans*- and *cis*-**C3** have been solved by X-ray diffraction analysis from a single crystal where the two isomers crystallize together in an equimolar ratio. Figure **4.1** displays the molecular structure of both isomers whereas their main crystallographic data and selected bond distances and angles can be found in the Supporting Information section (Tables **S4.1** and **S4.2**). In both cases, the Ru metal centers adopt an octahedrally distorted type of coordination where the trpy-P-Et ligand is bonded in a meridional manner and the pypz-Me ligand acts in a didentate fashion. The sixth coordination site is occupied by the chlorido ligand. All bond distances and angles are within the expected values for this type of complexes[190,363,434] although the quality of the diffraction data does not allow a precise discussion of structural parameters, in particular those corresponding to the pypz-Me ligand (see experimental section).

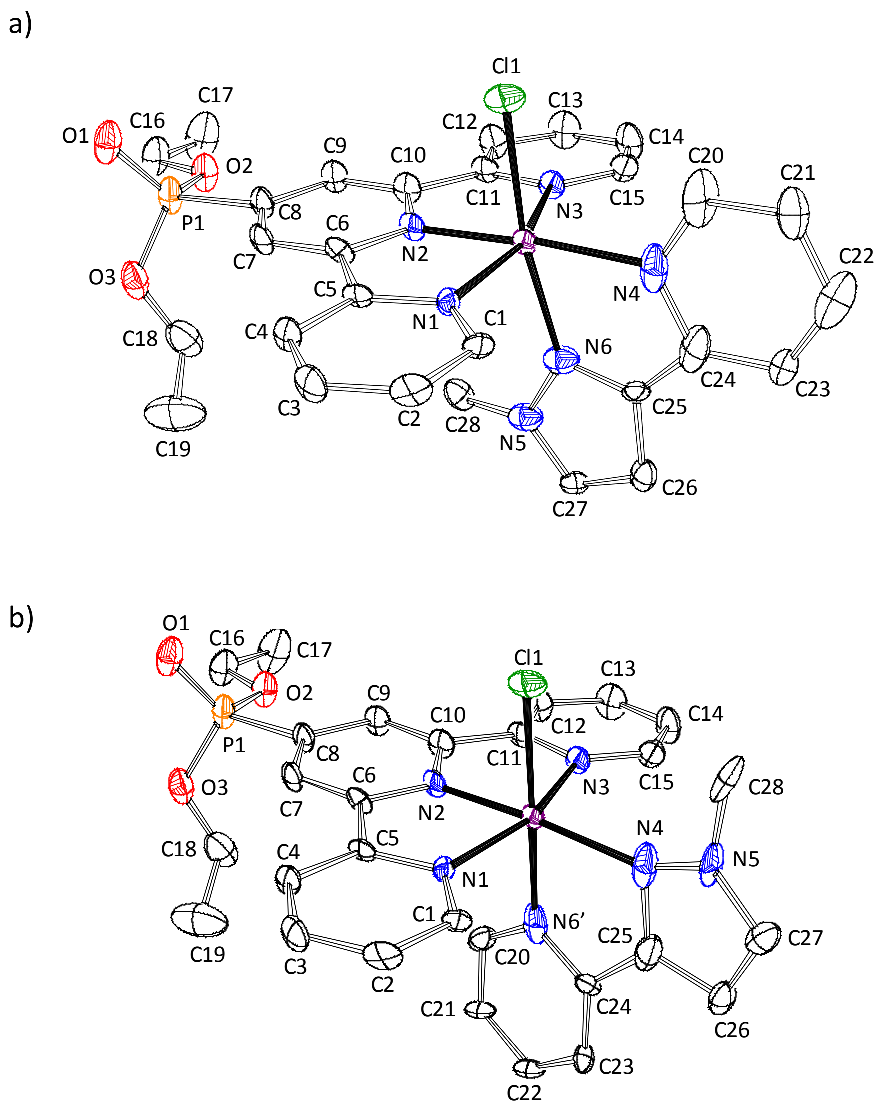
a)
Cl1
C17
C16
O1
O2
C9
C10
C12
C13
C14
C20
C21
C11
N3
C15
P1
C8
C6
N2
C7
N4
C22
O3
C5
N1
C1
C4
C18
N6
C24
C23
C3
C2
C25
C28
N5
C19
C26
C27
b)
O1
C16
C17
Cl1
C13
O2
C9
C14
C10
C12
P1
C8
C11
N3
C15
C28
O3
C7
C6
N2
C18
C5
N4
C4
N1
N5
C1
N6′
C25
C27
C19
C3
C20
C2
C24
C21
C26
C23
C22

Figure 4.1. Ortep plot and labelling schemes for compounds *trans*-**C3** and *cis*-**C3**.

The N(1)-Ru-N(2) and N(2)-Ru-N(3) angles are 80º and 81.1º respectively, showing the geometrical restrictions imposed by the tridentate trpy-P-Et ligand, which is considered to define the equatorial plane of the structure; as a consequence of this, the other two equatorial angles, N(1)-Ru-N(4) and N(3)-Ru-N(4), are larger than the 90º expected for an ideal octahedral geometry.

4.2. Spectroscopic properties

The IR spectra for both complexes (Figures **S4.1** and **S4.2**) show vibrations around 1200, 1000 and 800 cm^{-1} that can be respectively assigned to $\upsilon_{P=O}$, $\upsilon_{P\text{-}O\text{-}c}$ and $\upsilon_{P\text{-}C}$ stretching modes. In the case of **C4**, it can be observed a band around 3000 that can be assigned to $\upsilon_{O\text{-}H}$ stretching.

The one-dimensional (1D) and two-dimensional (2D) NMR spectra of both complexes were registered in d$_6$-acetone and are presented in Figure **4.2** and Supporting Information (Figures **S4.3**-**S4.5**). The resonances found for both complexes are consistent with the structures obtained in the solid state. The combination of 1D and 2D NMR spectra allows identifying all the resonances for the complexes. Two sets of signals can be found in ^{1}H-NMR: one in the aromatic region corresponding to the nitrogen ligands and the other in the aliphatic region assigned to the ethyl groups bound to phosphonate and the methyl group of de pypz-Me ligand. It is worth mentioning the difference observed in the chemical shift of H20 for the two isomers: in the case of *trans* isomer this signal is found at 10.16 ppm whereas for the *cis* isomer it appears at 8.17 ppm. This difference is due to the deshielding effect of the spatially close Cl ligand in the case of the *trans* isomer.

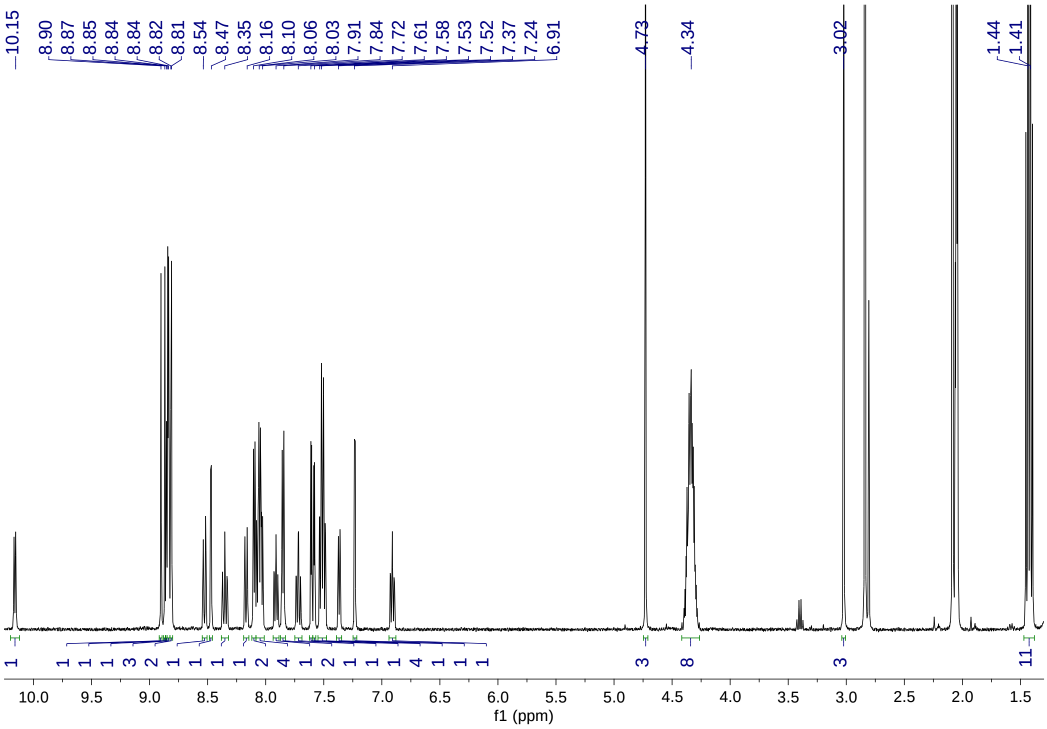

Figure 4.2. ^{1}H-NMR spectrum of *trans* and *cis*-**C3**, 400 MHz, acetone-d$_6$.

The UV-Vis spectra for both complexes **C3** and **C4** registered in CH$_2$Cl$_2$ are displayed in Figure **4.3**. The complexes exhibit ligand based π-π* bands below 350 nm and relatively intense bands above 350 nm mainly due to dπ(Ru)-π*(L) MLCT transitions.[435]

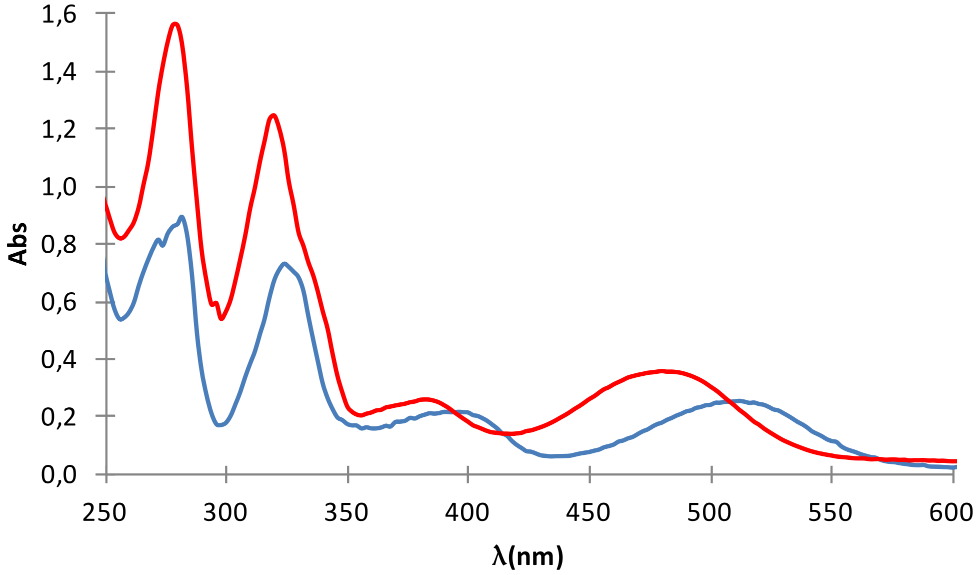

Figure 4.3. UV-vis spectra of 0.03 mM of complexes **C3** (blue) and **C4** (red) in CH$_2$Cl$_2$.

As can be seen in Figure **4.3**, for the Ru-Cl complex the MLCT bands are shifted to longer wavelengths with regard to the corresponding Ru-OH$_2$ complex because of the relative destabilization of the dπ(Ru) levels provoked by the anionic chlorido ligand.[436-438]

4.3. Electrochemical properties

The redox properties of the complexes **C3** and **C4** have been determined by cyclic voltammetry (CV) and differential pulse voltammetry (DPV) experiments. Chloridocomplex **C3** exhibits a reversible monoelectronic Ru(III/II) redox wave at $E_{1/2}$ around 0.93 V versus SCE and the corresponding CV is shown in Figure **4.4**.

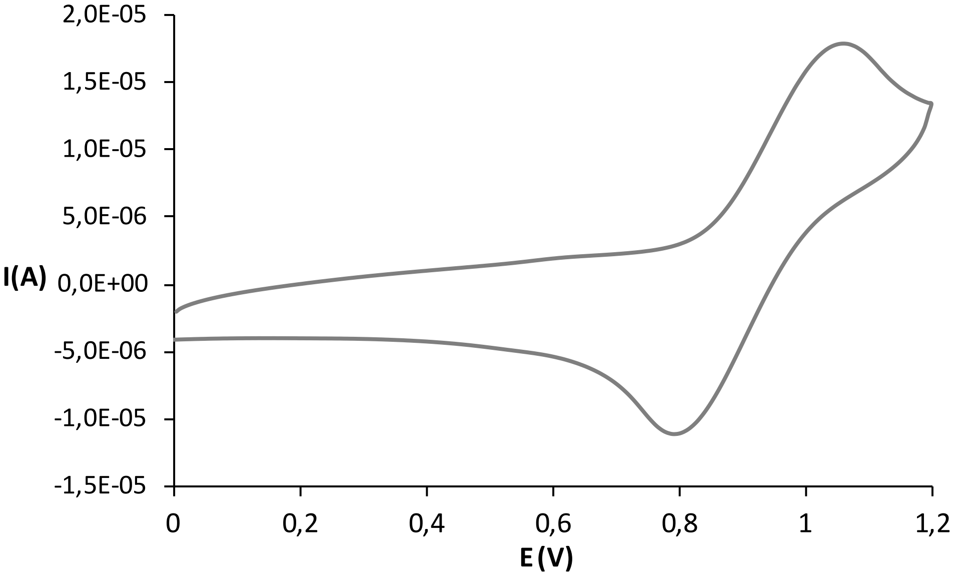

Figure 4.4. Cyclic voltammogram of **C3** in CH_2Cl_2.

Comparing the redox potential of **C3** and that of the analogous complex [RuCl(trpy)(pypz-Me)], described in the literature,[190] it can be observed that the presence of the phosphonate groups leads to an increase in the redox potential (0.93 V for **C3** *vs*. 0.80 V for [RuCl(trpy)(pypz-Me)]), as a result of the higher electron-withdrawing capacity of the trpy-P-Et ligand, that provokes a destabilization of the Ru(III) species. This is also in agreement with the enhanced lability of the chlorido ligand found for complex **C3**, as described previously in the *Synthesis and crystal structures* section.

On the other hand, aqua complex **C4** exhibits a reversible wave at $E_{1/2}$ around 0.5 V *vs* SCE in water at pH= 7 (Figure **4.5**) corresponding to the Ru(IV/II) redox couples of the two *cis* and *trans*-**C4** isomers, which display closely similar potential values.

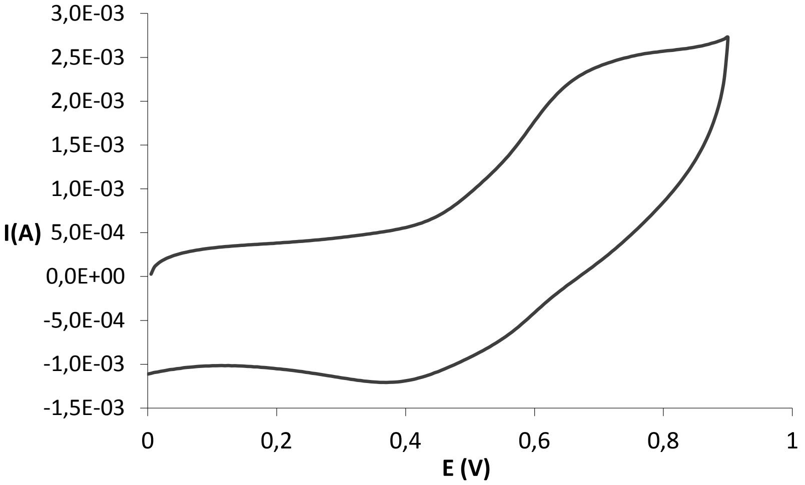

Figure 4.5. Cyclic Voltammogram of **C4** in water at pH =7.

Differential pulse voltammetry (DPV) was performed in acetonitrile for compound **C4**, with the idea to distinguish the respective redox processes for the two isomers of **C4**. Figure **4.6** displays the DPV obtained at pH = 6.4 and, as can be observed, the two redox pairs partially overlap but distinctive potential values, at $E_{1/2}$ of 0.6 and 0.5 V, can be drawn after deconvolution of the wave registered (see below). Thus, by comparison with the analogous complex $[Ru(trpy)(pypzMe)OH_2)]^{2+}$ previously described in the literature,[190] the redox pair at $E_{1/2}$ of 0.6 V can be assigned to the *cis*-**C4** isomer whereas the process at $E_{1/2}$ = 0.5V corresponds to the *trans*-**C4** isomer.

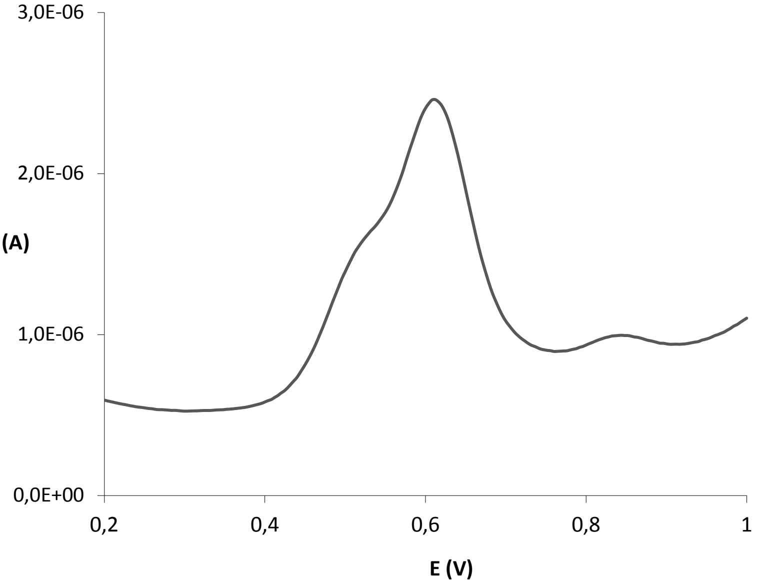

Figure 4.6. Differential Pulse Voltammetry of **C4** in water at pH= 6.4.

The redox properties of Ru-aqua complexes are pH dependent (Figure **4.7**) because of the capacity of the aqua ligand to lose protons upon oxidation of the complex, which also makes the upper oxidation states easily accessible:

$$[\mathrm{Ru^{II}(trpy\text{-}P\text{-}Et)(pypz\text{-}Me)(H_2O)}]^{2+} \longrightarrow [\mathrm{Ru^{III}(trpy\text{-}P\text{-}Et)(pypz\text{-}Me)(OH)}]^{2+} + H^+ + e^- \quad (1)$$

$$[\mathrm{Ru^{III}(trpy\text{-}P\text{-}Et)(pypz\text{-}Me)(OH)}]^{2+} \longrightarrow [\mathrm{Ru^{IV}(trpy\text{-}P\text{-}Et)(pypz\text{-}Me)(O)}]^{2+} + H^+ + e^- \quad (2)$$

This pH-dependent behavior is manifested in DPV experiments performed at different pH values, as can be observed in Figure **4.7** for three different pH values:

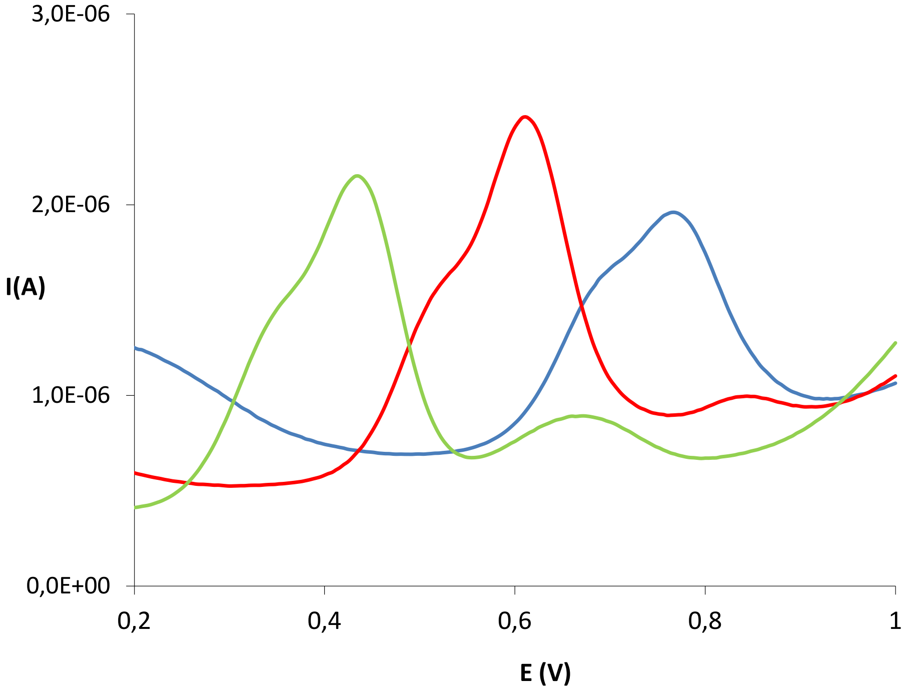

Figure 4.7. Differential pulse voltammetries of **C4** in water at pH=2.6 (blue), 6.4 (red) and 8.8 (green).

As mentioned earlier, a mathematical deconvolution treatment of the DPV registered allows the independent assignment of the redox potentials for the two isomeric species present in **C4**. Thus, their respective Pourbaix diagrams, which plot $E_{1/2}$ versus pH, can be represented, and are exhibited in Figures **4.8** and **4.9** for *trans*-**C4** and *cis*-**C4** respectively. Both complexes *trans* and *cis*-**C4** show a unique pH-dependent redox process throughout the whole pH range with a change in the slope value (from approximately 58 to 30 mV/pH unit) at pH around 7.6 and 9.6, respectively, a behavior that is generally indicative of the occurrence of a two-electron (IV/II) redox process. The changes in the slope correspond to the pKa values of the Ru(II) or Ru(III) species and are indicated by vertical lines in each case.

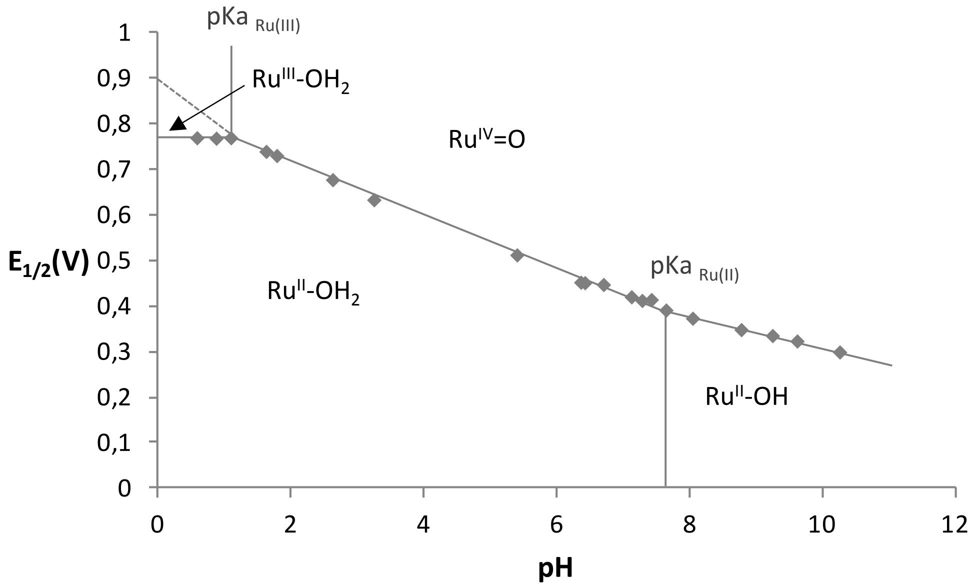

Figure 4.8. Pourbaix diagram of *trans*-**C4**. The pH-potential regions of stability for the various oxidation states and their dominant proton compositions are indicated.

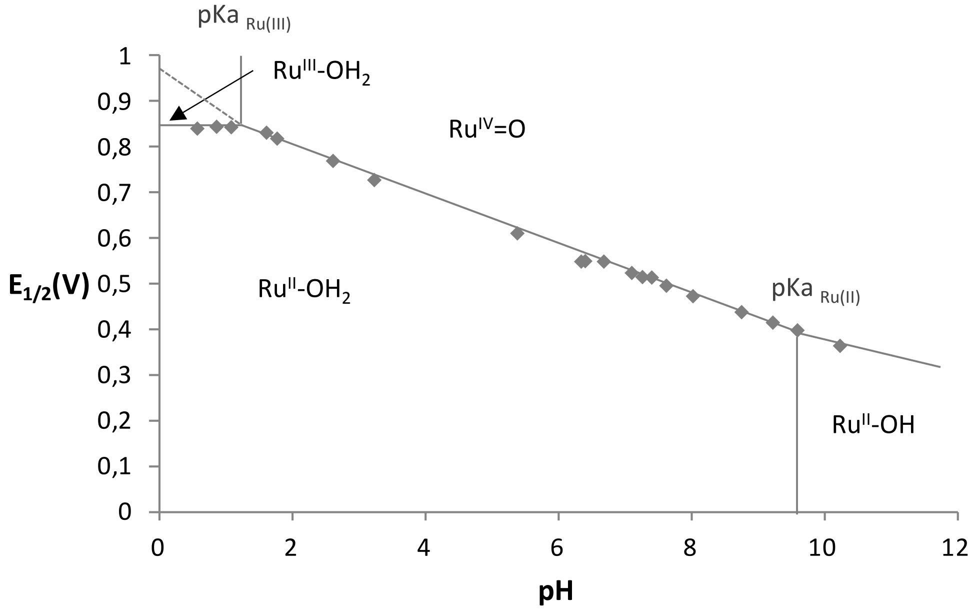

Figure 4.9. Pourbaix diagram of *cis*-**C4**. The pH-potential regions of stability for the various oxidation states and their dominant proton compositions are indicated.

Complete electrochemical and thermodynamic information regarding the Ru-aqua type of complex can be extracted from these Pourbaix diagrams and the data corresponding to *trans*- and *cis*-**C4**, together with that of similar complexes described in the literature that contain trpy/trpy-R and bidentate N-donor ligands, are displayed in Table **4.1**. In all entries of the table, the notation *cis* or *trans* (to the aqua ligand) is referred to a ligand having higher σ-donor (or lower π-acceptor) capacity than a pyridyl ring.

Table 4.1. pK_a and electrochemical data (pH = 7, $E_{1/2}$ in V vs SCE) for aqua complexes described in this chapter and others for purposes of comparison.

Entry	Compound	$E_{1/2}$ (III/II)	$E_{1/2}$ (IV/III)	ΔE (IV/II)[a]	E (IV/II)[b]	pK_a(II)	pK_a(III)	ref.
1	*trans*-**C4**	0.42[c]		<0	0.42	7.6	1.1	[d]
2	*cis*-**C4**	0.52[c]		<0	0.52	9.6	1.5	[d]
3	*trans*-[Ru(trpy)(pypzMe)OH_2)]$^{2+}$	0.39	0.57	180	0.48	10.1	0.95	190
4	*cis*-[Ru(trpy)(pypzMe)OH_2)]$^{2+}$	0.47	0.52	50	0.495	10.75	1.65	190
5	*trans*-[Ru(trpy)(pyrpy-O)OH_2]$^{+}$	0.55[c]		<0	0.55	9.75	1.21	190
6	[Ru(trpy-P)(bpm)OH_2)]$^{2+}$	0.66[c]		<0	0.66			363
7	[Ru(trpy)(bpy)OH_2)]$^{2+}$	0.57	0.74	0.17	0.65	9.7	1.7	177

[a] ΔE = $E_{1/2}$(IV/III) - $E_{1/2}$(III/II) in mV. [b] Average value calculated according to: E(IV/II) = [$E_{1/2}$(IV/III) + $E_{1/2}$(III/II)]/2, in V. [c] $E_{1/2}$(IV/II) in V. [d] This chapter

A first look at Table **4.1** shows that both isomers of complex **C4** (entries 1 and 2) present Ru(III/II) potential values slightly higher than the analogous *cis*- and *trans*-[Ru(trpy)(pypzMe)OH_2)]$^{2+}$ complexes (entries 3 and 4), which is in accordance with the electron-withdrawing character of the phosphonate group of the trpy-P-Et ligand. Another complex also containing this modified trpy ligand (entry 6) displays the higher Ru(III/II) potential value of the set of complexes compared in Table **4.1**.

Nevertheless, the $E_{1/2}$ values are not only governed by the electronic properties of the ligands but also by the geometry of the complex. Thus, when comparing for instance entries 1 and 2 or 3 and 4 in Table **4.1** one can see that coordination of a relatively good σ-donor (or less π-acceptor) ligand in a *trans* fashion with respect to the aqua ligand, as in the case for the *trans* isomers, lowers $E_{1/2}$(III/II) with respect to the analogous *cis* isomers hence stabilizing the high oxidation state species.[439,440]

However, in complexes displaying two monoelectronic processes (entries 3 and 4), the effect on the Ru(IV/III) wave seems to be reversed and, consequently, the difference between Ru(IV/III) and Ru(III/II) *E* values (ΔE, see Table **4.1**) is increased for the *trans* geometry. Thus, the occurrence of a bielectronic process seems to arise from a specific balance between the geometry and the σ-donor and π-acceptor properties of the ancillary ligands.[441]

Finally, regarding the pKa values for the Ru(II) species, the **C4** isomers display lower pKa values than the corresponding $[Ru(trpy)(pypzMe)OH_2)]^{2+}$ isomers (7.6 and 9.6 *vs.* 10.1 and 10.75 for *trans* and *cis*, see entries 1-4). This higher acidic character for **C4** is again in accordance with the enhanced electron-withdrawing nature of the trpy-P-Et ligand when compared to trpy. The geometry also influences pKa(II) values, with a higher acidity for the isomers having the more electron-withdrawing ligand in *trans* to the aqua ligand.

4.4. Catalytic epoxidation of alkenes

The catalytic activity of the ruthenium aquacomplexes *trans* and *cis*-**C4** was checked in the epoxidation of *cis-β*-methylstyrene in dichloromethane and using iodobenzene as oxidant. No epoxidation occurred in the absence of catalyst. In Table **4.2** the catalytic results are shown, other previously reported complexes are also included for comparison purposes.

Within the epoxidation area a particularly interesting reaction is the stereoselective epoxidation of *cis*-alkenes.[197,396,442- 447] This is an important issue specially because the well-known and efficient Jacobsen's Mn-salen complexes generally give mixtures of *cis* and *trans*-epoxides.[448,449] The *cis→trans* isomerization in epoxidation processes involving *cis* alkenes is a common phenomenon due to the higher thermodynamic stability of the *trans* epoxides. To undergo such isomerization, a rotation around the C-C bond is required involving the presence of a relatively long-lived free substrate radical during the oxygen transfer process.[74,81,450]

Table 4.2. Catalytic epoxidation of *cis-β*-methylstyrene by Ru complexes using $PhI(OAc)_2$ as oxidant.[a]

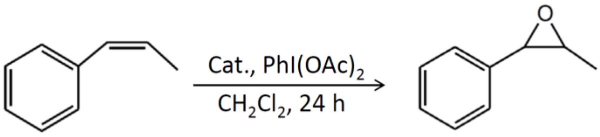

Entry	Compound	Conversion (%)	Selectivity (%)[b]	% of *cis*-epoxide	ref.
1	**C4**	>99	70	>99	this chapter
2	*trans*-$[Ru(trpy)(pypzMe)OH_2)]^{2+}$	90	99	98	190
3	*cis*-$[Ru(trpy)(pypzMe)OH_2)]^{2+}$	>99	86	97	190
4	$[Ru(trpy\text{-}P)(bpm)OH_2)]^{2+}$	>99	68	>99	363

[a] Conditions: complex (1.25 μmol), substrate (125 μmol), $PhI(OAc)_2$ (250 μmol), CH_2Cl_2 (2.5 mL), 25°C, 24 h, biphenyl (125 μmol) as internal standard.

[b] Selectivity for epoxide, (Yield/Conversion)x100.

As we can observe in Table **4.2**, the mixture of isomers **C4** presents high levels of conversion and selectivity for the epoxide, comparable to the other complexes described. The corresponding *cis*-epoxide was detected as the major product, with no formation of the *trans*-epoxide. This result indicates that, if an alkene-localized radical species was formed as intermediate, the closure of the ring would be much faster than the C-C rotation at the radical intermediate that would lead to the *trans* epoxide product. This is in agreement with a potential O-atom transfer concerted mechanism, which is in turn consistent with the low stability of Ru(III) that favors $2e^-$ versus $1e^-$ transfer process.[75,451]

It is worth to notice here that complexes $[Ru(trpy)(pypzMe)OH_2)]^{2+}$(entries 2 and 3), display similar degree of conversion and selectivity than $[Ru(trpy\text{-}P\text{-}Et)(pypzMe)OH_2)]^{2+}$, **C4**, (entry 1) in epoxidation. This validates the use of complex **C4** to prepare heterogeneous catalytic systems to be compared with $[Ru(trpy)(pypzMe)OH_2)]^{2+}$ as their homogeneous counterparts. The preparation and evaluation of such heterogeneous systems will be seen in Chapter 5.

4.5. Catalytic hydration of nitriles

We have checked the previously reported complex $[\mathrm{Ru(trpy)(pypzMe)OH_2)}]^{2+}$ (equimolar mixture of *cis* and *trans* isomers) in the hydration of different nitriles using water as a solvent at 80ºC. Conversion and selectivity values are summarized in Table **4.3**, together with the conditions used in the catalysis. This compound constitutes the first example of aqua complex of ruthenium containing N-donor ligands successfully applied to hydration of nitriles described in the literature.

Table 4.3. Ru-catalyzed hydration of nitriles to amides in water using aquacomplex $[\mathrm{Ru(trpy)(pypzMe)OH_2)}]^{2+}$ as catalyst.[a]

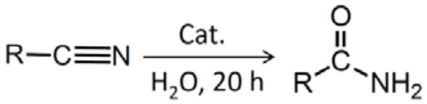

Entry	Substrate	Conversion (%)	Selectivity (%)[b]
1	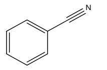	35	>98
2	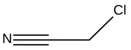	60	70
3	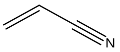	42	>98
4	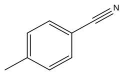	21	>98
5	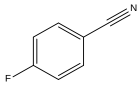	49	64
6	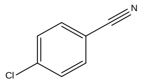	34	>98
7	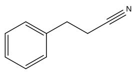	17	>98

[a] Reactions performed at 80ºC using 1 mmol of nitrile in 3 ml of water. [Substrate]:[Ru] = 100 : 1. Time: 20 h. [b] Selectivity = (amide yield/substrate conversion) x 100.

As can be observed in Table **4.3**, **C4** was found to be active towards nitrile hydration despite obtaining only moderate conversion. In most cases, high selectivity values were obtained except in two cases (entries 2 and 5) where a certain amount of the corresponding acid has been also detected.

The electronic properties of the substrates influence the extent of the hydration reaction, provided that a nucleophilic attachment of water (or hydroxo anions) on the nitrile carbon atom takes place.[268,270] Lower performances are displayed by substrates either linked to aliphatic groups (entry 7) or having *para*-electron donating groups in the aromatic ring (entry 4). Otherwise, halide-substituted benzonitriles (entries 5 and 6) are expected to display better performances thanks to the electron-withdrawing character of the halide substituents (inductive effect). However, in the case of *p*-chlorobenzonitrile the performance is lowered indicating that a deactivating effect, probably caused by the resonance delocalization of the Cl lone pairs throughout the aromatic system, is taking place. This is in contrast with the activating effect that Cl substituent has on the aliphatic substrate (entry 2), where the electronic influence is dominated by the electronegativity of the Cl substituent.

The catalytic activity of the ruthenium aquacomplex $[Ru(trpy\text{-}P\text{-}Et)(pypzMe)OH_2)]^{2+}$, **C4**, was checked in the hydration of benzonitrile as a test substrate in water to compare with the results displayed in Table **4.3**. Both aquacomplexes show a similar catalytic activity with moderate conversion values (30% for **C4** and 35% for $[Ru(trpy)(pypzMe)OH_2)]^{2+}$) and high selectivity values (>98% for both complexes). We can expect a similar behavior in the hydration of different substrates for both compounds.

In summary, in this chapter we have synthesized and characterized two new ruthenium complexes: Ru-Cl and Ru-OH_2 with one tridentate (trpy-P-Et) and one bidentate (pypzMe) ligands. Both complexes have been fully characterized by structural, analytical and spectroscopic techniques. In the case of the clorocomplex **C3** two isomers were obtained, although their separation resulted difficult due to their similar solubility. Unlike other complexes found in the literature, aqua complex **C4** was easily obtained after refluxing chlorido complex **C3** in water. After the redox characterization of the isomeric Ru-aqua complexes, Pourbaix diagrams could be obtained and they indicated the occurrence of a two-electron (IV/II) redox process for both isomers.

Complex **C4** was tested in epoxidation of alkenes and hydration of nitriles. In the case of the epoxidation, where *cis*-β-methylstyrene was used as a test substrate, **C4** presents high levels of conversion and stereoselectivity that were comparable to other complexes described in the literature taken as reference. The high stereoselectivity obtained indicates that the reaction is due either to a concerted mechanism or to a pathway involving a short-lived radical intermediate that closes the epoxide ring prior to *cis*→*trans* isomerization.

For the hydration of nitriles, we have tested the previously reported complex $[Ru(trpy)(pypzMe)OH_2)]^{2+}$ using different nitrile substrates and high values of selectivity were achieved in most of the cases, with moderate conversion values in some cases. The catalytic activity of **C4** was checked in the hydration of benzonitrile and the results were similar to the results obtained using complex $[Ru(trpy)(pypzMe)OH_2)]^{2+}$. These results will allow us to compare the performance of these catalysts with their homologous heterogeneous systems as will be described in Chapter 5.

Chapter 5

Heterogeneous catalytic systems based on [Ru (trpy-P)(pypz-Me)X]$^{n+}$ (X = Cl, H_2O) complexes. Evaluation of the catalytic activity in epoxidation and hydration reactions.

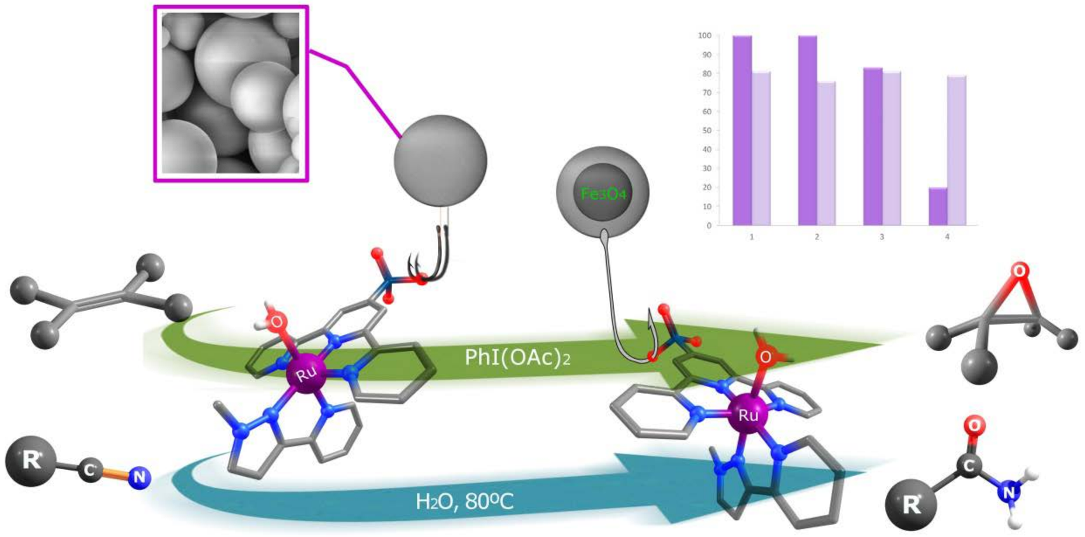

Phosphonated terpyridine complexes with general formula [Ru^{II}(trpy-P)(pypz-Me)X]$^{n+}$ (X = Cl, H_2O) have been anchored onto three different silica supports *via* covalent bonds. These new materials have been fully characterized by ICP-AES, SEM, TGA and spectroscopic techniques. The redox properties of heterogeneous Ru-OH_2 complexes together with their reactivity in alkene epoxidation and nitrile hydration have been studied. The results obtained have been compared with the analogous homogeneous systems.

5.1. Strategies for the immobilization of Ru complexes

The immobilization method used for the heterogenization of $[Ru^{II}Cl(trpy\text{-}P)(pypz\text{-}Me)]^{+}$ and $[Ru^{II}(trpy\text{-}P)(pypz\text{-}Me)OH_2]^{2+}$ described in this chapter is based on a covalent binding between the modified terpyridine (trpy-P) ligands and silica particles through phosphonate groups (Scheme **5.1**), allowing a strong interaction between the catalyst and the support.

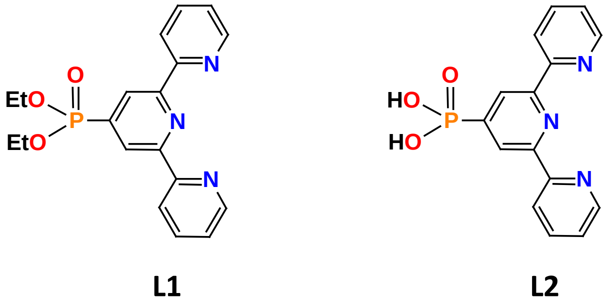

Scheme 5.1. Terpyridine ligands modified with phosphonate linking groups.

In this chapter, three different SiO_2 supports were used: silica aerogel particles (**SP1**), silica mesoporous particles (**SP2**) and silica-coated Fe_3O_4 magnetic particles (**MSP**). Two different strategies, numbered 1a/b and 2 (see Scheme **5.2**) were followed for the immobilization of the complexes, depending on the order in which the products were anchored. In strategy 1, the modified ligand is first attached to the silica particles and the catalyst is thereafter generated *in situ*, whereas strategy 2 consists on the direct anchoring of the previously synthesized complex **C3**.

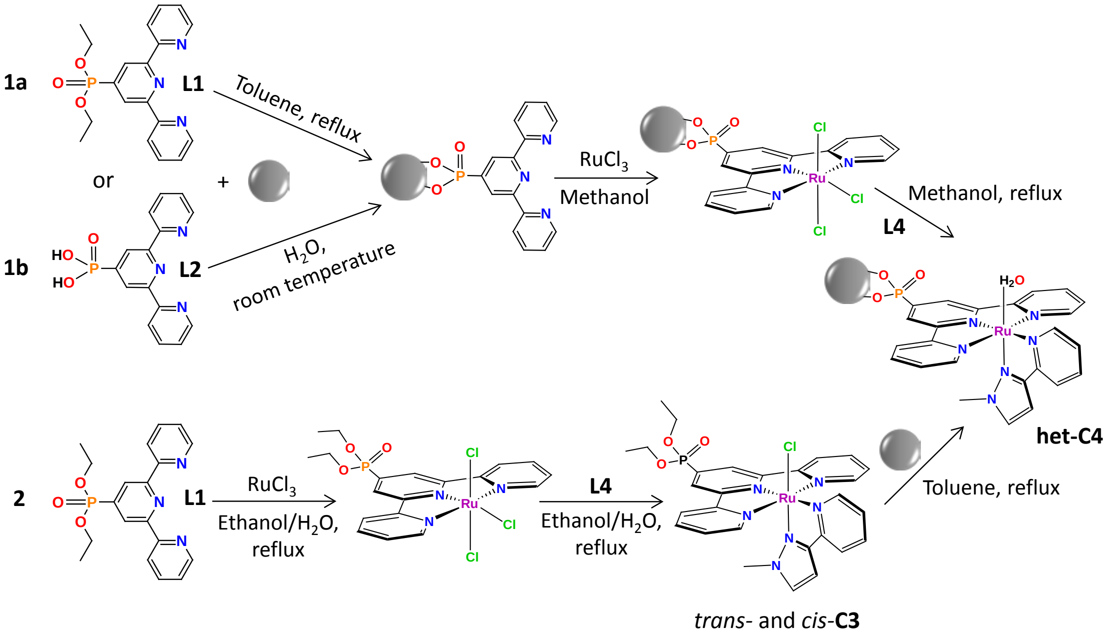
1a
L1
or
+
1b
L2
Toluene, reflux
H_2O, room temperature
$RuCl_3$
Methanol
Methanol, reflux
L4
het-C4
2
L1
$RuCl_3$
Ethanol/H_2O, reflux
L4
Ethanol/H_2O, reflux
Toluene, reflux
trans- and *cis*-**C3**

Scheme 5.2. Synthetic strategies for the immobilization of the complexes (**L4** represents the bidentate pypz-Me ligand). Grey spheres represent the silica particles.

There are few examples in the literature where strategy 1 was used.[364] The second one is more common[354,363] and there are also reports for a third type of strategy where a linker is attached to the particles before the ligand itself.[158,452] The two strategies used in this chapter are discussed next.

1) Functionalization of the supports with the corresponding trpy-P ligand

Two different terpyridyl ligands (Scheme **5.1**) were used for the functionalization of the supports. In the first step, a tridentate trpy-P ligand (**L1** or **L2**) was anchored to the silica particles. In our case, **L2** was anchored to **SP1**, **SP2** and **MSP** whereas **L1** was anchored only to **SP1** and **MSP**. For the immobilization of the diethylphosphonate **L1** ligand, a reflux in toluene was needed (Scheme **5.2**, 1a) in order to achieve the hydrolysis of the ethyl groups. In contrast, for the immobilization of **L2** much milder conditions could be used, obtaining the modified silica by simply stirring overnight a solution of the ligand in water in presence of the corresponding SiO_2 particles, at room temperature (Scheme **5.2**, 1b).

In the second step, $RuCl_3$ was coordinated to the trpy-functionalized supports in methanol. The $RuCl_3$(trpy-P)-functionalized particles were washed, centrifuged and dried in a hot air oven. Afterwards, the bidentate **L4** ligand was coordinated to ruthenium at the $RuCl_3$(trpy-P)-functionalized particles by reflux in methanol using NEt_3 as reducing agent, leading to the final Ru(II) aquacomplex **C4** attached to the corresponding support. The resulting heterogeneous systems were centrifuged, washed and dried in a hot air oven. It is important to note here that the final supported product was the aquacomplex instead of the expected **C3** chloridocomplex. This is also the case for strategy 2 (see below) and is probably due to the use of non-anhydrous solvents in the last step of each heterogenization route, leading to the exchange of the chlorido ligand by an aquo ligand.

As will be described below (section 5.2.2) the amount of Ru anchored was lower when following strategy 1a and, for this reason, strategy 1b was chosen for the three supports used.

2) Attachment of the complex previously synthesized

For this strategy, a mixture of *trans*- and *cis*-[RuCl(trpy-P-Et)(pypz-Me)](PF_6), **C3** (chapter 4), was used to be anchored to **SP2**. As mentioned earlier, a reflux in toluene (with addition of acetone after 4 hours of reflux to further solubilize complex **C3**, see experimental section) was needed in this case for the hydrolysis of the ester groups, and these conditions also lead to the hydrolysis of the chlorido ligand at the attached complex, generating the corresponding aquacomplex **C4**.

An alternative anchoring protocol using a mixture of toluene/acetone as refluxing solvent from the beginning of the process was tested. However, under these conditions the exchange of chlorido ligand by aquo ligand happened before the hydrolysis of the ester groups causing the anchorage of the complex through the aqua ligand position preferentially, leading to a blockage of the labile position needed for catalysis.

5.2. Characterization of supports

The different techniques used for the characterization of the supports described below correspond to the **C4**-modified particles except for the physical parameters, which are given for the naked silica supports.

5.2.1. Physical parameters of the silica supports used

The physical parameters were measured on the various silica supports prior to the attachment of the complex or ligand and are summarized in Table **5.1**. As can be observed, the silica aerogel particles (**SP1**) present a bimodal size distribution in contrast to mesoporous silica particles (**SP2**) and silica-coated magnetic particles (**MSP**) that present a unique average size value. The specific surface areas (S_{BET}) of the three supports are quite different, with **SP2** having the highest surface area value whereas **MSP** presents the lowest area.

Table 5.1. Physical parameters of the silica supports used.

Support	Particle size (nm)	Pore		S_{BET} (m^2/g)	% Fe_3O_4
		Volume (cm^3/g)	Size (nm)		
SP1	~1700 ~3900	0.151	1.4	322	-
SP2	~200	0.002	4	886	-
MSP	~173	0.034	5.9	25	7.2

5.2.2. Atomic Emission Spectroscopy (ICP-AES)

From the ICP-AES experiments, the amount of Ru complex covalently anchored to the supports was obtained. The results obtained for the three supports using different strategies are shown in Table **5.2**.

Table 5.2. Amount of Ru anchored in the different supports.

Support	Strategy	Average Ru (%)[a]	Ru (mmol/g silica)
SP1	1a	0.023	$2.3 \cdot 10^{-3}$
	1b	0.0164	$1.6 \cdot 10^{-3}$
SP2	1b	0.95	0.094
	2	0.52	0.052
MSP	1a	0.46	0.045
	1b	0.075	$7.4 \cdot 10^{-3}$

[a] % g of Ru/100 g silica support

As can be observed in Table **5.2**, strategy 1a and 1b (starting from the ethyl or the acid trpy-P ligand respectively, see Scheme **5.2**) were tested for supports **SP1** and **MSP** and, in both cases, strategy 1a becomes the most effective probably due to the harsher reaction conditions used, necessary to hydrolyze the ethyl groups of the phosphonate ligand. Strategy 1b was also used with support **SP2**, yielding the highest amount of Ru anchored. For this reason, this support was chosen to test strategy 2 (direct anchoring of the complex). However, a lower amount of Ru was anchored when compared to strategy 1b, probably due to the incomplete hydrolysis of the ester groups so that fewer points of anchorage were available.

5.2.3. SEM images

Scanning electron microscopy (SEM) was performed on the three types of supports after functionalization, and the images obtained are displayed in Figure **5.1**. As can be observed, all supports maintain their particle size and morphology after the attachment process. Figure **S5.1** (supporting information) shows the SEM images obtained for supports **SP1** and **SP2** before anchoring the complex (MSP particles had been previously prepared and characterized by the group of Prof. Anna Roig, from ICMAB, and were not further characterized prior to their functionalization).

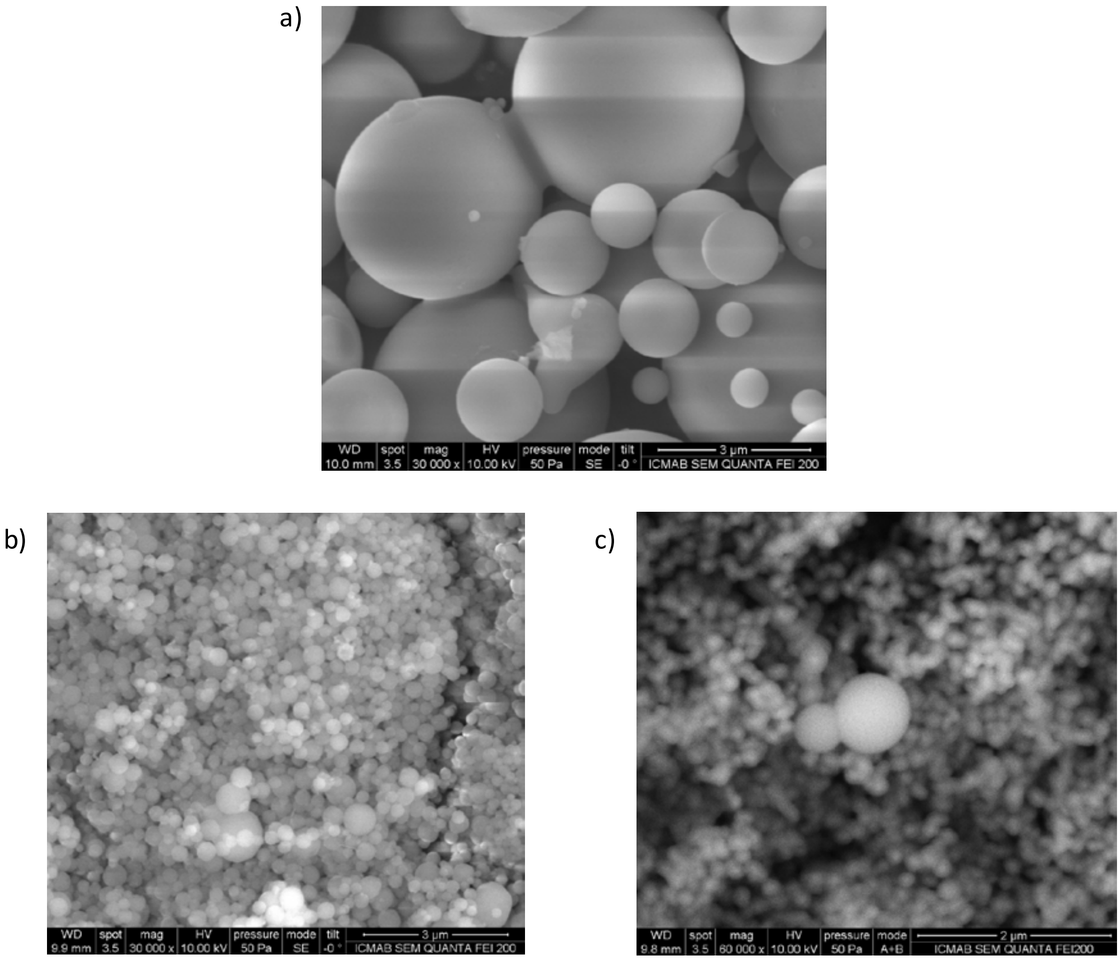
a)
WD spot mag HV pressure mode tilt 3 µm
10.0 mm 3.5 30 000 x 10.00 kV 50 Pa SE -0 ° ICMAB SEM QUANTA FEI 200
b)
WD spot mag HV pressure mode tilt 3 µm
9.9 mm 3.5 30 000 x 10.00 kV 50 Pa SE -0 ° ICMAB SEM QUANTA FEI 200
c)
WD spot mag HV pressure mode 2 µm
9.8 mm 3.5 60 000 x 10.00 kV 50 Pa A+B ICMAB SEM QUANTA FEI200

Figure 5.1. SEM images of a) **SP1** b) **SP2** and c) **MSP** after the anchoring of the Ru complex.

5.2.4. Thermal studies (TGA)

Thermogravimetric profiles have been registered for the naked **SP2** support and for the three (**SP1**, **SP2** and **MSP**) supports after anchoring the Ru complex, and the results obtained are shown in Figure **5.2**. In all cases, the supports present an initial weight loss at temperatures below 150˚C, corresponding to the evaporation of adsorbed solvent. At temperatures above 300˚C, the weight loss for the three functionalized supports corresponds to the release of the Ru complex. For **SP1** (prepared following strategy 1a) the weight loss was 3.1%, whereas it was of 7.7% for **SP2** and 3.9% for **MSP** (both prepared through strategy 1b).

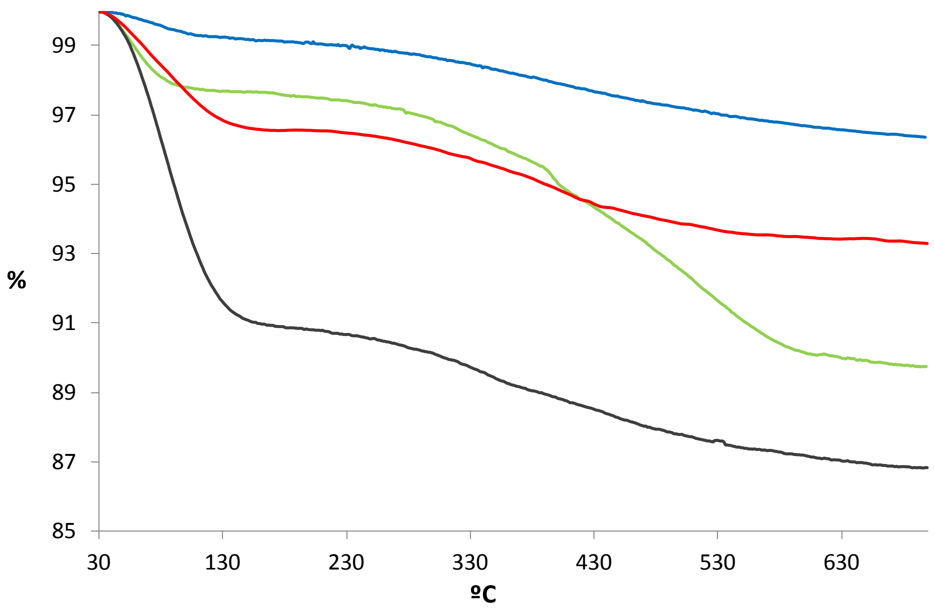

Figure 5.2. Thermogravimetric profiles of **SP2** (blue), **SP1-C4** (red), **SP2-C4** (green), **MSP-C4** (grey).

5.2.5. Spectroscopic properties

The spectroscopic and electrochemical characterization of the modified nanoparticles has been performed on **SP2** functionalized systems. Regarding the spectroscopic properties, the **C4-**modified supports have been characterized through IR and UV-vis spectroscopies. Figure **5.3** displays the IR spectra for **SP2** and **SP2-C4** and, as can be observed in the inset, the modified silica **SP2-C4** shows bands around 2900-3000 cm^{-1} that can be assigned to $\upsilon_{N\text{-}H}$ and $\upsilon_{C\text{-}H}$ stretching modes of the supported trpy-P ligand.

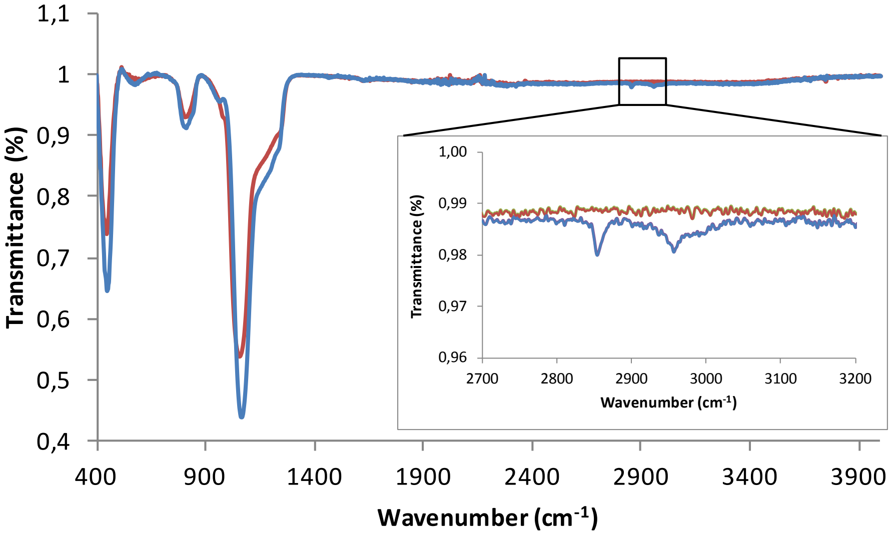

Figure 5.3. IR spectra of **SP2** (red) and **SP2-C4** (blue).

The UV-Vis spectra for **SP2-C4** obtained through strategies 1b and 2 have been registered on a suspension of the heterogeneous support in dichloromethane and are displayed in Figure **5.4** together with the UV-vis spectrum corresponding to the **C4** aquacomplex (Chapter 4). The anchored complex exhibits ligand based π-π* bands below 350 nm and relatively intense bands above 350 nm mainly due to dπ(Ru)-π*(L) MLCT transitions[435] that are similar to those obtained for the homogeneous complex **C4**.We can then assert that the anchored **C4** complex is analogous to that previously synthesized in solution.

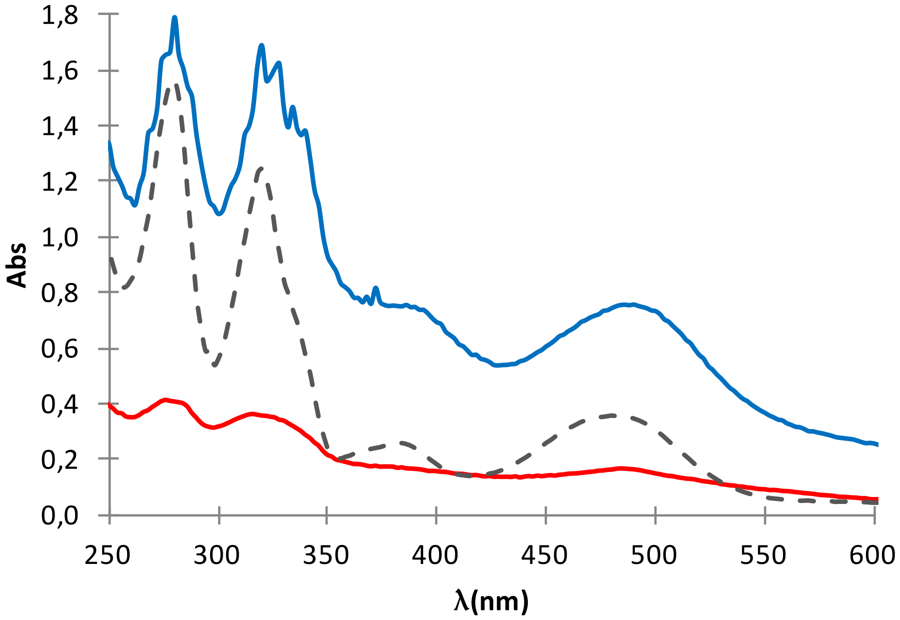

Figure 5.4. UV-vis spectra for **SP2-C4** obtained through strategy 1b (red), 2 (blue) and homogeneous complex **C4** (dotted grey).

5.2.6. Electrochemical properties

The redox properties of the **SP2-C4** have been investigated by cyclic voltammetry (CV) and differential pulse voltammetry (DPV) experiments by settling a layer of the heterogeneous functionalized particles on the working electrode surface. Figure **5.5** displays the differential pulse voltammetry obtained for **SP2-C4** together with that of the homogeneous complex **C4** for purposes of comparison. The cyclic voltammetries of **SP2-C4** in MeOH and in aqueous phosphate buffer are shown in the supporting information (Figure **S5.2**).

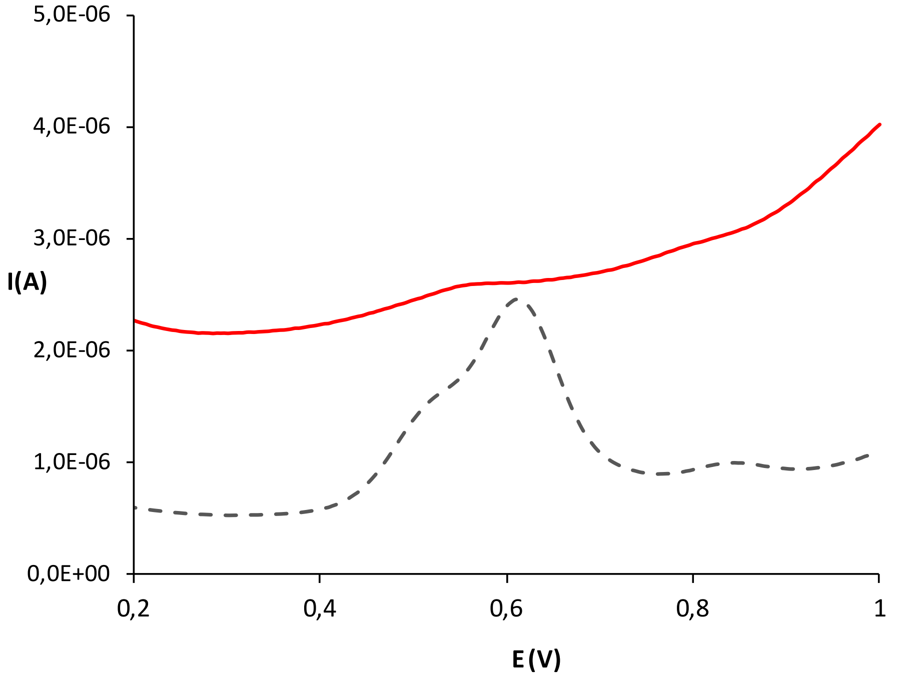

Figure 5.5. Differential Pulse Voltammetry of **SP2-C4** (red) and homogeneous complex **C4** (dotted grey) in water at pH=6.4.

In Figure **5.5**, it can be seen that the potential obtained for **SP2-C4** corresponds to the average of the potential obtained for the two isomers of **C4** (Chapter 4). The DPV experiment performed on the **C4**-modified support does not allow the distinction of the two waves for the *cis*- and *trans*- isomers of the complex though an isomeric mixture is expected to be formed in the heterogeneous supports as suggested by the UV-vis spectrum obtained (section 5.2.5).

As mentioned in Chapter 4, the redox properties of Ru-aqua complexes are pH dependent due to the simultaneous exchange of protons and electrons during the redox processes, and this dependence can be plotted as E vs. pH (Pourbaix) diagrams. The Pourbaix diagram obtained for a **SP2-C4** sample prepared through strategy 1b is shown in Figures **5.6** and **S5.3** displays the diagram corresponding to the functionalized support prepared by means of strategy 2.

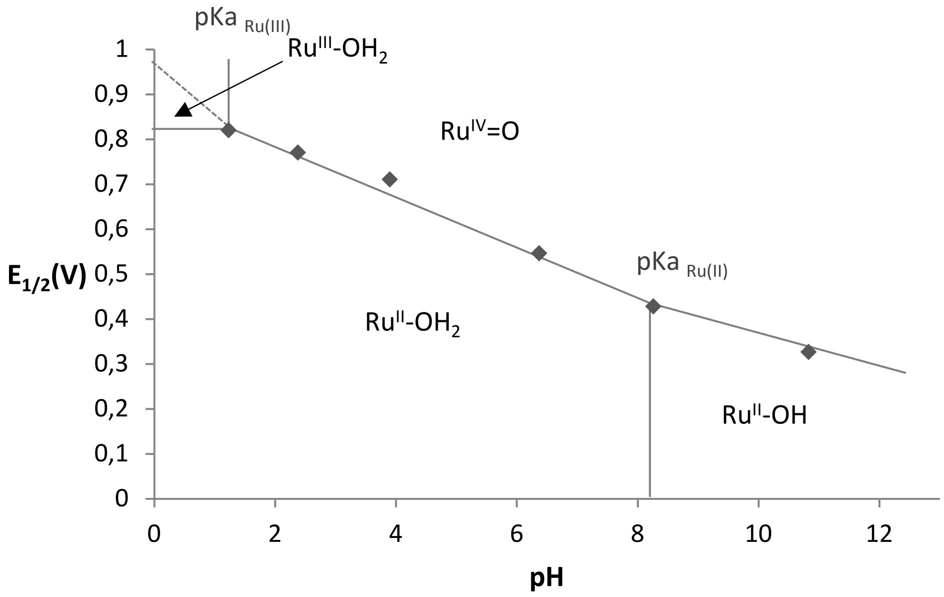

Figure 5.6. Pourbaix diagram of **SP2-C4** obtained through strategy 1b. The pH-potential regions of stability for the various oxidation states and their dominant proton compositions are indicated.

The change of $E_{1/2}$ value with pH displayed by the heterogeneous **SP2-C4** system confirms that the species anchored is indeed the aquacomplex, not the chloridocomplex. On the other hand, a comparison with the analogous diagrams obtained for the two isomers of complex $[Ru(trpy\text{-}P\text{-}Et)(pypz\text{-}Me)(H_2O)]^{2+}$, **C4** (Chapter 4), evidences a parallel behavior in heterogeneous and homogeneous phase. However, such a comparison must be cautious because, as mentioned earlier, the DPV technique does not allow differentiating the redox processes for the two isomers present and, consequently, the Pourbaix diagrams displayed in Figures **5.6** and **S5.3** correspond to an average of the data for *cis*- and *trans*- isomers.

5.3. Catalytic activity

5.3.1. Catalytic epoxidation of alkenes

The heterogeneous catalytic activity of the ruthenium aquacomplex anchored onto two different supports (**SP2-C4** and **MSP-C4**) was checked in the epoxidation of a diversity of alkenes in dichloromethane and using $PhI(OAc)_2$ as oxidant (peracetic acid was also tested but the conversion values were low). All substrates were tested under analogous conditions (catalyst:substrate:oxidant, 1:100:200). No epoxidation occurred in the absence of catalyst. **SP1-C4** was not evaluated due to the low quantity of Ru anchored, as can be seen in section 5.2.2.

In the case of **SP2-C4**, a preliminary essay of the catalytic activity was performed using two different samples of the catalyst obtained through strategies 1b and 2, to check whether there was an influence of the heterogenization strategy on the catalytic performance. The substrate tested was styrene and the conversions obtained were similar thus confirming that the supports prepared through different strategies are comparable. Then, only the heterogeneous catalyst prepared though route 1b has been used for the rest of the substrates tested.

First of all, the reaction time for epoxidation was optimized for **SP2-C4**. Table **5.3** reports the conversion values for three alkene substrates registered at different periods. A first glance at Table **5.3** shows that for the aromatic substrates (styrene and *cis*-β-methylstyrene) total conversion was attained in 6 h reaction whereas for the aliphatic 4-vynilcyclohexene substrate longer reaction times were needed.

Table 5.3. Optimization of the reaction time on the catalytic oxidation of alkenes by **SP2-C4** using $PhI(OAc)_2$ as oxidant.[a]

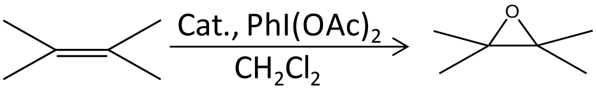

Substrate	Time (h)	Conversion (%)
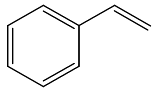	2	47
	4	88
	6	>99
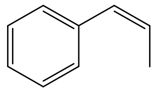	2	13
	4	96
	6	>99
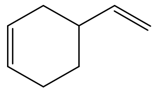	2	43
	6	86
	24	>99

[a] Conditions: **SP2-C4** (1 μmol Ru), substrate (100 μmol), $PhI(OAc)_2$ (200 μmol), CH_2Cl_2 (2.5 mL), 25^{o}C, biphenyl (100 μmol) as internal standard.

The recyclability of the heterogeneous catalytic systems was also investigated. After a first reaction run, the sample of **SP2-C4** catalyst used was centrifuged, washed with dichloromethane and settled together with a second load of substrate, solvent and oxidant. In the epoxidation of styrene, a reaction time of 6 h was set for each run (Figure **5.7a**) taking into account the time needed for complete conversion of this substrate (Table **5.3**). However, the conversion value decreased dramatically after the first run. Then, a similar experiment (Figure **5.7b**) was performed keeping each of the catalytic runs throughout 15 h and the conversion values were improved, indicating that the low conversion values obtained in the first case (6h per run) were the consequence of slow kinetics in heterogeneous phase and are not due to catalyst deactivation. On the other hand, as can be observed in Figure **5.7**, selectivity values above 70% were achieved for the epoxide product in all cases.

a)

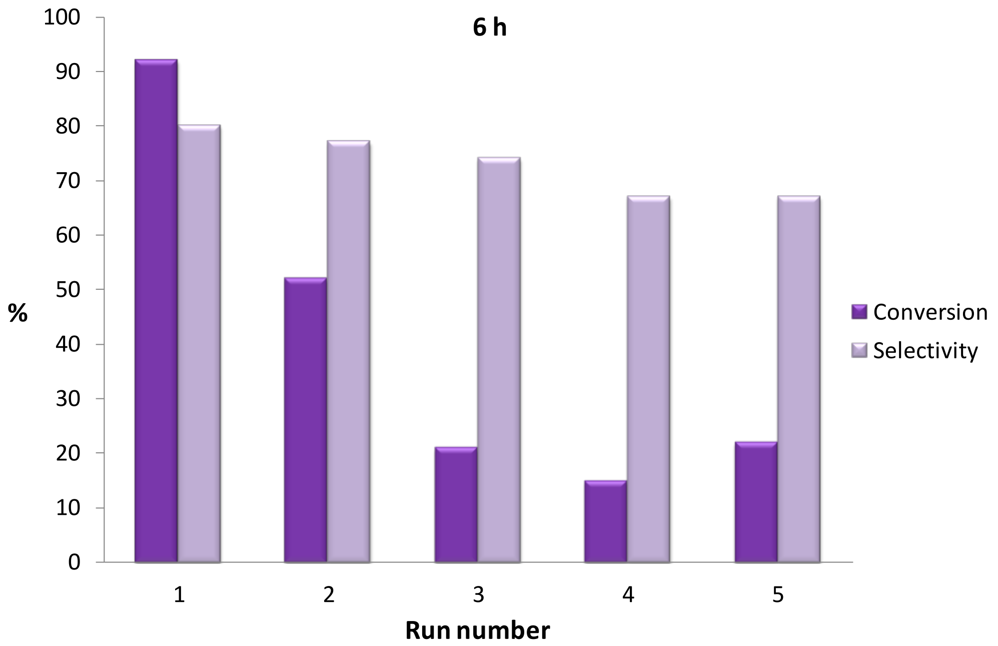

b)

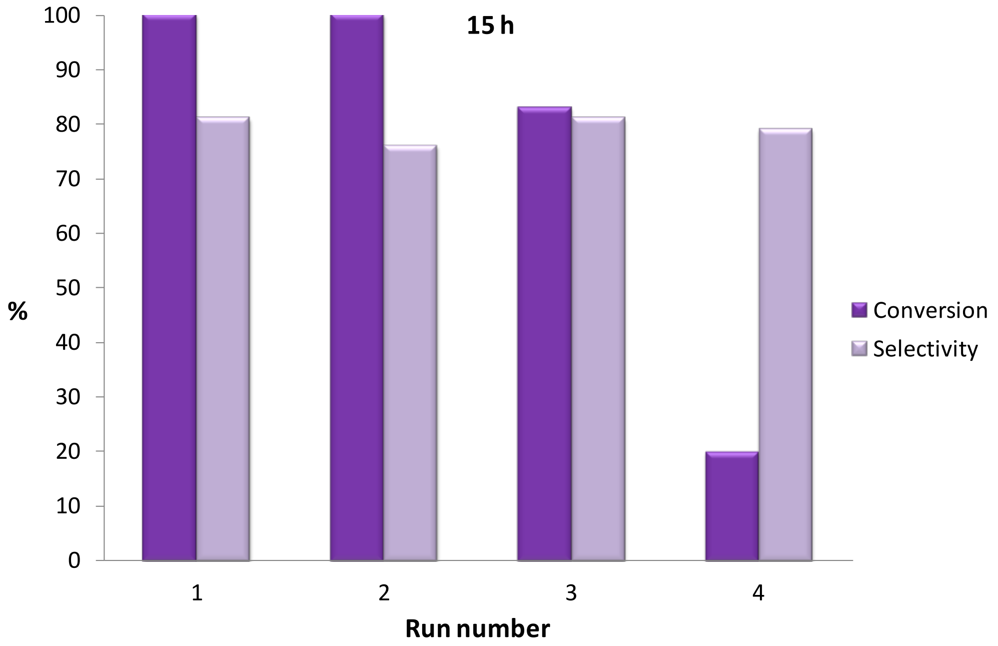

Figure 5.7. Conversion and selectivity values obtained throughout a number of consecutive reuses of catalyst **SP2-C4** in the epoxidation of styrene: a) 6 h per run; b) 15 h per run.

The recyclability of the catalytic **SP2-C4** system has been also investigated on other substrates. The results obtained for a number of consecutive runs on *cis*-β-methylstyrene, 4-vinylcyclohexene and 1-octene are displayed in Figures **5.8**-**5.10**.

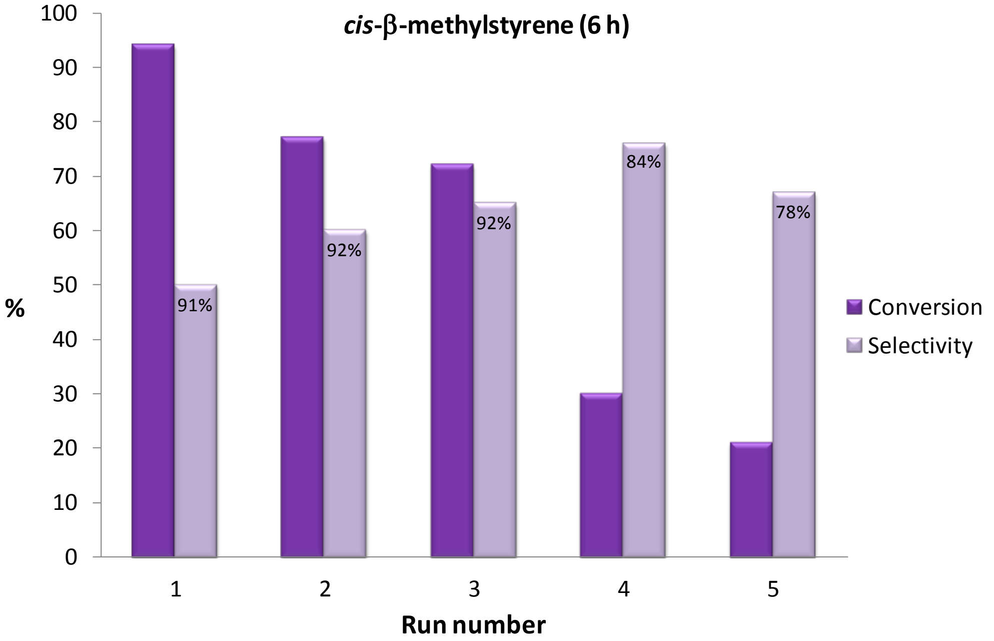

Figure 5.8. Conversion and selectivity values obtained throughout a number of consecutive reuses of complex **SP2-C4** in the epoxidation of *cis*-b-methylstyrene. The number on the column of selectivity represents the percent of *cis* isomer obtained.

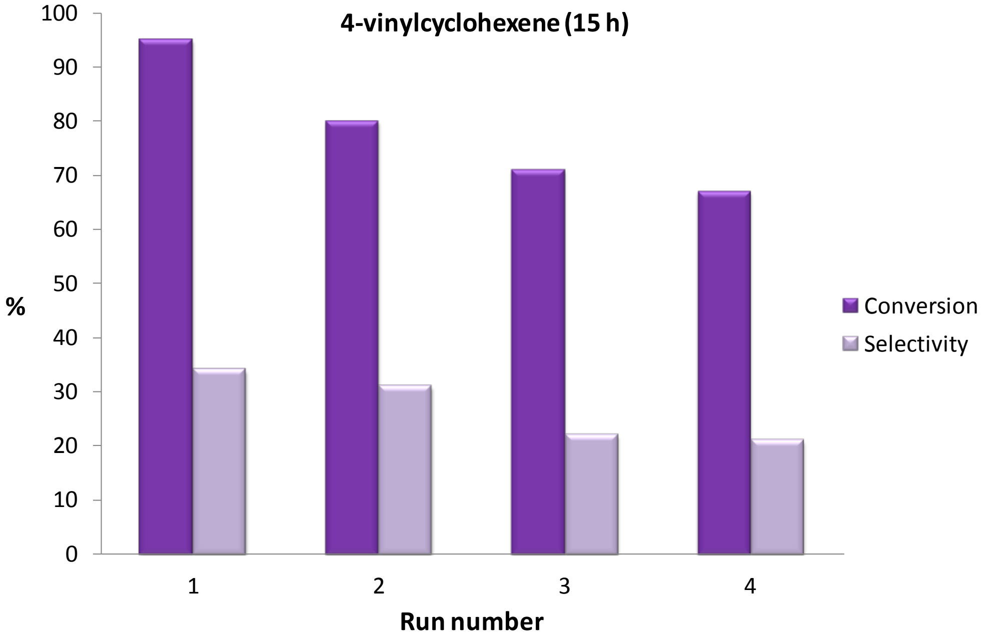

Figure 5.9. Conversion and selectivity values obtained throughout a number of consecutive reuses of complex **SP2-C4** in the epoxidation of 4-vinylcyclohexene.

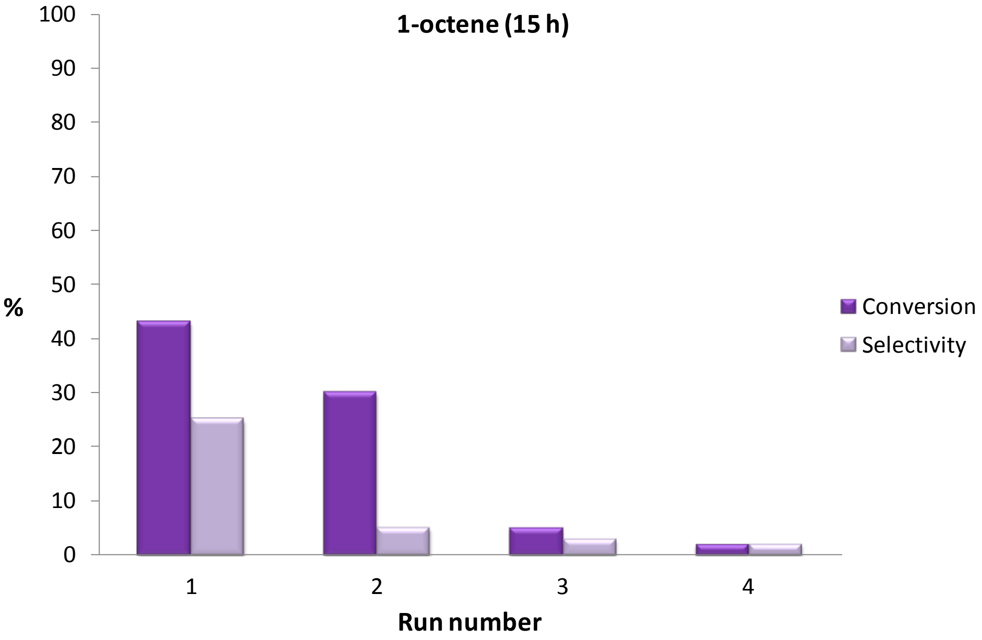

Figure 5.10. Conversion and selectivity values obtained throughout a number of consecutive reuses of complex **SP2-C4** in the epoxidation of 1-octene.

Figures **5.8**-**5.10** evidence that the catalyst maintains good conversion values for *cis*-β-methylstyrene and 4-vinylcyclohexene substrates for 3-4 runs whereas the less activated 1-octene displays much lower activity. The overall turnover numbers are 172 for *cis*-β-methylstyrene, 108 for 4-vinylcyclohexene and 12 for 1-octene. The selectivity for the epoxide is also well maintained except for this latest substrate, with a dramatic drop of selectivity at the second run and practically null conversion at the fourth run. In the case of *cis*-β-methylstyrene the stereoselectivity for the *cis*-epoxide is maintained around 80-90% through all the runs, whereas for 4-vinylcycloxexene the epoxidation takes place exclusively at the ring position in all cases. This stereoselectivity value is slightly lower than that obtained for the epoxidation of this substrate with complex **C4** in homogeneous phase (Chapter 4) which was practically stereospecific (>99%) and thus evidences an influence of the silica support on this behavior, probably slowing the closure of the ring in a potential radical intermediate species.[75,451]

The reusability of the **MSP-C4** system has been tested in the epoxidation of styrene under the same conditions. The results obtained are displayed in Figure **5.11**.

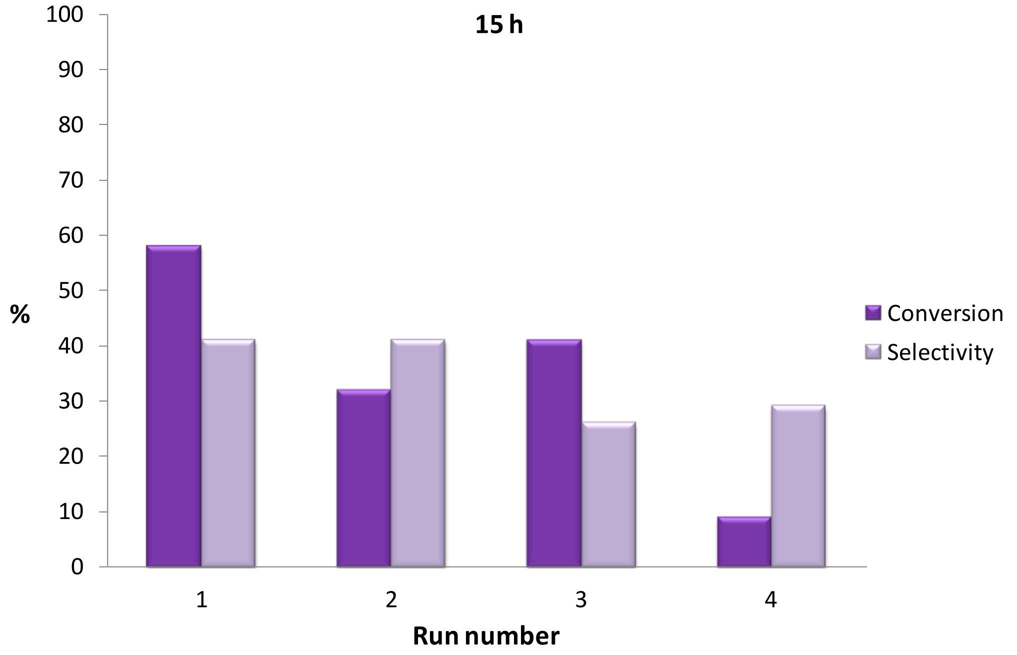

Figure 5.11. Conversion and selectivity values obtained throughout a number of consecutive reuses of catalyst **MSP-C4** in the epoxidation of styrene.

As it can be observed in Figure **5.11**, the overall values of conversion and selectivity are moderate to low in the epoxidation of styrene using **MSP-C4** as catalyst and are clearly lower than the results obtained for this substrate with catalyst **SP-C4** under the same reaction conditions. This is striking since the amount of Ru catalyst anchored is similar for **SP2** and **MSP** particles and thus an important influence of the silica heterogeneous support on the catalytic performance is manifested. The origin of this difference could arise from the enormous contrast in the surface area values between the two silica supports (886 m^2/g for **SP2** and only 25 m^2/g for **MSP**, see Table **5.1**), that would entail the molecules of anchored **C4** catalyst being placed much closer to each other at the **MSP** support, either hindering the approach of the substrate to the active site or alternatively favoring the catalyst self-deactivation. On the other hand, the pore volume is much higher for **MSP** (0.034 cm^3/g) than for **SP2** (0.002 cm^3/g) and this could involve slower kinetics for the approach and release of substrates/products within the pore region.

Catalyst leaching is an important problem which can lead to a progressive decrease of heterogeneous catalytic activity throughout the successive runs, and can also cause difficulty to unravel whether the activity arises from the heterogeneous or homogeneous (leached) catalyst. Thus, the amount of Ru complex was measured through ICP-AES in the reaction solvent for a whole set of reuses on a specific substrate. In all cases, the quantity of Ru present in the final solution was below the detection limit of the technique, a value that, at its maximum, would correspond to 1.8-2% of the initial Ru anchored. We can then assert that leaching of Ru is negligible for the heterogeneous systems described.

5.3.2. Catalytic hydration of nitriles

We have performed preliminary tests on the catalytic activity of the **SP2-C4** heterogeneous system for the hydration of nitriles under neutral conditions using water as solvent at 80^{o}C. Benzonitrile was chosen as test substrate and an initial conversion value around 10% after 20 hours of reaction was obtained. After reusing the catalyst in subsequent runs, the conversion decreased gradually. However, although the low performance, high values of selectivity for the amide product (>98%) were obtained in all cases. In order to improve the conversion values longer reaction times (up to 72 h) were checked. Under these conditions the conversion at the first run was improved (24%) but it dropped drastically at the second run.

In summary, in this chapter the heterogenization of complex **C4** was successfully achieved using three different strategies (1a, 1b and 2) on **SP1**, **SP2** and **MSP** supports. The supports have been fully characterized through physical measurements before functionalization, and by a variety of spectroscopic and electrochemical techniques after the Ru catalyst was anchored. The characterization of the functionalized supports indicates that the Ru species anchored is similar to that previously obtained in solution.

The heterogeneous system **SP2-C4** was effective in the epoxidation of a variety of olefin substrates and, in the case of *cis*-β-methylstyrene, the stereoselectivity for the *cis*-epoxide was maintained throughout the different runs, although it attained a value slightly lower than the analogous homogeneous catalyst **C4**, indicating an influence of the silica support. For **MSP**, the conversion and selectivity values obtained were moderate, manifesting a different effect of the **SP** and **MSP** substrates on the catalytic performance. Finally, the catalytic hydration of nitriles mediated by **SP-C4** resulted in a significantly lower performance when compared to the homogeneous **C4** system.

Chapter 6

Ru(II) complexes containing dmso and pyrazolyl ligands as catalysts for nitrile hydration in environmentally friendly media.

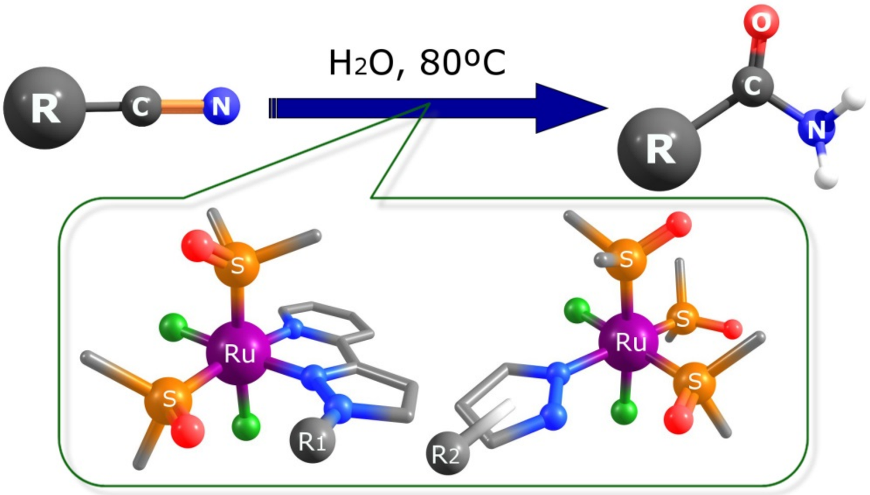

New efficient catalytic systems for nitrile hydrolysis to the corresponding amides in pure water or in glycerol as solvent are described. The catalysts employed are new ruthenium (II) complexes containing dmso and pyrazolyl ligands, which have been fully characterized through structural, analytical and spectroscopic techniques. Studies on linkage isomerization of dmso ligands and photoinduced substitution by solvent were carried out for some complexes. It is outstanding the conversion and selectivity obtained in the catalytic hydration of nitriles when using either aromatic or aliphatic substrates. The reuse of the catalysts has been explored for the first time in ruthenium-mediated nitrile hydration catalysis.

6.1. Synthesis and crystal structures

The schematic syntheses for all the complexes described in this chapter, together with the ligands used, are outlined in Scheme **6.1**. Reaction of equimolecular amounts of [RuCl$_2$(dmso)$_4$], **C2**, and the pypz-R$_1$ (R$_1$ = H, Me), R$_2$-pz-H (R$_2$ = H, CH$_3$, NO$_2$, CF$_3$) or Br-Hind ligands in methanol, ethanol or dichloromethane at reflux under nitrogen atmosphere and in the absence of light produces the *cis*-Cl *cis*-dmso complex **C5**, *cis*-Cl *trans*-dmso complex **C6** and the *cis*-Cl, *fac*-dmso complexes **C7**-**C11**, respectively (compound **C7** has been previously synthesized[426] but in this chapter, we introduce a new synthetic method together with a complete characterization of the complex). In the complexes, the nomenclature *cis* or *trans* refers to the relative position of two identical monodentate ligands (Cl or dmso).

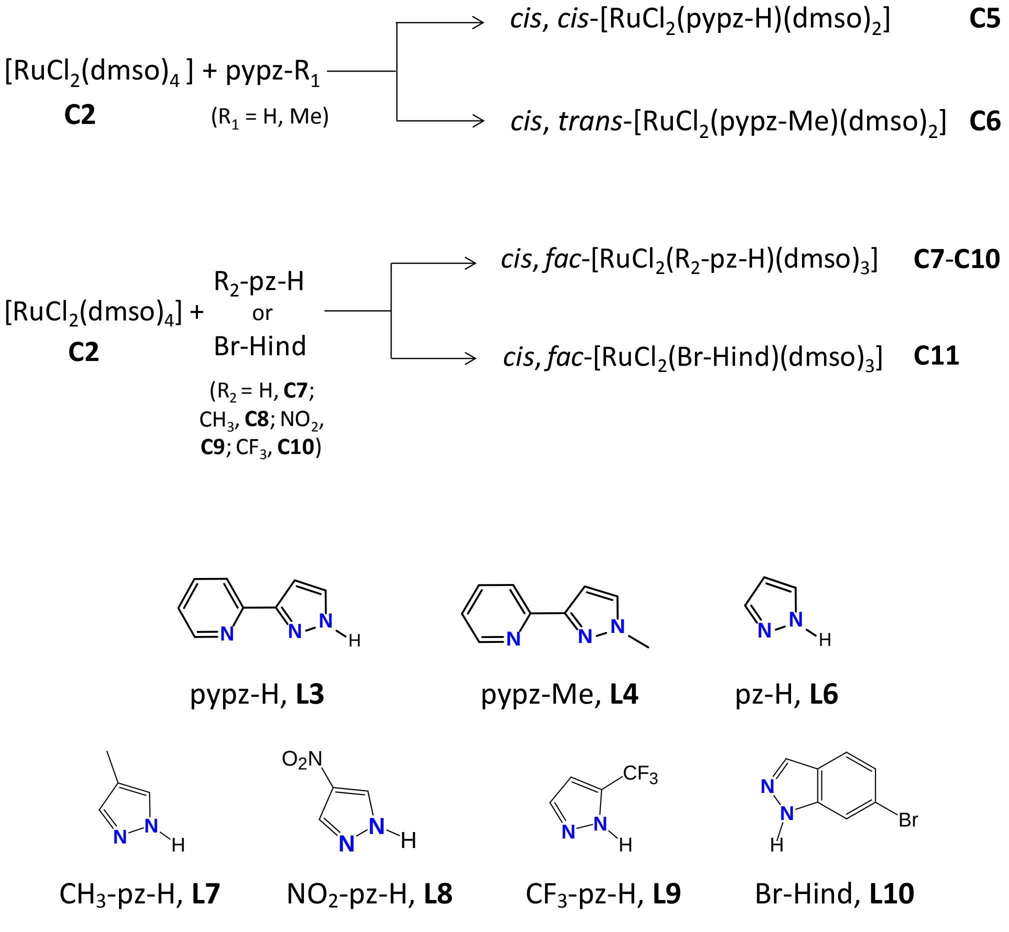
[RuCl2(dmso)4] + pypz-R1
C2
(R1 = H, Me)
cis, cis-[RuCl2(pypz-H)(dmso)2] C5
cis, trans-[RuCl2(pypz-Me)(dmso)2] C6
[RuCl2(dmso)4] + R2-pz-H or Br-Hind
C2
(R2 = H, C7; CH3, C8; NO2, C9; CF3, C10)
cis,fac-[RuCl2(R2-pz-H)(dmso)3] C7-C10
cis,fac-[RuCl2(Br-Hind)(dmso)3] C11
pypz-H, L3
pypz-Me, L4
pz-H, L6
CH3-pz-H, L7
NO2-pz-H, L8
CF3-pz-H, L9
Br-Hind, L10

Scheme 6.1. Synthetic strategy **C5**-**C11** and ligands used.

The substitution of two dmso ligands in **C2** by the unsymmetrical ligand pypz-R_1 (R_1 = H, Me) can potentially lead to six different stereoisomers (including two pairs of enantiomers) for complexes **C5** and **C6** which are depicted in Scheme **6.2a**, whereas three different isomers can be formed for complexes **C7**-**C11** (Scheme **6.2b**).

a)

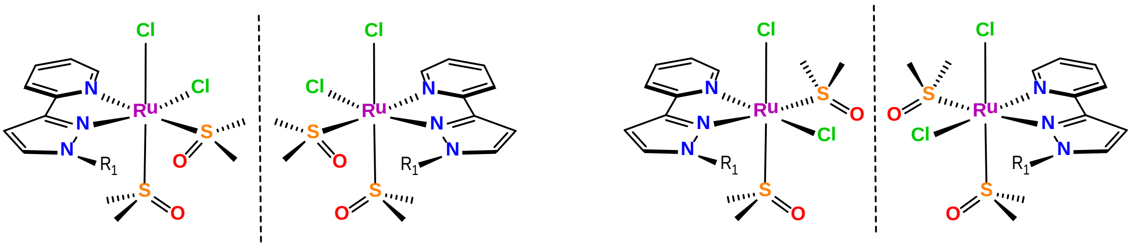

Δ *cis*-Cl *cis*-dmso **(a)** Λ *cis*-Cl *cis*-dmso **(a)** Λ *cis*-Cl *cis*-dmso **(b)** Δ *cis*-Cl *cis*-dmso **(b)**

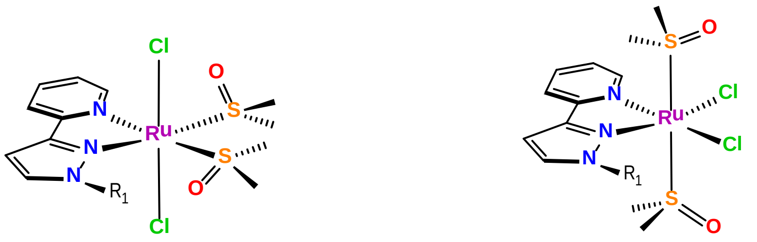

trans-Cl *cis*-dmso **(c)** *cis*-Cl *trans*-dmso **(d)**

b)

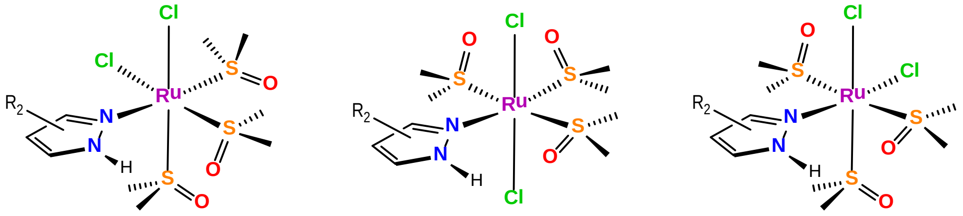

cis-Cl *fac*-dmso **(e)** *trans*-Cl *mer*-dmso **(f)** *cis*-Cl *mer*-dmso **(g)**

Scheme 6.2. Possible stereoisomers for complexes: a) **C5**, **C6** and b) **C7**-**C11**.

It is remarkable that we have detected a single geometrical isomer for all the complexes described except for compounds **C6** and **C11**, either when the reflux time is limited to 15' or when it is extended up to 24h. For complex **C5** the pair of enantiomers Λ/Δ-**(a)** has been isolated, whereas for complexes **C7-C10** the *cis*-Cl *fac*-dmso **(e)** isomer is specifically obtained. The formation of a single isomer in this type of compounds can be rationalized taking into account the following structural and electronic factors:

a) Ru(II) is a d^6 ion, it forms strong bonds with N-donor ligands and they do not exchange in solution with other coordinated ligands, thus minimizing geometrical reorganization after pypz-R_1 or R_2-Pz-H coordination.[453,454]

b) The existence of a strong hydrogen bonding between the oxygen atom of a dmso ligand and the pyrazolic hydrogen atom (Scheme **6.2**).

c) The synergistic π-donor and π-acceptor effects among the Cl and dmso ligands mutually placed in *trans*.

In complex **C5**, all these factors account for the formation of the **(a)** isomer, which presents a *trans* relative disposition of Cl and dmso ligands together with a dmso-$H_{pyrazolyl}$ hydrogen bond. However, for the structurally similar compound **C6** we have detected a mixture of two different isomers independently of the refluxing time. The major isomer found is surprisingly the *cis*-Cl *trans*-dmso-**C6d** compound that was separated and isolated, and for which the X-ray structure has been solved (see Figure **6.1**). From ^{1}H-NMR experiments (Figure **S6.9a**) we have tentatively postulated that the minor isomer obtained together with **C6d** is Λ/Δ *cis*-Cl *cis*-dmso-**C6a** since a doublet signal is found at δ around 9.6 ppm that can be presumably assigned to the highly deshielded 2-pyridyl H1 atom in *cis* position with regard to a Cl ligand (see **6.1** for the numbering scheme). This is the case for the major **C6d** isomer (δ = 9.5 ppm) and also for other Ru complexes containing Cl and pyridyl ligands in *cis* such as the trpy-P chloridocomplexes described in Chapter 4. The preference for the **C6d** isomer in this case, where the formation of pyazolyl H-bonds is not possible, is not easy to explain but is probably governed by steric factors that place the two bulky dmso ligands in *trans* to each other.

Regarding the tris(dmso) complexes **C7**-**C10**, the *cis*-Cl *fac*-dmso **(e)** isomer formed is the one that best fulfills the structural and electronic factors mentioned above and the compounds are specifically obtained under this form. Complex **C11** is a mixture of isomers but with **C11e** also being the major form (NMR spectra are gathered in Figure **S6.14**). The minor isomer displays the signal corresponding to the pyrazole H7 atom (see Figure **6.2** for numbering scheme) upfield when compared to the chemical shift in **(e)**, which is in accordance with this H7 atom being in *cis* to a dmso ligand instead of a Cl ligand, a conformation consistent with **(f)** and **(g)** isomers. In this case, we could postulate the minor isomer to be **C11g** because it settles a *trans* Cl-Ru-dmso axis in contrast to the more disfavored Cl-Ru-Cl *trans* disposition in **(f)**. However, isolation of the minor isomer would be necessary to confirm this hypothesis.

The crystal structures of complexes **C5**-**C11** have been solved by X-ray diffraction analysis. Figures **6.1** and **6.2** display the molecular structure of all complexes whereas their main crystallographic data and selected bond distances and angles can be found in the Supporting Information section (Tables **S6.1**-**S6.3** and **S6.5**). In all cases, the Ru metal center adopts an octahedrally distorted type of coordination. In complex **C5** and **C6**, the pypz-R_1 ligand acts in a didentate fashion and the other coordination sites are occupied by two chlorido and two dmso ligands, which adopt a *cis* coordination with respect to each other in the case of **C5.** For complex **C6**, the two dmso ligands are disposed in a *trans* position whereas the two chlorido ligands adopt a *cis* coordination. In complexes **C7**-**C11**, the corresponding pyrazol or indazol ligand is coordinated *trans* respect to one dmso ligand which is in facial disposition with the two remaining dmso. The two chlorido ligands adopt a *cis* coordination. All bond distances and angles are within the expected values for this type of complexes.[103,455- 459]

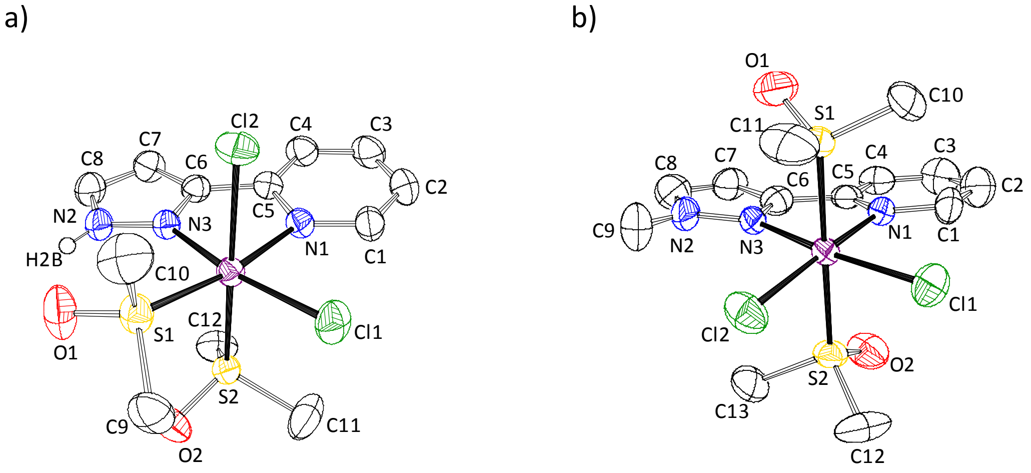

Figure 6.1. Ortep plot and labeling schemes for compounds **C5** and **C6**.

For complex **C5**, it is interesting to note that the Ru-N1 bond length (2.123 Å), where the pyridyl N atom is placed *trans* to the S atom of dmso, is larger than the distance found for Ru-N3 (2.031 Å) bond, where the ligand in *trans* with respect to the pyrazole ring is a Cl atom. This denotes the stronger *trans* influence of the dmso ligand with respect to the chlorido ligand, since a shorter Ru-N bond distance should be expected for the more π-acceptor pyridyl ring as is the case in complex **C6**, where both Ru-N1 and Ru-N3 bond lengths are similar (about 2.06 Å).

For **C5** and **C6**, the N(1)-Ru(1)-N(3) angles are 76.92(6)˚ and 77.7(2)˚ showing the geometrical restrictions imposed by the didentate ligands, which are considered to define the equatorial plane of the structure; as a consequence of this, the rest of the equatorial angles are in most of cases larger than the 90^o expected for an ideal octahedral geometry.

As we have mentioned previously, complexes **C5**, and **C7**-**C11** display strong hydrogen bonds between the oxygen atoms of the equatorial dmso ligands and the hydrogen atoms of the corresponding pyrazole or indazol rings (H(2b)-O(1) = 2.194 Å, **C5**; H(2D)–O(1) = 2.012 Å, **C7**; H(2)–O(3) = 2.012 Å, **C8**; H(2A)–O(5) = 1.86 Å, **C9**; H(2)–O(1) = 1.891 Å, **C10**; H(2B)–O(3) = 1.952 Å, **C11**). In the case of complexes bearing monodentate ligands these H-interactions are stronger than the analogous bonds found in complex **C5** containing the didentate pypz-H ligand, due to the lower geometrical restrictions of the monodentate R_2-pz-H ligands with respect to pypz-H.

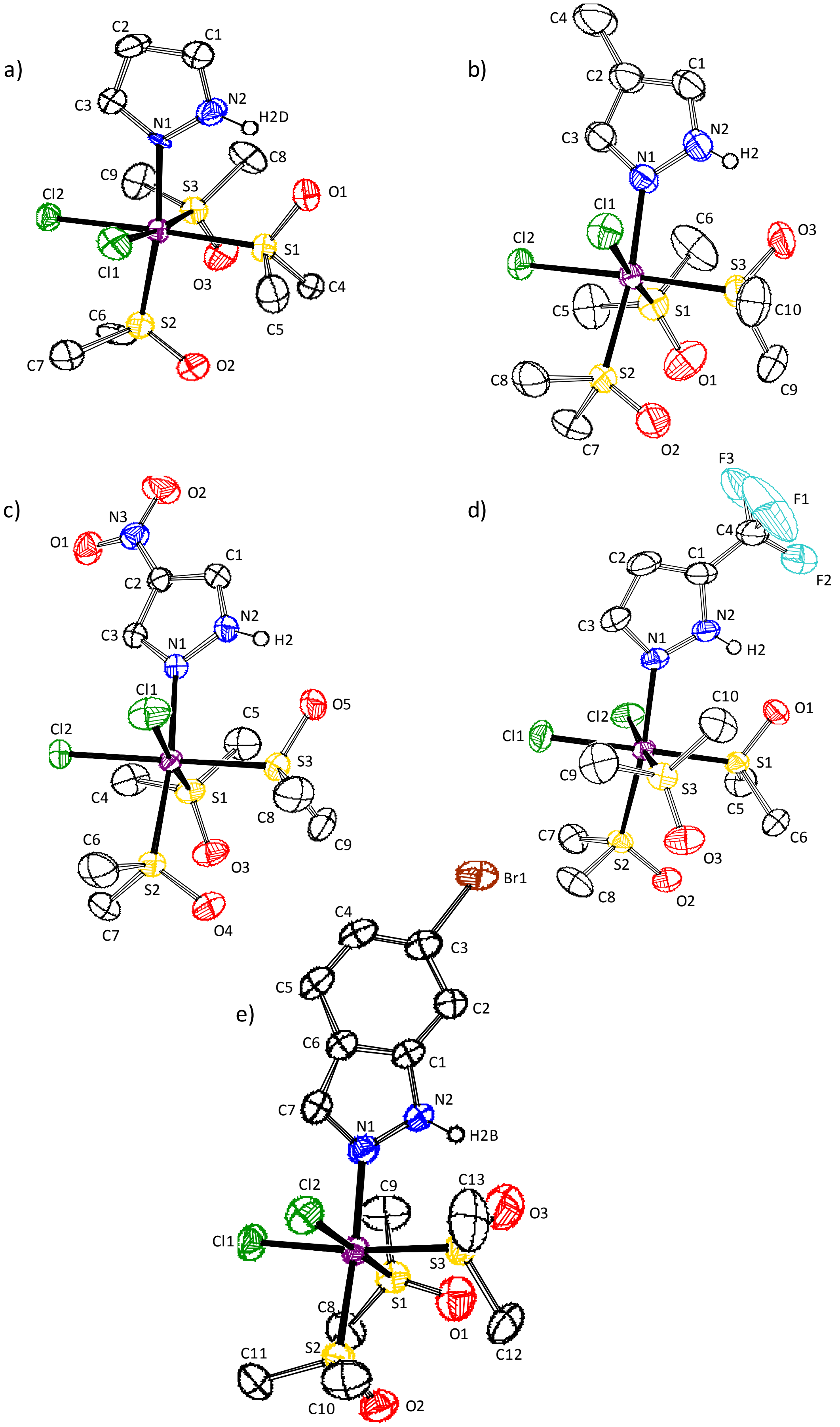
a)
C2
C1
C3
N2
H2D
N1
C9
C8
Cl2
S3
O1
Cl1
O3
S1
C4
C5
C6
S2
C7
O2
b)
C4
C1
C2
C3
N2
H2
N1
Cl1
C6
O3
Cl2
S3
C5
S1
C10
O1
C8
S2
C9
C7
O2
c)
O2
N3
O1
C1
C2
N2
C3
N1
H2
Cl1
O5
C5
Cl2
S3
C4
S1
C8
C9
C6
O3
S2
O4
C7
d)
F3
F1
C4
C2
C1
F2
N2
C3
N1
H2
C10
O1
Cl2
Cl1
S1
C9
S3
C5
C7
C6
O3
S2
C8
O2
Br1
C4
C3
C5
C2
e)
C6
C1
N2
C7
N1
H2B
Cl2
C9
C13
O3
Cl1
S3
S1
C8
O1
C12
C11
S2
C10
O2

Figure 6.2. Ortep plots and labeling schemes for compounds **C7**-**C11**.

It is interesting to note that in **C7**-**C11** , where the pyrazolyl ring has a dmso ligand in *trans* position, the Ru-N_{pz} bond length is larger than the analogous distance observed for complexes **C5** and **C6**, where a Cl ligand is located in *trans*, again evidencing the *trans* influence of dmso respect to the chlorido ligand (Ru-N_{pz} bond distances: Ru-N(1): 2.145 Å, **C7** and **C10**; 2.146 Å, **C8**; 2.12 Å, **C9**; 2.141 Å, **C11**, whereas Ru-N(3): 2.031 Å for **C5** and 2.058 Å for **C6**).

6.2. Spectroscopic properties

The IR spectra for all complexes (Figures **S6.1**-**S6.7**) show a band around 1100-1090 cm^{-1} that can be assigned to a $\upsilon_{S=O}$ stretching, and the absence of any significant vibration in the 930-920 cm^{-1} range indicates a sulfur-bonded dmso complex,[103,434,458] as confirmed by the X-ray structures obtained.

The one-dimensional (1D) and two-dimensional (2D) NMR spectra of complexes **C5**-**C11** were registered in CD_3CN, CD_2Cl_2 or methanol and are presented in Figure **6.3** and in the Supporting Information (Figures **S6.8**-**S6.14**). The resonances found for all complexes are consistent with the structures obtained in the solid state. The complexes exhibit two sets of signals: one in the aromatic region corresponding to the N-donor ligands and the other one in the aliphatic region assigned to the methyl groups of the bonded dmso ligands and to the pyrazole methyl group of complex **C6**. In all cases, the resonances of the aromatic region are easily identified through the COSY and NOESY spectra.

Complex **C5** and **C6** are asymmetric molecules and they generate four different methyl resonances for the dmso ligands. In **C5**, the resonances at lower chemical shift (2 and 3.02 ppm) are assigned to the C11 and C12 methyl groups of the axial dmso ligand, due to the anisotropic effect of the aromatic ligand. On the other hand, the resonances of C9 and C10 methyl groups (found at 3.52 and 3.54 ppm) for the equatorial dmso ligand are influenced by the deshielding effect of the close Cl ligands. In the aromatic region, the pyrazolic hydrogen H2b is easily identified downfield at 13.10 ppm. On the other hand, the deshieding effect exerted by the equatorial Cl ligand over the alfa pyridyl H1 atom allows its identification at δ = 9.43 ppm.

In the case of complex **C6**, the resonances at lower chemical shift are assigned to methyl groups C10 and C12 (2.93 ppm) thanks to the NOE effects: a NOE resonance is observed between H10/H12 and the pyridyl hydrogen H1 (9.50 ppm) whereas a second one is found between C11/C13 (3.10 ppm) with the methyl group C9 (4.28 ppm).

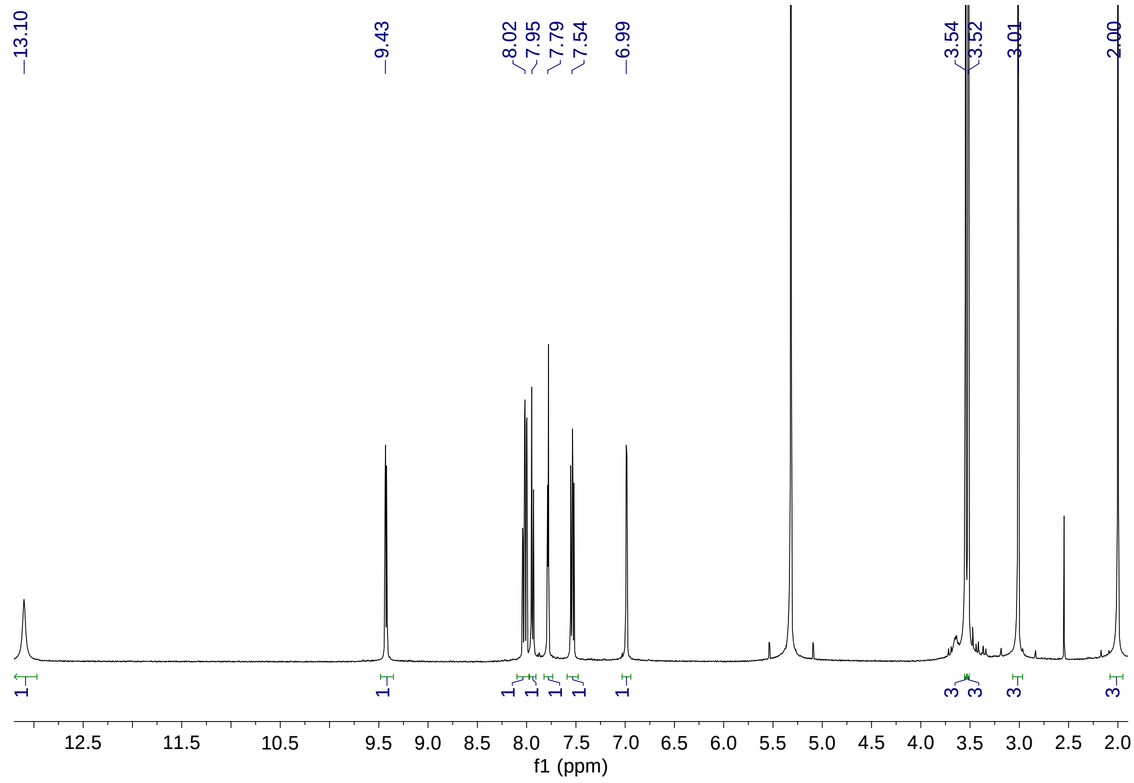

Figure 6.3. ^{1}H-NMR spectrum of **C5**, 400 MHz, CD_2Cl_2.

Complexes **C7**-**C11** show three resonances corresponding to the dmso ligands with no magnetically equivalent methyl groups per ligand. NOE effects observed between the pyrazolic hydrogen and two methyl groups in these compounds allow identifying two of the dmso ligands unambiguously; the resonances of the remaining dmso ligands are tentatively assigned on the basis of the deshielding effect produced by the two Cl ligands (see Chapter 3).

The UV-Vis spectra of complexes **C5**-**C11** are displayed in Figure **6.4** and in the Supplementary Information (Figures **S6.15**-**S6.18**) and the spectral features of complexes are presented in the experimental section and in Table **6.1**. The complexes exhibit very intense ligand based π-π* bands below 300 nm and relatively intense bands above 300 nm mainly due to dπ-π* MLCT transitions.[435]

Table 6.1. UV-vis spectroscopic features in CH_2Cl_2 for complexes **C5**-**C11**.

Compound	**λmax, nm (ε, $M^{-1}\cdot cm^{-1}$)**
$[Ru^{II}Cl_2(pypz\text{-}H)(dmso)_2]$, **C5**	264 (27904), 320 (4150), 408 (1914)
$[Ru^{II}Cl_2(pypz\text{-}Me)(dmso)_2]$,**C6**	277 (21913), 366 (5669)
$[Ru^{II}Cl_2(pz\text{-}H)(dmso)_3]$, **C7**	356 (463)
$[Ru^{II}Cl_2(CH_3\text{-}pz\text{-}H)(dmso)_3]$, **C8**	359 (574)
$[Ru^{II}Cl_2(NO_2\text{-}pz\text{-}H)(dmso)_3]$, **C9**	310 (329)
$[Ru^{II}Cl_2(CF_3\text{-}pz\text{-}H)(dmso)_3]$, **C10**	356 (560)
$[Ru^{II}Cl_2(Br\text{-}Hind)(dmso)_3]$, **C11**	280 (10931), 343 (532)

In general, the lower aromatic character of the monodentate R_2-pz-H ligands when compared to didentate pypz-R_1 involves ligand orbitals of higher energy for the former and, consequently, provokes a blue-shift of the dπ-π* bands for complexes **C7**-**C11** when compared to **C5** and **C6**, in parallel with a decrease of the molar extinction coefficients. The intraligand π-π* bands are also affected in a similar manner and, for complexes **C7**-**C10**, these bands are sufficiently blue-shifted as to be out of the solvent range. It is striking to see that complex **C11**, which contains the conjugated Br-Hind ligand, displays lower energy π-π* absorptions that can be indeed observed at wavelengths above 250 nm. However, the aromatic ring in this case is not directly bound to the ruthenium metal center and thus the energy of the dπ-π* bands in **C11** are not affected to a significant extent.

Figure **6.4** displays the UV-vis spectra of complexes **C5**, **C6** and **C7**. As can be observed, the substitution of a H atom in the pypz-H ligand by a methyl group induces an hypsochromic shift of the dπ-π* absorptions that would be in accordance with an enhanced electron density donation from the pypz-H ligand to the metal, thanks to a certain acidity of the ligand.

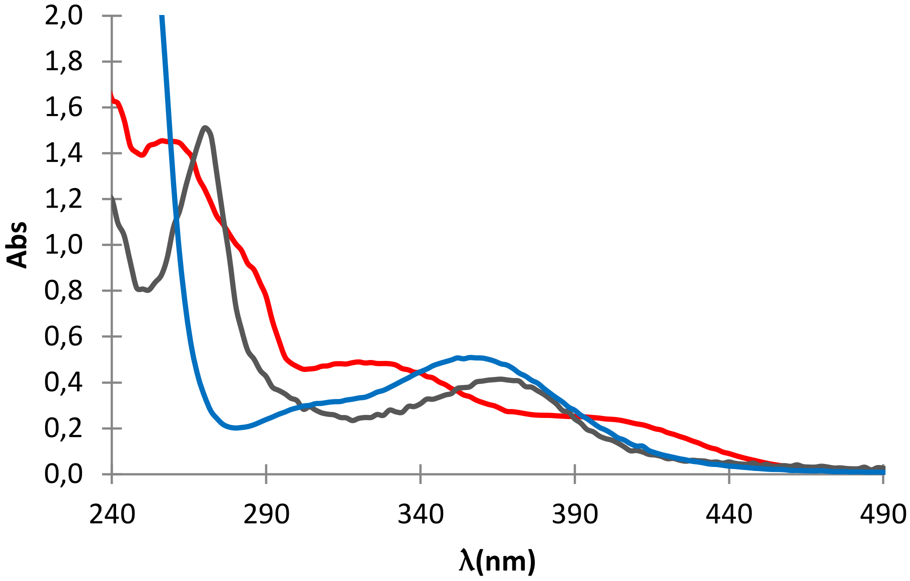

Figure 6.4. UV-visible spectra of 0.1 mM solutions of **C5** (red) and **C6** (grey) and a 1.1 mM solution of **C7** (blue), in CH_2Cl_2.

6.3. Electrochemical properties and linkage isomerization

The redox properties of complexes **C5**-**C11** have been determined by cyclic voltammetry (CV) experiments that are displayed in Figures **6.5**, **6.6** and in the Supporting Information (Figures **S6.19**-**S6.21**). The electrochemical data of complexes are presented in Table **6.2**. In the case of complexes **C7**-**C11**, a quantitative dmso linkage isomerization takes place (see below) and the values given in Table **6.2** are the corresponding anodic and cathodic peak potential values.

Table 6.2. Electrochemical data (CH_3CN +0.1M TBAH *vs*. Ag/AgCl) for complexes **C5**-**C11**.

Compound	$E_{1/2}$ (III/II) (V)	E_{pa} (V) [Ru^{II}-S→ Ru^{III}-S]	E_{pc} (V) [Ru^{II}-O→ Ru^{III}-O]
[$Ru^{II}Cl_2$(pypz-H)(dmso)$_2$], **C5**	0.98[a] (1.09)[b]		
[$Ru^{II}Cl_2$(pypz-Me)(dmso)$_2$],**C6**	0.92[a,b]		
[$Ru^{II}Cl_2$(pz-H)(dmso)$_3$], **C7**		1.60	0.82
[$Ru^{II}Cl_2$(CH_3-pz-H)(dmso)$_3$], **C8**		1.49	0.75
[$Ru^{II}Cl_2$(NO_2-pz-H)(dmso)$_3$], **C9**		1.62	0.86
[$Ru^{II}Cl_2$(CF_3-pz-H)(dmso)$_3$], **C10**		1.73	0.85
[$Ru^{II}Cl_2$(Br-Hind)(dmso)$_3$], **C11**		1.66	0.85

[a] *vs*. SCE; [b] in CH_2Cl_2 +0.1M TBAH

Complexes **C5** and **C6**, containing didentate pypz-R_1 (R_1 = H, Me) ligands, exhibit reversible monoelectronic Ru(III/II) redox waves at $E_{1/2}$ values of 0.98 and 0.92 V *vs.* SCE, respectively (the different solvent used is not expected to significantly influence the potential value). We can observe that the redox potential value slightly decreases in complex **C6**, and this can be due to the presence of the CH_3 substituent in the pypz ligand, which is of σ-donor character and thus provokes the stabilization of the Ru(III) species. On the other hand, the different geometry of the two complexes could also have an influence on the redox potential as has been described for other Ru complexes with N-donor ligands,[76,93,460] though this factor is expected to exert little influence.

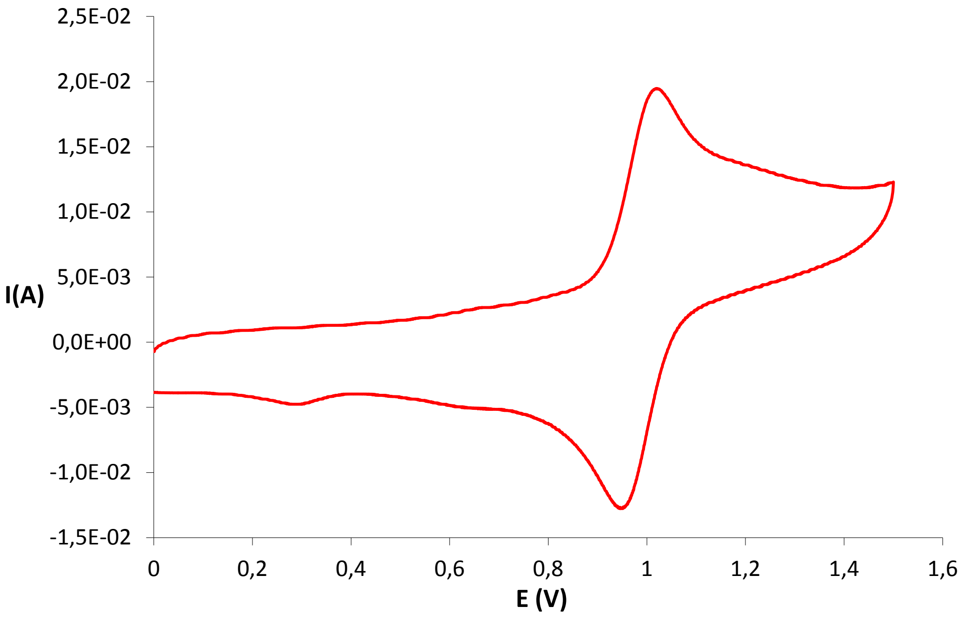

Figure 6.5. Cyclic voltammogram of **C5** in CH_3CN.

For complexes **C7**-**C11**, containing monodentate R_2-pz-H ligands, the electrochemically irreversible CVs obtained suggest the occurrence of a quantitative dmso ligand linkage isomerization process in all cases (see below) yielding irreversible redox waves and consequently a comparison can be done only on the basis of the anodic E_{pa} values. As can be observed in Table **6.2**, a slight increase in the oxidation potential values, E_{pa} [Ru^{II}-S→Ru^{III}-S], for complexes **C7**-**C11** takes place along with the stronger π-acceptor capacity of the nitrogen ligands. This trend is in line with the electronic characteristics of the R_2 substituents on the pyrazole ligands. Thus compound **C8**, containing a methyl σ-donor substituent, presents the lowest E_{pa} value whereas complexes **C9**-**C11,** containing electron withdrawing substituents, display higher E_{pa} values than **C7**, with an unsubstituted pyrazole. However, the effect of the electron-withdrawing substituents in the potential values is clearly stronger for complex **C10**, containing the CF_3-pz-H ligand. This fact could be due to the more extensive electronic delocalization of the NO_2- and Ph- substituents over the pyrazolic ring in **C9** and **C11**, which would presumably favour a weaker π-acceptor character of these ligands and therefore a moderate increase of the E_{pa} value.

On the other hand, when comparing the $E_{1/2}$ value obtained for **C5** with the E_{pa} [Ru^{II}-S → Ru^{III}-S] oxidation process of **C7**, the formal substitution of the pyridyl ring of the pypz-H ligand present in **C5** by a third dmso ligand in **C7** shifts the Ru^{III}-S/Ru^{II}-S potential value to clearly upper values owing of the higher π-acceptor capacity of the dmso ligand. This shift to higher $E_{1/2}$ values is shown by all the pyrazole complexes **C7**-**C11** though with small differences arising from the distinctive substituents on the corresponding R$_2$-Pz-H ligands.

As mentioned above, the pyrazole complexes **C7**-**C11** undergo a dmso linkage isomerization process. This can be illustrated by the cyclic voltammogram of **C8** in acetonitrile at a scan rate of 0.1 V and starting the potential scanning at E_{init} = 0 V (see Figure **6.6**, blue line). The CV shows an anodic wave at E_{pa} = 1.49 V *vs* Ag/AgCl, which corresponds to the oxidation of Ru^{II}(dmso-S) species to Ru^{III}(dmso-S) (the notation *dmso-S* indicates that the dimethylsulfoxide ligand is coordinated to ruthenium via the sulfur atom). This species undergoes a fast linkage isomerism forming Ru^{III}(dmso-O), see Scheme **6.3**. Upon scanning to low potential, the isomerized species undergoes reduction at E_{pc}= 0.75 V to form Ru^{II}(dmso-O) and then rearranges restoring the initial complex. This shift to lower potential values (0.75 vs 1.49 V) for the O-coordinated dmso complex is due to the lower electron-withdrawing ability of the O-coordinated dmso, then making the upper oxidation states of Ru more accessible.

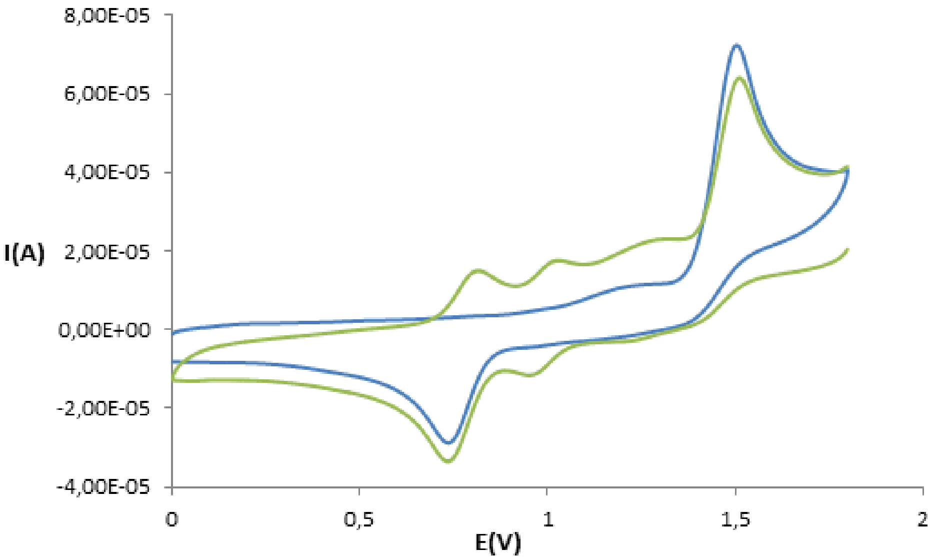

Figure 6.6. Cyclic voltammetry for complex **C8** in CH_3CN starting the scanning at E_{init} = 0 V (blue) and at E_{init} = 1.8 V applying an equilibration time of 10 min (green).

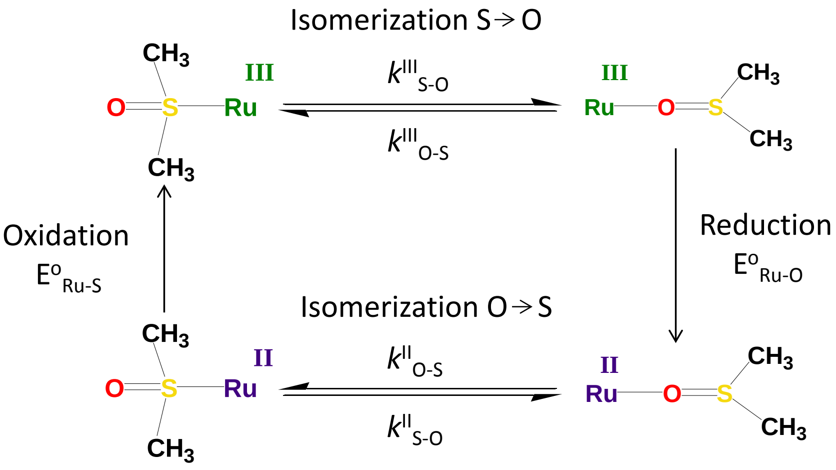
Isomerization S→O
$k^{III}_{S\text{-}O}$
$k^{III}_{O\text{-}S}$
III
III
Oxidation
$E^o_{Ru\text{-}S}$
Reduction
$E^o_{Ru\text{-}O}$
Isomerization O→S
$k^{II}_{O\text{-}S}$
$k^{II}_{S\text{-}O}$
II
II

Scheme 6.3. Isomerization and redox processes of a Ru-dmso complex.

This isomerization process becomes more evident by starting the potential scanning at E_{init} = 1.8V and applying an equilibration time of 10 minutes prior to the cathodic scan (see Figure **6.6**, green line). As can be observed an additional reversible wave appears at $E_{1/2}$= 0.98 V, corresponding probably to the substitution of one dmso ligand by acetonitrile that may have taken place during the 10-minutes oxidation period.

The behavior displayed by complex **C8** is also shown by the whole set of R_2-pz-H complexes **C7**-**C11**, with comparable shifts for the respective potential values upon isomerization (Table **6.2**). These values of shifts are in the same range as those observed in complexes where only one dmso ligand isomerizes,[96,119,461-462] suggesting that such is the case for complexes **C7**-**C11** during the electrochemical process. To the best of our knowledge, compounds **C7**-**C11** are the first reported $Ru(dmso)_3$ species displaying this type of isomerization linkage that had been previously described only for Ru compounds containing one or two dmso ligands[96,119,461-462]

On the other hand, pypz-R_1 complex **C5** also undergoes a dmso linkage isomerization process, though it is not complete on the scale time of the cyclic voltammetry. A throughout kinetic study has been carried out on the linkage isomerization experimented by complexes **C5** and **C8**, following the method described in the literature by Nicholson and Shain[463] and detailed step by step below.

The scan rates (υ) directly influence the intensity of waves of the cyclic voltammograms and this dependence provides information about the participation of chemical reactions coupled with electrochemical processes as is the example of dmso linkage isomerization shown in Scheme **6.3**. From the scan rate dependent cyclic voltammograms, it is possible to estimate the linkage isomerism rates and equilibrium constants. We have calculated these constants for compounds **C5** and **C8** both containing pyrazolyl type of ligands and the results have been compared with other Ru complexes described in the literature. To do so, cyclic voltammetries at different scan rates, starting the potential scanning from the lower and upper points of the CV range, have been registered for both complexes in CH_2Cl_2 (chosen as solvent with the idea to avoid ligand solvolysis). Figures **6.7** and **6.8** show the corresponding CV obtained for complex **C5**, whereas those corresponding to complex **C8** are displayed in Figures **6.9** and **6.10**.

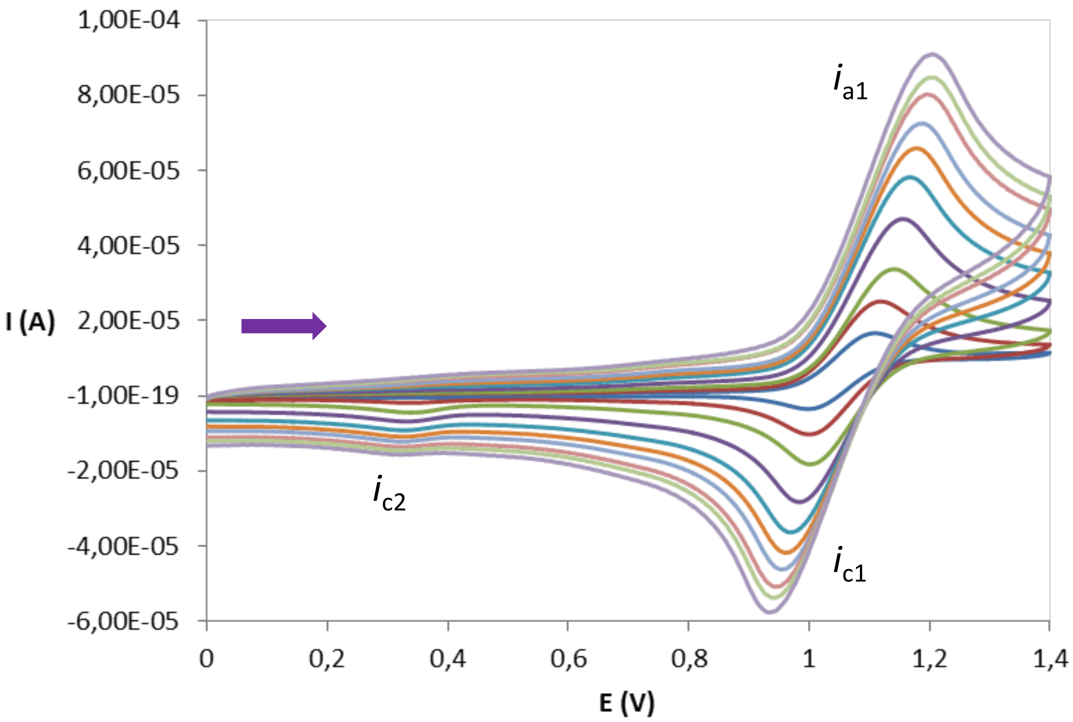

Figure 6.7. Cyclic voltammograms of **C5** in CH_2Cl_2 (TBAH, 0.1M) vs Ag/AgCl starting from E_{init} = 0 V. Arrow indicates initial scan direction; scan rate: 0.20 - 8 V/s.

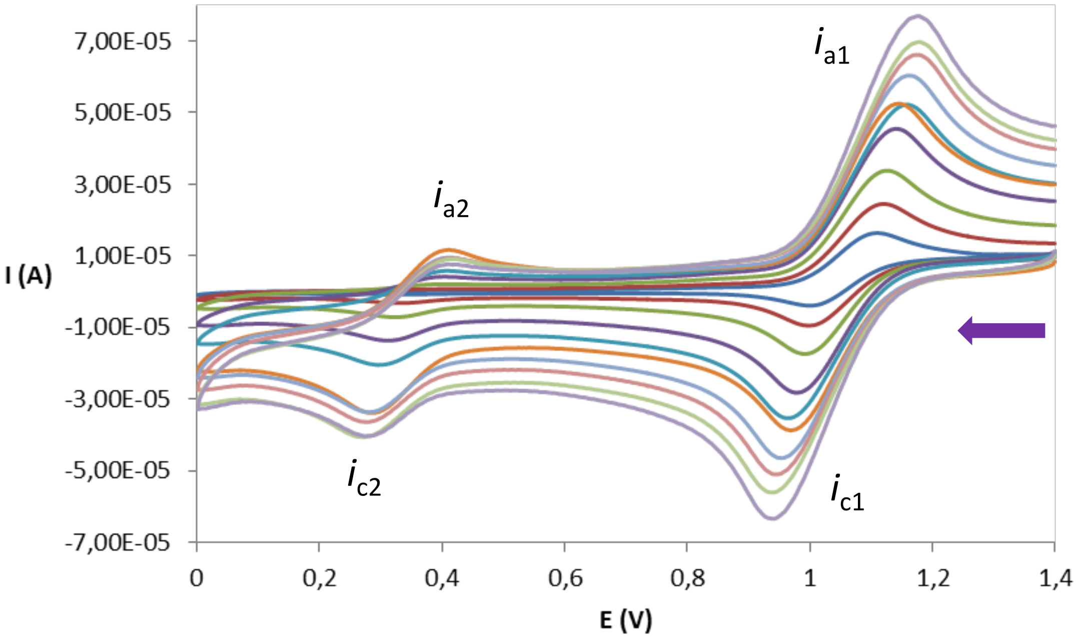

Figure 6.8. Cyclic voltammograms of **C5** in CH_2Cl_2 (TBAH 0.1M) vs Ag/AgCl starting from E_{init} = 1.4 V. Arrow indicates initial scan direction; scan rates: 0.20 - 8 V/s.

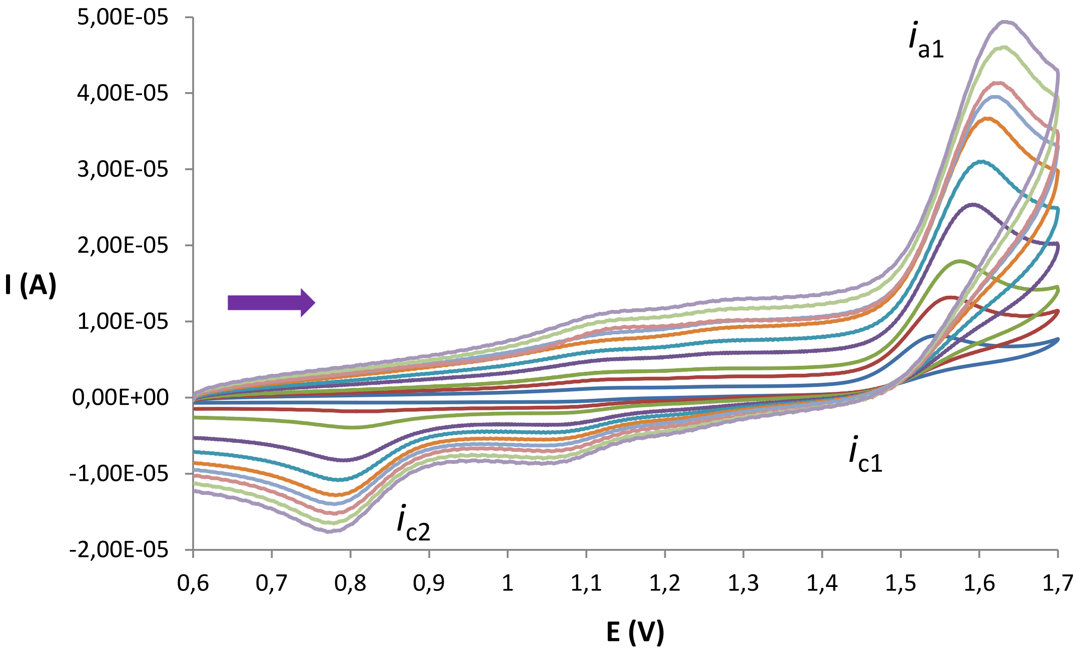

Figure 6.9. Cyclic voltammograms of **C8** in CH_2Cl_2 (TBAH, 0.1M) vs Ag/AgCl starting from 0 V. Arrow indicates initial scan direction; scan rate: 0.20 - 8 V/s.

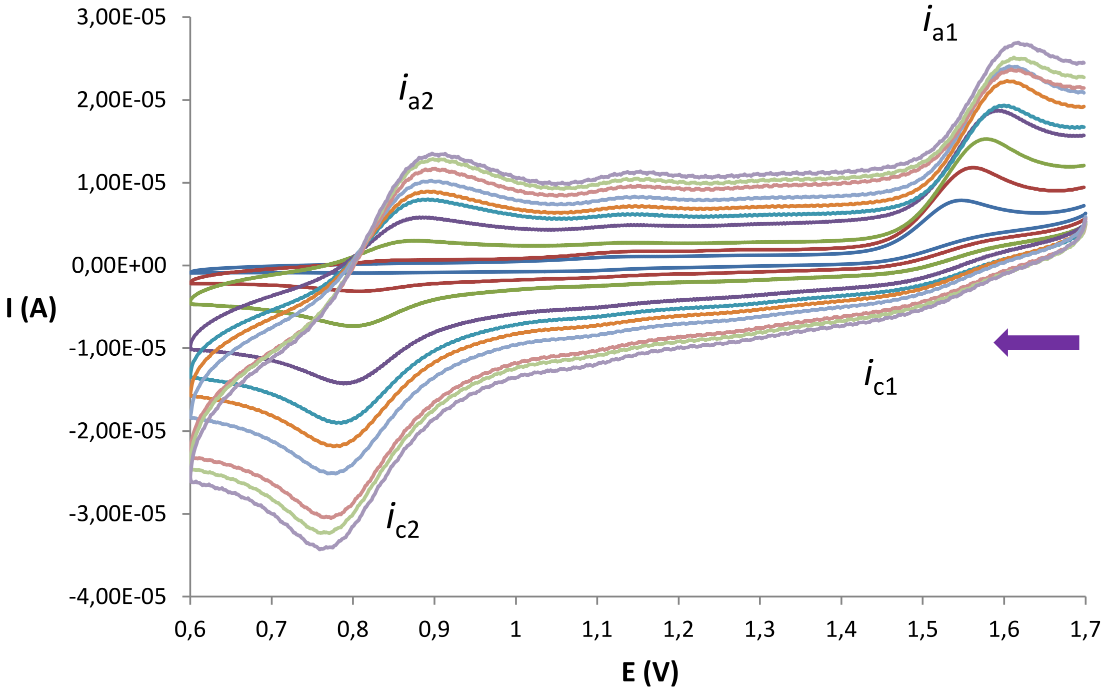

Figure 6.10. Cyclic voltammograms of **C8** in CH_2Cl_2 (TBAH, 0.1M) vs Ag/AgCl starting from 1.7 V. Arrow indicates initial scan direction; scan rate: 0.20 - 8 V/s.

The equilibrium constant (K_{O-S}^{III}) for the Ru^{III}-O⇆Ru^{III}-S reaction can be obtained in each case from cyclic voltammograms recorded through starting the potential scanning from the upper E_{init} values (1.4 V for **C5** and 1.7 V for **C8**, with 1 minute of equilibration time at the initial potential in both cases) and applying Equation **6.1**, where i_c is the cathodic peak intensity, a = RT/nF, υ is the scan rate and K is the equilibrium constant (the set of formulas used for all the calculations with details of the different parameters involved are gathered in Table **S6.6**). Plotting the ratio i_{c1}/i_{c2} *vs* υ^{-1} and extrapolating υ to infinite in order to obtain the intercept values results in K_{O-S}^{III} = 1.39 for **C5** (Figure **S6.22**) and K_{O-S}^{III} = 0.036 for **C8** (Figure **S6.23**).

$$\frac{i_{c1}}{i_{c2}} = a \cdot \frac{1}{v} + K_{O-S}^{III}$$

Equation 6.1

The kinetic isomerization constants (k_{O-S}^{III} and k_{S-O}^{III}) are calculated from plotting $\upsilon^{1/2}$ *vs.* the i_d/i_k ratio (Equation **6.2**), where n is the number of exchanged electrons (1 in this case), $l = k_{O-S}^{III} + k_{S-O}^{III}$ and the rest of parameters are defined in Table **S6.6**. The i_d/i_k ratio was calculated by measuring i_k (which equals to i_{c1} values at the reverse scan set of voltammetries, Figure **6.8** for complex **C5** and Figure **6.10** for complex **C8**) and i_d (which corresponds to the i_{a1} values measured starting the CVs from 0 V, Figures **6.7** and **6.9**). The plots obtained for Equation **6.2** are shown in Figures **S6.24** and **S6.25** for **C5** and **C8** respectively.

$$\sqrt{v} = \frac{1}{\frac{0.471}{K_{O-S}^{III}} \cdot \sqrt{\frac{nFl}{RT}}} \cdot \frac{i_d}{i_k} - \frac{1.02}{\frac{0.471}{K_{O-S}^{III}} \cdot \sqrt{\frac{nFl}{RT}}}$$

Equation 6.2

From the value of slope obtained, and considering that $K_{O-S}^{III} = k_{O-S}^{III}/k_{S-O}^{III}$, the following kinetic constants can be obtained: k_{O-S}^{III} = 0.176 s^{-1} and k_{S-O}^{III} = 0.126 s^{-1} for **C5** and k_{O-S}^{III} = 0.019 s^{-1} and k_{S-O}^{III} = 0.53 s^{-1} for **C8**.

With the equilibrium constant K_{O-S}^{III} and assuming that $E°$ = $E_{1/2}$ for each linkage isomer, Equation **6.3** can be used to obtain K_{O-S}^{II}, yielding values of $1.34 \cdot 10^{12}$ for **C5** and $1.53 \cdot 10^{12}$ for **C8**.

$$K^{II} = K^{III} + e^{\frac{F}{RT} \cdot (E^0_{Ru-S} - E^0_{Ru-O})}$$

Equation 6.3

The kinetic isomerization constants in the Ru^{II} oxidation state (k_{O-S}^{II} and k_{S-O}^{II}) can be calculated from plotting ln($i_{a1}/\upsilon^{1/2}$) *vs.* υ^{-1} (Equation **6.4**,[464] Figures **S6.26** and **S6.27**), giving values of k_{O-S}^{II} = 0.11 s^{-1} and k_{S-O}^{II} = $8.2 \cdot 10^{-14}$ s^{-1} for **C5** and k_{O-S}^{II} = 0.072 s^{-1} and k_{S-O}^{II} = $4.7 \cdot 10^{-14}$ s^{-1} for **C8**. These results are gathered in Table **6.3** together with other complexes described in the literature.

$$ln\left(\frac{i_{a1}}{\sqrt{v}}\right) = k_{O-S}^{II} \cdot \frac{1}{v} + b$$

Equation 6.4

Table 6.3. Thermodynamic and kinetic parameters for the linkage isomerization of **C5** and **C8** complexes, together with Ru-dmso complexes described in the literature.[a]

Entry	Compound	K_{O-S}^{III}	k_{O-S}^{III} (s^{-1})	k_{S-O}^{III} (s^{-1})	K_{O-S}^{II}	k_{O-S}^{II} (s^{-1})	k_{S-O}^{II} (s^{-1})
1	*cis,cis*-[RuCl$_2$(pypz-H)(dmso)$_2$], **C5**	1.39	$1.76 \cdot 10^{-1}$	$1.26 \cdot 10^{-1}$	$1.34 \cdot 10^{12}$	$1.1 \cdot 10^{-1}$	$8.2 \cdot 10^{-14}$
2	*cis,fac*-[RuCl$_2$(CH$_3$-pz-H)(dmso)$_3$], **C8**	0.036	$1.9 \cdot 10^{-2}$	$5.3 \cdot 10^{-1}$	$1.53 \cdot 10^{12}$	$7.2 \cdot 10^{-2}$	$4.7 \cdot 10^{-14}$
3	*cis,cis*-[RuCl$_2$(H3p)(dmso)$_2$][119]	1.7	$2.8 \cdot 10^{-1}$	$1.7 \cdot 10^{-1}$	$5.2 \cdot 10^{11}$	$4.9 \cdot 10^{-1}$	$9.3 \cdot 10^{-14}$
4	*trans,cis*-[RuCl$_2$(H3p)(dmso)$_2$][119]	0.27	$5.7 \cdot 10^{-2}$	$2.2 \cdot 10^{-1}$	$5.3 \cdot 10^{8}$	$8.7 \cdot 10^{-2}$	$1.6 \cdot 10^{-10}$
5	*trans,cis*-[RuCl$_2$(bpp)(dmso)$_2$]$^{-}$ [96]	0.26	$1.7 \cdot 10^{-2}$	$6.5 \cdot 10^{-2}$	$6.5 \cdot 10^{9}$	$1.3 \cdot 10^{-1}$	$2.1 \cdot 10^{-11}$
6	*out*-[Ru(L^2)(trpy)(dmso)]$^{+}$ [461]	0.13	$7.7 \cdot 10^{-2}$	$6.0 \cdot 10^{-1}$	$5.5 \cdot 10^{8}$	$2.5 \cdot 10^{-1}$	$4.6 \cdot 10^{-10}$

[a] H3p is 5-phenyl-3-(2-pyridyl)-1*H*-pyrazole, L^2 is 5-phenyl-3-(pyridin-2-yl)pyrazolate and bpp is 3,5-(2-pyridyl)pyrazolate.

As can be seen in Table **6.3**, K_{O-S}^{II} values indicate that, in Ru^{II} redox state, the dmso ligand in compounds **C5** and **C8** displays a high preference to be bound to the metal through the S atom in both cases, and the thermodynamic stability of this form is slightly higher in **C8** than in **C5**. The major stability of complex **C5** with regard to the structurally similar compounds of entries 3-5 in the Ru(II) state is not easy to explain but could be related to the distinctive electronic characteristics and the higher volume of the H3p and bpp ligands when compared to pypz-H. Also, in complexes *trans,cis*-$[RuCl_2(H3p)(dmso)_2]$ and *trans,cis*-$[RuCl_2(bpp)(dmso)_2]^-$ (entries 4 and 5) the *trans* disposition of the two chlorido ligands probably diminishes the overall electron density on the Ru metal center then facilitating the Ru-S → Ru-O isomerization. A similar argument would explain the lower relative stability of complex *out*-$[Ru(L^2)(trpy)(dmso)]^+$ (entry 6) where only one anionic (the deprotonated L^2) ligand is present.

In the Ru^{III} state, linkage isomerization takes place in both complexes (as evidenced by the cyclic voltammetries discussed above) but, as can be inferred from K_{O-S}^{III} values, the Ru-S bound form is still dominant for complex **C5** whereas complex **C8** presents a marked preference for the Ru^{III}-O isomer, which is one or two orders of magnitude higher than the rest of the complexes in Table **6.3**. This is in accordance with the CVs of Figures **6.8** and **6.10**, where the Ru^{III}-S→Ru^{II}-S reduction process is observed only for complex **C5** whilst complex **C8** displays a complete isomerization towards the Ru-O form. Steric factors could be responsible for the higher stability of the isomerized form in **C8** since three S-bound dmso ligands would probably encounter significant steric hindrance when coordinating in facial arrangement the smaller Ru(III) ion.

Complex **C8** also presents a higher $\boldsymbol{k_{S-O}^{III}}$ kinetic constant than **C5** and this could be due to the presence of an additional S-bound dmso ligand in **C8** instead of the pypz-H ring in **C5**. A larger number of π-acceptor auxiliary ligands will presumably increase the Ru-S→Ru-O isomerization rate upon Ru(II) oxidation, and this is in accordance with complex *out*-$[Ru(L^2)(trpy)(dmso)]^+$ (entry 5) being the one with the highest $\boldsymbol{k_{S-O}^{III}}$ value as it contains four π-acceptor pyridyl ligands and only one anionic pyrazolate ring coordinated to Ru. However, it is noticeable that complex **C8**, in spite of bearing two anionic π-donor Cl ligands, presents a $\boldsymbol{k_{S-O}^{III}}$ value comparable to that found for the complex in entry 5, then evidencing the remarkable influence exerted by the third dmso ligand over the isomerization process in **C8**. As mentioned above, steric factors arising from the facial coordination of three S-bound dmso ligands to a small Ru(III) ion could be determinant to increase the isomerization rate. The high kinetic rates for the Ru^{III}-S → Ru^{III}-O process in **C8** and *out*-$[Ru(L^2)(trpy)(dmso)]^+$ are also consistent with the high degree of isomerization observed experimentally for both complexes.[461]

6.4. Photoinduced substitution reactions

6.4.1. Photochemical study of $[RuCl_2(pypz\text{-}H)(dmso)_2]$ (C5) and $[RuCl_2(CH_3\text{-}pz\text{-}H)(dmso)_3]$ (C8) in acetonitrile and chloroform.

In order to obtain some information about the lability of the ligands in the synthesized complexes, we have investigated the photochemical behavior of complexes **C5** and **C8** (Scheme **6.4**).

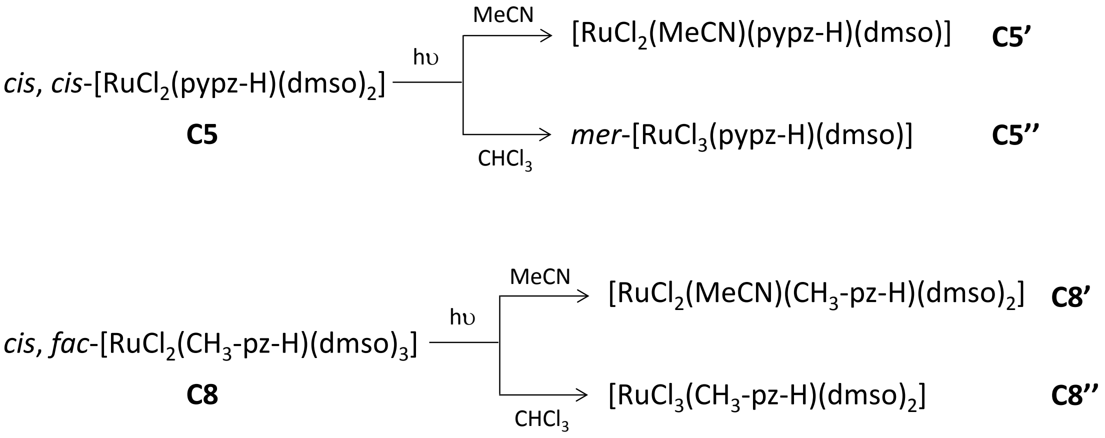
MeCN
hυ
cis, cis-[RuCl2(pypz-H)(dmso)2]
C5
[RuCl2(MeCN)(pypz-H)(dmso)]
C5'
CHCl3
mer-[RuCl3(pypz-H)(dmso)]
C5''
MeCN
hυ
cis, fac-[RuCl2(CH3-pz-H)(dmso)3]
C8
[RuCl2(MeCN)(CH3-pz-H)(dmso)2]
C8'
CHCl3
[RuCl3(CH3-pz-H)(dmso)2]
C8''

Scheme 6.4. Photochemical transformation of complexes **C5** and **C8**.

A 0.65 mM and 1mM solutions of **C5** and **C8**, respectively, in acetonitrile have been exposed to visible light at room temperature and their evolution has been monitored through UV-visible, NMR and cyclic voltammetric experiments. Upon exposure to light for a few minutes, the color of the solutions change from light to deep yellow, indicating the occurrence of light induced processes. A 80 W lamp was used as light source to irradiate the complexes and the spectrophotometric changes were monitored using a UV-Vis apparatus.

The evolution of the UV-Vis spectra of **C5** (Figure **6.11**) shows one isosbestic point at 340 nm confirming the net conversion to a new compound that presumably corresponds to *cis*-[RuCl$_2$(MeCN)(pypz-H)(dmso)], **C5'**, as inferred from spectrophotometric, cyclic voltammetric and NMR experiments (*vide infra*). In the UV-vis spectra, a shift of the MLTC bands to lower energy absorptions is observed for the new complex **C5'**, as expected from the higher σ-donor and lower π-acceptor capacity of the MeCN ligand with regard to dmso, that provokes a relative destabilization of the dπ(Ru) orbital.

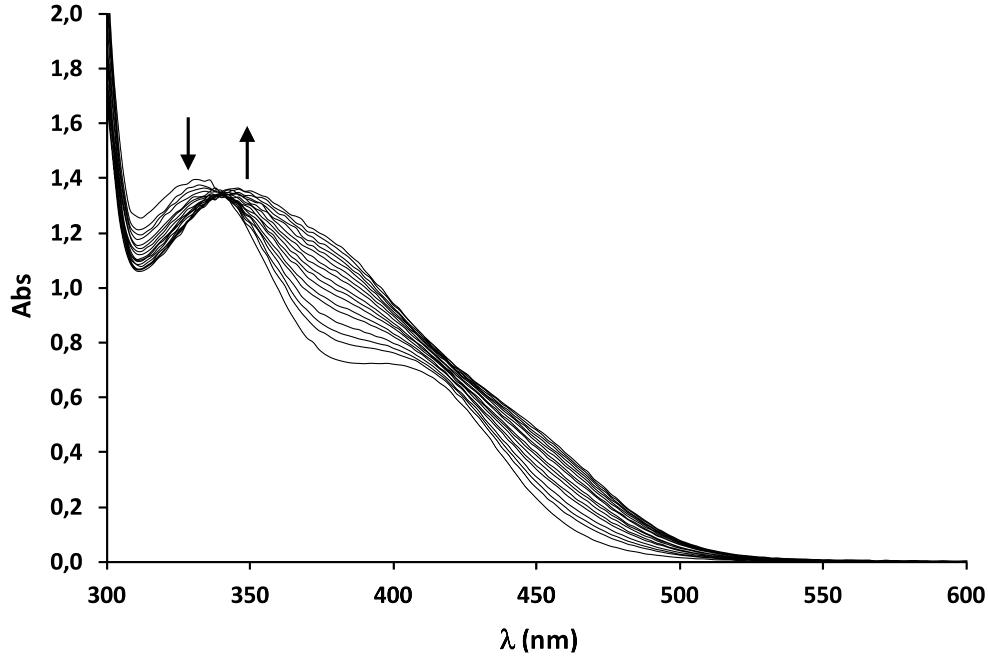

Figure 6.11. UV-visible spectroscopy corresponding to the photochemical transformation of a 0.7 mM solution of **C5** into **C5'.**

The changes in the ^{1}H-NMR spectrum of the aliphatic region upon **C5→C5'** photochemical substitution (Figure **S6.28**) clearly show that free dmso (δ 2.6 ppm) is progressively generated, along with the appearance of new signals which reveal the presence of two different species during the substitution process. The four dmso singlets of **C5** (located at 1.98, 2.92, 3.44 and 3.48 ppm) gradually decrease and are almost quantitatively replaced in 40 minutes by the resonances of free dmso and two new resonances at 3.38 and 3.45 ppm. From the chemical shifts of the new signals obtained, that present chemical shifts close to those of the equatorial C9 and C10 dmso methyl groups in the original complex, we can assert that the released dmso ligand is the one formerly occupying the axial coordination site. This is consistent with:

a) the fact that the remaining equatorial dmso ligand is stabilized by H-bonding with the pyrazole ring in *cis*.

b) the axial dmso ligand is labilized thanks to a kinetic *trans* effect exerted by the Cl(2) ligand.

The substitution process has also been followed through cyclic voltammetry (CV) experiments (Figure **6.12**). The initial redox wave at 0.98 V progressively decreases upon irradiation, in parallel with the appearance of a new reversible wave at 0.64 V. This value is consistent with the substitution of one dmso by MeCN to generate complex **C5'** since the substitution of an anionic Cl ligand by a neutral MeCN would generate much higher redox potentials.[82] The new wave observed around 1.2 V corresponds to the oxidation of free dmso.

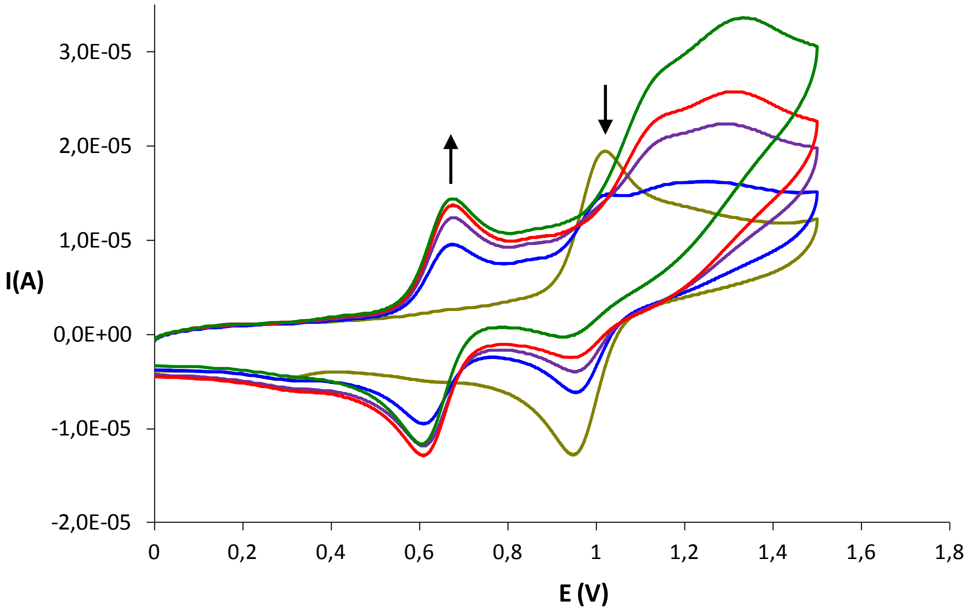

Figure 6.12. Cyclic voltammograms of **C5** (1mM in 0.1M TBAH acetonitrile solution) after irradiation: t = 0, 21, 45, 70 and 85 minutes.

Similar experiments have been performed to monitor the dmso sustitution by solvent in complex **C8**. The UV-Vis spectra of an acetonitrile solution of **C8** registered during 90 minutes under irradiation (Figure **S6.29**) show two isosbestic points at 327 and 403 nm and a new MLCT band appears a higher wavelength, 432 nm, confirming the substitution of a dmso ligand by a less π-acceptor acetonitrile ligand and the formation of a new compound that presumably corresponds to $[RuCl_2(MeCN)(CH_3\text{-pz-H})(dmso)_2]$, **C8'**, as inferred from NMR experiments and cyclic voltammetry (Figures **S6.30** and **S6.31**). However, keeping the irradiation for longer led to the disappearance of the isosbestic points, consequently indicating that further ligand substitutions must be taking place.

The changes in the ^{1}H-NMR spectrum of the aliphatic region upon **C8**→**C8**' photochemical substitution (Figure **S6.30**) clearly show that free dmso (δ 2.6 ppm) is progressively generated along with the disappearance of the three dmso singlets, located at 3.40, 3.36 and 3.1 ppm. Two new resonances, with equal integration value, appear at 3.04 and 3.26 ppm, corresponding to compound **C8'**. The appearance of only two signals indicates the formation of a complex with two magnetically equivalent dmso ligands and consequently we can assert that the released dmso ligand is the one located *trans* to the pyrazolic ring.

The substitution process has also been followed through cyclic voltammetry (CV) experiments. Figure **S6.31** shows the appearance of a new reversible wave at lower potential ($E_{1/2}$ = 1.04 V) than that of the former Ru-S_{dmso} complex (E_{pa} = 1.49 V), also consistent with the substitution of one dmso by MeCN, together with the wave corresponding to the oxidation of free dmso at 1.2 V.

Isomerization of dmso (discussed in section 6.3.) and the substitution process by acetonitrile have been described in the literature with compounds containing one or two dmso ligands[96,119,461-462,465] but, to the best of our knowledge, these are the first $Ru(dmso)_3$ compounds that present this behavior.

Similar experiments were carried out for **C5** and **C8** in chloroform, chosen as non-coordinating solvent, with the aim to evaluate the photochemical behavior of the complexes in particular regarding the dmso linkage isomerization. However, after irradiating a solution of complex **C5** in chloroform for 12 h the solution color changed from yellow to red-brown and, on the basis of similar systems described in the literature,[119] we could unravel that the substitution of one dmso ligand by a chlorido ligand and the subsequent oxidation of Ru^{II} to Ru^{III} had taken place, leading to the formation of a new complex, $[Ru^{III}Cl_3(pypz\text{-}H)(dmso)]$ (**C5**''). The light-induced reaction of Ru^{II} complexes with $CHCl_3$ has already been described and seems to be initiated by high-energy transitions of the complex.[119]

The new **C5''** complex was isolated by precipitation with ether, and suitable crystals for X-ray diffraction analysis were obtained. The corresponding ORTEP plot is shown in Figure **6.13**, where it can be observed that the complex displays a distorted octahedral geometry with a meridional disposition of the three chlorido ligands. The main crystallographic data and selected bond distances and angles for the structure can be found in Tables **S6.1** and **S6.4**.

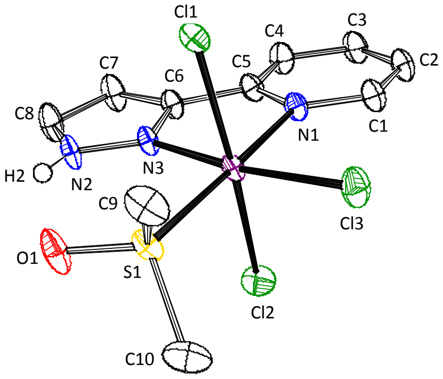

Figure 6.13. Ortep plot and labeling scheme for compound **C5''**.

The structural features of compound **C5''** are similar to other trichlorido compounds described in the literature.[119] It is remarkable that, despite the Ru(II)→Ru(III) oxidation, the dmso ligand is coordinated by the sulfur atom so that no linkage isomerization has taken place, probably due to the stabilization of the remaining dmso ligand by an intramolecular hydrogen bond and the weakened Lewis acid character of the metal by the presence of an additional strong σ-donor chlorido ligand, as previously reported in the literature.[119]

The CV registered after irradiation (Figure **S6.32**) shows that this substitution provokes a potential decrease from 1.09 to 0.05 V due to the additional electron-donating ability of the new chlorido ligand. The evolution of the UV-Vis spectra is depicted in Figure **6.14**, and the final spectrum, corresponding to **C5''** (Figure **S6.33**), shows spectral features such as those displayed by other similar compounds described.[119] A shift to lower energy absorptions is observed due to the higher σ-donor and lower π-acceptor capacity of the Cl ligand with regard to dmso, that provokes a destabilization of the dπ (Ru) donor orbital**.** Also, a different pattern of absorption bands was observed with additional Clpπ-Ru-dπ* LMCT in the visible region.[459] Two isosbestic points at 328 and 352 nm are found, confirming the net conversion from **C5** to **C5''**.

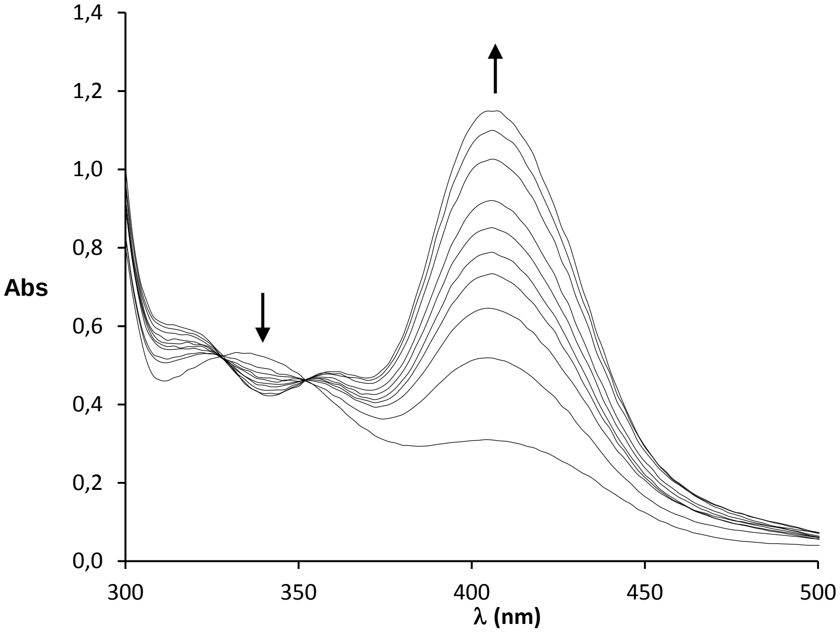

Figure 6.14. UV-visible spectra corresponding to the photochemical transformation of a 0.25 mM solution of **C5** into **C5''** in chloroform during 60 minutes. Isosbestic points are found at 328 and 352 nm.

On the other hand, the irradiation of a chloroform solution of compound **C8** lead to a color change from yellow to brown presumably due, as described above for **C5**, to a dmso substitution by chlorido with concomitant oxidation of Ru^{II} to Ru^{III}, generating the new complex $[Ru^{III}Cl_3(CH_3\text{-pz-H})(dmso)_2]$, **C8''**. The CV registered after irradiation, starting the potential scanning at -0.2 V vs Ag/AgCl (Figure **S6.34**), shows two new redox processes at $E_{1/2}$ = 0.1 V and 0.3 V that, unlike the former **C8** Ru(III/II) wave, are electrochemically reversible. We have further investigated the electrochemical behavior displayed by complex **C8''** through differential pulse voltammetry at different initial equilibrium times and starting the potential scanning from -0.2 or +0.6 V. The voltammetries obtained are displayed in Figure **6.15** and, as can be observed, the redox process at $E_{1/2}$ = 0.3 V is manifested only when the potential scanning starts at low E values (Figure **6.15a**). Moreover, upon lengthening the equilibrium time the relative intensity of this redox process (compared to that at $E_{1/2}$ = 0.1 V) increases from approximately 1:1 at equilibrium time = 0 s up to 1:2.5 at equilibrium time = 180 s. The reverse scanning potential (Figure **6.15b**) mostly displays the $E_{1/2}$ = 0.1 V redox process independently of the equilibrium time applied. Taking into account these observations a plausible explanation is that, unlike the case of complex **C5''**, the irradiation of **C8** leads mainly to the formation of a $\mathrm{Ru}^{\mathrm{III}}$ complex (**C8''**) where one of the two remaining dmso ligands has undergone linkage isomerization and is bound through its O atom. This compound, that displays a Ru(III/II) redox process at $E_{1/2}$ = 0.1 V, experiences a partial Ru-O → Ru-S isomerization upon reduction to Ru(II), generating a new isomer with $E_{1/2}$ = 0.3 V where the two dmso ligands are coordinated through their S atoms.

As mentioned earlier, complex **C5''** does not display any dmso linkage isomerization and the different behavior shown by **C5''** and **C8''** could be explained by several factors:

a) only one dmso ligand remains coordinated in **C5''** which in addition is stabilized through H-bonding with the pyrazolyl ring.

b) two dmso ligands are present in **C8''** but, presumably, only one of them will be stabilized through H-bonding interaction with the pyrazole ligand.

c) as discussed earlier, a dmso ligand presents higher π-acceptor character than a pyridyl ring and, consequently, the overall electron-withdrawing character of the ligands is enhanced in **C8''** if compared to **C5''**, thus facilitating the isomerization towards the less π-acceptor O-bound dmso.

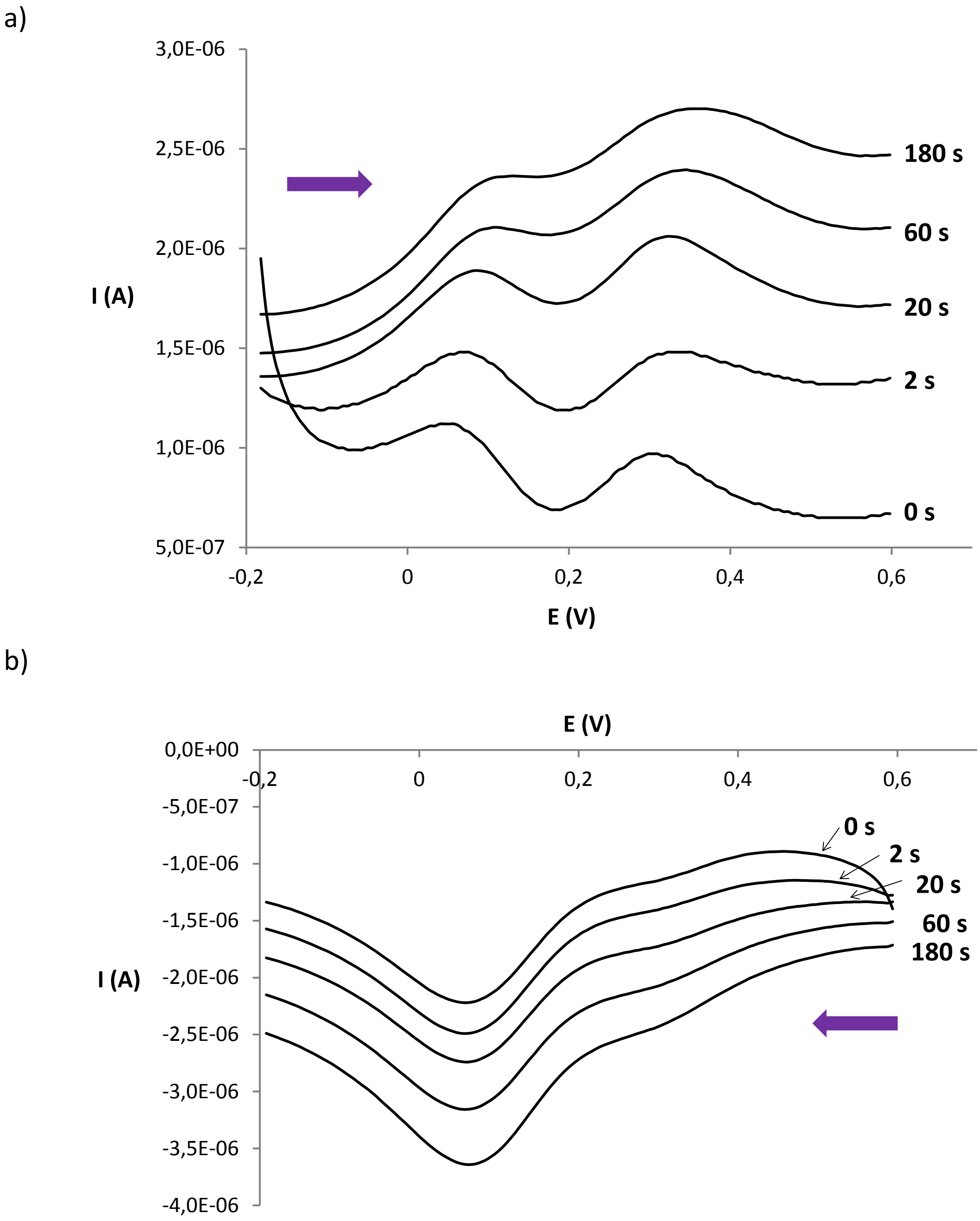

Figure 6.15. DPV of a solution of complex **C8''** in dichloromethane, starting the scanning of potential at -0.2 V (a) and at 0.6 V (b). The equilibrium time applied in each case (0-180 s) is indicated.

On the other hand, the difference between the potential values for the O- and S-bound dmso forms in **C8''** (approximately 0.2 V) is lower than that displayed by complexes **C5** or **C7**-**C11** (see Figures **6.6** and **6.8**) which is around 0.6-0.7 V. This could be explained by the increased electron density at the Ru metal center in **C5''** and **C8''** thanks to the third anionic chlorido ligand that probably balances to a higher extent the electron-withdrawing character of a S-bound dmso. Unfortunately, the isolation of suitable crystals for the X-ray diffraction structure of this species has not been achieved so the presence of a O-bound dmso cannot be unambiguously confirmed. Yet, the low potential values observed are in agreement with the substitution of one dmso by a choro ligand owing to the higher electron-donating character of the latter.

The evolution of the UV-Vis spectra for the generation of **C8''** is depicted in Figure **S6.35** and is also consistent with this hypothesis because it shows a shift to lower energy absorptions that could be due to the higher σ-donor and lower π-acceptor capacity of the Cl ligand with regard to dmso and the consequent destabilization of the dπ (Ru) orbital**.**

6.4.2. Photochemical study of [RuCl$_2$(pypz-H)(dmso)$_2$] (C5) in water.

To shed some light on the changes undergone by the catalysts under the experimental conditions of the hydration process, a 0.15 mM solution of complex **C5** in H_2O was kept at 60^{o}C and the evolution was followed by UV-vis spectroscopy. For the first 2 hours (Figure **6.16**), isosbestic points were found at 280 and 302 nm, thus indicating the net formation of a unique complex species presumably by substitution of a dmso ligand by water (see below). However, keeping the temperature for longer (up to 4 hours) led to the disappearance of the isosbestic points, consequently indicating that further ligand substitutions must be taking place.

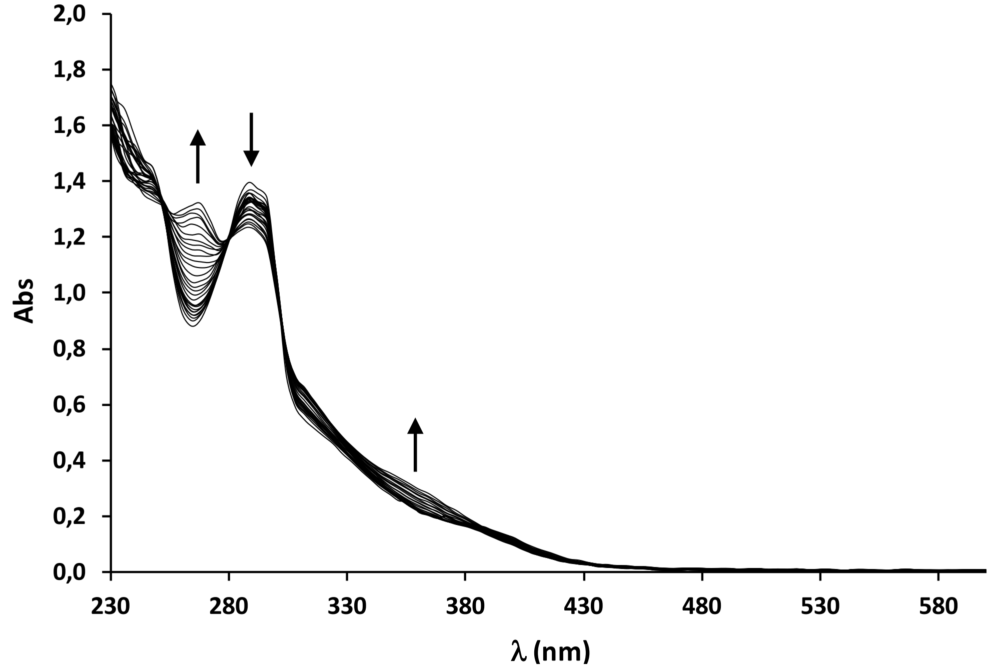

Figure 6.16. Evolution of an aqueous solution of complex **C5** by warming at 60ºC for 2h. Isosbestic points are found at 280 and 302 nm.

A similar evolution is observed when irradiating an aqueous solution of **C5** at room temperature with visible light. Figure **S6.36** displays the final spectra obtained after the two procedures described, evidencing that the same type of species is obtained either though the thermal or the photochemical solvolysis. However, in the case of photosubstitution, the spectrum corresponding to the initial complex **C5** completely vanishes within 1.5 hours, thus indicating that the photochemical substitution process is faster than the thermal one. In both cases, a new MLCT band appears at higher wavelength (around 355 nm), which is consistent with the replacement of a dmso ligand by a less π-acceptor aqua ligand.

6.5. Catalytic hydration of nitriles

We have checked all our complexes in the catalytic hydration process of different nitriles under neutral conditions using water as solvent at 80ºC. The remaining substrate has been quantified through GC chromatography with biphenyl as the internal standard and the hydrolysis products have been analyzed by NMR spectroscopy and compared to pure samples of the corresponding amide and acid derivatives. Conversion and selectivity values for [RuCl$_2$(pypz-H)(dmso)$_2$], **C5**, and [RuCl$_2$(pz-H) (dmso)$_3$], **C7**, are summarized in Table **6.4**, together with the conditions used in the catalysis.

Firstly, blank experiments without any catalyst were carried out by keeping the substrates in water at 80ºC for 20h. In all cases, the nitrile was quantitatively recovered except for the aliphatic chloronitriles (chloro and dichloroacetonitrile), were a conversion around 40% was achieved in both cases. However, no traces of the amide product were found after the blank test for the chloroacetonitrile substrate, in contrast to the dichloroacetonitrile, were the amide was quantitatively formed. Thus, the latest substrate was not further tested in catalytic experiments.

As we can observe in Table **6.4**, both complexes were found to be active towards nitrile hydration, with moderate to high conversion values. However, the most remarkable feature is the excellent selectivity observed for the corresponding amides in the vast majority of cases, with the exception of p-fluorobenzonitrile in **C5** mediated hydrolysis (entry 4) where a minor amount (lower than 10%) of the corresponding acid has been also detected. Regarding the ether substrate in entry 2, we have observed the hydrolytic cleavage of the C-O bond in the hydration reaction using **C5** as catalyst, yielding around 5% of benzonitrile. Among all the substrates tested, the hydration of acrylonitrile (entry 7) is particularly interesting, where the industrially relevant acrylamide product is quantitatively obtained when the hydration process is mediated by complex **C7**. Selectivity with catalyst **C5** is lower and unidentified products are generated together with acrylamide.

Table 6.4. Ru-catalyzed hydration of nitriles to amides in water using complexes **C5** and **C7** as catalysts[a]

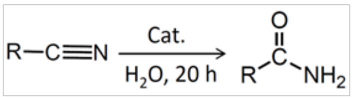

Entry	Substrate	C5		C7	
		Conv. (%)	Select. (%)[b]	Conv. (%)	Select. (%)[b]
1	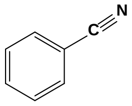	75	>98	80[c]	>98
2	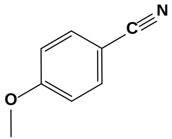	36[c]	>98[c]	-	-
3	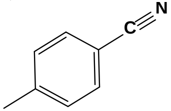	13	>98	45	>98
4	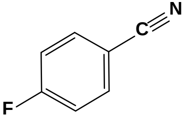	62	90	88	>98
5	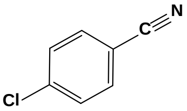	37	>98	55	>98
6	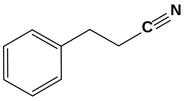	26	>98	41	>98
7	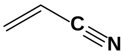	23	80	61	>98
8	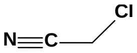	85	>98	53	>98

[a] Reactions performed at 80°C using 1 mmol of nitrile in 3 ml of water. [Substrate]:[Ru] ratio = 100:1. Time: 20 h reaction.

[b] Selectivity for the amide is determined by ^{1}H-NMR analysis of the reaction mixture

[c] 5% of conversion corresponds to cleavage of the ether group. Selectivity is calculated with regard to the conversion of the ether substrate.

The general mechanism currently accepted in the hydration of nitriles begins with a substitution process, where a ligand is replaced by the corresponding nitrile in the metal coordination environment and a subsequent nucleophilic attack of water (or hydroxo anions) on the nitrile carbon atom takes place (see Introduction, section 1.4.2).[246,268,270] The electronic characteristics of the ligands in the catalyst influence the ability of the metal to activate the nitrile substrate: a high electron-withdrawing character of the ligands will drive the metal to a stronger activation of the coordinated nitrile substrate, making it more susceptible to a water (or hydroxo) nucleophilic attack. In parallel, electron-withdrawing substituents on the nitrile substrates will lead to a similar activating effect.

A first look at the conversion values in Table **6.4** is in agreement with the accepted mechanism described above since complex **C7**¸ with three highly π-acceptor dmso ligands, is the one displaying the higher conversions for almost all the substrates tested. The effect of three dmso on the properties of **C7** had already been manifested in the electrochemical properties (section 6.3), with a Ru(III/II) redox potential around 0.4 V higher than that of **C5**. Another factor that could explain the better performance of **C7** is the enhanced flexibility of a putative intermediate species which would contain only monodentate ligands bound to the metal center, in parallel with the occurrence of a larger number of potentially labile sites (presumably those occupied by dmso ligands). Decoordination of dmso is supported by the observations on ligand substitution discussed in the previous section and that free dmso is found in all cases when analyzing the hydrolysis products by NMR spectroscopy.

As mentioned above, the electronic properties of the substrates also influence the extent of the hydration reaction. Thus, lower performances are observed in Table **6.4** for substrates either linked to aliphatic groups (entry 6) or having *para*-electron donating groups in the aromatic ring (entries 2 and 3). On the other hand, halide-substituted benzonitriles (entries 4 and 5) are expected to display better performances thanks to the electron-withdrawing character of the halide substituents (inductive effect). However, in the case of *p*-chlorobenzonitrile the performance is clearly lowered for both catalysts when compared to benzonitrile, indicating that a deactivating effect, probably caused by the resonance delocalization of the Cl lone pairs throughout the aromatic system, is taking place (the same resonance effect is expected to be much less significant for the smaller fluoride substituent). This is in contrast with the activating effect that Cl substituents have on the aliphatic substrates (entry 8), where the electronic influence is dominated by the electronegativity of the Cl substituents, leading in both cases to a considerable degree of hydrolysis without need of a catalyst (though in this latest case the amide product is not obtained, as mentioned in the description of the blank experiments).

The catalytic activity of [RuCl$_2$(pypz-Me)(dmso)$_2$], **C6**, was also checked in the hydration of benzonitrile, acrylonitrile and chloroacetonitrile obtaining conversion values of 66%, 42% and 46% respectively. In all cases high values of selectivity (>98%) were obtained. Comparing it with **C5**, it can be seen that lower conversion values were obtained in the case of **C6** for benzonitrile and chloroacetonitrile, but the acrylonitrile substrate is hydrolyzed more effectively (23% conversion for **C5** and 42% for **C6**). It seems that electronic factors could be dominant in the **C5**-catalyzed nitrile hydration as the more activated substrates are better hydrolyzed, and this factor is not as determinant in complex **C6**, where more balanced conversion values are found for the substrates tested. The differences could arise from the presence of the pyrazolic hydrogen atom in **C5**, but we must take into account that two different isomers were obtained for **C5** and **C6** and this could induce a distinctive catalytic activity.

The R$_2$-pz-H complexes **C8**-**C11** have also been tested in the hydration of two nitrile substrates (benzonitrile and acrylonitrile). Conversion and selectivity values are summarized in Table **6.5**, together with the results obtained with these substrates using complex **C7** as catalyst for purposes of comparison.

Table 6.5. Ru-catalyzed hydration of nitriles to amides in water using complexes **C7**-**C11** as catalysts.[a]

Substrate	**C7**		**C8**		**C9**		**C10**		**C11**	
	Conv. (%)	**Select.[b] (%)**	**Conv. (%)**	**Select.[b] (%)**	**Conv. (%)**	**Select.[b] (%)**	**Conv. (%)**	**Select.[b] (%)**	**Conv. (%)**	**Select.[b] (%)**
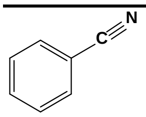	80	>98	29	>98	85	>98	24	>98	30	>98
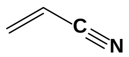	61	>98	35	>98	29	>98	53	>98	43	>98

[a] Reactions performed at 80°C using 1 mmol of nitrile in 3 ml of water. [Substrate]:[Ru] ratio = 100:1. Time: 20 h reaction.

[b] Selectivity for the amide is determined by ^{1}H-NMR analysis of the reaction mixture.

As we can observe in Table **6.5**, all complexes were found to be active towards nitrile hydration with moderate values of conversion in most cases though in some particular cases, such as the benzonitrile hydration with complexes **C7** and **C9**, conversion values above 80% are attained. The most remarkable feature is the excellent selectivity observed for the corresponding amides in all cases. Regarding the hydration of benzonitrile with compound **C10** we have observed a change in the color of the solution during the catalytic process probably due to the degradation of the catalyst. It is interesting to emphasize the performance of these compounds in the hydration of acrylonitrile, where the industrially relevant acrylamide product is quantitatively obtained in all cases.

The relatively good performance of these tris(dmso) compounds could be explained, as discussed above, by the electronic characteristics of the catalysts and the occurrence of a higher number of potentially labile sites (presumably those occupied by dmso ligands). As in **C5** mediated catalysis, decoordination of dmso is supported by the fact that free dmso is found in all cases when analyzing the hydrolysis products by NMR spectroscopy. However, some differences in the conversion values are observed between the catalysts for a specific substrate that are likewise originated by the distinctive characteristics of the monodentate R_2-pz-H ligands, as the rest of ligands and the catalyst geometry are identical for all **C7**-**C11** complexes.

An influence of the electronic characteristics of the ligands is evidenced in Table **6.5** when using benzonitrile as substrate. Indeed, an enhanced performance is found, as expected, for complex **C9** having the NO_2 electron-withdrawing substituent when compared to **C7**, and a decrease in conversion is shown for the methyl-pyrazole complex **C8**, with a more σ-donor ligand. The Br-phenyl complex **C11** would also be expected to display better activity than **C7** but this is not the case, probably due to a certain delocalization effect of the π electron density of the Br-phenyl ring on the pyrazole, as discussed previously in the electrochemical behavior (section 6.3). Complex **C10** is also expected to display improved activity but, as mentioned earlier, it undergoes a color change during the catalytic process that most certainly indicates a catalyst deactivation, thus yielding the lowest conversion value for this substrate.

The comparison of catalysts **C7**-**C11** in the hydration of acrylonitrile follows a tendency similar to that described above for benzonitrile for most of the catalysts: complex **C8** displays lower activity than **C7** and complex **C11** performance is lower than expected and it is comparable to that of **C8**. In this case, complex **C10**, with the CF_3 substituent, displays the highest conversion value amongst all the substituted pyrazole catalysts (**C8**-**C11**) though it is only comparable (not better) than that displayed by the unsubstituted pyrazole complex **C7**. Finally, complex **C9** displays a low conversion value that is not easily explained and that might involve significant changes in the catalyst structure at the high temperatures of the catalytic experiments that affect mainly the non-activated substrate acrylonitrile.

Given the efficacy of catalysts **C5** and **C7** in the nitrile hydration reaction, we proceeded to test their reusability in water and glycerol as single solvents. As mentioned previously, glycerol appears as a valuable solvent potentially useful for the immobilization of homogeneous catalysts. In this context we have carried out a preliminary test on the reuse of these catalysts using *p*-fluorobenzonitrile and benzonitrile as substrates (the nitriles chosen are the ones displaying better results among the ones previously tested for both catalysts, see Table **6.4**), and the results are shown in Table **6.6**. It is noticeable that the amide product (which is evaluated after the last run for each set of reuses) is obtained quantitatively in all cases.

A first glance at Table **6.6** allows evidencing that the first run was slower in glycerol than in water for a given substrate. Both catalysts could be reused for at least a second run and, in the case of aqueous media, the overall turnover number was above 175 for both substrates and catalysts. However, the decrease of activity observed after the first cycle was very pronounced in water, in contrast to the case of glycerol, where both catalysts maintain their performance unaltered for a second run. Yet, the overall TON in glycerol is lower than in water (121 and 146 for entries 2 and 4 of Table **6.6**, respectively). To the best of our knowledge, this is the first metal-based catalytic system applied to nitrile hydration catalysis in glycerol media. Although the performance obtained in glycerol is slightly lower than in water, it could also be a promising solvent for this kind of reactions.

Table 6.6. Consecutive reuses of catalysts **C5** and **C7** in the hydration of nitriles to amides in water and glycerol.[a]

Entry	Substrate	Cat.	Solvent	Run	Conv. (%)
1	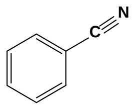	**C5**	H_2O	1	86
		C5	H_2O	2	35
		C5	H_2O	3	49
		C5	H_2O	4	20
		C5	H_2O	5	2
2	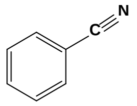	**C5**	Glycerol	1	62
		C5	Glycerol	2	59
		C5	Glycerol	3	1
3	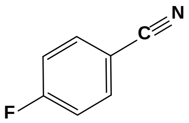	**C7**	H_2O	1	88
		C7	H_2O	2	55
		C7	H_2O	3	27
		C7	H_2O	4	5
4	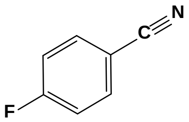	**C7**	Glycerol	1	48
		C7	Glycerol	2	56
		C7	Glycerol	3	42
		C7	Glycerol	4	2

[a] Reactions performed at $80^{o}C$ using 1 mmol of nitrile in 3ml of water. [Substrate]:[Ru] ratio = 100:1. Time: 20 h reaction.

In summary, in this chapter we have developed a new family of ruthenium dmso compounds which have been fully characterized by structural, analytical and spectroscopic techniques. For all complexes the crystal structures have been obtained and solved by X-ray diffraction analysis. It can be observed that in all cases, the Ru metal center adopts an octahedrally distorted type of coordination.

The redox properties of all complexes **C5**-**C11** have been compared and in general, complexes with monodentate ligands R_2-pz-H (R_2 = H, CH_3, NO_2, CF_3 or Br-Hind) have higher redox potentials than complexes with didentate ligands pypz-R_1 (R_1 = H, Me), due to the stronger π-acceptor capacity of the additional dmso ligand with regard to the pyridyl ring of pypz-R_1. The cyclic voltammograms of **C5** and **C8** suggest the existence of a dmso linkage isomerization process which goes in parallel to the oxidation of Ru^{II}(dmso-S) species to Ru^{III}(dmso-O). The scan rate dependent cyclic voltammograms permitted to estimate the rates of linkage isomerization and the thermodynamic properties of both complexes, evidencing a markedly higher preference of complex **C8** for the O-bound dmso form in the oxidation state Ru^{III} when compared to that of **C5**, in accordance with the high degree of linkage isomerization found for **C8** in electrochemical oxidation experiments.

Diferent photoinduced substitution reactions were studied for **C5** and **C8** in acetonitrile, chloroform and water through UV-visible, NMR and cyclic voltammetry experiments. After irradiating a solution of both complexes in chloroform, a substitution of one dmso ligand for a Cl took place leading to the formation of trischlorido complexes (**C5’’** and **C8’’**, respectively). It was possible to isolate crystals for **C5’’** and the X-ray structure obtained confirms this ligand substitution process.

A possible mechanism for the nitrile hydration could be initiated in the case of our catalysts by the substitution of one or more dmso ligands by the solvent (water in our case), as traces of free dmso are found in the NMR spectra after performing the catalytic reaction. Thus, dmso ligands would constitute the labile coordination sites that could allow the coordination of the corresponding nitrile to the metal center. The improved efficiency of **C7** versus **C5** could arise from the higher number of potentially labile coordination sites, together with the enhanced electron-withdrawing character of the ligands. For **C6**, we have observed high values of selectivity despite conversion values were moderate compared to **C5**. In the case of **C8**-**C11**, high values of selectivity were obtained although moderate values of conversion were achieved.

For the nitrile hydration in water and glycerol media all complexes have displayed a highly remarkable selectivity for the amide products as well as moderate recyclability in solution. These compounds constitute the first example of ruthenium dmso compounds successfully applied to this type of reactions in environmentally friendly media, and the essays described in glycerol are the first reported for this type of catalytic process in such solvent.

Chapter 7

Synthesis and heterogenization of complex [RuCl$_2$(pypz-Si)(dmso)$_2$] on SiO$_2$ supports. Evaluation of the catalytic activity in hydration of nitriles.

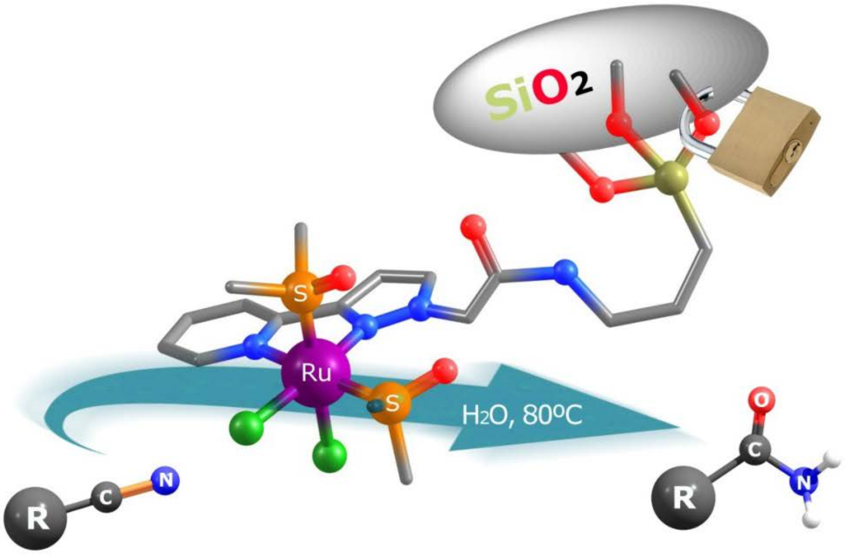

A ruthenium complex, [RuCl$_2$(pypz-Si)dmso$_2$], has been synthesized and has been anchored onto SiO$_2$ supports *via* covalent bonds. The complex and the functionalized silica supports have been characterized by spectroscopic and electrochemical techniques. Preliminary studies related to nitrile hydration catalysis in water were carried out with both homogeneous and heterogeneous catalytic systems.

7.1. Synthesis of [RuCl$_2$(pypz-Si)(dmso)$_2$]

The (3-triethoxysilylpropyl)[3-(2-pyridyl)-1-pyrazolyl]acetic amide ligand (pypz-Si), **L5**, was prepared according to literature procedures[424,425] and was characterized through NMR and ESI-MS where a peak at m/z = 407.1, corresponding to M+H$^+$, was observed. . Reaction of equimolar amounts of [RuCl$_2$(dmso)$_4$], **C2**, and the pypz-Si ligand, **L5**, in ethanol at reflux under nitrogen atmosphere produces complex **C12**. The synthetic strategies followed for the preparation of ligand **L5** and the Ru^{II} complex **C12** are outlined in Scheme **7.1**.

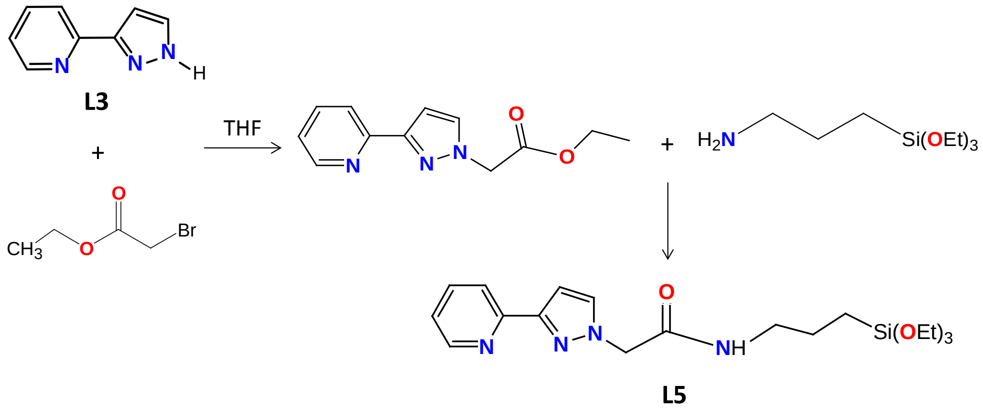

$$\underset{\textbf{C2}}{\mathrm{RuCl_2(dmso)_4}} \xrightarrow[\text{ethanol}]{\textbf{L5}} \mathrm{RuCl_2(pypz\text{-}Si)(dmso)_2} \qquad \textbf{C12}$$

Scheme 7.1. Synthetic strategies for the syntheses of ligand **L5** and complex **C12**.

The substitution of two dmso ligands in **C2** by the unsymmetrical ligand pypz-Si can potentially lead to six different stereoisomers (including two pairs of enantiomers) for complex **C12** that are analogous to those depicted for complexes **C5** and **C6** in Chapter 6 (see Figure **S7.1**). The ^{1}H-NMR spectrum of complex **C12** (Figure **S7.3**) evidences the coordination of the ligand to Ru, but it displays wide and low-defined signals probably arising from the formation of a mixture of isomers. The flexibility of the triethoxysilyl chain attached to the pypz ligand may also contribute to widen the NMR signals. Although a full assignation cannot be carried out, the presence of aromatic resonances at high δ values (around 9.8 ppm) probably points out to the formation of **2a** or **2d** isomers that present the alfa pyridyl atom in *cis* with regard to a Cl ligand, thus with an intense deshielding effect as discussed in chapter 6 for complexes **C5** and **C6**.

7.2. Spectroscopic and electrochemical properties

The UV-Vis spectrum of complex **C12** is displayed in Figure **7.1** and its spectroscopic features are shown in Table **7.1** together with those for the analogous complexes **C5** and **C6**. The spectrum exhibits a similar shape and maximum wavelength absorptions to those of complex [RuCl$_2$(pypz-Me)(dmso)$_2$], **C6,** obtained in Chapter 6, which is in accordance with the coordination of an alkyl substituted pypz ligand in both cases. Ligand based π-π* bands are observed below 300 nm along with relatively intense bands above 300 nm mainly due to dπ-π* MLCT transitions (see Table **7.1**).[435]

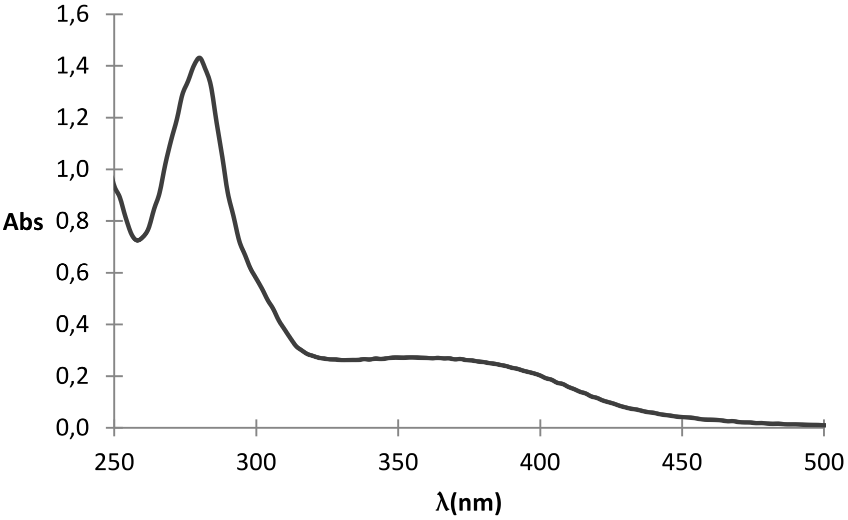

Figure 7.1. UV-visible spectrum of 0.08 mM **C12** in methanol.

Table 7.1. UV-vis spectroscopic features for complexes **C5**, **C6** and **C12**.

Compound	λmax, nm (ε, M^{-1}·cm^{-1})	Reference
[Ru^{II}Cl$_2$(pypz-Si)(dmso)$_2$], **C12**	282 (23184), 374 (4340)^a	This chapter
[Ru^{II}Cl$_2$(pypz-H)(dmso)$_2$], **C5**	264 (27904), 320 (4150), 408 (1914)^b	Chapter 6
[Ru^{II}Cl$_2$(pypz-Me)(dmso)$_2$],**C6**	277 (21913), 366 (5669)^b	Chapter 6

^{a} in methanol; ^{b} in CH$_2$Cl$_2$

The redox properties of complex **C12** have been determined by cyclic voltammetry (CV) experiments and the voltammetry obtained for the complex in dichloromethane is displayed in Figure **7.2**. The complex exhibits two irreversible redox processes (an oxidation at at E_{pa} = 1.21 V and a reduction at E_{pc} = 0.48 V) along with a quasireversible monoelectronic redox wave at $E_{1/2}$ =0.73 V *vs.* SCE. All these redox processes would agree with the occurrence of different isomers (as stated by NMR experiments), presumably corresponding in some cases to dmso linkage isomers given the relatively high differences in the potential values. A comparison with the analogous complexes **C5** and **C6** (Table **7.2**) seems to indicate that the Ru(III/II) process for the Ru-S_{dmso} species would correspond to the irreversible oxidation found at 1.21 V and the wave at E_{pc} = 0.48 V could be the reduction of the related Ru-O_{dmso} species generated after linkage isomerization (in a similar way to the behavior displayed by pyrazole complexes **C7**-**C11**, Chapter 6) but a precise assignation necessary goes through the separation and independent characterization of the isomeric species.

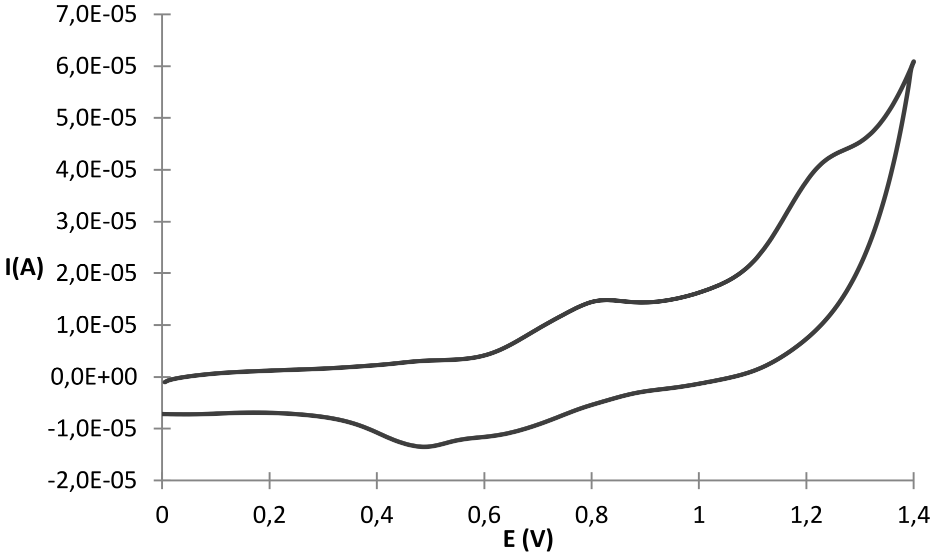

Figure 7.2. Cyclic voltammogram of **C12** in CH_2Cl_2.

Table 7.2. Electrochemical data (CH_2Cl_2 +0.1M TBAH *vs*. SCE) for complexes **C5**, **C6** and **C12**.

Compound	$E_{1/2}$ (V)	References
[$Ru^{II}Cl_2$(pypz-Si)$(dmso)_2$], **C12**	1.21^a 0.73 0.48^b	This chapter
[$Ru^{II}Cl_2$(pypz-H)$(dmso)_2$], **C5**	1.1	Chapter 6
[$Ru^{II}Cl_2$(pypz-Me)$(dmso)_2$],**C6**	0.92	Chapter 6

[a]E_{pa} value; [b]E_{pc} value

7.3. Strategies for the immobilization of the Ru complex

The immobilization method used for the heterogenization of [$Ru^{II}Cl_2$(pypz-Si)$(dmso)_2$] (**C12**) explained in this chapter is based on covalent binding, consequently a strong interaction between the catalyst and the support is achieved. In order to create this covalent bond the -N-(3-(triethoxysilyl)propyl)acetamide group was attached to pypz to generate the **L5** ligand (see Scheme **7.1** for ligand structure) that will be used to bond the surface of silica particles through the terminal triethoxysilyl groups.

In this chapter, silica mesoporous particles (**SP2**) as the ones previously used in Chapter 5 were chosen as heterogeneous support. The functionalization of these supports and the immobilization of the complexes were performed through two different synthetic strategies that are outlined in Scheme **7.2** and are further detailed below.

Strategy I) Functionalization of the supports with the ligand

In the first step, **L5** was anchored to **SP2** by a reflux in toluene in order to achieve the hydrolysis of the ester groups and consequently the functionalization of the support with the ligand.

In the second step, [$RuCl_2(dmso)_4$] was coordinated to the ligand-functionalized particles in ethanol and the resulting **SP2-C12**modified silica was centrifuged, washed with methanol and dried in a hot air oven.

Strategy II) Attachment of the previously synthesized complex

For this strategy, **C12** was directly anchored to **SP2**. A reflux in toluene was needed for the hydrolysis of the ester groups. The resulting **SP2-C12** modified silica was centrifuged, washed with methanol and dried in a hot air oven.

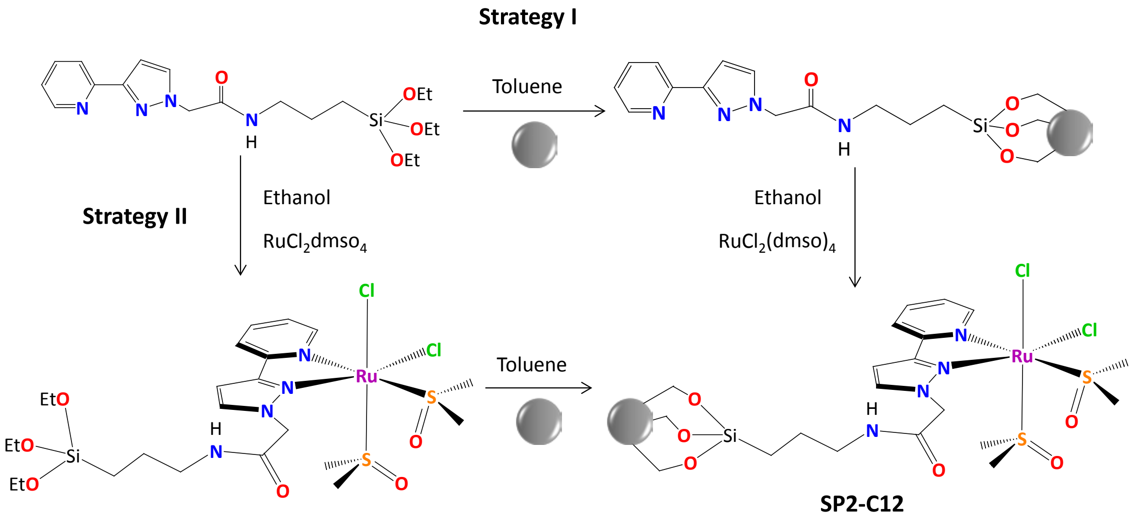

Scheme 7.2. Synthetic strategies for immobilization of **C12**. Grey spheres represent the **SP2** silica particles.

As stated in Chapter 5, there are few examples in the literature where strategy I is used.[364] The second one is more frequent[354,363] and other strategies involving the anchoring of a linker prior to the ligand are also described.[158,335]

7.4. Characterization of the functionalized supports

The characterization of the heterogeneous supports was made in the final step of the synthesis. The coloration of the resulting support may be used as a first visual indication of the success of the reaction. Both strategies led to **SP2-C12** final products with very similar spectroscopic and electrochemical characteristics and therefore the discussion that follows is based only on the results obtained for silica particles prepared through strategy II.

The amount of catalyst anchored onto the silica supports was determined by atomic emission (ICP-AES) spectroscopy. For strategy I, 3.5% Ru anchored was obtained, whereas this value increases to 4.5% for strategy II.

The functionalized **SP2-C12** particles were characterized by UV-visible spectroscopy (Figure **7.3**). The UV-Vis spectrum obtained for **SP2-C12** was compared with that of the homogeneous compound **C12**, confirming that the immobilized species is indeed complex **C12** based on the similarity of the respective spectra. The complex exhibits ligand based π-π* bands below 300 nm and relatively intense bands above 300 nm mainly due to dπ(Ru)-π*(L) MLCT transitions.[435] The π-π* bands suffer a slight shift towards lower wavelengths with respect to complex **C12**, probably due to the presence of the silica support which may affect the polarity of the complex environment modifying λ values.[466,467] We must also take into account that the UV-vis spectrum for **SP2-C12** particles is registered on a suspension of the particles in methanol whereas the homogeneous complex **C12** is characterized in solution.

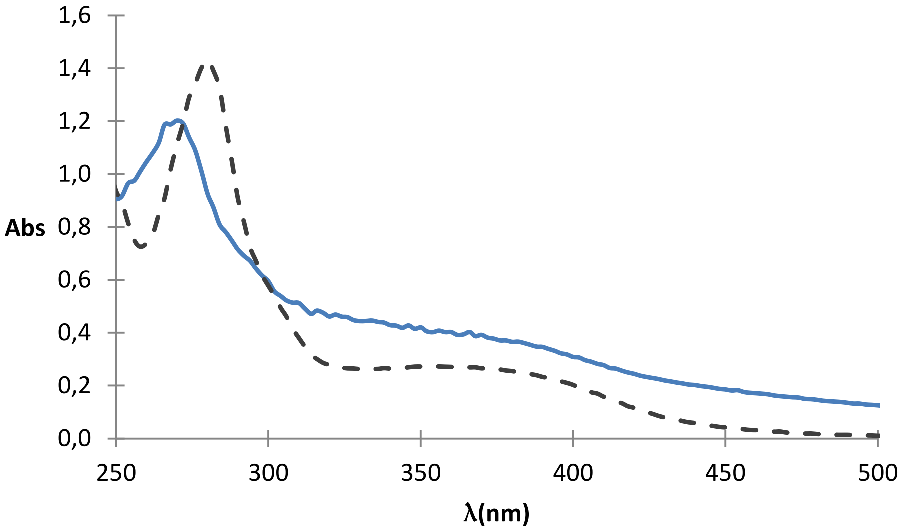

Figure 7.3. UV-vis spectra for **SP2-C12** (blue) and homogeneous complex **C12** (dotted grey) in methanol.

The electrochemical properties of the **SP2-C12** have been studied by differential pulse voltammetry (DPV) experiments and the voltammetry obtained is displayed in Figure **7.4**.

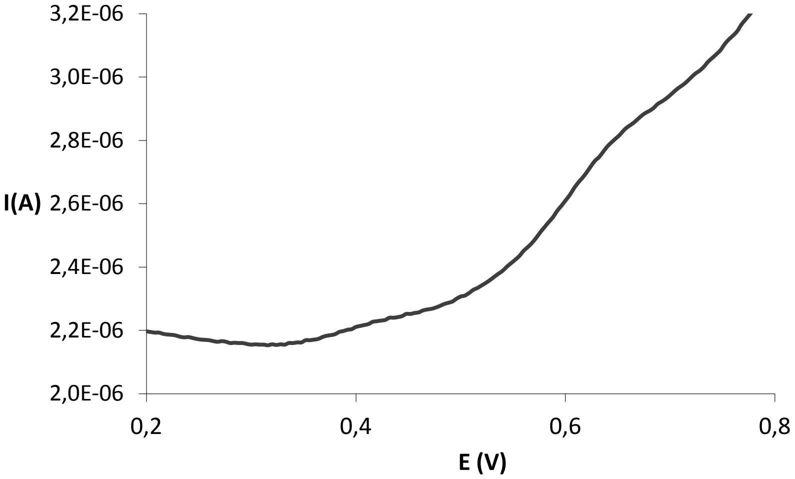

Figure 7.4. Differential pulse voltammetry of **SP2-C12** in CH_2Cl_2.

As can be observed, two redox processes are observed at $E_{1/2}$ = 0.42 V and $E_{1/2}$ = 0.68 V *vs.* SCE which are values similar to that registered for two of the redox processes exhibited by complex **C12** in cyclic voltammetry (Table **7.2**). The slight differences with regard to the values corresponding to **C12** could be due to the influence of the silica support. Thus, the electrochemical properties of **C12** are roughly maintained after heterogenization on the silica particles.

7.5. Catalytic activity in hydration of nitriles

The catalytic activity of the ruthenium complex **C12** and its analogous heterogeneous system **SP2-C12** were checked in the hydration of two nitrile substrates under neutral conditions using water as solvent at 80ºC. It is important to remark here that these catalytic essays are preliminary since separation and characterization of the different isomers in complex **C12** would be necessary to establish solid correlations between structure and catalytic performance. Benzonitrile and acrylonitrile were used as test substrates. Table **7.3** shows the preliminary results obtained with complex **C12** in homogeneous nitrile hydration, together with the conversion and selectivity values attained with [RuCl$_2$(pypz-H)(dmso)$_2$], **C5**, and [RuCl$_2$(pypz-Me)(dmso)$_2$], **C6** (chapter 6) for comparison purposes.

Table 7.3. Ru-catalyzed hydration of nitriles to amides in water using complexes **C5**, **C6** and **C12** as catalyst. [a]

Substrate	**C12**		**C5**		**C6**	
	Conv. (%)	**Select.[b] (%)**	**Conv. (%)**	**Select.[b] (%)**	**Conv. (%)**	**Select.[b] (%)**
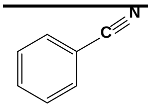	29	96	75	>98	35	>98
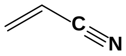	39	>98	23	80	42	>98

[a] Reactions performed at 80°C using 1 mmol of nitrile in 3 ml of water. [Substrate]:[Ru] ratio = 100:1. Time: 20 h reaction.

[b] Selectivity for the amide is determined by ^{1}H-NMR analysis of the reaction mixture.

As we can observe in Table **7.3**, complex **C12** was found to be active towards nitrile hydration with high values of selectivity, despite only moderate values of conversion were obtained. It is striking to see that the catalytic ability of complex **C12** is in the range of that observed previously for complex **C6** that also contains an alkyl-pyrazole ligand, indeed evidencing that the pyrazole H atom is a determinant factor in the reactivity of this type of complexes. Steric arguments could also play a role in **C12** mediated catalysis given the higher volume and the chain flexibility of the triethoxysilyl ligand **L5** that could somewhat hinder the substrate approach and, indeed, the conversion values are slightly lower for **C12** than for **C6**, but it does not seem to constitute a crucial factor in reactivity.

The heterogeneous catalytic hydration with **SP2-C12** as catalyst has been preliminary tested using benzonitrile and acrylonitrile as substrates and the results obtained for benzonitrile are shown in Table **7.4**, where the performances of three consecutive reuses of the catalytic system are displayed (the conversions attained for acrylonitrile were below 10% and are not included in the table). As can be observed, low conversion values were obtained but with excellent selectivity for the amide product.

The complexes show a slightly decrease of the conversion values with the successive runs but the selectivity for the amide is well maintained. As mentioned in the introduction, the control of the activity in heterogeneous catalytic systems is not easy since active sites are placed in a microporous environment that often causes diffusion control of the catalyzed reaction and thus reduces the activity and the selectivity degree. In this case, the conversions are indeed lower than the analogous homogeneous system but keeping an excellent selectivity.

Table 7.4. Ru-catalyzed hydration of benzonitrile to benzamide in water using the heterogeneous **SP2-C12** system as catalyst throughout three consecutive reuses.[a]

Substrate	**Run 1**		**Run 2**		**Run 3**	
	Conv. (%)	**Select.[b] (%)**	**Conv. (%)**	**Select.[b] (%)**	**Conv. (%)**	**Select.[b] (%)**
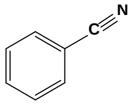	16	>98	12	>98	<10	95

[a] Reactions performed at 80ºC using 1 mmol of nitrile in 3 ml of water. [Substrate]:[Ru] ratio = 100:1. Time: 20 h reaction.

[b] Selectivity for the amide is determined by ^{1}H-NMR analysis of the reaction mixture.

In summary, in this chapter we have synthesized and characterized a new compound, [RuCl$_2$(pypz-Si)(dmso)$_2$] (**C12**) and its heterogenization onto silica particles was successfully achieved using two different strategies. Both catalysts (homogeneous and heterogeneous) have been characterized by spectroscopic and electrochemical techniques.

The UV-Vis spectra for **SP2-C12** has been compared with that of the homogeneous compound **C12** in solution, confirming the immobilization of the complex on the silica surface. The bands observed for **SP2-C12** suffer a slight shift towards lower wavelengths with respect to complex **C12**, probably due to the presence of silica support.

The redox properties of homogeneous and heterogeneous systems have been compared and several different redox processes are found in both cases. For the heterogeneous complex **SP2-C12** a slightly lower potential value is obtained when compared with the analogous homogeneous complex **C12** that could be due to the influence of the silica support.

Preliminary studies on nitrile hydration in water using **C12** as catalyst have displayed a degree of performance comparable to that of the pypz-Me complex **C6**, thus manifesting the influence of the presence or absence of the pyrazole H atom on catalysis. The heterogeneous **SP2-C12** system has also been tested displaying a highly remarkable selectivity for the amide product as well as moderate recyclability despite low conversion values were obtained.

CONCLUSIONS

Chapter 8

Conclusions

- Two new ruthenium complexes containing the tridentate trpy-P-Et and the nonsymmetric didentate pypz-Me ligands, $[Ru^{II}Cl(trpy\text{-}P\text{-}Et)(pypz\text{-}Me)](PF_6)$ (**C3**) and $[Ru^{II}(trpy\text{-}P\text{-}Et)(pypz\text{-}Me)(OH_2)](PF_6)_2$ (**C4**), have been synthesized and thoroughly characterized by structural, analytical and spectroscopic techniques.

- In the case of the chloridocomplex **C3** a mixture of two isomers (*cis* and *trans*) with similar solubility are obtained in an approximate equimolar ratio. The crystal structure of a 1:1 mixture of *trans* and *cis*-**C3** has been solved through X-ray diffraction analysis, showing a distorted octahedral environment for the Ru metal center.

- The aqua complex **C4** was easily obtained after refluxing the chlorido complex **C3** in water without the need of Ag^+ as precipitating reagent, unlike in the synthesis of the analogous $[Ru(trpy)(pypz\text{-}Me)OH_2)]^{2+}$ complex. This evidences a different influence of electronic factors arising from the phosphonate group of the trpy-P-Et ligand.

- The redox characterization of the Ru-aqua **C4** isomers showed the occurrence of a two-electron (IV/II) redox process in both cases, with slightly higher *E* values than that found for the analogous *cis*- and *trans*-$[Ru(trpy)(pypz\text{-}Me)(OH_2)]^{2+}$ complexes. The pKa values for the Ru(II) species are also lower than those of the analogous trpy complexes and both observations are in accordance with the electron-withdrawing character of the phosphonate group of the trpy-P-Et ligand in **C4**. The geometrical factors also determine the differences observed between the two isomers of a specific complex.

- Compound **C4** was tested in the epoxidation of *cis*-β-methylstyrene showing high levels of conversion and selectivity for the *cis*-epoxide, with no formation of the *trans*-epoxide. This behavior is consistent with the occurrence of a bielectronic (IV/II) redox process in the catalysts that favors $2e^-$ versus $1e^-$ transfer, as is the case for the two isomers of catalyst **C4**.

- Compounds **C4** and $[Ru(trpy)(pypz\text{-}Me)(OH_2)]^{2+}$ were checked in the hydration of benzonitrile showing a similar catalytic performance, with moderate conversion and high selectivity values. The hydration of other nitriles using the aquacomplex

$[Ru(trpy)(pypz\text{-}Me)(OH_2)]^{2+}$ as catalyst displayed moderate conversion and high selectivity values in most cases, where the electronic properties of the substrates influence the extent of the hydration reaction.

- The immobilization of **C4** was successfully achieved using two different strategies in different supports (**SP1**, **SP2** and **MSP**) through the functionalization of the terpyridine ligand with a phosphonate group (trpy-P) that allowed either the anchoring of this ligand onto the surface of the different supports and the subsequent preparation of compounds (strategy 1), or the immobilization of the previously synthesized Ru complexes onto the supports (strategy 2)

- The **C4**-functionalized supports were fully characterized through ICP-AES, SEM and TGA, together with spectroscopic and electrochemical techniques. This characterization corroborates that the Ru compounds anchored are similar to that obtained in solution, without modifying the coordination and electronic properties of the latter.

- The heterogeneous systems **SP2-C4** and **MSP-C4** were tested as catalysts in epoxidation of alkenes and hydration of nitriles. **SP2-C4** was effective in the epoxidation of a variety of olefin substrates and, in the case of *cis*-β-methylstyrene, it presented high levels of conversion and stereoselectivity for the *cis* epoxide. System **MSP-C4** showed moderate conversion and selectivity values in the epoxidation of styrene with lower values than that displayed by the analogous **SP2-C4** catalyst, manifesting a different effect of the SP and MSP supports on the catalytic performance.

- The reutilization of systems **SP2-C4** and **MSP-C4** in the epoxidation of alkenes has been evaluated demonstrating the effective recyclability of the catalytic system and keeping moderate conversion and selectivity values up to 3 or 4 successive runs, in all cases. The stereoselectivity for the *cis*-epoxide was maintained through different reuses of the **SP2-C4** catalytic system, although it attained a value slightly lower than the analogous homogeneous catalyst **C4**, indicating an influence of the silica support

- Heterogeneous system **SP2-C4** was also checked in the hydration of benzonitrile and low values of nitrile conversion were achieved but with high values of selectivity for the amide. The system was reused and a loss of activity was observed throughout the consecutive runs.

- A new family of ruthenium dmso complexes containing different pyrazole ligands, $[RuCl_2(pypz\text{-}H)(dmso)_2]$ (**C5**), $[RuCl_2(pypz\text{-}Me)(dmso)_2]$ (**C6**), $[RuCl_2(pz\text{-}H)(dmso)_3]$ (**C7**), $[RuCl_2(CH_3\text{-}pz\text{-}H)(dmso)_3]$ (**C8**), $[RuCl_2(NO_2\text{-}pz\text{-}H)(dmso)_3]$ (**C9**), $[RuCl_2(CF_3\text{-}pz\text{-}H)(dmso)_3]$ (**C10**) and $[RuCl_2(Br\text{-}Hind)(dmso)_3]$ (**C11**), has been synthesized and thoroughly characterized in solution and in solid state. The compounds have been mostly obtained as a single geometrical isomer and this can be rationalized taking into account structural and electronic factors as strong hydrogen bonding and synergistic electronic effects among ligands.

- For all complexes the crystal structures have been solved by X-ray diffraction analysis and it can be observed that in all cases the Ru metal center adopts an octahedrally distorted type of coordination. The characterization in solution is also consistent with the structures obtained in the solid state.

- The redox properties of complexes **C5**-**C11** have been investigated. Electrochemically irreversible Ru(II)/Ru(III) redox processes at potential values around 1.5-1.7 V are observed for the monodentate pyrazole complexes **C7**-**C11**, and the differences are consistent with the electronic characteristics of the substituents on the pyrazole ligands. In the case of complexes with didentate pyrazole ligands (**C5**-**C6**), reversible waves are observed at lower potential values than that displayed by complexes **C7**-**C11**. The difference in the redox potential values between the two groups of complexes (with didentate or monodentate ligands) is explained by the stronger π-acceptor capacity of the additional dmso ligand with regard to the pyridyl ring of pypz-R_1 (R_1 = H or Me).

- For complexes **C7**-**C11** a quantitative Ru-S → Ru-O linkage isomerization process of a dmso ligand is observed in parallel with the oxidation of Ru^{II}(dmso-S) species to

Ru^{III}(dmso-O). Complex **C5** also displays a certain degree of linkage isomerization though it is not as extensive as that observed for **C7**-**C11**. The isomerization process has been studied in a deeper way for complexes **C5** and **C8** through scan rate dependent cyclic voltammograms and the rates of linkage isomerization and the thermodynamic properties were calculated, confirming the above observations.

- The thermodynamic parameters determined for **C5** and **C8** allow concluding that, in Ru^{II} redox state, the dmso ligand in compounds **C5** and **C8** displays a high preference to be bound to the metal through the S atom. In oxidation state (III), complex **C8** presents a higher $\boldsymbol{k_{S-O}^{III}}$ kinetic isomerization constant than **C5** probably due to the presence of an additional S-bound dmso ligand in **C8** (instead of the pypz-H pyridyl ring in **C5**) that further lowers the electron density at the metal center. Steric factors might also favor the linkage isomerization in **C8** since three S-bound dmso ligands would probably encounter significant steric hindrance when coordinating in facial arrangement the smaller Ru(III) ion.

- Diferent photoinduced substitution reactions were studied for **C5** and **C8** in acetonitrile, chloroform and water through UV-visible, NMR and cyclic voltammetric experiments which allow evidence that, after irradiation of the complexes solutions, a substitution of one dmso ligand for solvent took place in the case of acetonitrile and water, whereas a new chlorido ligand was coordinated to Ru upon irradiation in chloroform. The Cl$^-$ coordination occurs in parallel with a Ru(II) to Ru(III) oxidation, leading to the formation of the trichlorido **C5’’** and **C8’’** complexes. For **C5’’**, it was possible to isolate crystals and the X-ray structure obtained confirms the coordination of the remaining dmso ligand through its S atom despite the II→III oxidation of the Ru metal center. In contrast, Ru-S to Ru-O linkage isomerization is postulated in **C8''** from DPV experiments that evidence two distinctive redox processes when starting the scanning potential from low *E* values.

- The nitrile hydration catalysis has been evaluated for complexes **C5**-**C11** in water as solvent using different nitrile substrates and moderate to high conversion values with excellent selectivity for the amide product were observed in most cases. A comparison of the activities displayed by complexes **C5** and **C7** evidences an improved efficiency for the latter, which could be explained by the higher number of potentially labile coordination sites as a plausible mechanism involves the initial decoordination of a dmso ligand. The enhanced electron-withdrawing character of an additional dmso ligand in **C7** can also contribute to increase the electron-withdrawing character of the metal center thus facilitating the activation of the nitrile substrate. For **C6**, we have observed high values of selectivity despite conversion values were moderate compared to **C5**, thus evidencing the positive influence of the H atom of the pyrazole ring on the catalytic performance. In the case of **C8**-**C11**, high values of selectivity were obtained although moderate values of conversion were achieved which, on the other hand, display a certain dependence on the electronic characteristics of the different R_2-pz-H ligands coordinated to Ru in each catalyst.

- The reusability of catalysts **C5** and **C7** in nitrile hydration carried out in water and glycerol media was evaluated using benzonitrile and 4-(trifluoromethyl)benzonitrile as substrates, displaying a highly remarkable selectivity for the amide products as well as moderate recyclability in solution.

- A new compound containing the triethoxysilyl-functionalized ligand pypz-Si, $[RuCl_2(pypz\text{-}Si)(dmso)_2]$ (**C12**), has been synthesized and characterized and its heterogenization onto silica particles was successfully achieved using the two strategies described for the anchoring of catalyst **C4**. Both catalysts (homogeneous and heterogeneous) have been characterized by spectroscopic and electrochemical techniques. Preliminary studies on homogeneous nitrile hydration in water using **C12** as catalyst and benzonitrile or acrylonitrile as substrates have displayed a degree of performance comparable to that of the pypz-Me complex **C6**, again manifesting the influence of the pyrazole H atom on catalysis as much better performance was observed for the analogous complex **C5**, containing the pypz-H ligand. The heterogeneous **SP2-C12** system has also been tested showing a highly remarkable selectivity for the amide product as well as moderate recyclability, although low conversion values were obtained.

In general, this work collects the syntheses and thorough study of new Ru compounds as catalysts in important transformations as epoxidation of alkenes and nitrile hydration reactions. The immobilization of these compounds onto different silica supports allows the reutilization of the catalysts in the mentioned processes. As global findings we can note the following:

- Ruthenium terpyridine complexes constitute the first example of compounds with stoichiometry $[Ru(trpy\text{-}R)(pypz\text{-}Me)(OH_2)]^{n+}$ (where R can be H or a phosphonate group) that have been studied as catalysts in the nitrile hydration reaction. The immobilization of the catalysts leads to significantly lower performance when compared to the analogous homogeneous catalysts, indicating an influence of the silica support. On the other hand, the silica-supported heterogeneous systems can be applied and reused in olefin epoxidation with good upkeep of the olefin conversion and epoxide selectivity values.

- Ruthenium dmso compounds are the first examples of complexes containing dmso ligands successfully applied to nitrile hydration reaction in environmentally friendly media, where electronic and geometrical factors of ligands and substrates are responsible for the distinctive catalytic behavior. The essays described in glycerol are the first reported for this type of process in such solvent.

- Complexes containing dmso ligands display higher conversion degrees in nitrile hydration than terpyridine complexes though high values of selectivity were achieved in both cases. This fact could be explained by the higher number of potentially labile coordination sites in the former, since the possible mechanism most commonly accepted involves the initial decoordination of a ligand.

REFERENCES

Chapter 9

References

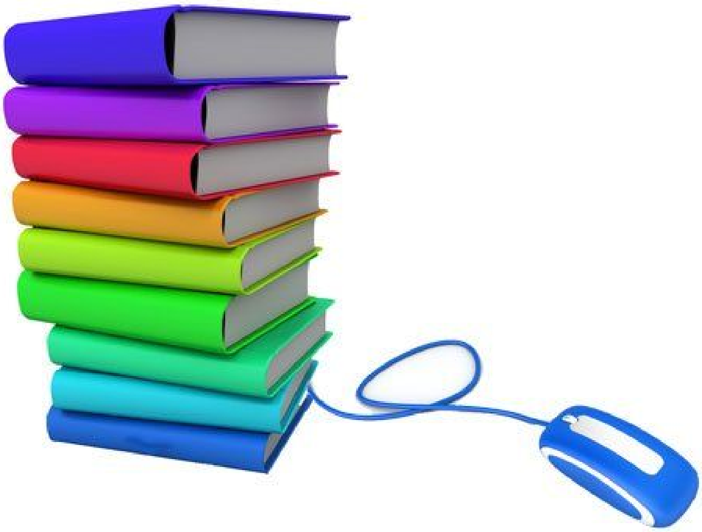

[1] Griffith, W. P. *Chem. Soc. Rev*. **1992**, *21*, 179.

[2] Bruneau, C. *Ruthenium catalysts and fine chemistry*; Springer-Verlag: Berlin, **2004**.

[3] Meyer, T. J. *Pure Appl. Chem*. **1990**, *62*, 1003.

[4] Qu, P.; Thompson, D. W.; Meyer, G. J. *Langmuir* **2000**, *16*, 4662.

[5] Butler, J.; George, M.; Schoonover, J.; Dattelbaum, D.; Meyer, T. *Coord. Chem. Rev*. **2007**, *251*, 492.

[6] Meyer, T. J.; Huynh, M. H. V. *Inorg. Chem*. **2003**, *42*, 8140.

[7] Seok, W. K.; Meyer, T. J. *Inorg. Chem*. **2005**, *44*, 3931.

[8] Goeltz, J. C.; Hanson, C. J.; Kubiak, C. P. *Inorg. Chem*. **2009**, *48*, 4763.

[9] Ley, S. V.; Norman, J.; Griffith, W. P.; Marsden, S. P. *Synthesis* **1994**, *7*, 639.

[10] Whittall, I. R.; McDonagh, A. M.; Humphrey, M. G.; Samoc, M. *Adv. Organomet. Chem*. **1999**, *43*, 349.

[11] Coe, B. *J. Acc. Chem. Res*. **2006**, *39*, 383.

[12] Green, K.; Cifuentes, M.; Corkery, T.; Samoc, M.; Humphrey, M. *Angew. Chem. Int. Ed*. **2009**, *48*, 7867.

[13] Coe, B. J. *Coord. Chem. Rev*. **2013**, *257*, 1438.

[14] Desplanches, C.; Ruiz, E.; Alvarez, S. *Eur. J. Inorg. Chem*. **2003**, *2003*, 1756.

[15] Mikuriya, M.; Yoshioka, D.; Handa, M. *Coord. Chem. Rev*. **2006**, *250*, 2194.

[16] Wang, D.; Yang, H.-Q.; Wu, G.-H.; Hou, X.-F.; Yang, J.-H. *Inorg. Chem. Commun*., **2014**, *46*, 241.

[17] Upadhyay, A.; Rajpurohit, J.; Singh, M. K.; Dubey, R.; Srivastava, A. K.; Kumar, A.; Rajaraman, G.; Shanmugam, M. *Chem. Eur. J*. **2014**, *20*, 6061.

[18] Fillaut, J.; Andriès, J.; Marwaha, R. D.; Lanoë, P.; Lohio, O.; Toupet, L.; Gareth Williams, J. *J. Organomet. Chem*. **2008**, *693*, 228.

[19] Kizaki, T.; Abe, T.; Matsumoto, T.; Ogo, S. *Chem. Lett*. **2010**, *39*, 128.

[20] Chen, X.-M.; Wu, G.-H.; Chen, J.-M.; Jiang, Y.-Q.; Chen, G.-N.; Oyama, M.; Chen, X.; Wang, X.-R. *Biosens. Bioelectron*. **2010**, *26*, 872.

[21] Aquino, M. A. *Coord. Chem. Rev*. **1998**, *170*, 141.

[22] Yoshida, J.; Watanabe, G.; Kakizawa, K.; Kawabata, Y.; Yuge, H. *Inorg. Chem*. **2014**, *52*, 11042.

[23] Bergamo, A.; Sava, G. *Dalton Trans*., **2007**, 1267.

[24] Silva, D. D. O. *Anticancer Agents Med. Chem*. **2010**, *10*, 312.

[25] Ji, L.; Zheng, W.; Lin, Y.; Wang, X.; Lü, S.; Hao, X. Luo, Q.; Li, X.; Yang, L.; Wang, F. *Eur. J. Med. Chem*. **2014**, *77*, 110.

[26] Vos, J. G.; Kelly, J. M. *Dalton Trans*. **2006**, *41*, 4869.

[27] Zhang, S.; Ding, Y.; Wei, H. *Molecules* **2014**, *19*, 11933.

[28] Xie, P.-H. Hou, Y.-J.; Wei, T.-X.; Zang, B.-W.; Cao, Y.; Huang, C.-H. *Inorg. Chim. Acta* **2000**, *308*, 73.

[29] Chen, C.; Pootrakulchote,N.; Wu, S.; Wang, M.; Li, J.; Tsai, J.; Wu, C.; Zakeeruddin, S. M.; Grätzel, M. *J. Phys. Chem. C*. **2009**, *113*, 20752.

[30] Sirimanne, P.; Winther-Jensen, B.; Weerasinghe, H.; Cheng, Y. *Thin Solid Films* **2010**, *518*, 2871.

[31] Yin, J.-F.; Velayudham, M.; Bhattacharya, D.; Lin, H.-C.; Lu, K.-L. *Coord. Chem. Rev*. **2012**, *256*, 3008.

[32] Kurzeev, S. A.; Medved'ko, A. V.; Grinberg, V. A.; Kozyukhin, S. A.; Emets, V. V.; Sadovnikav, A. A.; Baranchikov, A. E.; Ivanov, V. K.; Andreev, V. N.; Nizhnikovskii, E. A. *J. Rus. Inorg. Chem*. **2014**, *59*, 658.

[33] Barigelletti, F.; Flamigni, L. *Chem. Soc. Rev*. **2000**, *29*, 1.

[34] Belser, P.; De Cola, L.; Hartl, F.; Adamo, V.; Bozic, B.; Chriqui, Y.; Iyer, V. M.; Jukes, R. T. F.; Kühni, J.; Querol, M.; Roma, S.; Salluce, N. *Adv. Funct. Mater*. **2006**, *16*, 195.

[35] Mishra, L.; Yadaw, A. K.; Govil, G. *Indian J. Chem., Sect. A: Inorg., Bioinorg., Phys., Theor. Anal. Chem*. **2003**, *42A*, 1797.

[36] Newkome, G. R.; Cho, T. J.; Moorefield, C. N.; Mohapatra, P. P.; Godínez, L. A. *Chem. Eur. J*. **2004**, *10*, 1493.

[37] Delaney, S.; Pascaly, M.; Bhattacharya, P. K.; Han, K.; Barton, J. K. *Inorg. Chem*. **2002**, *41*, 1966.

[38] Zhang, Q.; Liu, J.; Liu, J.; Zhang, P.; Ren, X.; Liu, Y.; Huang, Y.; Ji, L. *J. Inorg. Biochem*. **2004**, *98*, 1405.

[39] Zhang, Q.; Liu, J.; Ren, X.; Zhang, P. *Transit. Metal. Chem*. **2005**, *30*, 285.

[40] Tan, L.; Zhang, S.; Liu, X.; Xiao, Y. *Aust. J. Chem*. **2008**, *61*, 725.

[41] Liu, Y.; Liang, Z.; Li, Z.; Zeng, C.; Yao, J.; Huang, H.; Wu, F. *Biometals* **2010**, *23*, 739.

[42] He, X.; Zeng, L.; Yang, G.; Xie, L. Sun, X.; Tan, L. *Inorg. Chim. Acta* **2013**, *408*, 9.

[43] Ding, F.; Sun, Y.-G.; Verpoort, F.; Dragutan, V.; Dragutan, I. *J. Mol. Cat. A-Chem.* **2014**, *386*, 86.

[44] Chan, K.-H.; Guan, X.; Lo, V. K.-Y.; Che, C.-M. *Angew. Com. Int. Ed.* **2014**, *53*, 2982.

[45] Hemelaere, R.; Caijo, F.; Mauduit, M.; Carreaux, F.; Carboni, B. *Eur. J. Org. Chem.* **2014**, 3328.

[46] Ascic, E.; Ohm, R. G.; Petersen, R.; Hansen, M. R.; Hansen, C. L.; Madsen, D.; Tanner, D.; Nielsen, T. E. *Chem. Eur. J.* **2014**, *20*, 3297.

[47] Bokare, A. D.; Choi, W. *J. Haz. Mat.* **2014**, *275*, 121.

[48] Pagliaro, M.; Campestrini, S.; Ciriminna, R. *Chem. Soc. Rev.* **2005**, *34*, 837.

[49] Bagh, B.; McKinty, A. M.; Lough, A. J.; Stephan, D. W. *Dalton Trans.* **2014**, *43*, 12842.

[50] Aguiló, J.; Francàs, L.; Hiu, H. J.; Bofill, R.; Garcia-Anton, J.; Benet-Buchholz, J.; Llobet, A.; Escriche, L.; Sala, X. *Cat. Sci. Tech.* **2014**, *4*, 190.

[51] Fernandez-Zumel, M. A.; Kiefer, G.; Thommes, K.; Scopelliti, R.; Severin, K. *Eur. J. Inorg. Chem.* **2010**, 3596.

[52] Siffert, N.; Bühl, M. *J. Am. Chem. Soc.* **2010**, *132*, 8056.

[53] Duman, S.; Özkar, S. *Int. J. Hyd. Ener.* **2013**, *38*, 180.

[54] Aydemir, M.; Baysal, A. *J. Organomet. Chem.* **2010**, *695*, 2506.

[55] Anitha, P.; Manikandan, R.; Endo, A.; Hashimoto, T.; Viswanathamurthi, P. *Spect. Acta Part A: Mol. Biomol. Spect.* **2012**, *99*, 174.

[56] Zeng, L.; Wu, F.; Li, Y.-Y.; Dong, Z.-R.; Gao, J.-X. *J. Organomet. Chem.* **2014,** *762*, 34.

[57] Ok, F.; Aydemir, M.; Durap, F.; Baysal, A. *Appl. Organomet. Chem.* **2014**, *28*, 38.

[58] Mandal, S.; Samanta, S.; Mondal, T. K.; Goswami, S. *Organometallics* **2012**, *31*, 5282.

[59] Reddy, M. C.; Jeganmohan, M. *Org. Lett.* **2014**, *16*, 4866.

[60] Mangold, S. L.; O'Leary, D. J.; Grubbs, R. H. *J. Am. Chem. Soc.* **2014**, *136*, 12469.

[61] Hartung, J.; Dornan, P. K.; Grubbs, R. H. *J. Am. Chem. Soc.* **2014**, *136*, 13029.

[62] Antonucci, A.; Bassetti, M.; Bruneau, C.; Dixneuf, P. H.; Pasquini, C. *Organometallics* **2010**, *29*, 4524.

[63] van Leeuwen, P. W. N. M. *Homogeneous Catalysis: Understanding the Art*; Springer **2004**.

[64] Brandt, W. W.; Dwyer, F. P.; Gyarfas, E. C. *Chem. Rev.* **1954**, *54*, 959.

[65] Dwyer, F. P.; Mellor, D. P. *Chelating Agents and Metal Chelates;* Academic Press: New York **1964**.

[66] Durham, B.; Caspar, J. V.; Nagle, J. K.; Meyer, T. J. *J. Am. Chem. Soc.* **1982**, *104*, 4803.

[67] Pugh, J. R.; Bruce, M. R. M.; Sullivan B. P.; Meyer, T. J. *Inorg. Chem.* **1991**, *30*, 86.

[68] Dovletoglou, A.; Adeyemi, S. A.; Meyer, T. J. *Inorg. Chem.* **1996**, *35*, 4120.

[69] Costentin, C.; Robert, M.; Saveant, J.-M. *Chem. Rev.* **2010**, *110*, PR1-PR40.

[70] Eggleston, D. S.; Goldsby, K. A.; Hodgson, D. J.; Meyer, T. J. *Inorg. Chem.* **1985**, *24*, 4573.

[71] Moyer, B. A.; Meyer, T. J. *J. Am. Chem. Soc.* **1978**, *100*, 3601.

[72] Moyer, B. A.; Meyer, T. J. *Inorg. Chem.* **1981**, *20*, 436.

[73] Binstead, R. A.; Moyer, B. A.; Samuels, G. J.; Meyer, T. J. *J. Am. Chem. Soc.* **1981**, *103*, 2897.

[74] Meyer, T. J. *J. Electrochem. Soc.* **1984**, *131*, 221C.

[75] Masllorens, E.; Rodríguez, M.; Romero, I.; Roglans, A.; Parella, T.; Benet-Buchholz, J.; Poyatos, M.; Llobet, A. *J. Am. Chem. Soc.* **2006**, *128*, 5306.

[76] Dakkach, M.; Atlamsani, A.; Parella, T.; Fontrodona, X.; Romero, I.; Rodríguez, M. *Inorg. Chem.* **2013**, *52*, 5077.

[77] Takeuchi, K.J.; Thompson, M.S.; Pipes, D.W.; Meyer, T.J. *Inorg. Chem.* **1984**, *23*, 1845.

[78] Roecker, L.; Kutner, W.; Gilbert, J.A.; Simmons, M.; Murray, R.W.; Meyer, T.J. *Inorg. Chem.* **1985**, *24*, 3784.

[79] Suen, H.F.; Wilson, S.W.; Pomerantz, M.; Walsh, J.K. *Inorg. Chem.* **1989**, *28*, 786.

[80] Llobet, A. *Inorg. Chim. Acta* **1994**, *221*, 125.

[81] Keene, F.R. *Coord. Chem. Rev.* **1999**, *187*, 121.

[82] Gerli, A.; Reedijk, J.; Lakin, M.T.; Spek, A.L. *Inorg. Chem.* **1995**, *34*, 1836.

[83] Masllorens Llinàs, Ester. *Preparació de nous catalitzadors basats en complexos de Ru i Pd, i el seu ancorament a polímers conductors per a la fabricació de materials multifuncionals*. Universitat de Girona, **2006**. <http://hdl.handle.net/10803/8038>

[84] Concepcion, J.J.; Jurss, J.W.; Templeton, J.L.; Meyer, T.J. *J. Am. Chem. Soc.* **2008**, *130*, 16462.

[85] Dakkach, M.; Fontrodona, X.; Parella, T.; Atlamsani, A.; Romero, I.; Rodríguez, M. *Dalton Trans.* **2014**, *43*, 9916.

[86] Lindquist, I.; Einarsson, P. *Acta Chem. Scand.* **1959**, *13*, 420.

[87] Cotton, F. A.; Elder, R. C. *J. An. Chem. Soc.* **1960**, *82*, 2986.

[88] Meek, D. W.; Straub, D. K.; Drago, R. S. *Bull. Chem. Soc. Japan* **1960**, *33*, 861.

[89] Cotton, F. A.; Francis, R. *J. Inorg. Nucl. Chem.* **1961**, *17*, 62.

[90] Evans, I. P.; Spencer, A.; Wilkinson, G. *J. Chem. Soc., Dalton Trans*. **1973**, *2*, 204.

[91] Alessio, E.; Mestroni, G.; Nardin, G.; Attia, W. M.; Calligaris, M.; Sava, G.; Zorzet, S. *Inorg. Chem.* **1988**, *27*, 4099.

[92] Alessio, E. *Chem. Rev*. **2004**, *104(9)*, 4203.

[93] Mola, J.; Romero, I.; Rodríguez, M.; Bozoglian, F.; Poater, A.; Sola, M.; Parella, T.; Benet-Buchholz, J. *Inorg. Chem*. **2007**, *46*, 10707.

[94] Khan, M. M. T.; Mohiuddin, R.; Vancheesan, S.; Swamy, B. *Ind. J. Chem. Section A: Inorg., Phys., Theor.& Anal.* **1981**, *20A*, 564.

[95] Van der Drift, R. C; Sprengers, J. W.; Bouwman, E.; Mul, W. P.; Kooijman, H.; Spek, A. L.; Drent, E. *Eur. J. Inorg. Chem.* **2002**, *8*, 2147.

[96] Sens, C.; Rodríguez, M.; Romero, I.; Llobet, A.; Parella, T.; Sullivan, B. P.; Benet-Buchholz, J. *Inorg. Chem*. **2003**, *42*, 2040.

[97] Shan, N.; Adams, H.; Thomas, J. A. *Inorg. Chim. Acta* **2006**, *359*, 759.

[98] Martínez, R.; Ramón, D. J.; Yus, M. *Eur. J. Org. Chem.* **2007**, 1599.

[99] Wang, L.; Duan, L.; Stewart, B.; Pu, M.; Liu, J.; Privalov, T.; Sun, L. *J. Am. Chem. Soc.* **2012**, *134*, 18868.

[100] Bolyog-Nagy, E.; Udvardy, A.; Joó, F.; Kathó, A. *Tetrahedron Lett.* **2014**, *55*, 3615.

[101] Sava, G.; Gagliardi, R.; Bergamo, A.; Alessio, E.; Mestroni, G. *Anticancer Res*. **1999**, *19*, 969.

[102] Bergamo, A.; stucco, G.; Gava, B.; Cocchietto, M.; Alessio, E.; Serli, B.; Iengo, E.; Sava, G. *J. Pharm. And Exp. Therap.* **2003**, *305*, 725.

[103] Bratsos, I.; Simonin, C.; Zangranado, E.; Gianferrara, T.; Bergamo, A.; Alessio, E. *Dalton Trans.* **2011**, *40*, 9533.

[104] David, S.; Perkins, R. S.; Fronczek, F. R.; Kasiri, S.; Mandal, S. S.; Srivastava, R. S. *J. Inorg. Biochem.* **2012**, *111*, 33.

[105] Alagesan, M.; Bhuvanesh, N. S. P.; Dharmaraj, N. *Dalton Trans.* **2014**, *43*, 6087.

[106] Sava, G.; Pacor, S.; Mestroni, G.; Alessio, E. *Clin. Exp. Met.* **1992**, *10*, 273.

[107] Mestroni, G.; Alessio, E.; Sava, G.; Pacor, S. Coluccia, M.; Boccarelli, A. *Metal-based drugs* **1994**, *1*, 41.

[108] Alessio, E.; Iengo, E.; Zorzet, S.; Bergamo, A.; Coluccia, M.; Boccarelli, A.; Sava, G. *J. Inorg. Biochem.* **2000**, *79*, 173.

[109] Alessio, E.; Mestroni, G.; Bergamo, A.; Sava, G. *Curr. Top. Med. Chem.* **2004**, *4*, 1525.

[110] Bratsos, L.; Jedner, S.; Gianferrara, T.; Alessio, E. *Chimia* **2007**, *61*, 692.

[111] Alessio, E.; Macchi, M.; Heath, S. L.; Marzilli, L. G. *Inorg. Chem*. **1997**, *36*, 5614.

[112] Hesek, D.; Inoue, Y.; Everitt, S. R. L.; Ishida, H.; Kunieda, M.; Drew, M. G. B. *Chem. Commun.* **1999**, 403.

[113] Malik, K. Z.; Robinson, S. D.; Steed, J. W. *Polyhedron* **2000**, *19*, 1589.

[114] Ashton, P. R.; Ballardini, R.; Balzani, V.; Credi, A.; Dress, K. R.; Ishow, E.; Cornelis, J.; Kocian, O.; Preece, J. A.; Spencer, N.; Stoddart, J. F.; Venturi, M.; Wenger, S. *Chem. Eur. J.* **2000**, *6*, 3558.

[115] Ballardini, R.; Balzani, V.; Credi, A.; Gandolfi, M. T.; Venturi, M. *Int. J. Photoen.* **2001**, *3*, 63.

[116] Baranoff, E.; Collin, J. P.; Furusho, J.; Furusho, Y.; Laemmel, A. C.; Sauvage, J. P. *Inorg. Chem.* **2002**, *41*, 1215.

[117] Smith, M. K.; Gibson, J. A.; Young, C. G.; Broomhead, J. A.; Junk, P. C.; Keene, F. R. *Eur. J. Inorg. Chem.* **2000**, 1365.

[118] Kato, M.; Takayanagi, T.; Fujihara, T.; Nagasawa, A. *Inorg. Chim. Acta* **2009**, *362*, 1199.

[119] Roeser, S.; Maji, S.; Benet-Buchholz, J.; Pons, J.; Llobet, A. *Eur. J. Inorg. Chem.* **2013**, 232.

[120] Jin, Y.; Rack, J. J. *Isr. J. Chem.* **2013**, *53*, 280.

[121] Alessio, E.; Bolle, M.; Milani, B.; Mestroni, G.; Faleschini, P.; Geremia, S.; Calligaris, M. *Inorg. Chem.* **1995**, *34*, 4716.

[122] Pearson, R. G. *J. Chem. Educ.* **1968**, *45*, 643.

[123] Okumura, T.; Morishima, Y.; Shiozaki, H.; Yagyu, T.; Funahashi, Y.; Ozawa, T.; Jitsukawa, K.; Masuda, H. *Bull. Chem. Soc. Jpn.* **2007**, *80*, 507.

[124] Martínez, R.; Brand, G. J.; Ramón, D. J.; Yus, M. *Tetrahedron Lett.* **2005**, *46*, 3683.

[125] Khenkin, A. M.; Shimon, L. J. W.; Neumann, R. *Inorg. Chem.* **2003**, *42*, 3331.

[126] Gonsalvi, L.; Arends, I. W. C. E.; Sheldon, R. A. *Chem. Commun.* **2002**, *3*, 202.

[127] Riley, D. P.; Oliver, J.D. *Inorg. Chem.* **1986**, *25*, 1814.

[128] Srivastava, R. S.; Milani, B.; Alessio, E.; Mestroni, G. *Inorg. Chim. Acta* **1992**, *191*, 15.

[129] Muhherjee, D. K.; Palit, B. K.; Saha, C. R. *J. Mol. Catal.* **1994**, *88*, 57.

[130] Jitsukawa, K.; Shiozaki, H.; Masuda, H. *Tetrahedron Lett.* **2002**, *43*, 1491.

[131] Sava, G.; Pacor, S,: Mestroni, G.; Alessio, E. *Anticanc. Drugs* **1992**, *3*, 25.

[132] Sava, G.; Zorzet, S.; Turrin, C.; Vita, F.; Soranzo, M.; Zabucchi, G.; Cocchietto, M.; Bergamo, A.; DiGiovine, S.; Pezzoni, G.; Sartor L.; Garbisa, S. *Clin. Cancer Res.* **2003**, *9*, 1898.

[133] Bacac, M.; Hotze, A. C. G.; Van der Schilden, K.; Haasnoot, J. G.; Pacor, S.; Alessio, E.; Sava, G.; Reedijk, J. *J. Inorg. Biochem.* **2004**, *98*, 402.

[134] Gava, B.; Zorzet, P.; Spessotto, P.; Cocchietto, M.; Sava, G. *J. Pharmacol. Exp. Ther.* **2006**, *317,* 284.

[135] Antonarakis, E. S.; Emadi, A. *Cancer Chemoth. Pharm.* **2010**, *66*, 1.

[136] Iengo, E.; Mestroni, G.; Geremia, S.; Calligaris, M.; Alessio, E. *J. Chem. Soc. Dalton* **1999**, 3361.

[137] Serli, B.; Iengo, E.; Gianferrara, T.; Zangrando, E.; Alessio, E. *Metal-Based Drugs* **2001**, *8*, 9.

[138] Velderes, A. H.; Bergamo, A.; Alessio, E.; Zangrando, E.; Haasnoot, J. G.; Casarsa, C.; Cocchietto, M.; Zozet, S.; Sava, G. *J. Med. Chem.* **2004**, *47*, 1110.

[139] Groessl, M.; Reisner, E.; Hartinger, C. G.; Eichinger, R.; Semenova, O.; Timerbaev, A. R.; Jakupec, M. A.; Arion, V. B.; Keppler, B. K. *J. Med. Chem.* **2007**, *50*, 2185.

[140] Hudej, R.; Miklavcic, D.; Cemazar, M.; Todorovic, V.; Sersa, G.; Bergamo, A.; Sava, G.; Martincic, A.; Scancar, J.; Keppler, B. K.; Turel, I. *J. Memb. Biol.* **2014**, *247*, 1239.

[141] Hartinger, C. G.; Zorbas-Seifried, S.; Jakupec, M. A.; Kynast, B.; Zorbas, H.; Keppler, B. K. *J. Inorg. Biochem.* **2006**, *100*, 891.

[142] Sheldon, R. A.; Kochi, J. K. *Metal Catalyzed Oxidation of Organic Compounds*; Academic Press; New York, **1981**.

[143] Meunier, B. Ed. *Biomimetic Oxidations Catalyzed by Transition Metal Complexes*, Imperial College Press, **2000**.

[144] Bäckvall, J. E. *Modern Oxidation Methods*, Wiley-VCH: Weinheim, **2004**.

[145] Bruijnincx, P. C. A.; van Koten, G.; Gebbink, R. J. M. K. *Chem. Soc. Rev*. **2008**, *37*, 2716.

[146] Crabtree, R.H. *Oxidation Catalysis by Transition Metal Complexes*, in *Encyclopedia of Inorganic and Bioinorganic Chemistry*, John Wiley & Sons: New York, **2011**.

[147] Lippard, S.J.; Berg, J.M. *Principles of Bioinorganic Chemistry*, University Science Books: Mill Valley, California, **1994**.

[148] Chauhan, S. M. S.; Ray, P. C. *Bioinorg. Med. Chem. Let.* **1991**, *1*, 601.

[149] Han, J. H.; Yoo, S. K.; Seo, J. S.; Hong, S. J.; Kim, S. K.; Kim, C. *Dalton Trans.* **2005**, 402.

[150] Bolzon, L. B.; Airoldi, H. R.; Zanardi, F. B.; Granado, J. G.; Iamamoto, Y. *Microp. and mesop. Mat.* **2013**, *168*, 37.

[151] Mathur, P.; Crowder, M.; Dismukes, G.C. *J. Am. Chem. Soc.* **1987**, *109*, 5227.

[152] Dismukes, G.C. *Chem. Rev*. **1996**, *96*, 2909

[153] Palopoli, C.; Bruzzo, N.; Hureau, C.; Ladeira, S.; Murgida, D.; Signorella, S. *Inorg. Chem.* **2011**, *50*, 8973

[154] Murahashi, S. I.; Komiya, N. *Cat. Today* **1998**, *41*, 339.

[155] Csjernyik, G.; Ell, A. H.; Fadini, L.; Pugin, B.; Bäckvall, J.-E. *J. Org. Chem.* **2002**, *67*, 1657.

[156] Babu, B. P.; Endo, Y.; Bäckvall, J.-E. *Chem. Eur. J.* **2012**, *18*, 11524.

[157] Endo, Y.; Bäckvall, J.-E. *Chem. Eur. J.* **2012**, *18*, 13609.

[158] Papfotiou, F.; Karidi, K.; Garoufis, A.; Louloudi, M. *Polyhedron* **2013**, *52*, 634.

[159] Meunier, B.; de Visser, S. P.; Shaik, S. *Chem. Rev*. **2004**, *104*, 3947.

[160] Tabushi, I.; Kodera, M.; Yokoyama, M. *J. Am. Chem. Soc*. **1985**, *107*, 4466.

[161] Groves, J. T.; Nemo, T. E.; Myers, R. S. *J. Am. Chem. Soc.* **1979**, *101*, 1032.

[162] Sheldon, R. A. *Metalloporphyrins in Catalytic Oxidations*; Marcel Dekker; New York, **1994**.

[163] Jitsukawa, K.; Oka, Y.; Einaga, H.; Masuda, H. *Tetrahedron Lett.* **2001**, *42*, 3467.

[164] Sono, M.; Roach, M.P.; Coulter, E. D.; Dawson, J. H. *Chem. Rev*. **1996**, *96*, 2841.

[165] Groves, J. T. *Cytochrome P450: Structure, Mechanism and Biochemistry*, 3rd ed., Ed. Ortiz de Montellano, P.R.; Kluwer Academic/Plenum Publishers: New York, **2005**, Ch 1.

[166] Meunier, B. *Chem. Rev*. **1992**, *92*, 1411.

[167] Groves, J. T. *J. Inorg. Biochem*. **2006**, *100*, 434.

[168] Nam, W. *Acc. Chem. Res*. **2007**, *40*, 522.

[169] de Oliveira, F. T.; Chanda, A.; Banerjee, D.; Shan, X.; Mondal, S.; Que Jr. L.; Bominaar, E.L.; Münck, E.; Collins, T. J. *Science* **2007**, *315*, 835.

[170] Lee, J. Y.; Lee, Y.-M.; Kotani, H.; Nam, W.; Fukuzumi, S. *Chem. Commun*. **2009**, 704.

[171] Shaik, S.; Cohen, S.; Wang, Y.; Chen, H.; Kumar, D.; Thiel, W. *Chem. Rev*. **2010**, *110*, 949.

[172] Costas, M. *Coord. Chem. Rev*. **2011**, *255*, 2912.

[173] Lanucara, F.; Crestoni, M. E. *Chem. Eur. J*. **2011**, *17*, 12092.

[174] Murahashi, S.-L.; Komiya, N. *Ruthenium in Organic Synthesis*; Wiley-VCH: Weinheim, Germany, **2004**.

[175] Lebeau, E. L.; Binstead, R. A.; Meyer, T. J. *J. Am. Chem. Soc.* **2001**, *123*, 10535.

[176] Binstead, R. A.; McGuire, M. E.; Dovletoglou, A.; Seok, W. K.; Roecker, L. E.; Meyer, T. J. *J. Am. Chem. Soc.* **1992**, *114*, 173.

[177] Gilbert, J. A.; Gersten, S. W.; Meyer, T. J. *J. Am. Chem. Soc.* **1982**, *104*, 6872.

[178] Gilbert, J.; Roecker, L.; Meyer, T. J. *Inorg. Chem.* **1987**, *26*, 1126.

[179] Seok, W. K.; Dobson, J. C.; Meyer, T. J. *Inorg. Chem.* **1988**, *27*, 3.

[180] Roecker, L.; Dobson, J. C.; Vining, W. J.; Meyer, T. J. *Inorg. Chem.* **1987**, *26*, 779.

[181] Moyer, B. A.; Sipe, B. K.; Meyer, T. J. *Inorg. Chem.* **1981**, *20*, 1475.

[182] Stultz, L. K.; Binstead, R. A.; Reynolds, M. S.; Meyer, T. J. *J. Am. Chem. Soc.* **1995**, *117*, 2520.

[183] Tse, M. K.; Klawonn, M.; Bhor, S.; Döbler, C.; Anilkumar, G.; Hugo, H.; Mägerlein, W.; Beller, M. *Org. Lett.* **2005**, *7*, 987.

[184] Roecker, L.; Meyer, T. J. *J. Am. Chem. Soc.* **1987**, *109*, 746.

[185] Roecker, L.; Meyer, T. J. *J. Am. Chem. Soc.* **1986**, *108*, 4066.

[186] Stultz, L. K.; Huynh, M. H. V.; Binstead, R. A.; Curry, M.; Meyer, T. J. *J. Am. Chem. Soc.* **2000**, *122*, 5984.

[187] Balavoine, G.; Eskenazi, C.; Meunier, F.; Rivière, H. *Tetrahedron Lett.* **1984**, *25*, 3187.

[188] Bailey, A. J.; Griffith, W. P.; White, A. J. P.; Williams, D.J. *J. Chem. Soc., Chem. Commun.* **1994**, 1833.

[189] Jitsukawa, K.; Oka, Y.; Yamaguchi, S.; Masuda, H. *Inorg. Chem.* **2004**, *43*, 8119.

[190] Dakkach, M.; López, M. I.; Romero, I.; Rodríguez, M.; Atlamsani, A.; Parella, T.; Fontrodona, X.; Llobet, A. *Inorg. Chem.* **2010**, *49*, 7072.

[191] Dobson, J. C.; Seok, W. K.; Meyer, T. J. *Inorg. Chem.* **1986**, *25*, 1513.

[192] Bressan, M.; Morvillo, A. *J. Chem. Soc., Chem. Commun.* **1988**, 650.

[193] Higuchi, T.; Ohtake, H.; Hirobe, M. *Tetrahedron Lett.* **1989**, *30*, 6545.

[194] Zhang, J.-L.; Che, C.-M. *Chem. Eur. J.* **2005**, *11*, 3899.

[195] Fisher, J. M.; Fulford, A.; Bennett, P. S. *J. Mol. Catal.* **1992**, *77*, 229.

[196] Barf, G. A.; van den Hoek, D.; Sheldon, R.A. *Tetrahedron* **1996**, *52*, 12971.

[197] Chatterjee, D. *J. Mol. Cat. A: Chem.* **2009**, *310*, 174.

[198] Bailey, C. L.; Drago, R. S. *J. Chem. Soc., Chem. Commun.* **1987**, 179.

[199] Leung, W. H.; Che, C. M.; Yeung, C. H.; Poon, C. K. *Polyhedron* **1993**, *12*, 2331.

[200] Hudlicky, M. *Oxidations in Organic Chemistry*, ACS Monograph, Vol. 186, **1990**.

[201] Bruneau, C.; Dixneuf, P. H.; Arends, I. W. C. E.; Kodama, T.; Sheldon, R. A. *Ruthenium Catalysts and Fine Chemistry*; Springer Berlin/Heidelberg: **2004**, Vol. 11, 277.

[202] Sheldon, R. A. *J. Mol. Catal.* **1980**, *7*, 107.

[203] Joergensen, K. A. *Chem. Rev.* **1989**, *89*, 431.

[204] Banu, A.; Stan, R.; Matondo, H.; Perez, E.; Rico-Lattes, I.; Lattes, A. *C. R. Chim.* **2005**, *8*, 853.

[205] Upjohn, *J. Am.Chem. Soc*. **1956**, 6213.

[206] Barf, G. A.; Sheldon, R. A. *J. Mol. Catal. A: Chem.* **1995**, *98*, 143.

[207] Chatterjee, D. *Coord. Chem. Rev.* **2008**, *252*, 176.

[208] Fung, W.-H.; Yu, W.-Y.; Che, C.-M. *J. Org. Chem.* **1998**, *63*, 7715.

[209] Groves, J. T.; Stern, M. K. *J. Am. Chem. Soc.* **1987**, *109*, 3812.

[210] Castellino, A. J.; Bruice, T. C. *J. Am. Chem. Soc.* **1988**, *110*, 158.

[211] Castellino, A. J.; Bruice, T. C. *J. Am. Chem. Soc.* **1988**, *110*, 7512.

[212] Groves, J. T.; Stern, M. K. *J. Am. Chem. Soc.* **1988**, *110*, 8628.

[213] Chatterjee, D.; Sengupta, A.; Mitra, A. *Polyhedron* **2007**, *26*,178.

[214] Sala, X.; Santana, N.; Serrano, I.; Plantalech, E.; Romero, I.; Rodríguez, M.; Llobet, A.; Jansat, S.; Gómez, M.; Fontrodona, X. *Eur. J. Inorg. Chem.* **2007**, 5207.

[215] Serrano, I.; Sala, X.; Plantalech, E.; Rodríguez, M.; Romero, I.; Jansat, S.; Gómez, M.; Parella, T.; Stoeckli-Evans, H.; Solans, X.; Font-Bardia, M.; Vidjayacoumar, B.; Llobet, A. *Inorg. Chem.*, **2007**, *46*, 5381.

[216] Kaminskaia, N. V.; Kostic, N. M. *J. Chem. Soc., Dalton Trans.* **1996**, 3677.

[217] Zabicky, J. *The Chemistry of Amides*, Wiley-Interscience, New York, **1970**.

[218] Grenberg, A.; Breneman, C. M.; Liebman, J.F. *The amide linkage: Structural significance in chemisatry, biochemistry and materials science*, Wiley, New York, **2000**.

[219] Yamada H.; Kobayashi, M.; *Biosci. Biotechnol. Biochem*. **1996**, *60*, 1391.

[220] Bhattacharya, A.; Scott, B. P.; Nasser, N.; Ao, H.; Maher, M. P.; Dubin, A. E.; Swanson, D. M.; Shankley, M. P.; Wickenden, A. D.; Chaplan, S. R. *J.Pharmacol. Exp. Ther*. **2007**, *323*, 665.

[221] Lugo-Mas, P.; Dey, A.; Xu, L.; Davin, S. D.; Benedict, J.; Kaminsky, W.; Hodgson, K. O.; Hedman, B.; Solomon, E. I.; Kovacs, J. A. *J. Am. Chem. Soc*. **2006**, *128*, 11211.

[222] Kovacs, J. A. *Chem. Rev*. **2004**, *104*, 825.

[223] Endo, I.; Nojiri, M.; Tsujimura, M.; Nakasako, M.; Nagashima, S.; Yohda, M.; Odaka, M. *J. Inorg. Biochem*. **2001**, *83*, 247.

[224] van Pelt, S.; van Rantwijk, F.; Sheldon, R. A. *Focus on Catalysis Applications* (supplement to *Chimica Oggi/Chemistry Today*); Teknoscienze Srl: Milano, Italy, **2008**, *26*, 2.

[225] Sanchez, S.; Demain, A. L. *Org. Process Res. Dev.* **2011**, *15*, 224.

[226] Li, B.; Su, J.; Tao, J. *Org. Process Res. Dev.* **2011**, *15*, 291.

[227] Stein, M.; Breit, B. *Angew. Chem. Int. Ed*. **2013**, *52*, 2231.

[228] Reeves, J. T.; Tan, Z.; Marsini, M. A.; Han, Z. S.; Xu, Y.; Reeves, D. C.; Lee, H.; Lu, B. Z.; Senanayake, C. H. *Adv. Synth. Catal.* **2013**, *355*, 47

[229] Werkmeister, S.; Bornschein, C.; Junge, K.; Beller, M. *Chem. Eur. J.* **2013**, *19*, 4437.

[230] Allen C. L.; Williams, J. M. J. *Chem. Soc. Rev.* **2011**, *40*, 3405.

[231] Dopp, D.; Dopp, H. in *Methoden Org. Chem.* (Houben Weyl), vol. E5(2),Thieme Verlag, Stuttgart, **1985**, pp. 1024.

[232] Bailey, P. D.; Mills, T. J.; Pettecrew, R.; Price, R. A. in A.R. Katritzky, R.J.K. Taylor (Eds.), *Comprehensive Organic Functional Group Transformations II*, vol. 5, Elsevier, Oxford, **2005**, pp. 201.

[233] Montalbetti, C. A. G. N.; Falque, V. *Tetrahedron* **2005**, *61*, 10827.

[234] Valeur, E.; Bradley, M. *Chem. Soc. Rev.* **2009**, *38*, 606.

[235] Pattabiraman, V. R.; Bode, J. W. *Nature* **2011**, *480*, 471.

[236] Singh, C.; Kumar, V.; Sharma, U.; Kumar, N.; Singh, B. *Curr. Org. Synth.* **2013,** *10*, 241.

[237] Moorthy, J. N.; Singhal, N. *J. Org. Chem*. **2005**, *70*, 1926.

[238] Kornblum, N.; Singaram, S. *J.Org. Chem*. **1976**, *44*, 4727.

[239] Katrizky, A. R.; Pilarski, B.; Urogdi, L. *Synthesis,* **1989**, 949.

[240] Kobayashi, M.; Shimizu, S. *Curr. Opin. Chem. Biol.* **2000**, *4*, 95.

[241] Prasad, S.; Bhalla, T. C. *Biotechnol. Adv.* **2010**, *28*, 725.

[242] Ramteke, P. W.; Maurice, N. G.; Joseph, B.; Wadher, B. J. *Biotechnol. Appl. Biochem.* **2013,** *60*, 459.

[243] Tao, J.; Xu, J.-H. *Curr. Opin. Chem. Biol.* **2009**, *13*, 43.

[244] Kumar, D.; Masitas, C. A.; Nguyen, T. N.; Grapperhaus, C. A. *Chem. Commun.* **2013**, *49*, 294.

[245] De Santis, G.; Di Cosimo, R. *Biocatalysis for the Pharmaceutical Industry: Discovery, Development and Manufacturing*, ed. Tao, J.; Lin, G.-Q.; Liese, A. Wiley-VCH, Weinheim, **2009**.

[246] Ahmed, T. J.; Knapp, S. M. M.; Tyler, D. R. *Coord. Chem. Rev.* **2011**, *255*, 949.

[247] Tamura, M.; A. Satsuma and K.-I. Shimizu, *Cat. Sci. Tec.*, **2013**, *3*, 1386.

[248] Parkins, A. W. *Platinum Met. Rev.* **1996**, *40*, 169.

[249] Ghaffar, T.; Parkins, A. W. *Tetrahedron Lett*. **1995**, *36*, 8657.

[250] Ghaffar, T.; Parkins, A. W. *J. Mol. Catal. A: Chem*. **2000**, *160*, 249.

[251] North, M.; Parkins, A. W.; Shariff, A. N. *Tetrahedron Lett.* **2004**, *45*, 7625

[252] Akisanya, J.; Parkins, A. W.; Steed, J. W. *Org. Process Res. Dev*. **1998**, *2*, 274.

[253] Herzon, S. B.; Myers, A. G. *J. Am. Chem. Soc.* **2005**, *127*, 5342.

[254] Brown, L. E.; Landaverry, Y. R.; Davies, J. R.; Milinkevich, K. A.; Ast, S.; Carlson, J. S.; Oliver, A. G.; Konopelski, J. P. *J. Org. Chem.* **2009**, *74*, 5405.

[255] Feng, Y.; Jiang, X.; de Brabander, J. K. *J. Am. Chem. Soc.* **2012**, *134*, 17083.

[256] Goto, A.; Endo, K.; Saito, S. *Angew. Chem., Int. Ed*. **2008**, *47*, 3607.

[257] Diamond, S. E.; Grant, B.; Tom, G. M.; Taube, H. *Tetrahedron Lett.* **1974**, 15, 4025.

[258] Murahashi, S.-I.; Sasao, S.; Saito, E.; Naota, T. *J. Org. Chem*. **1992**, *57*, 2521.

[259] Murahashi, S.-I.; Sasao, S.; Saito, E.; Naota, T. *Tetrahedron,* **1993**, *49*, 8805.

[260] Murahashi, S.-I.; Naota, T. *Bull. Chem. Soc. Jpn.* **1996**, *69*, 1805.

[261] Murahashi, S.-I.; Takaya, H. *Acc. Chem. Res*. **2000**, *33*, 225.

[262] Fung, W. K.; Huang, X.; Man, M. L.; Ng, S. M.; Hung, M. Y.; Lin, Z.; Lau, C. P. *J. Am. Chem. Soc.* **2003**, *125*, 11539.

[263] Lau, C. P.; Ng, S. M.; Jia, G.; Lin, Z. *Coord. Chem. Rev.* **2007**, *251*, 2223.

[264] O'Connor, J. M.; Casey, C. P. *Chem. Rev.* **1987**, *87*, 307.

[265] Cadierno, V.; Díez, J.; Gamasa, M. P.; Gimeno, J.; Lastra, E. *Coord. Chem. Rev.* **1999**, *193-195*, 147.

[266] Zargarian, D. *Coord. Chem. Rev.* **2002**, *233-234*, 157.

[267] Kukushkin, V. Yu.; Pombeiro, A. J. L. *Chem. Rev.* **2002**, *102*, 1771.

[268] Katz, N. E.; Fagalde, F.; Lis de Katz, N. D.; Mellace, M. G.; Romero, I.; Llobet, A.; Benet-Buchholz, J. *Eur. J. Inorg. Chem*. **2005**, 3019.

[269] Kukushkin, V. Yu.; Pombeiro, A. J. L. *Inorg. Chim. Acta,* **2005**, *358*, 1.

[270] Mola, J.; Pujol, D.; Rodríguez, M.; Romero, I.; Sala, X.; Katz, N. E.; Parella, T.; Benet-Buchholz, J.; Fontrodona, X.; Llobet, A. *Aus. J. Chem*. **2009**, *62*, 1675.

[271] Leung, C. W.; Zheng, W.; Wang, D.; Ng, S. M.; Yeung, C. H.; Zhou, Z.; Lin, Z.; Lau, C. P. *Organometallics* **2007**, *26*, 1924.

[272] Oshiki, T.; Yamashita, H.; Sawada, K.; Utsunomiya, M.; Takahashi, K.; Takai, K. *Organometallics,* **2005**, *24*, 6287.

[273] Oshiki, T.; Hyodo, I.; Ishizuka, A. *J. Synth. Org. Chem. Jpn.* **2010**, *68*, 41.

[274] Muranaka, M.; Hyodo, I.; Okumura, W.; Oshiki, T. *Catal. Today* **2011**, *164*, 552.

[275] Borovik, A. S. *Acc. Chem. Res.* **2005**, *38*, 54.

[276] Ikariya, T.; Murata, K.; Noyori, R. *Org. Biomol. Chem.* **2006**, *4*, 393.

[277] Grotjahn, D.B. *Dalton Trans.* **2008**, 6497.

[278] Ikariya, T.; Gridnev, I.D. *Top. Catal.* **2010**, *53*, 894.

[279] Šmejkal, T.; Breit, B. *Organometallics* **2007**, *26*, 2461.

[280] Anastas, P. T.; Warner, J. C. *Green Chemistry: Theory and Practice*; Oxford University Press: Oxford, U.K., **1998**.

[281] Lancaster, M. *Handbook of Green Chemistry and Technology*; Clark, J. H.; Macquarrie, D. J. Eds.; Blackwell Publishing: Abingdon, U.K., **2002**.

[282] Poliakoff, M.; Fitzpatrick, J. M.; Farren, T. R.; Anastas, P. T. *Science,* **2002**, *297*, 807.

[283] Sheldon, R. A. *Green Chem*. **2005**, *7*, 267.

[284] Sheldon, R. A.; Arends, I.; Hanefeld, U. *Green Chemistry and Catalysis*; Wiley-VCH: Weinheim, Germany, **2007**.

[285] Li, C.-J. *Chem. Rev.* **2005**, *105*, 3095.

[286] Li, C.-J.; Chan, T. H. *Comprehensive Organic Reactions in Aqueous Media*; Wiley-VCH: Weinheim, Germany, **2007**.

[287] Lindström, U. M. *Organic Reactions in water*; Blackwell Publishing: Oxford, U. K., **2007**.

[288] Kerton, F. M. *Alternatives Solvents for Green Chemistry*; RSC Publishing: Cambridge, U.K., **2009**.

[289] Skouta, R. *Green Chem. Lett. Rev.* **2009**, *2*, 121.

[290] Anastas, P. T.; Li, C.-J. *Handbook of Green Chemistry*; Wiley-VCH: Weinheim, Germany, **2010**, Vol. 5.

[291] García-Álvarez, R.; Díez, J.; Crochet, P.; Cadierno, V. *Organometallics,* **2010**, *29*, 3955.

[292] Phillips, A. D.; Gonsalvi, L.; Romerosa, A.; Vizza, F.; Peruzzini, M. *Coord. Chem. Rev.* **2004**, *248*, 955.

[293] Shaughnessy, K. H. *Chem. Rev.* **2009**, *109*, 643.

[294] Zablocka, M.; Hameau, A.; Caminade, A.-M.; Majoral, J.-P. *Adv. Synth. Catal.* **2010**, *352*, 2341.

[295] Gonsalvi, L.; Peruzzini, M. *Catal. Met. Complexes* **2011**, *37*, 183.

[296] Cadierno, V.; Francos, J.; Gimeno, J. *Chem. Eur. J.* **2008**, *14*, 6601.

[297] Cadierno, V.; Diez, J.; Francos, J.; Gimeno, J. *Chem. Eur. J.* **2010**, *16*, 9808.

[298] García-Álvarez, R.; Díez, J.; Crochet, P.; Cadierno, V. *Organometallics,* **2011**, 30, 5442.

[299] García-alvarez, R.; Crochet, P.; Cadierno, V. *Green Chem.* **2013**, *15*, 46.

[300] García-Álvarez, R.; Zablocka, M.; Crochet, P.; Duhayon, C.; Majoral, J.-P.; Cadierno, V. *Green Chem*. **2013**, *15*, 2447.

[301] Li, C.-J.; Chen, L. *Chem. Soc. Rev.* 2006, **35**, 68.

[302] Lastra-Barreira, B.; Díez, J.; Crochet, P. *Green Chem*. **2009**, *11*, 1681.

[303] Tavor, D.; Sheviev, O.; Dlugy, C.; Wolfson, A. *Can. J. Chem.* **2010**, *88*, 305.

[304] Francos, J.; Cadierno, V. *Green Chem.* **2010**, *12*, 1552.

[305] Balieu, S.; El Zein, A.; De Sousa, R.; Jérôme, F.; Tatibouët, A.; Gatard, S.; Pouilloux, Y.; Barrault, J.; Rollin, P.; Bouquillon, S. *Adv. Synth. Catal.* **2010**, *352*, 1826.

[306] Lastra-Barreira, B.; Crochet, P. *Green Chem*. **2010**, *12*, 1311.

[307] Gu, Y.; Jérôme, F. *Green Chem*. **2010**, *12*, 1127.

[308] Díaz-Alvarez, A.; Francos, J.; Lastra-Barreira, B.; Crochet, P.; Cadierno, V. *Chem. Commun*. **2011**, *47*, 6208.

[309] Gladysz, J. *Chem. Rev.* **2002**, *102*, 3215.

[310] Bell, A. T. *Science* **2003**, *299*, 1688.

[311] Schlögl, R.; Abd Hamid, S. B. *Angew. Chem. Int. Ed.* **2004**, *116*, 1656.

[312] Cornils, B. *Applied homogeneous catalysis with organometallic compounds: a comprehensive handbook in three volumes*; 2n ed.; Wiley-VCH: Weinheim, **2002**.

[313] Ertl, G. *Handbook of heterogeneous catalysis.*; 2n ed.; Wiley-VCH; John Wiley distributor: Weinheim; Chichester, **2008**.

[314] Anastas, P. *Handbook of green chemistry.*; Wiley-VCH: Weinheim, **2009**.

[315] Francàs Forcada, Laia. *Ruthenium Complexes with Polynucleating Ligands and their Capacity to Catalytically Oxidize Water to Dioxyen.* Universitat Autònoma de Barcelona, 2011. <http://hdl.handle.net/10803/83973>

[316] Sheldon, R. A.; van Bekkum, H. *Fine Chemicals through Heterogeneous Catalysis*, Wiley-VCH, Weinheim, **2001.**

[317] Sheldon, R. A. *Chem. Commun.* **2008**, 3352.

[318] Meille, V. *Appl. Catal. A-Gen.* **2006**, *315*, 1.

[319] Campanati, M.; Fornasari, G.; Vaccari, *A. Catal. Today* **2003**, *77*, 299.

[320] Cozzi, F. *Adv. Synth. Catal.* **2006**, *348*, 1367.

[321] Dioos, B. M. L.; Vankelecom, I. F. J.; Jacobs, P. A. *Adv. Synth. Catal.* **2006**, *348*, 1413.

[322] McMorn, P.; Hutchings, G. *J. Chem. Soc. Rev.* **2004**, *33*, 108.

[323] Thomas, J. M.; Raja, R.; Lewis, D. W. *Angew. Chem. Int. Ed.* **2005**, *44*, 6456.

[324] Dal Santo, V.; Liguori, F.; Pirovano, C.; Guidotti, M. *Molecules* **2010**, *15*, 3829.

[325] Gheorghiu, C.C.; Salinas-Martínez de Lecea, C.; Román-Martínez, M. C. *Ap. Cat. A: General* **2014**, *478*, 194.

[326] Barbaro, P.; Liguori, F. *Chem Rev.* **2008**, *109*, 515.

[327] Parton, R. F.; Vankelecom, I. F. J.; Casselman, M. J. A.: Bezaukhanova, C. P.; Uytterhoeven, J. B.; Jacobs, P. A. *Nature* **1994**, *370*, 541.

[328] Knops-Gerrits, P.-P.; de Vos, D.; Thibault-Starzyk, F.; Jacobs, P. A. *Nature* **1994**, *369*, 543.

[329] Mori, K.; Kagohara, K.; Yamashite, H. *J. Phys. Chem. C* **2008**, *112*, 2593.

[330] Lee, C.-H.; Lin, H.-C.; Cheng, S.-H.; Lin, T.-S.; Mou, C.-Y. *J. Phys. Chem. C* **2009**, *113*, 16058.

[331] Dupont, J.; de Souza, R. F.; Suarez, P. A. *Chem. Rev*. **2002**, *102*, 3667.

[332] Freemantle, M. *Chem. Eng. News* **2001**, *79*, 21.

[333] Ranke, J.; Stolte, S.; Störmann, R.; Arning, J.; Jastorff, B. *Chem. Rev*. **2007**, *107*, 2183.

[334] Mutin, P. H.; Guerrero, G.; Vioux, A. *J. Mater. Chem.* **2005**, *15*, 3761.

[335] Ribeiro, S. M.; Serra, A. C.; Rocha Gonsalves, A. *Tetrahedron.* **2007**, *63*, 7885.

[336] Sayah, R.; Framery, E.; Dufaud, V. *Green Chem*. **2009**, *11*, 1694.

[337] Stamatis, A.; Giasafaki, D.; Christoforidis, K. C.; Deligiannakis, Y.; Louloudi, M. *J. Mol. Catal. A: Chem.* **2010**, *319*, 58.

[338] Hagiwara, R.; Ito, Y. *J. Fluorine Chem*. **2000**, *105*, 221.

[339] Huddleston, J. G.; Visser, A. E.; Reichert, W. M.; Willauer, H. D.; Broker, G. A.; Rogers, R. D. *Green Chem*. **2001**, *3*, 156.

[340] Ho, K.-P.; Wong, W.-L.; Lee, L. Y. S.; Lam, K.-M.; Chan, T. H.; Wong, K.-Y. *Chem. Asian J.* **2010**, *5*, 1970.

[341] Rich, J.; Manrique, E.; Molton, F.; Duboc, C.; Collomb, M.-N.; Rodríguez, M.; Romero, I. *Eur. J. Inorg. Chem.* **2014**, 2663.

[342] Corma, A.; Garcia, H. *Adv. Synth. Catal.* **2006**, *348*, 1391.

[343] Bergbreiter, D. E. *Chem. Rev.* **2002**, *102*, 3345.

[344] Sodhi, R. K.; Paul, S.; Clark, J. H. *Green Chem.* **2012**, *14*, 1649.

[345] Zucca, P.; Sanjust, E. *Molecules* **2014**, *19*, 14139.

[346] Zukal, A.; Opanasenko, M.; Rubes, M.; Nachtigall, P.; Nachtigall, P.; Jagiello, J. *Cat. Today* **2015**, *243*, 69.

[347] Fujii, S.; Matsuzawa, S.; Nakamura, Y.; Ohtaka, A.; Teratani, T.; Akamatsu, K.; Tsuruoka, T.; Nawafune, H. *Langmuir*, **2010**, *26*, 6230.

[348] Magdesieva, T. V.; Nikitin, O. M.; Levitsky, O. A.; Zinovyeva, V. A.; Bezverkhyy, I.; Zolotukhina, E. V.; Vorotyntsev, M. A. *J. Mol. Catal. A: Chem.*, **2012**, *353*, 50.

[349] Li, X. Y.; Zhu, M. Y.; Dai, B. *Appl. Catal. B*, **2013**, *142*, 234.

[350] Wise, D. L.; Winek, G. E.; Trantolo, D. J.; Cooper, T. M.; Gresser, J. D. *Electrical and Optical Polymer Systems*, Marcel Dekker Inc., New York, **1998**, vol. 17.

[351] Mola, J.; Mas-Marza, E.; Sala, X.; Romero, I.; Rodríguez, M.; Viñas, C.; Parella, T.; Llobet, A. *Angew. Chem. Int. Ed.* **2008**, *47*, 5830.

[352] Maeda, K.; Teramura, K.; Lu, D.; Takata, T.; Saito, N.; Inoue, Y.; Domen, K. *Nature* **2006**, *440*, 295.

[353] Qiu, X.; Miyauchi, M.; Yu, H.; Irie, H.; Hashimoto, K. *J. Am. Chem. Soc.* **2010**, *132*, 15259.

[354] Krebs, F.; Biancardo, M. *Sol. Energ. Mat. Sol. C.* **2006**, *90*, 142.

[355] Francàs, L.; Sala, X.; Benet-Buchholz, J.; Escriche, L.; Llobet, A. *Chem. Sus. Chem.* **2009**, *2*, 321.

[356] Patel, S. M.; Chudasama, U. V.; Ganeshpure, P. A. *J. Mol. Catal. A: Chem*. **2003**, *194*, 267.

[357] Dakkach, M.; Atlamsani, A.; Sebti, S. *Comp. Rend. Chim.* **2012**, *15*, 482.

[358] Parangi, T. F.; Wani, B. N.; Chudasama, U. V. *Ind. Eng. Chem. Res.* **2013**, *52*, 8969.

[359] Bautista, F. M.; Caballero, V.; Campelo, J. M.; Luna, D.; Marinas, J. M.; Romero, A. A.; Romero, I.; Serrano, I.; Llobet, A. *Top. Catal.* **2006**, *40*, 193.

[360] Caballero, V.; Bautista, F. M.; Campelo, J. M.; Luna, D.; Luque, R.; Marinas, J. M.; Romero, A. A.; Romero, I.; Rodríguez, M.; Serrano, I.; Hidalgo, J. M.; Llobet, A. *J. Mol. Cat. A: Chem.* **2009**, *308*, 41.

[361] Elanany, M.; Koyama, M.; Kubo, M.; Selvam, P.; Miyamoto, A. *Micropor. Mesopor. Mater.* **2004**, *71*, 5.

[362] Schmid, G. *Nanoparticles: From Theory to Application*; John Wiley&Sons, Incorporated, **2010**.

[363] Shylesh, S.; Schünemann, V.; Thiel, W. R. *Angew. Chem. Int. Ed.* **2010**, *49*, 3428.

[364] Vaquer, L.; Riente, P.; Sala, X.; Jansat, S.; Benet-Buchholz, J.; Llobet, A.; Pericàs, M. A. *Catal. Sci. Technol.* **2013**, *3*, 706.

[365] García-Garrido, S. E.; Francos, J.; Cadierno, V.; Basset, J.-M.; Polshettiwar, V. *Chem. Sus. Chem.* **2011**, *4*, 104.

[366] Baig, R. B. N.; Varma, R. S. *Chem. Commun.* **2012**, *48*, 6220.

[367] Taboada, E.; Solanas, R.; Rodríguez, E.; Weissleder, R.; Roig, A. *Adv. Funct. Mater.* **2009**, *19*, 2319.

[368] Kamonsatikul, C.; Khamnaen, T.; Phiriyawirut, P.; Charoenchaidet, S.; Somsook, E. *Catal. Commun.* **2012**, *26*, 1.

[369] Shi, F.; Tse, M. K.; Pohl, M.-M.; Brückner, A.; Zhang, S.; Beller, M. *Angew. Chem., Int. Ed.*, **2007**, *46*, 8866.

[370] Ligtenbarg, A.G.J.; Hage, R.; Feringa, B.L. *Coord. Chem. Rev.* **2003**, *237*, 89.

[371] Bolm, C. *Coord. Chem. Rev.* **2003**, *237*, 245.

[372] Maurya, M. R.; Saklani, H.; Kumar, A.; Chand, S. *Catal. Lett.* **2004**, *87*, 121.

[373] Maurya, M. R.; Sikarwar, S. *Catal.Commun.* **2007**, *8*, 2017.

[374] El-Qisiari, A. K.; Qaseer, H. A.; Henry, P. M. *Tetrahedron Lett.* **2002**, *43*, 4229.

[375] Severeyns, A.; De Vos, D. E.; Jacobs, P. A. *Green Chem.* **2002,** *4*, 380.

[376] Tada, M.; Muratsugu, S.; Kinoshita, M.; Sasaki, T; Iwasawa, Y. *J. Am. Chem. Soc.* **2010**, *132*, 713.

[377] Sels, B. F.; Villa, A. L.; Hoegaerts, D.; De Vos, D. E.; Pierre, A. J. *Topics Cat.* **2000**, *13*, 223.

[378] Lou, L.-L.; Yu, K.; Ding, F.; Zhou, W.; Peng, X.; Liu, S. *Tetrahedron Lett.* **2006**, *47*, 6513.

[379] Alkordi, M. H.; Liu, Y.; Larsen, R. W.; Eubank, J. F.; Eddaoudi, M. *J. Am. Chem. Soc.* **2008**, *130*, 12639.

[380] Faria, A. L.; Mac Leod, T. O. C.; Barros, V. R. P.; Assis, M. D. *J. Braz. Chem. Soc.* **2009**, *20*, 895.

[381] Parton, R. F.; Neys, P. E.; Jacobs, P. A.; Sosa, R. C.; Rouxhet, P. G. *J. Catal.* **1996**, *164*, 341.

[382] Zucca, P.; Sollai, F.; Garau, A.; Rescigno, A.; Sanjust, E. *J. Mol. Catal. A: Chem.* **2009**, *306*, 89.

[383] Halma, M.; Castro, K. A. D. d. F.; Prévot, V.; Forano, C.; Wypych, F.; Nakagaki, S. *J. Mol. Catal. A: Chem.* **2009**, *310*, 42.

[384] Ballesteros, R.; Fajardo, M.; Sierra, I.; del Hierro, I. *J. Mol. Cat. A: Chem.* **2009**, *310*, 83.

[385] Ballesteros, R.; Pérez, Y.; Fajardo, M.; Sierra, I.; del Hierro, I. *Microp. and mesop. Mat.* **2008**, *116*, 452.

[386] Luque, R.; Badamali, S. K.; Clark, J. H.; Fleming, M.; Macquarrie, D. J. *Appl. Cat. A: Gen.* **2008**, *341*, 154.

[387] Haas, G. R.; Kolis, J. W. *Organometallics* **1998**, *17*, 4454.

[388] Deubel, D. V.; Sundermeyer, J. R.; Frenking, G. *J. Am. Chem. Soc.* **2000**, *122*, 10101.

[389] Buffon, R.; Schuchardt, U. *J. Braz. Chem. Soc.* **2003**, *14*, 347.

[390] Maurya, M. R.; Kumar, A.; Pessoa, J. C. *Coord. Chem. Rev.* **2011**, *255*, 2315.

[391] Sels, B. F.; De Vos, D. E.; Buntinx, M.; Jacobs, P. A. *J. Catal.* **2003**, *216*, 288.

[392] Le, Y.; Yang, X.; Dai, W.-L-; Gao, R.; Fan, D. *Cat. Comm.* **2008**, *9*, 1838.

[393] Sofia, L. T. A.; Krishnan, A.; Sankar, M.; Raj, N. K.; Manikandan, P.; Rajamohanan, P. R.; Ajithkumar, T. G. *J. Phys. Chem. C* **2009**, *113*, 21114.

[394] Amini, M.; Haghdoost, M. M.; Bagherzadeh, M. *Coord. Chem. Rev.* **2014**, *168*, 83.

[395] Nestler, O.; Severin, K. *Org. Lett.* **2001**, *3*, 3907.

[396] Kobayashi, S.; Sugiura, M. *Adv. Synth. Catal.* **2006**, *348*, 1496.

[397] Che, C.-M.; Huang, J.-S. *Chem. Commun.* **2009**, 3996.

[398] Tsang, S. C.; Caps, V.; Paraskevas, I.; Chadwick, D.; Thompsett, D. *Angew. Chem. Int. Ed.* **2004**, *43*, 5645.

[399] Guin, D.; Baruwati, B.; Manorama, S. V. *Org. Lett.* **2007**, *9*, 1419.

[400] Jacinto, M. J.; Santos, O. H. C. F.; Jardim, R. F.; Landers, R.; Rossi, L. M. *Appl. Cat. A: Gen.* **2009**, *360*, 177.

[401] Rossi, L. M.; Cosata, N. J. S.; Silva, F. P.; Wojcieszak, R. *Green Chem.* **2014**, *16*, 2906.

[402] Kotani, M.; Koike, T.; Yamaguchi, K.; Mizuno, N. *Green Chem.* **2006**, *8*, 735.

[403] Shylesh, S.; Schweizer, J.; Demeshko, S.; Schünemann, V.; Ernst, S.; Thiel, W. R. *Adv. Synth. Cat.* **2009**, *351*, 1789.

[404] Shylesh, S.; Schünemann, V.; Thiel, W. R. *Angew. Chem. Int. Ed.* **2010**, *49*, 3428.

[405] Hu, A.; Yee, G. T.; Lin, W. *J. Am. Chem. Soc.* **2005**, *127*, 12486.

[406] Kurata, T.; Tamuro, A.; Murata, Y.; Nagashima, S.; Okano, T.; Ohfuchi, K. Jpn. Kokai Tokkyo Koho, *JP 48054021*, **1973**.

[407] Mizuno, T. Jpn. Kokai Tokkyo Koho, *JP 2005170821*, **2005**.

[408] Oshiki, T.; Ishizuka, A. Jpn. Kokai Tokkyo Koho, *JP 2009214099*, **2009**.

[409] Yamaguchi, K.; Matsushita, M.; Mizuno, N. *Angew. Chem. Int. Ed.* **2004**, *43*, 1576.

[410] Yamaguchi, K.; Mizuno, N. *Synlett* **2010**, 2365.

[411] Ishizuka, A.; Oshiki, T. *Chem. Lett.* **2009**, *38*, 360.

[412] Subramanian, T.; Pitchumani, K. *Catal. Commun.* **2012**, *29*, 109.

[413] Kim, A. Y.; Bae, H. S.; Park, S.; Park, S.; Park, K. H. *Catal. Lett.* **2011**, *141*, 685.

[414] Shimizu, K.; Imaiida, N.; Sawabe, K.; Satsuma, A. *Appl. Catal. A* **2012**, *421–422*, 114.

[415] Sherbow, T. J.; Downs, E. L.; Sayler, R. I.; Razink, J. J.; Juliette, J. J.; Tyler, D. R. *ACS Catal.* **2014**, *4*, 3096.

[416] Liu, Y.-M.; He, L.; Wang, M.-M.; Cao, Y.; He, H.-Y.; Fan, K.-N. *Chem. Sus. Chem.* **2012**, *5*, 1392.

[417] Kumar, S.; Das, P. *New J. Chem.* **2013**, *37*, 2987.

[418] Polshettiwar, V.; Varma, R. S. *Chem. Eur. J.* **2009**, *15*, 1582.

[419] Baig, R. B. N.; Varma, R. S. *Green Chem.* **2013**, *15*, 398.

[420] Woo, H.; Lee, K.; Park, S.; Park, K. H. *Molecules* **2014**, *19*, 699.

[421] Gawande, M. B.; Branco, P. S.; Nogueira, I. D.; Ghumman, C. A. A.; Bundaleski, N.; Santos, A.; Teodoro, O. M. N. D.; Luque, R. *Green Chem.* **2013**, *15*, 682.

[422] García-Álvarez, R.; Francos, J.; Tomás-Mendivil, E.; Crochet, P.; Cadierno, V. *J. Org. Chem.* **2014**, *771*, 93.

[423] Brunner, H.; Scheck, T. *Chem. Ber*. **1992**, *125*, 701.

[424] Thiel, W. R.; Angstl, M.; Priermeier, T. *Chem. Ber.* **1994**, *127*, 2373.

[425] Jia, M.; Thiel, W.R. *Chem. Commun.* **2002**, *20*, 2392.

[426] Taqui Khan, M. M.; Khan, N. H.; Kureshy, R. I.; Venkatasubramanian, K. *Polyhedron* **1992**, *11*, 431.

[427] Bruker Advanced X-raySolutions. SMART: Version 5.631, **1997**-**2002**.

[428] Bruker Advanced X-raySolutions. SAINT +, Version 6.36A, **2001**.

[429] Sheldrick, G. M. *Empirical Absorption Correction Program*, Universität Göttingen, **1996**.

[430] Bruker Advanced X-raySolutions. SADABS Version 2.10, **2001**.

[431] Sheldrick, G. M. *Program for Crystal Structure Refinement*, Universität Göttingen, **1997**.

[432] Bruker Advanced X-raySolutions. SHELXTL Version 6.14, **2000**-**2003**.

[433] Rilak, A.; Bratsos, I.; Zangrando, E.; Kljun, J.; Turel, I.; Bugarčić, Ž. D.; Alessio, E. *Inorg. Chem.* **2014**, *53*, 6113.

[434] Sens, C.; Rodríguez, M.; Romero, I.; Parella, T.; Benet-Buchholz, J.; Llobet, A. *Inorg. Chem*. **2003**, *42*, 8385.

[435] Balzani, V.; Juris, A.; Veturi, M. *Chem. Rev*. **1996**, *96*, 759.

[436] Bell-Loncella, E. T.; Bessel, C. A. *Inorg. Chim. Acta* **2000**, *303*, 199.

[437] Llanguri, R.; Morris, J. J.; Stanley, W. C. ; Bell-Loncella, E. T.; Turner, M.; Boyko, W. J.; Bessel, C. A. *Inorg. Chim. Acta* **2001**, *315*, 53.

[438] Passaniti, P.; Browne, W. R.; Lynch, F. C.; Hughes, D.; Nieuwenhuyzen, M.; James, P.; Maestry, M.; Vos, J. G. *J. Chem. Soc. Dalton.* **2002**, 1740.

[439] Leising, R. A.; Takeuchi, K. J. *Inorg. Chem.* **1987**, *26*, 4391.

[440] Bessel, C. A.; Leising, R. A.; Takeuchi, K. J. *J. Chem. Soc; Chem. Commun.* **1991**, 883.

[441] Lever, A. B. P. *Inorg. Chem.* **1990**, *29*, 1271.

[442] Mägerlein, W.; Dreisbach, C.; Hugl, H.; Tse, K.; Klawonn, M.; Bhor, S.; Beller, M. *Catal. Today* **2007**, *121*, 140.

[443] Tse, M. K.; Bhor, S.; Klawonn, M.; Anilkumar, G.; Jiao, H.; Spannenberg, A.; Döbler, C.; Mägerlein, W.; Hugl, H.; Beller, M. *Chem.-Eur. J.* **2006**, *12*, 1875.

[444] Benet-Buchholz, J.; Comba, P; Llobet, A.; Roeser, S.; Vadivelu, P.; Wadepohl, H.; Wiesner, S. *Dalton Trans.* **2009**, 5910.

[445] Barf, G. A.; Sheldon, R. A. *J. Mol. Catal. A: Chem.* **1995**, *102*, 23.

[446] Chowdhure, A. D.; Das, A.; Irshad, K.; Mobin, S. M.; Lahiri, G. K. *Inorg. Chem.* **2011**, *50*, 1775.

[447] Tse, M. K.; Döbler, C.; Bhor, S.; Klawonn, M.; Mägerleins, W.; Hugl, H.; Beller, M. *Angew. Chem. Int. Ed.* **2004**, *43*, 5255.

[448] Jacobsen, E. N.; Zhang, W.; Guler, M. L. *J. Am. Chem. Soc.* **1991**, *113*, 6703.

[449] Cavallo, L.; Jacobsen, H. *J. Org. Chem*. **2003**, *68*, 6202.

[450] Palucki, M.; Finney, N.S.; Pospisil, P.J.; Güler, M.L.; Ishida, T.; Jacobsen, E.N. *J. Am. Chem. Soc.* **1998**, *120*, 948.

[451] Yu, X.-Q.; Huang, J.-S.; Che, C.-M. *J. Am. Chem. Soc.* **2000**, *122*, 5337.

[452] Sodhi, R.K.; Paul, S.; Clark, J.H. *Green Chem.* **2012**, *14*, 1694.

[453] Suresh, I.; Aruna, S. K. *Indian J. Chem. B* **2003**, *42B*, 2805.

[454] Romero, I.; Rodríguez, M.; Llobet, A.; Collomb, M. N.; Deronzier, A.; Parella, T.; Stoeckli-Evans, H. *J. Chem. Soc. Dalton* **2000**, 1689.

[455] Alessio, E.; Iengo, E.; Zangrando, E.; Geremia, S.; Marzilli, P. A.; Calligaris, M. *Eur. J. Inorg. Chem.* **2000**, 2207.

[456] Calligaris, M. *Coord. Chem. Rev.*, **2004**, *248*, 351.

[457] Serli, B.; Zangrando, E.; Gianferrara, T.; Scolaro, C.; Dyson, P. J.; Bergamo, A.; Alessio, E. *Eur. J. Inorg. Chem.* **2005**, 3423.

[458] Mola, J.; Romero, M.; Rodríguez, M.; Bozoglian, F.; Poater, A.; Solà, M.; Parella, T.; Benet-Buchholz, J.; Fontrodona, X.; Llobet, A. *Inorg. Chem*. **2007**, *46*, 10707.

[459] Rack, J. J.; Gray, H. B. *Inorg. Chem.* **1999**, *38*, 2.

[460] Dakkach, M.; Fontrodona, X.; Parella, T. Atlamsani, A.; Romero, I.; Rodríguez, M. *Adv. Synth. Catal.* **2011**, *353*, 231.

[461] Benet-Buchholz, J.; Comba, P.; Llobet, A.; Roeser, S.; Vadivelu, P.; Wiesner, S. *Dalton Trans.* **2010**, *39*, 3315.

[462] Choudhuri, M. M. R.; Crutchley, R. J. *Inorg. Chem.* **2013**, *52*, 14404.

[463] Nicholson, R.S.; Shain, I. *Anal. Chem.* **1964**, *36*, 706.

[464] Silva, D.O.; Toma, H.E. *Can. J. Chem.* **1994**, *72* ,1705.

[465] Weisser, F.; Hohloch, S.; Plebst, S.; Schweinfurth, D.; Sarkar, B. *Chem. Eur. J.* **2014**, *20*, 781.

[466] Lever, A. B. P. *Inorganic electronic spectroscopy*, 2nd ed.; Elsevier: Amsterdam; Oxford, **1984.**

[467] Weinstein, J. A.; Tierney, M. T.; Davies, S.; Base, K.; Robeiro, A. A.; Grinstaff, M. W. *Inorg. Chem.* **2006**, *45*, 4544.

ANNEX

Annex

Supporting Information

Chapter 4

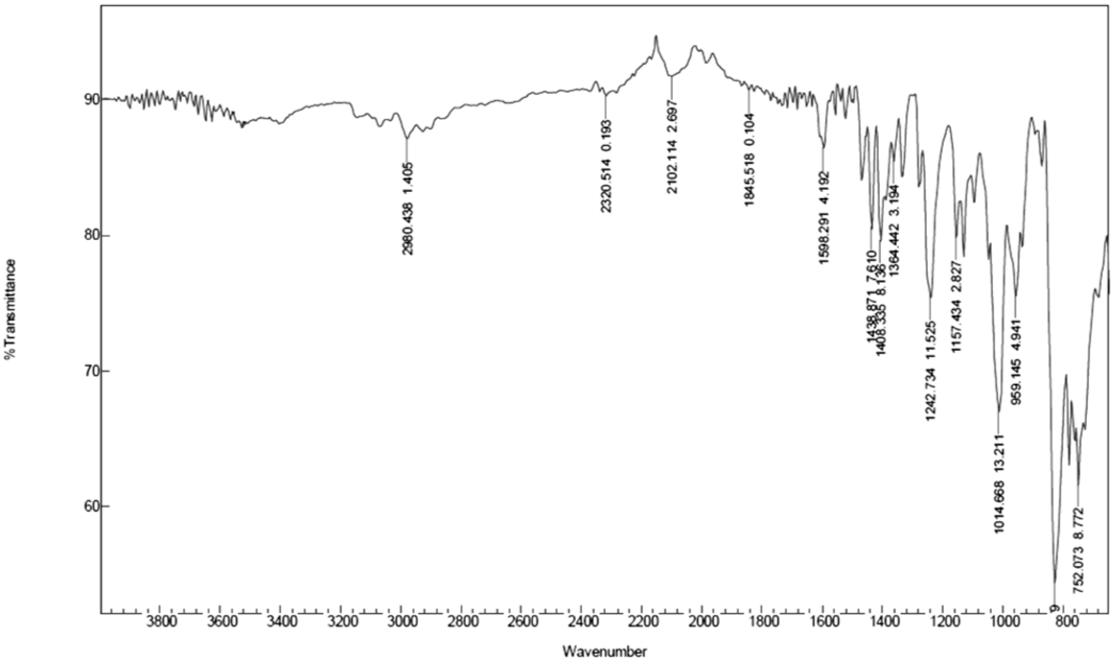

Figure S4.1. FTIR spectra of **C3**.

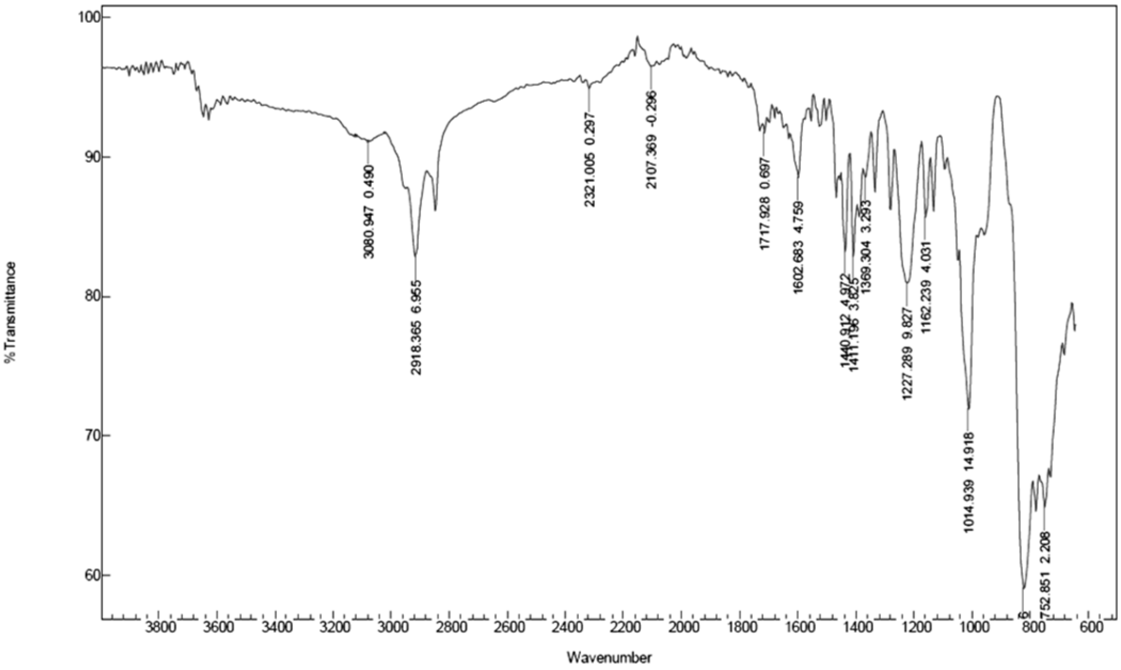

Figure S4.2. FTIR spectra of **C4**.

a)

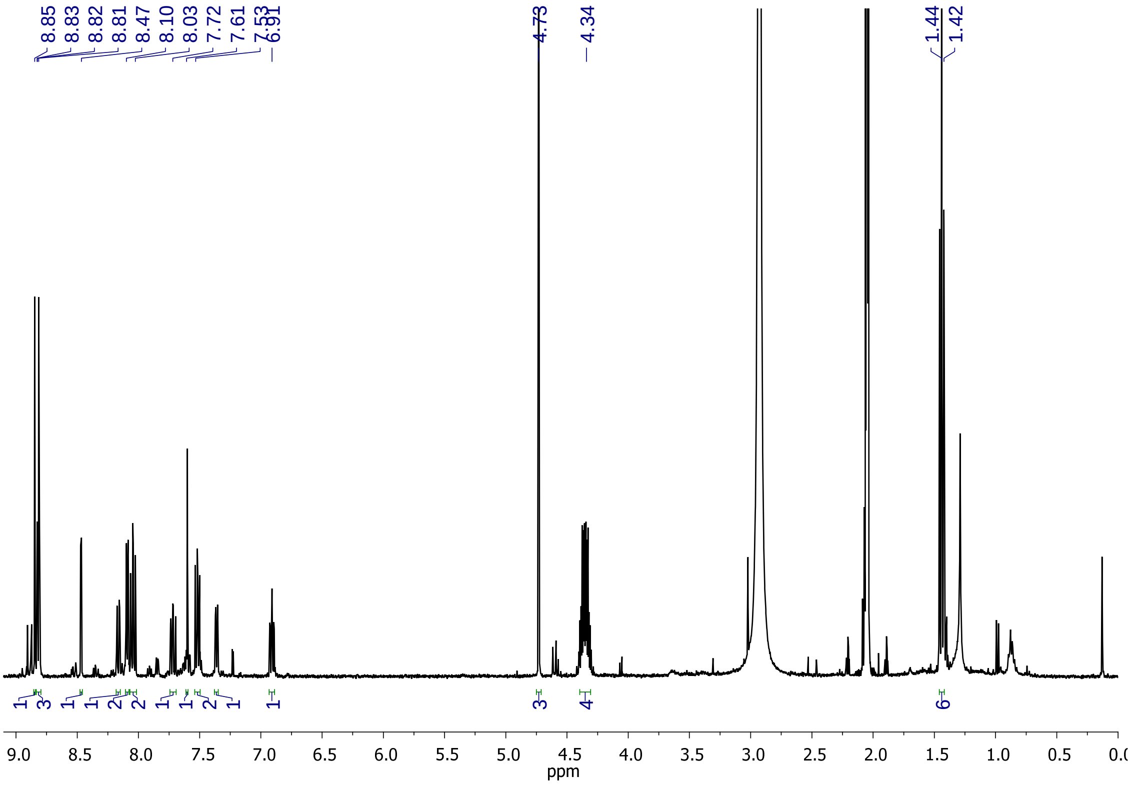
8.85
8.83
8.82
8.81
8.47
8.10
8.03
7.72
7.61
7.53
6.91
4.73
4.34
1.44
1.42
1
3
1
1
2
2
1
1
2
1
1
3
4
6
9.0
8.5
8.0
7.5
7.0
6.5
6.0
5.5
5.0
4.5
4.0
3.5
3.0
2.5
2.0
1.5
1.0
0.5
0.0
ppm

b)

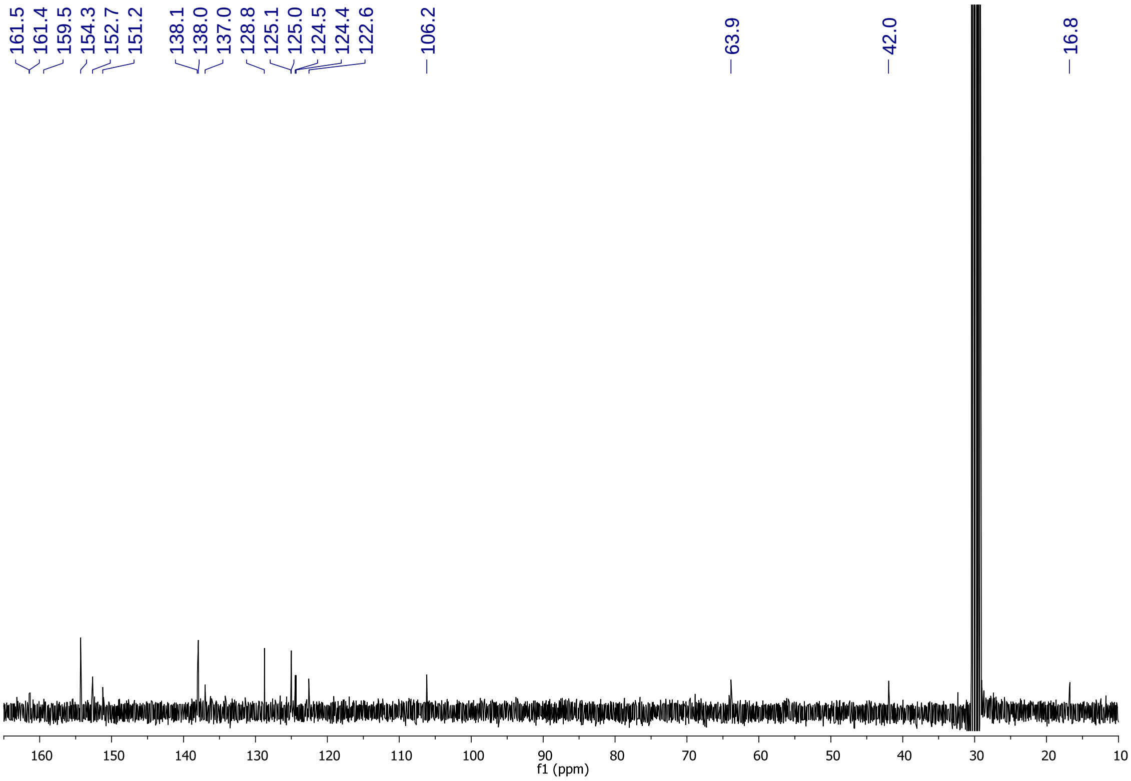
161.5
161.4
159.5
154.3
152.7
151.2
138.1
138.0
137.0
128.8
125.1
125.0
124.5
124.4
122.6
106.2
63.9
42.0
16.8
160
150
140
130
120
110
100
90
80
70
60
50
40
30
20
10
f1 (ppm)

c)

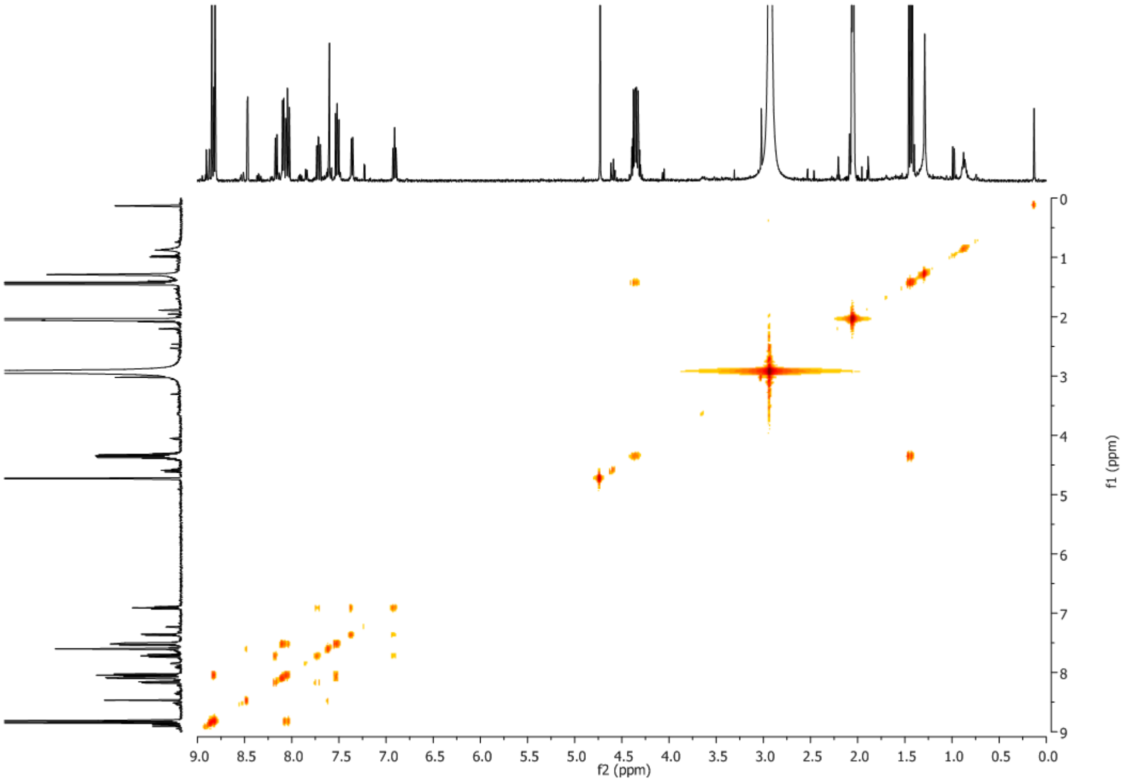
f2 (ppm)
9.0
8.5
8.0
7.5
7.0
6.5
6.0
5.5
5.0
4.5
4.0
3.5
3.0
2.5
2.0
1.5
1.0
0.5
0.0
f1 (ppm)
0
1
2
3
4
5
6
7
8
9

d)

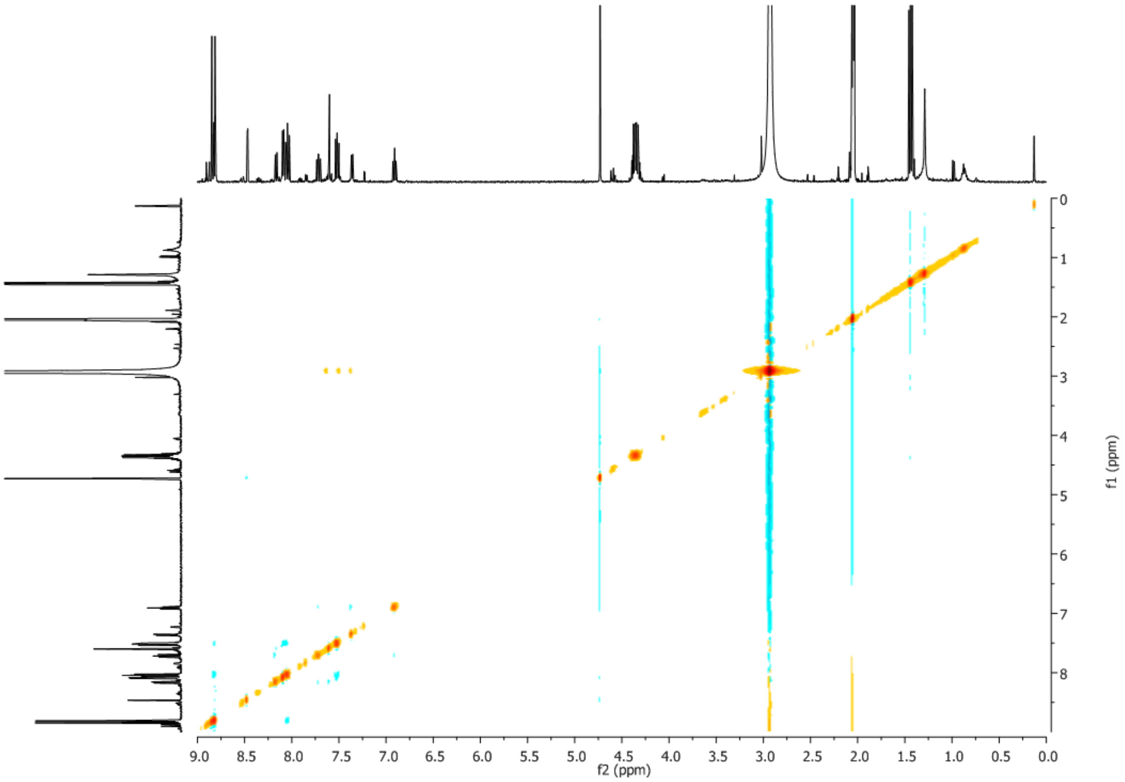
f2 (ppm)
9.0
8.5
8.0
7.5
7.0
6.5
6.0
5.5
5.0
4.5
4.0
3.5
3.0
2.5
2.0
1.5
1.0
0.5
0.0
f1 (ppm)
0
1
2
3
4
5
6
7
8

e)

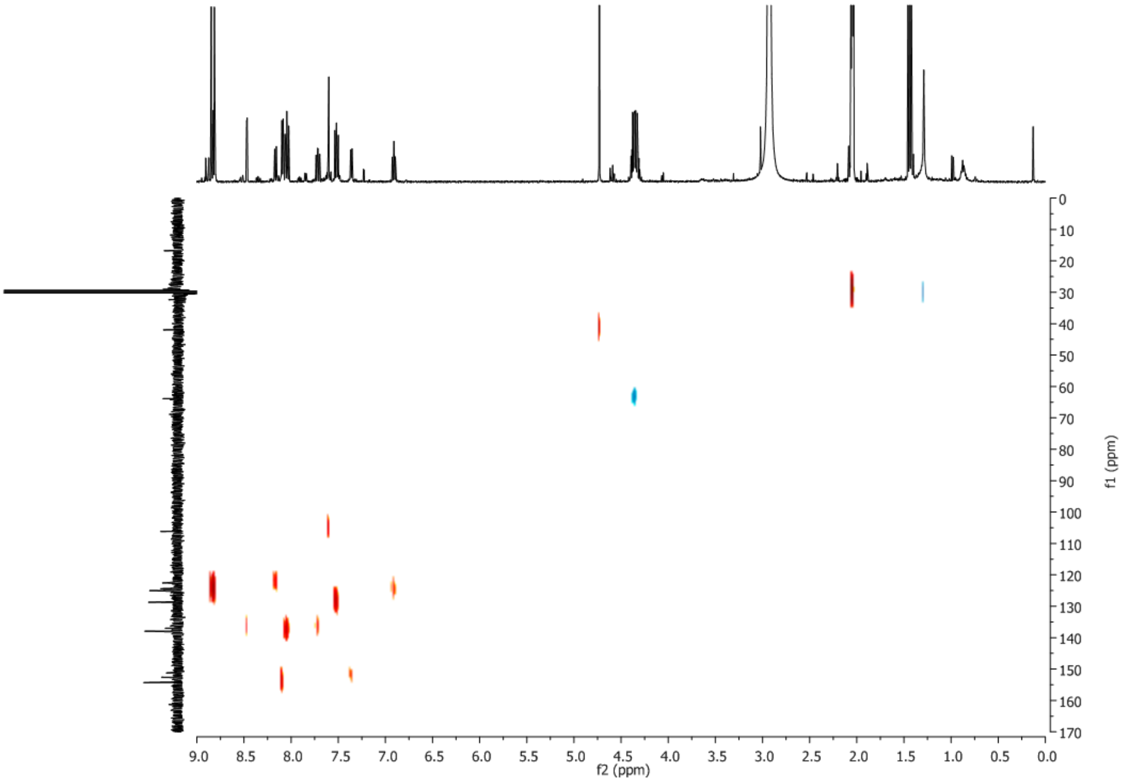

f)

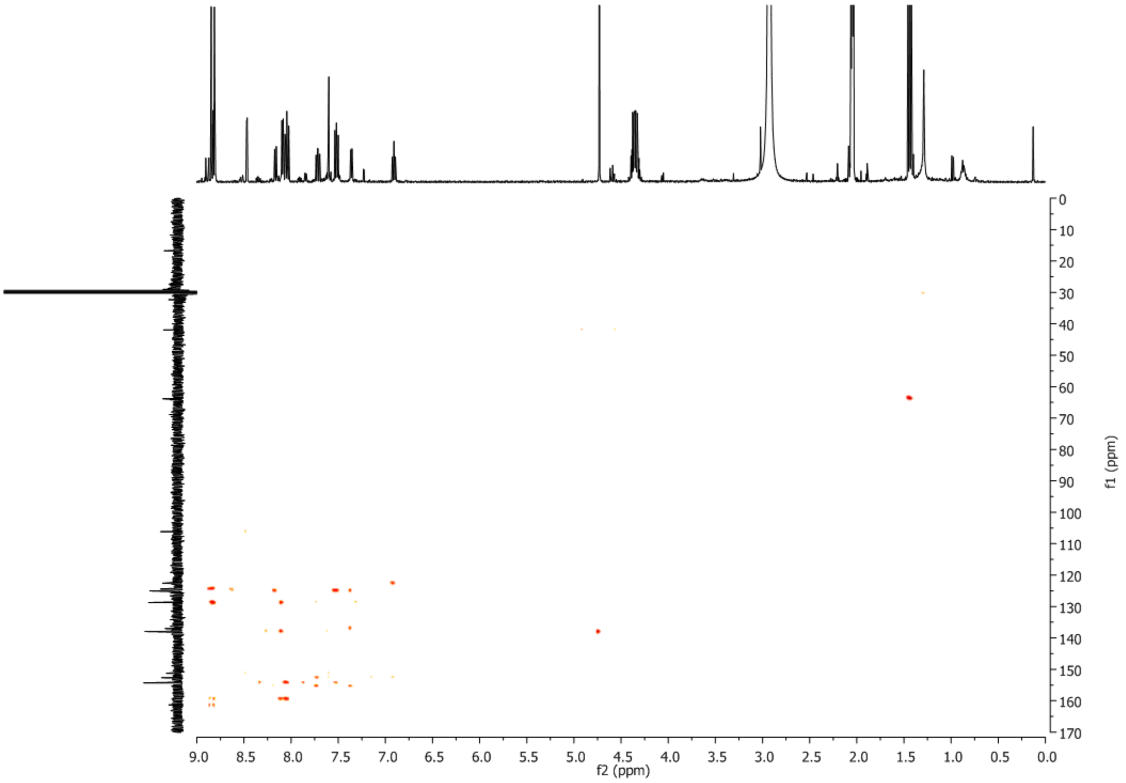

Figure S4.3. NMR spectra of *cis*-**C3**, 400 MHz, acetone-d_6: a) ^{1}H-NMR; b) ^{13}C-NMR; c) COSY; d) NOESY; e) ^{1}H-^{13}C HSQC, f) ^{1}H-^{13}C HMBC.

a)

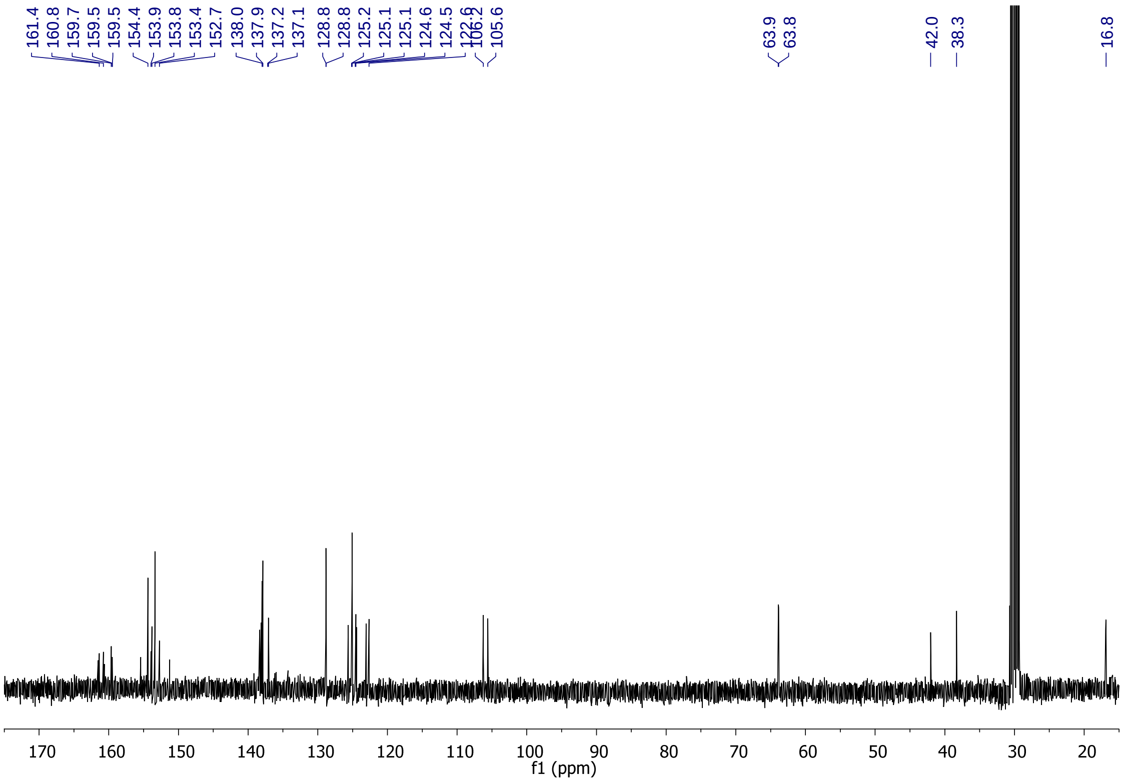
161.4
160.8
159.7
159.5
159.5
154.4
153.9
153.8
153.4
152.7
138.0
137.9
137.2
137.1
128.8
128.8
125.2
125.1
125.1
124.6
124.5
122.6
106.2
105.6
63.9
63.8
42.0
38.3
16.8
170
160
150
140
130
120
110
100
90
80
70
60
50
40
30
20
f1 (ppm)

b)

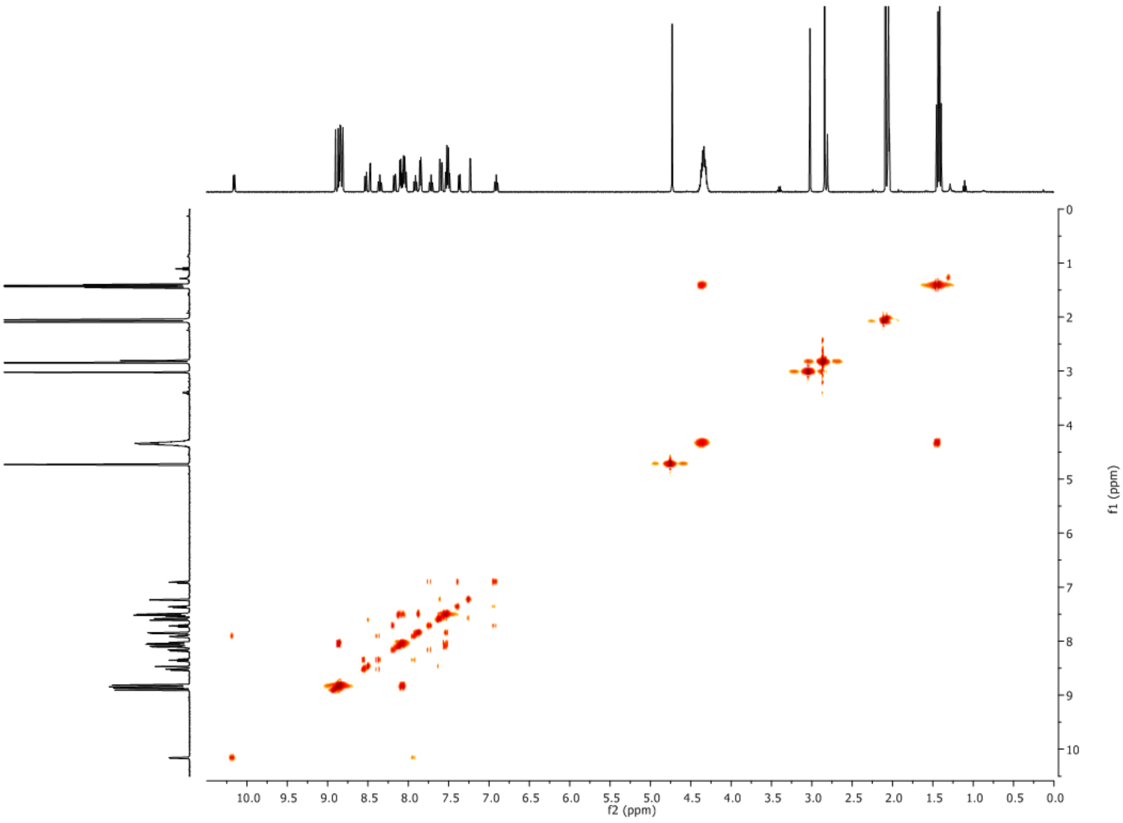
10.0
9.5
9.0
8.5
8.0
7.5
7.0
6.5
6.0
5.5
5.0
4.5
4.0
3.5
3.0
2.5
2.0
1.5
1.0
0.5
0.0
f2 (ppm)
0
1
2
3
4
5
6
7
8
9
10
f1 (ppm)

c)

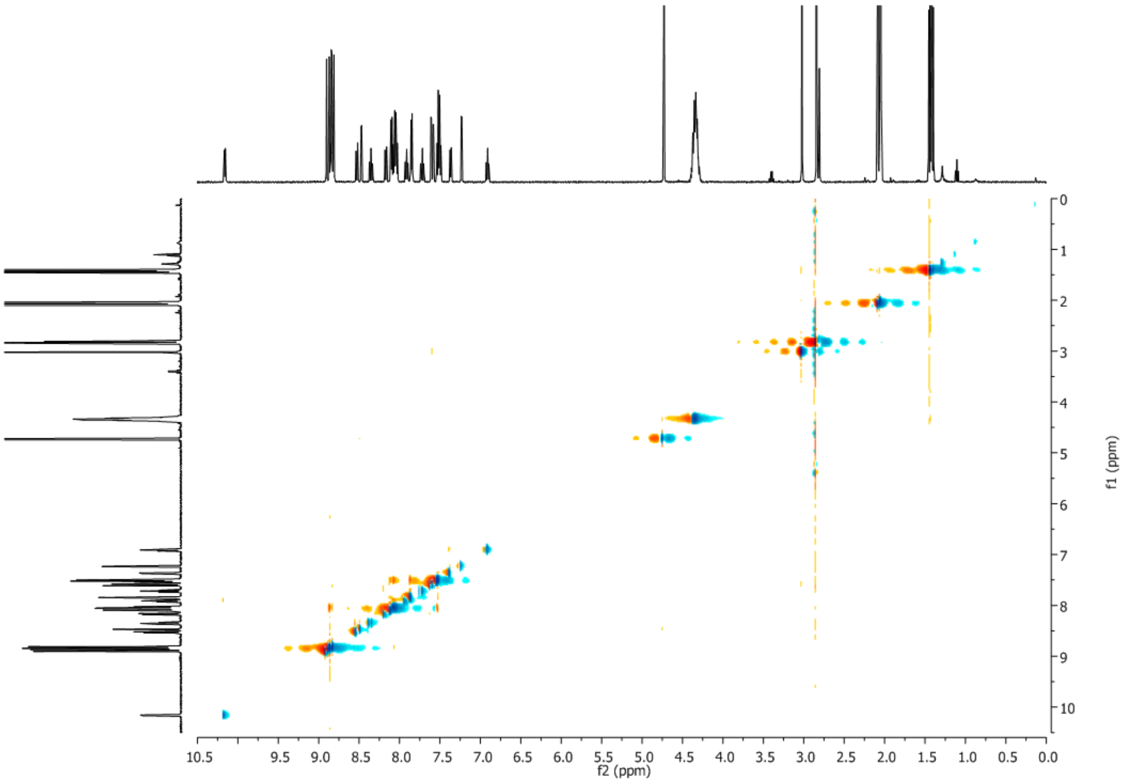
10.5
9.5
9.0
8.5
8.0
7.5
7.0
6.5
6.0
5.5
5.0
4.5
4.0
3.5
3.0
2.5
2.0
1.5
1.0
0.5
0.0
f2 (ppm)
0
1
2
3
4
5
6
7
8
9
10
f1 (ppm)

d)

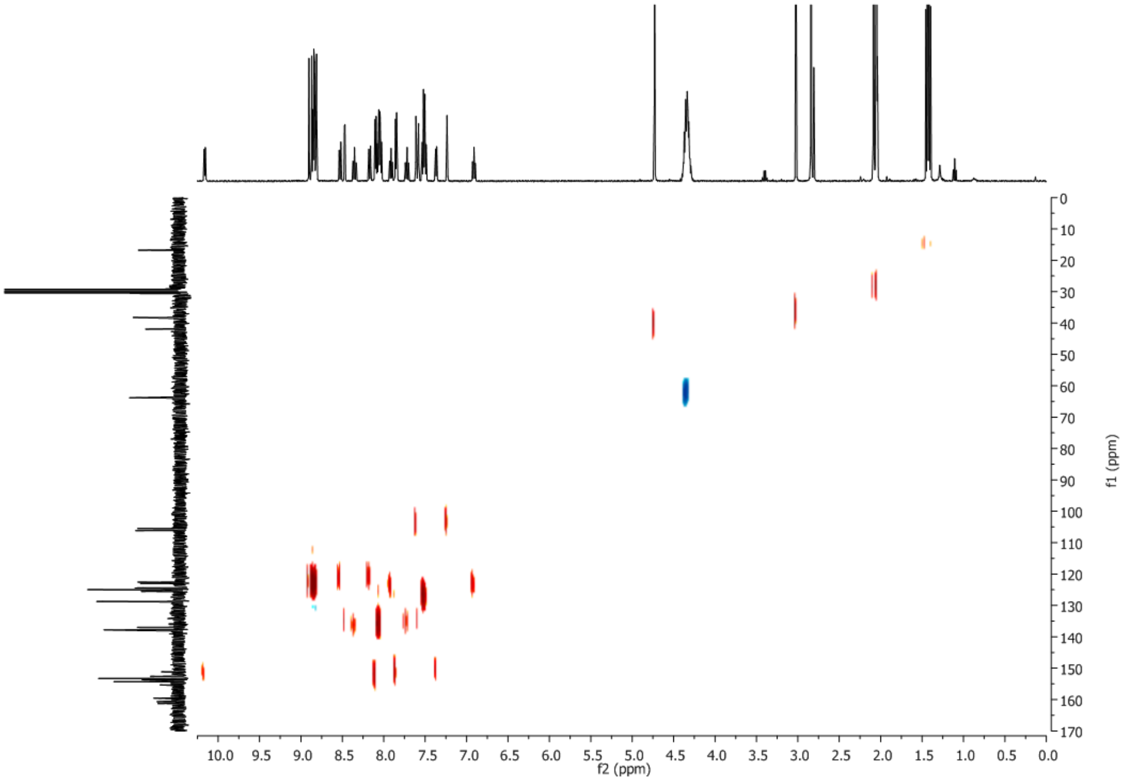
10.0
9.5
9.0
8.5
8.0
7.5
7.0
6.5
6.0
5.5
5.0
4.5
4.0
3.5
3.0
2.5
2.0
1.5
1.0
0.5
0.0
f2 (ppm)
0
10
20
30
40
50
60
70
80
90
100
110
120
130
140
150
160
170
f1 (ppm)

e)

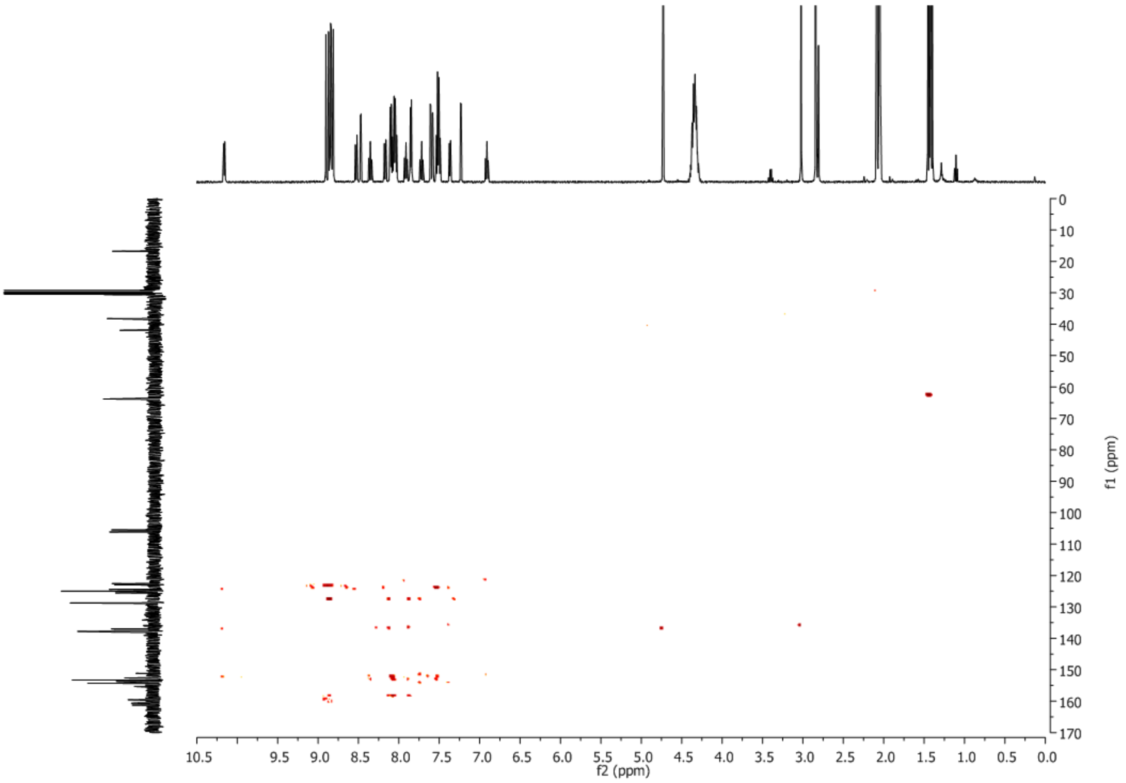

Figure S4.4. NMR spectra of *trans*- and *cis*-**C3**, 400 MHz, acetone-d_6: a) ^{13}C-NMR; b) COSY; c) NOESY; d) ^{1}H-^{13}C HSQC; e) ^{1}H-^{13}C HMBC.

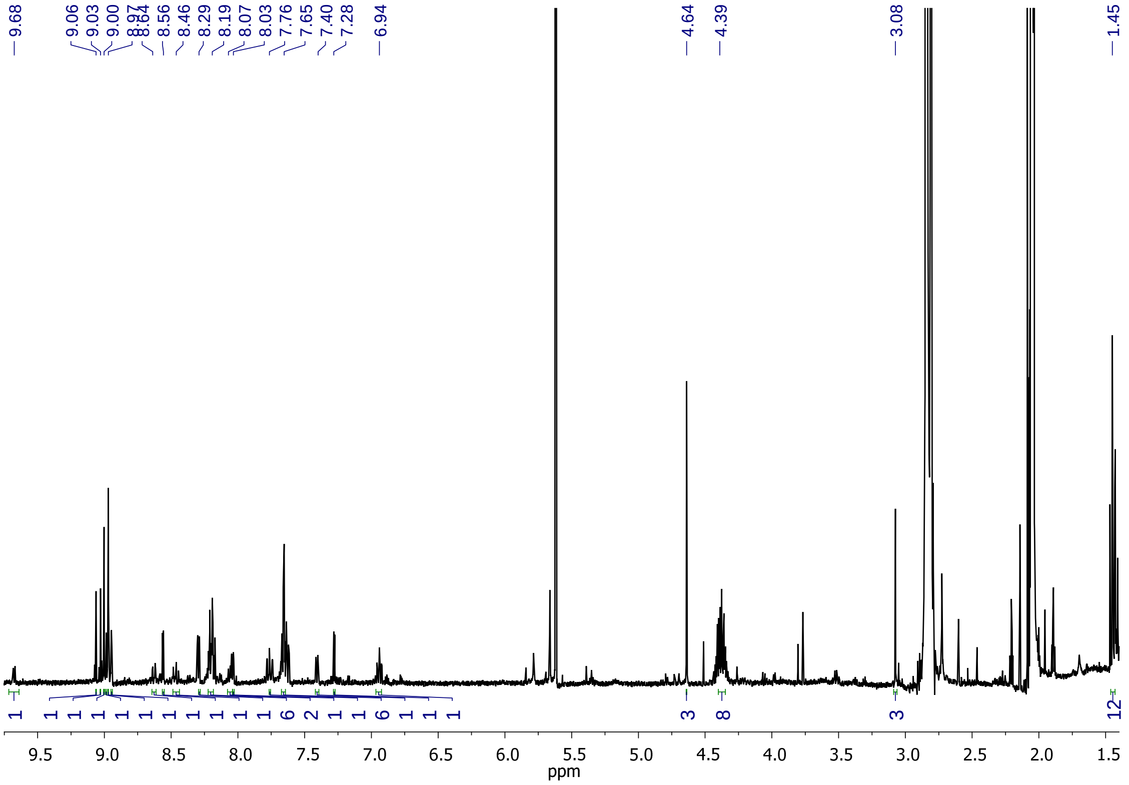

Figure S4.5. ^{1}H-NMR spectra of **C4**, 400 MHz, acetone-d_6.

Table S4.1. Crystallographic Data for Complex **C3**.

	C3
Empirical formula	$C_{31}H_{35}ClN_6O_4F_6P_2Ru$
Formula weight	868.11
Crystal system	Triclinic
Space group	P-1
a[Å]	8.834(3)
b[Å]	14.292(4)
c[Å]	15.293(5)
α[°]	101.867(6)
β[°]	106.652(5)
γ[°]	95.095(5)
V [$Å^3$]	1787.8(9)
Formula Units/ cell	2
Temp. [K]	100(2)
ρ_{calc}, [Mg/m^{-3}]	1.613
μ[mm^{-1}]	0.679
Final R indices,	$R_1 = 0.0759$
[I>2σ(I)]	$wR_2 = 0.1732$
R indices [all data]	$R_1 = 0.1242$ $wR_2 = 0.1963$

Table S4.2. Selected Bond Lengths (Å) and Angles (°) for **C3**.

	C3
Ru(1)-N(1)	2.081(6)
Ru(1)-N(2)	1.942(6)
Ru(1)-N(3)	2.084(6)
Ru(1)-N(4)	2.133(6)
Ru(1)-N(6)	2.091(17)
Ru(1)-N(6’)	2.049(9)
Ru(1)-Cl(1)	2.399(2)
N(1)-Ru(1)-N(2)	80.1(2)
N(1)-Ru(1)-N(3)	160.1(2)
N(1)-Ru(1)-N(4)	97.4(2)
N(1)-Ru(1)- N(6)	90.0(6)
N(1)-Ru(1)- N(6’)	89.1(4)
N(1)-Ru(1)-Cl(1)	89.46(18)
N(2)-Ru(1)- N(3)	80.1(2)
N(2)-Ru(1)- N(4)	175.9(3)
N(2)-Ru(1)- N(6)	104.5(6)
N(2)-Ru(1)- N(6’)	93.3(4)
N(2)-Ru(1)-Cl(1)	86.7(2)
N(3)-Ru(1)-N(4)	102.3(2)
N(3)-Ru(1)-N(6)	93.8(6)
N(3)-Ru(1)-N(6’)	90.9(4)
N(3)-Ru(1)-Cl(1)	90.57(19)
N(4)-Ru(1)-N(6)	72.2(6)
N(4)-Ru(1)-N(6’)	83.4(4)
N(4)-Ru(1)-Cl(1)	96.6(2)
N(6)-Ru(1)-Cl(1)	168.5(6)
N(6’)-Ru(1)-Cl(1)	178.5(4)

Chapter 5

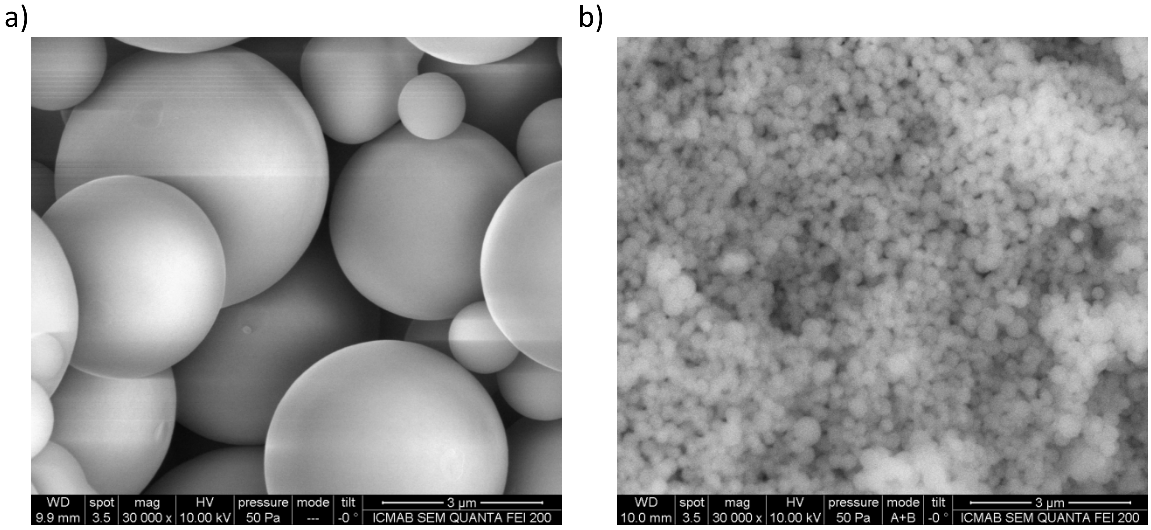
a)
b)
WD 9.9 mm | spot 3.5 | mag 30 000 x | HV 10.00 kV | pressure 50 Pa | mode --- | tilt -0 ° | 3 μm | ICMAB SEM QUANTA FEI 200
WD 10.0 mm | spot 3.5 | mag 30 000 x | HV 10.00 kV | pressure 50 Pa | mode A+B | tilt -0 ° | 3 μm | ICMAB SEM QUANTA FEI 200

Figure S5.1. SEM images of a) **SP1** b) **SP2** before functionalization with the Ru complex.

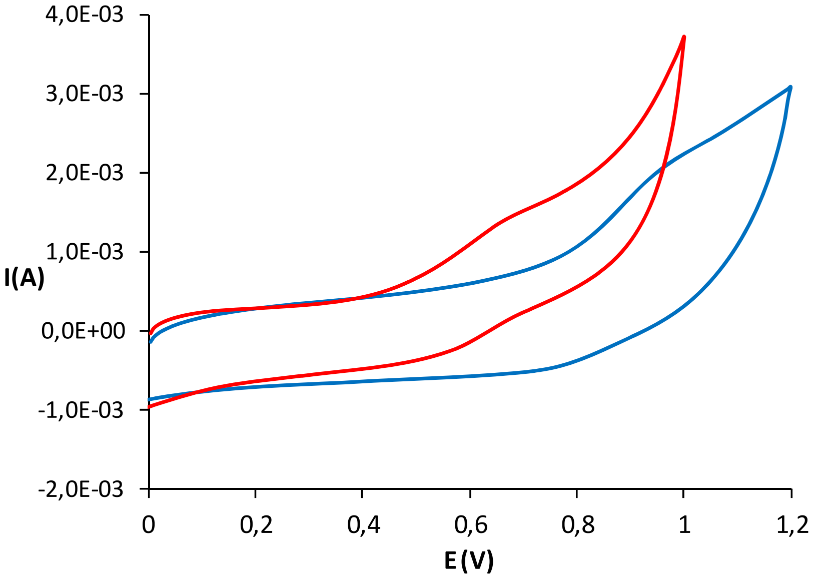

Figure S5.2. Cyclic voltammograms of **SP2-C4** in MeOH (blue) and in aqueous phosphate buffer, pH = 6.4 (red).

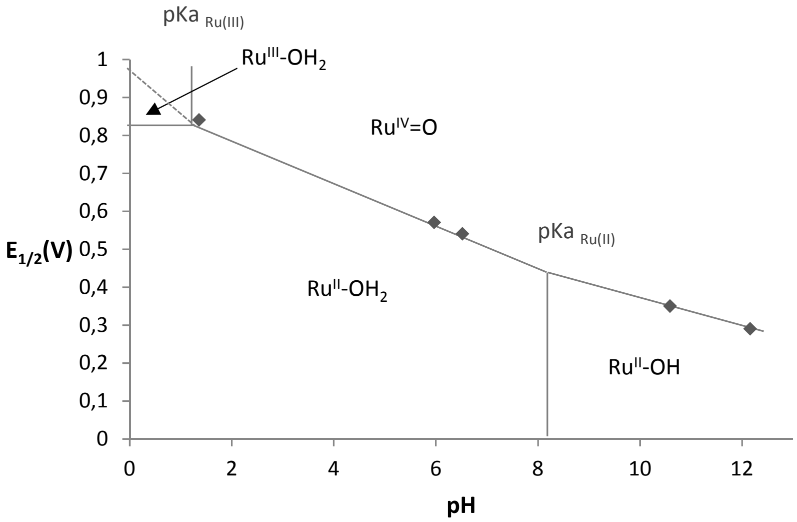

Figure S5.3. Pourbaix diagram for a **SP2-C4** sample obtained through strategy 2. The pH-potential regions of stability for the various oxidation states and their dominant proton compositions are based on the information displayed in Figure **5.6**.

Chapter 6

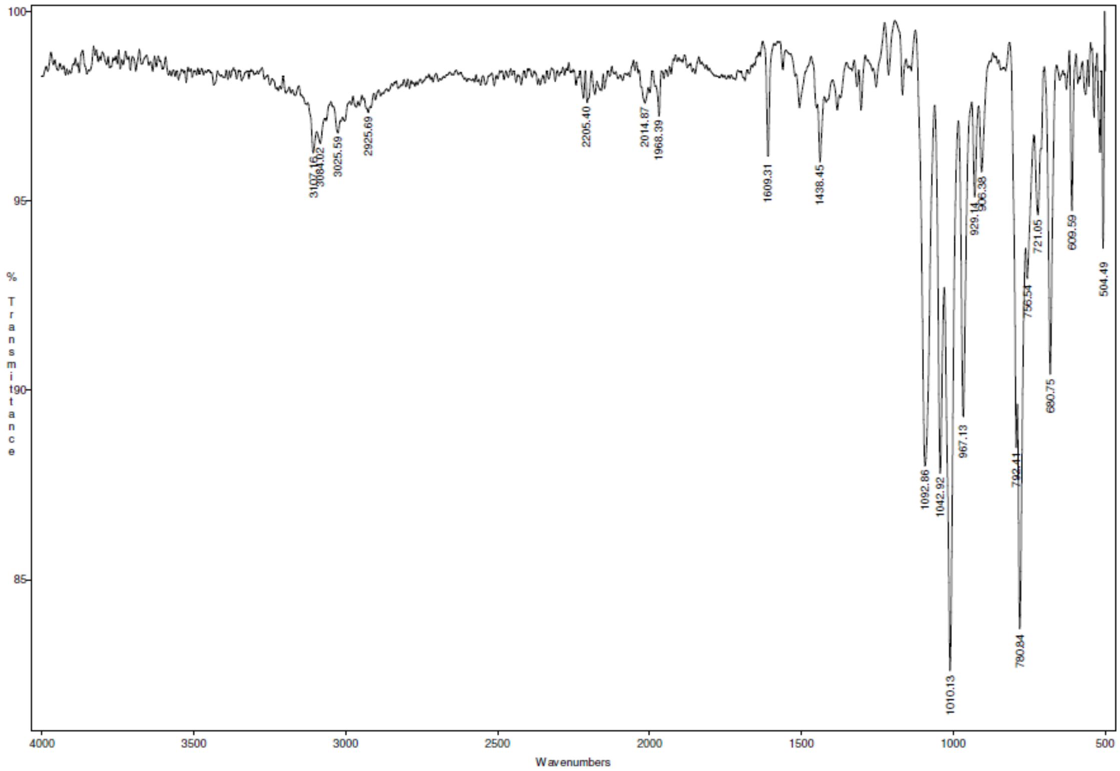

Figure S6.1. FTIR spectrum of **C5**.

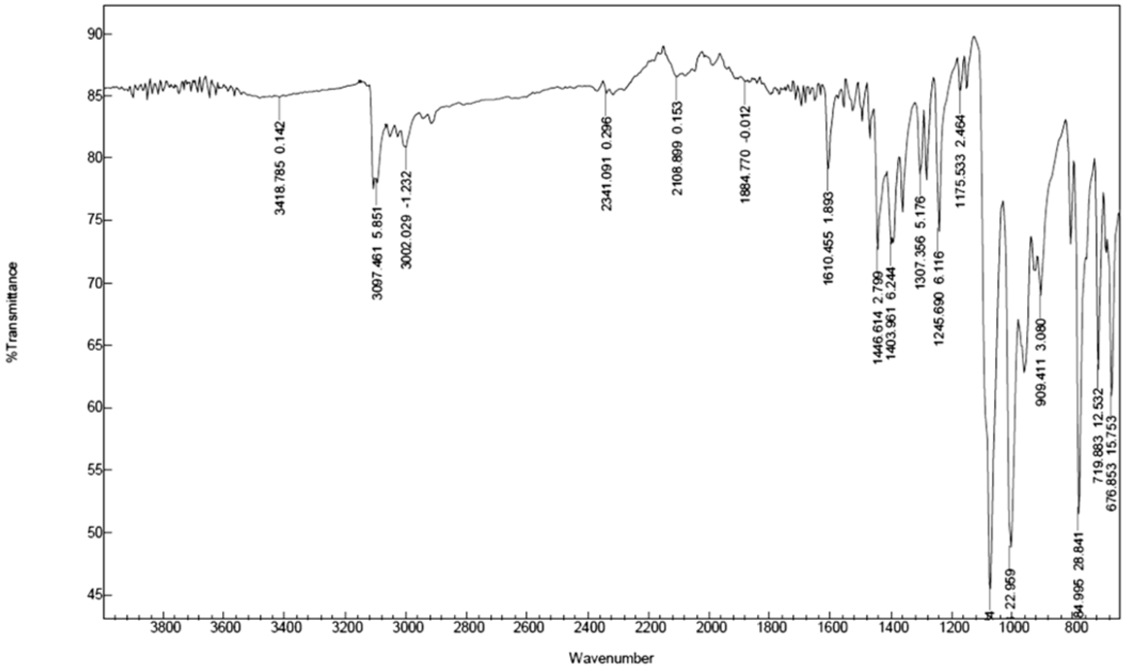

Figure S6.2. FTIR spectrum of **C6**.

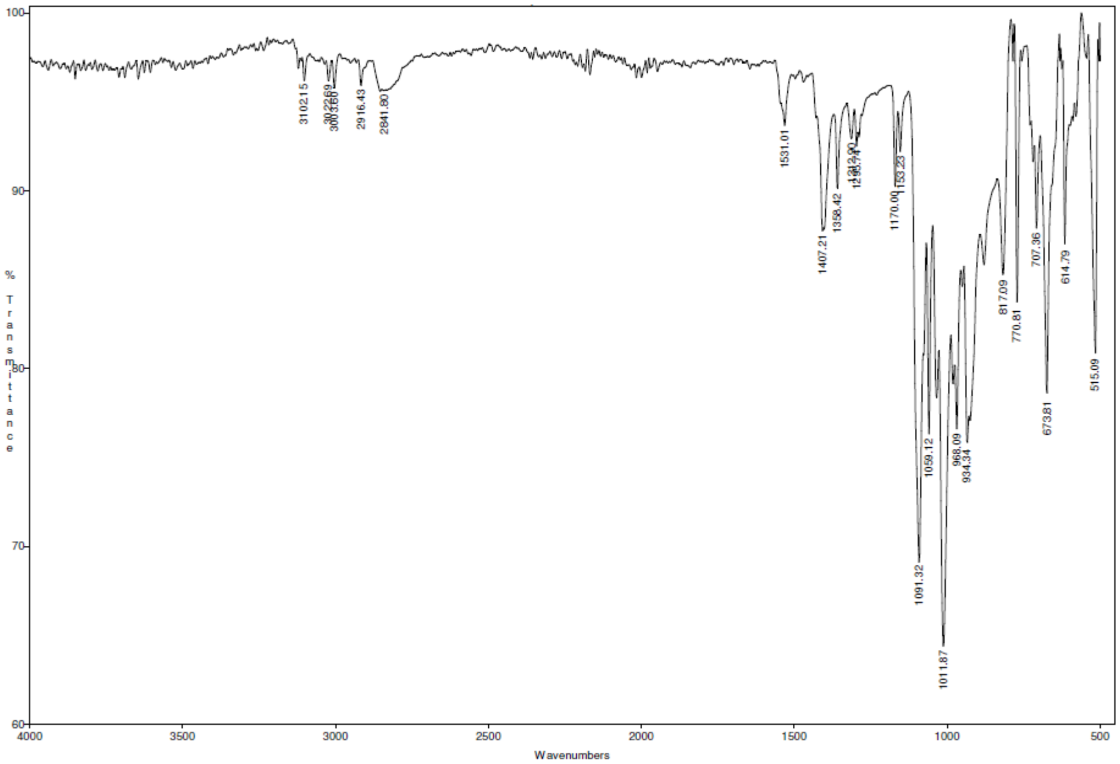

Figure S6.3. FTIR spectrum of **C7**.

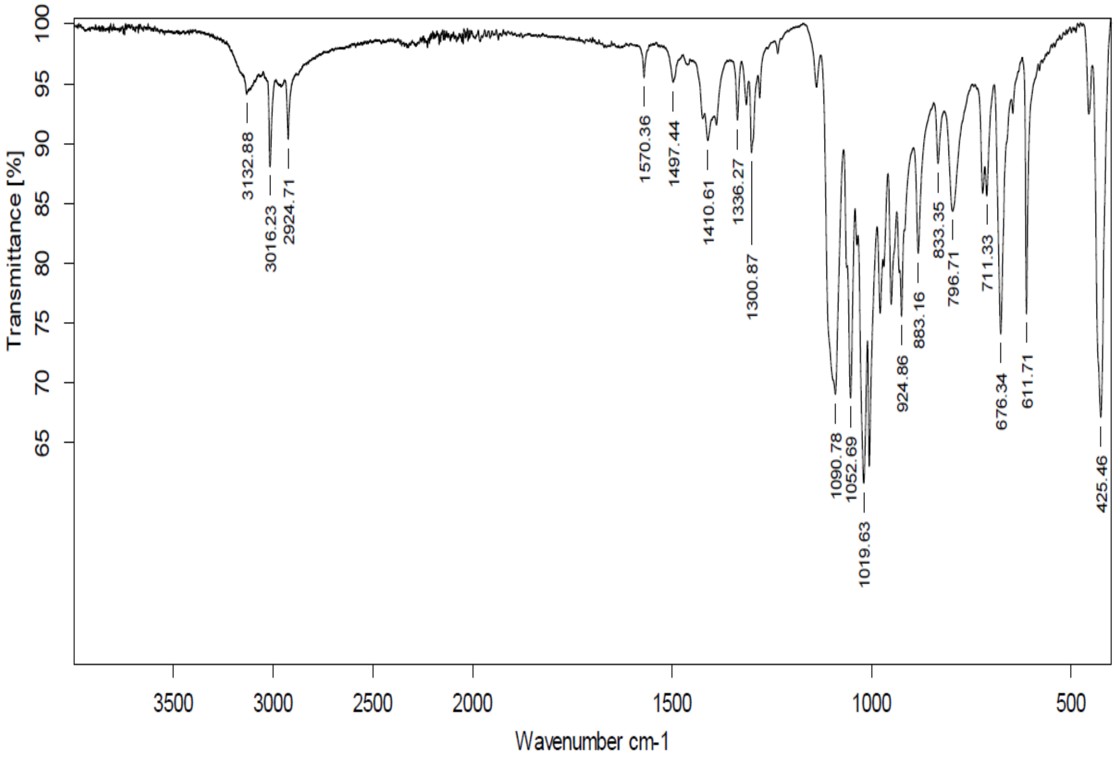

Figure S6.4. FTIR spectrum of **C8**.

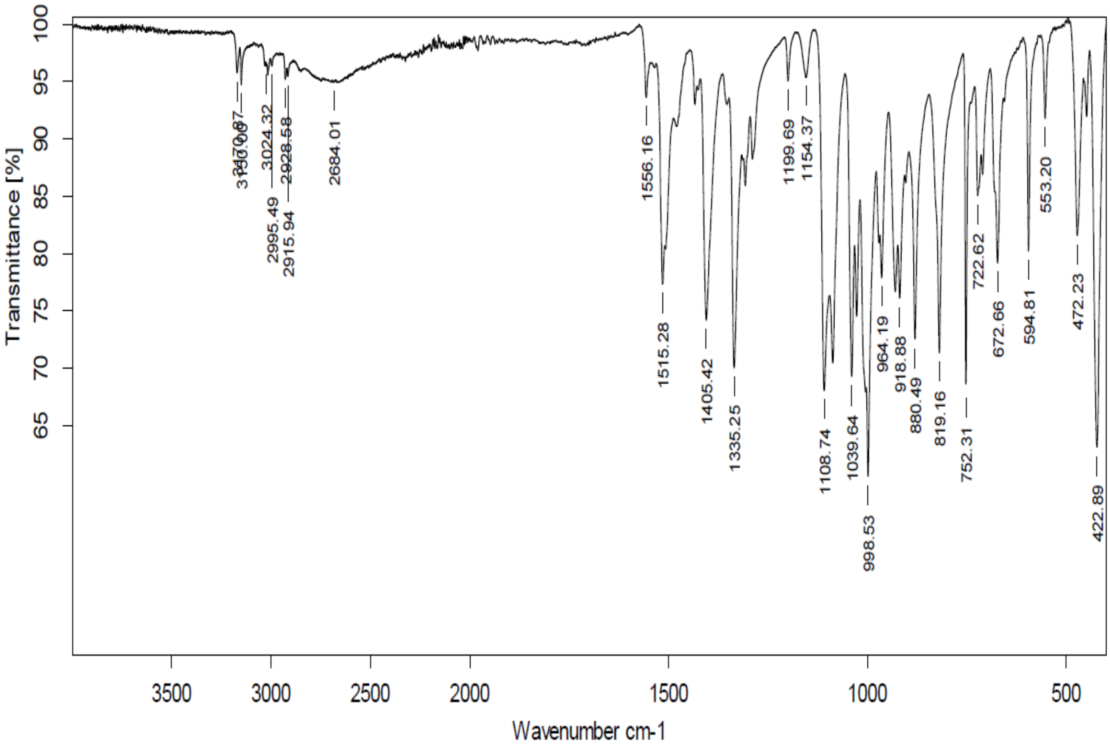

Figure S6.5. FTIR spectrum of **C9**.

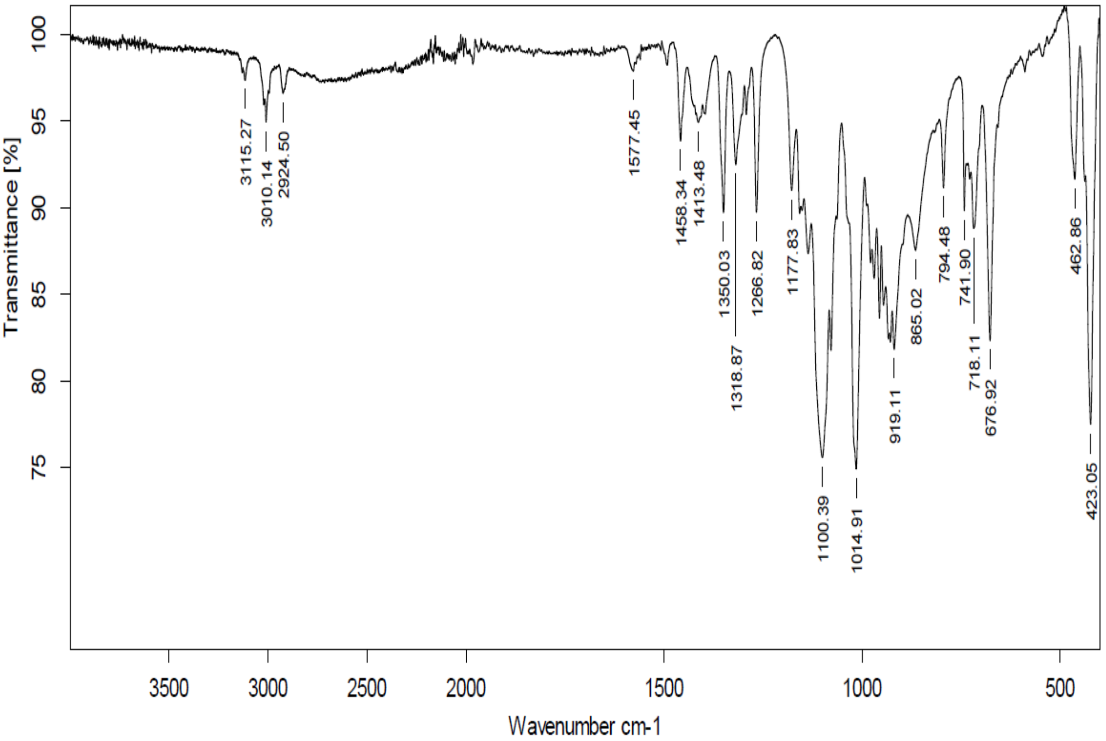

Figure S6.6. FTIR spectrum of **C10**.

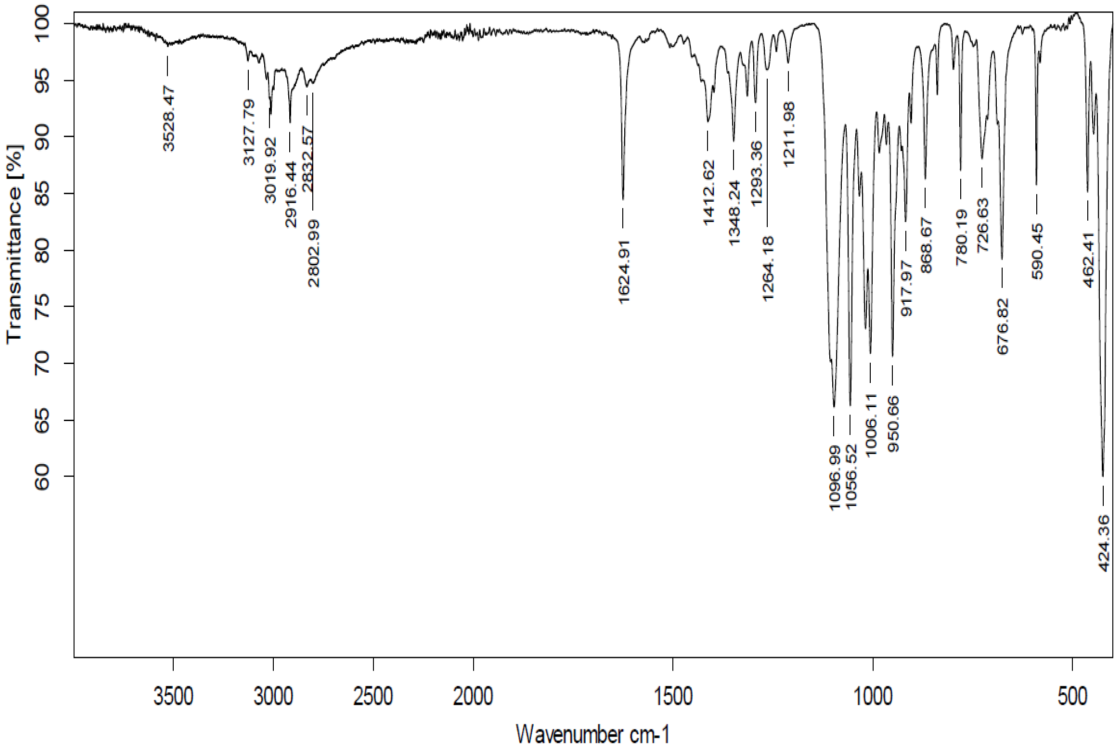

Figure S6.7. FTIR spectrum of **C11**.

a)

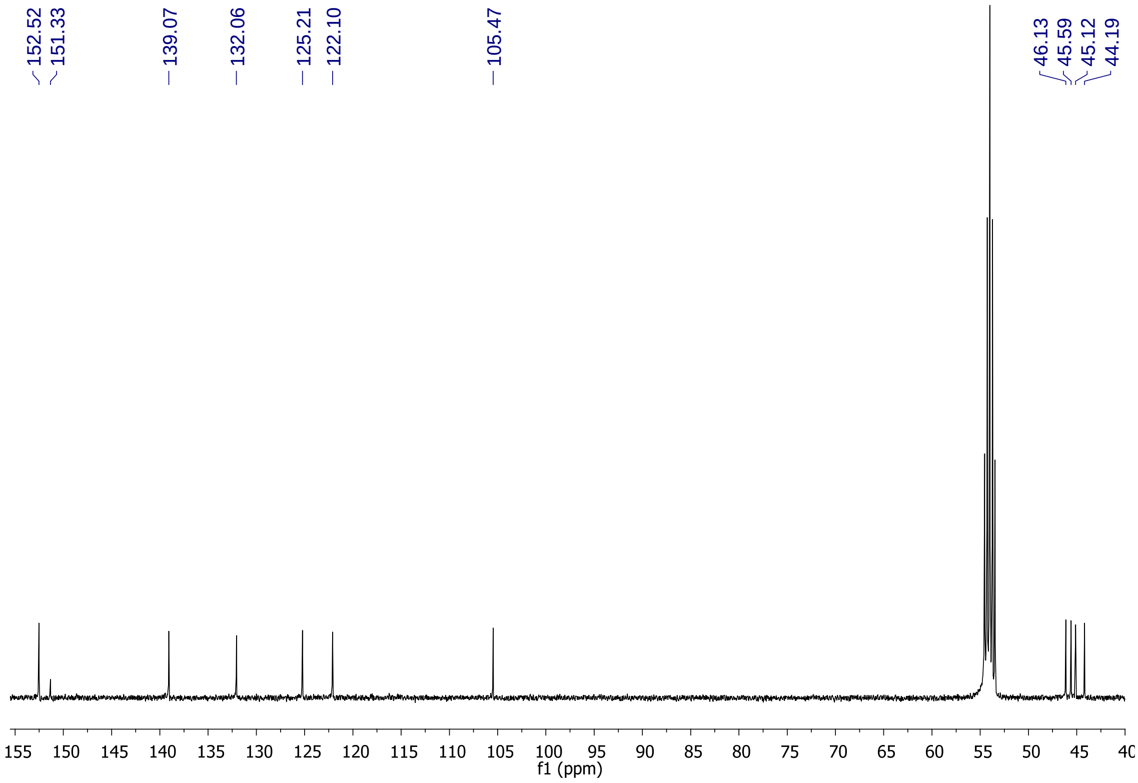

b)

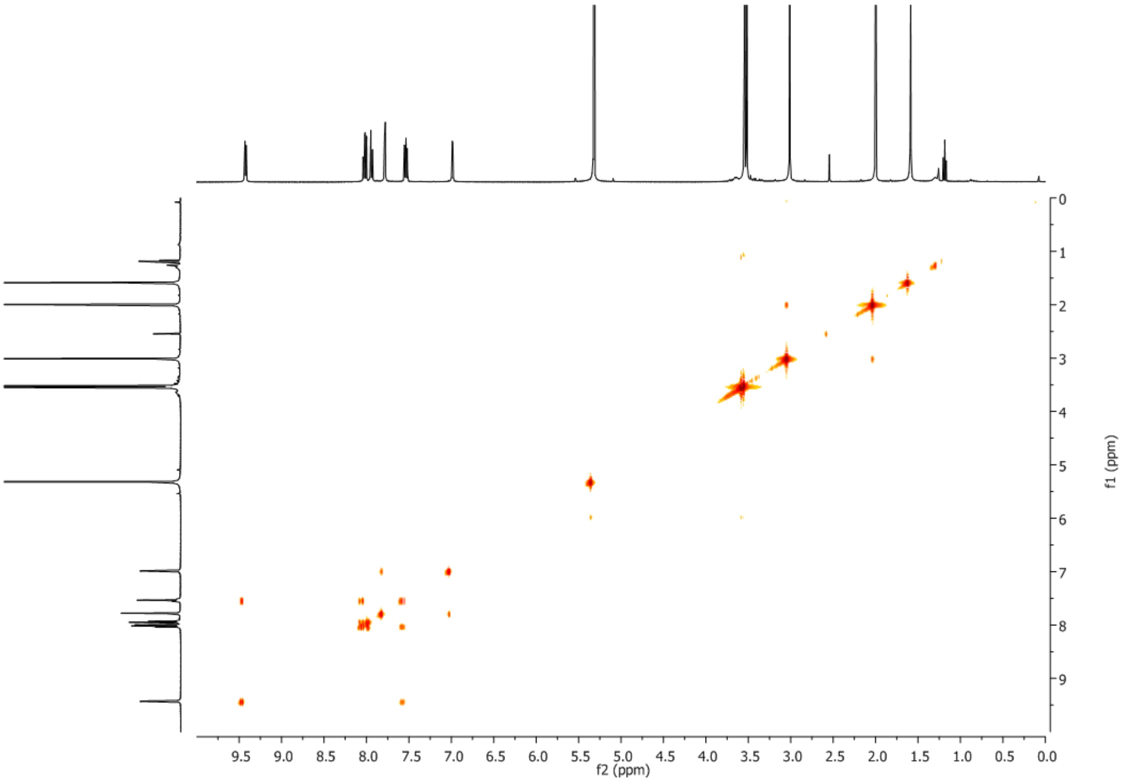
9.5
9.0
8.5
8.0
7.5
7.0
6.5
6.0
5.5
5.0
4.5
4.0
3.5
3.0
2.5
2.0
1.5
1.0
0.5
0.0
f2 (ppm)
0
1
2
3
4
5
6
7
8
9
f1 (ppm)

c)

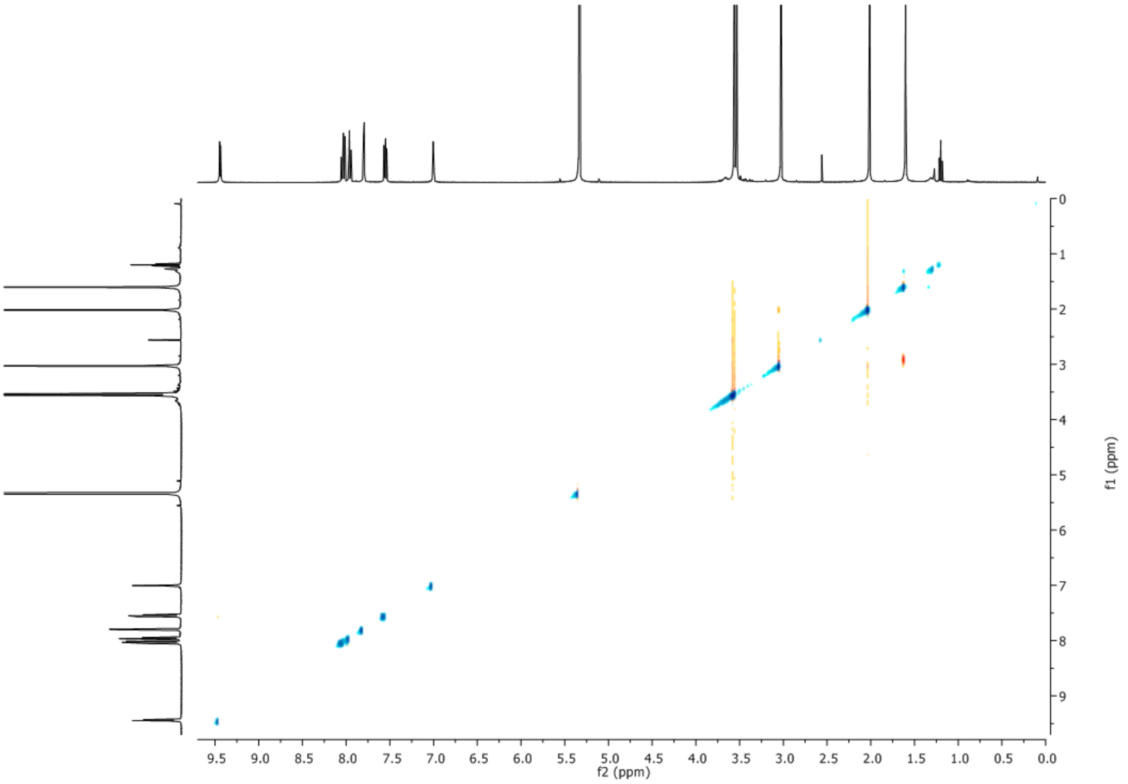
9.5
9.0
8.5
8.0
7.5
7.0
6.5
6.0
5.5
5.0
4.5
4.0
3.5
3.0
2.5
2.0
1.5
1.0
0.5
0.0
f2 (ppm)
0
1
2
3
4
5
6
7
8
9
f1 (ppm)

d)

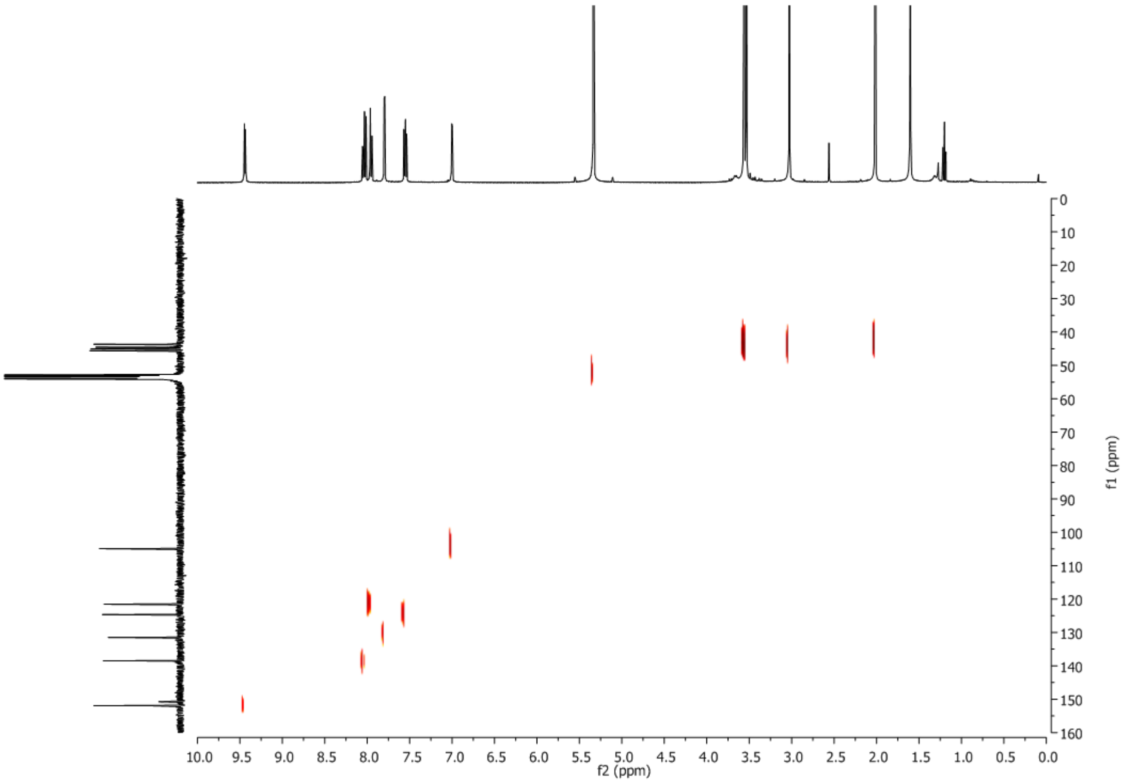

e)

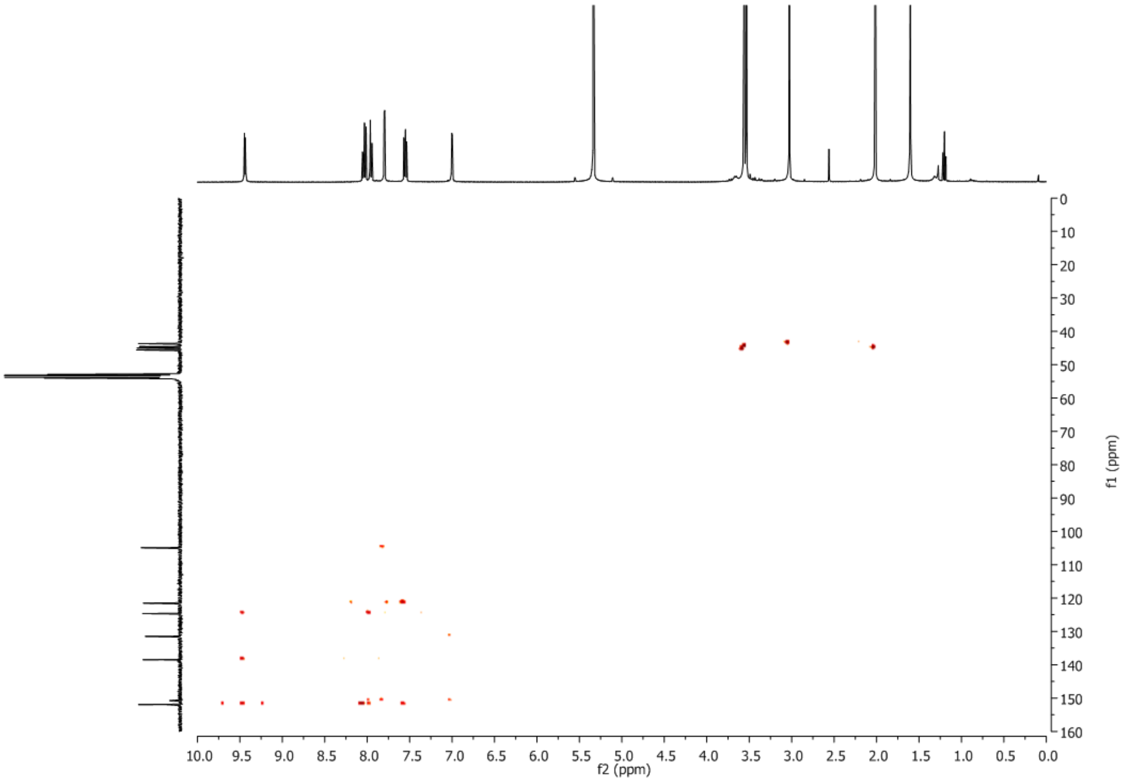

Figure S6.8. NMR spectra of **C5**, 400 MHz, CD_2Cl_2: a) ^{13}C-NMR; b) COSY; c) NOESY; d) ^1H-^{13}C HSQC, e) ^1H-^{13}C HMBC.

a)

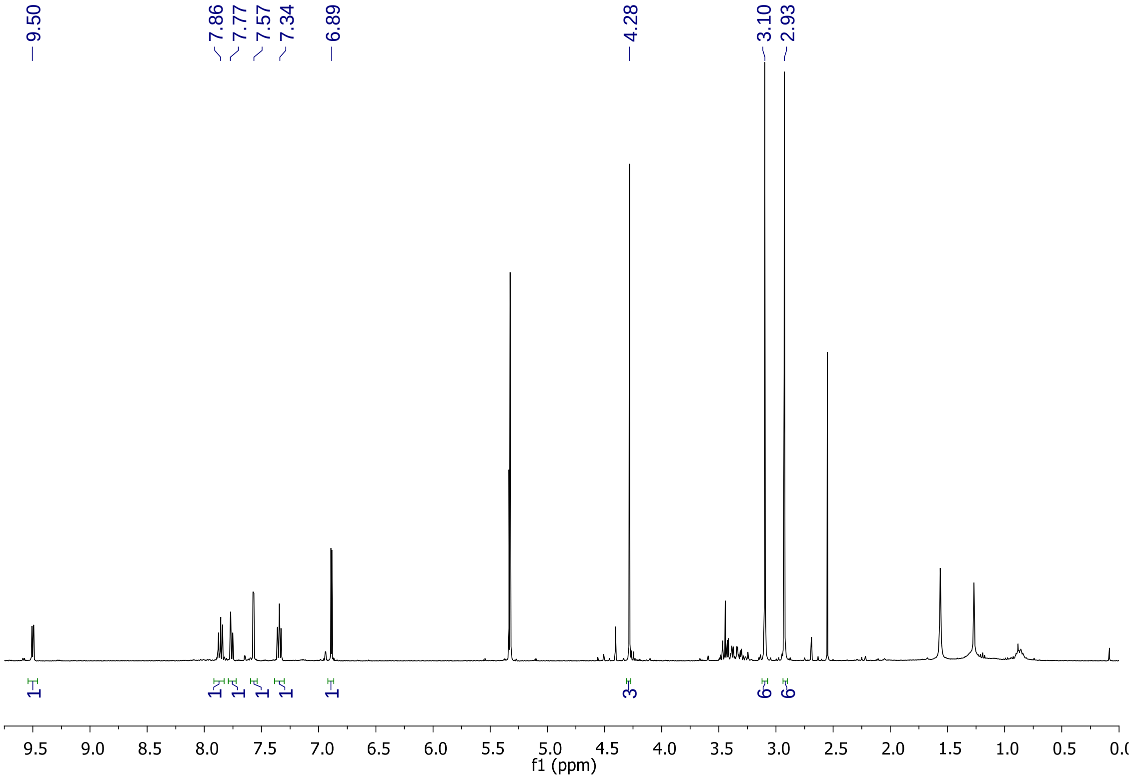
9.50
7.86
7.77
7.57
7.34
6.89
4.28
3.10
2.93
1
1
1
1
1
1
3
6
6
9.5
9.0
8.5
8.0
7.5
7.0
6.5
6.0
5.5
5.0
4.5
4.0
3.5
3.0
2.5
2.0
1.5
1.0
0.5
f1 (ppm)

b)

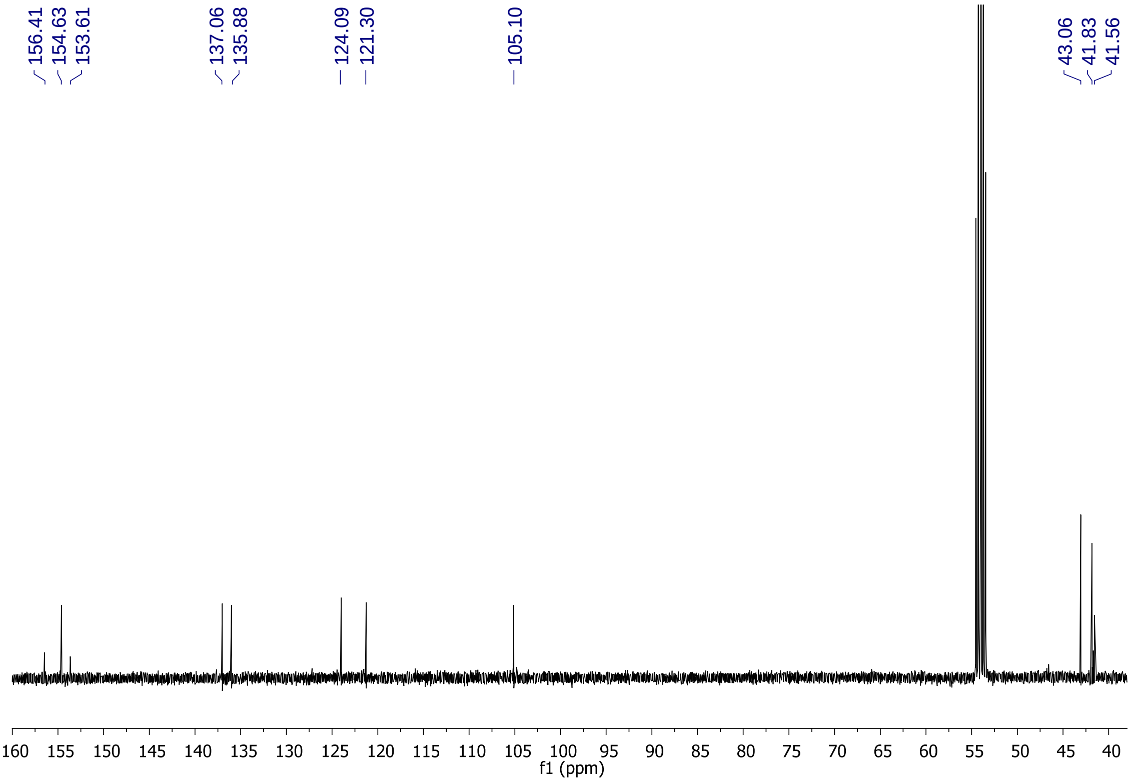
156.41
154.63
153.61
137.06
135.88
124.09
121.30
105.10
43.06
41.83
41.56
160
155
150
145
140
135
130
125
120
115
110
105
100
95
90
85
80
75
70
65
60
55
50
45
40
f1 (ppm)

c)

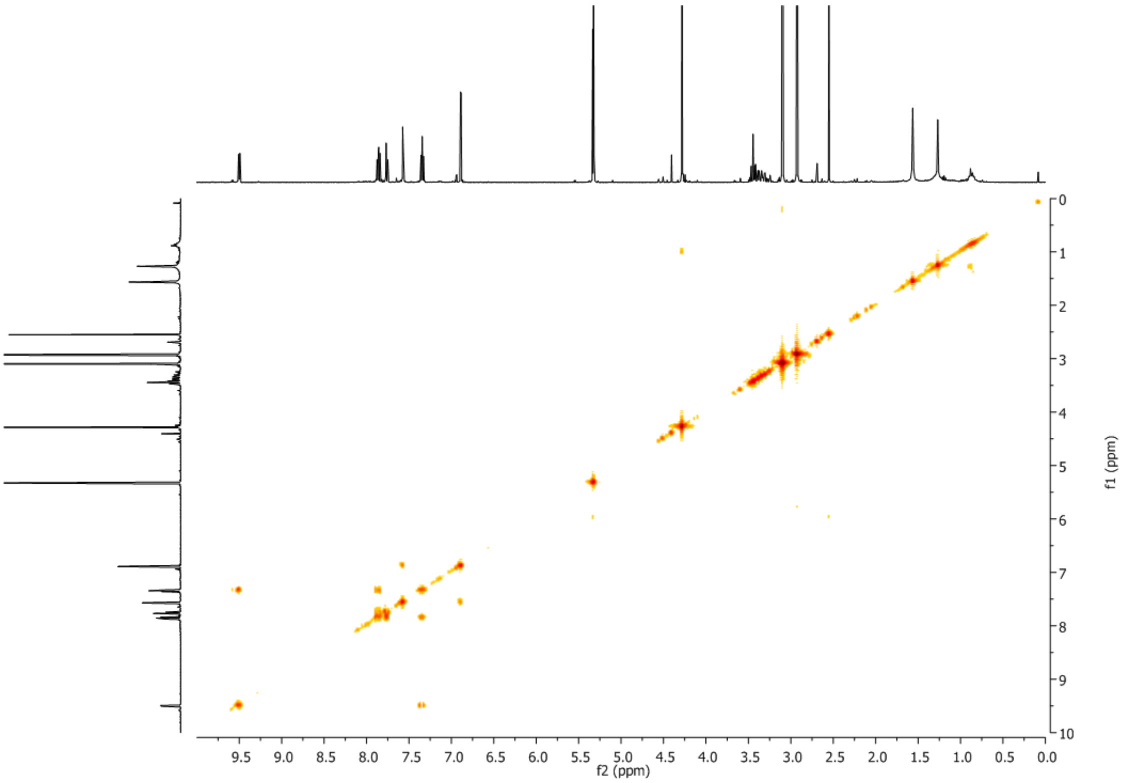
9.5
9.0
8.5
8.0
7.5
7.0
6.5
6.0
5.5
5.0
4.5
4.0
3.5
3.0
2.5
2.0
1.5
1.0
0.5
0.0
f2 (ppm)
0
1
2
3
4
5
6
7
8
9
10
f1 (ppm)

d)

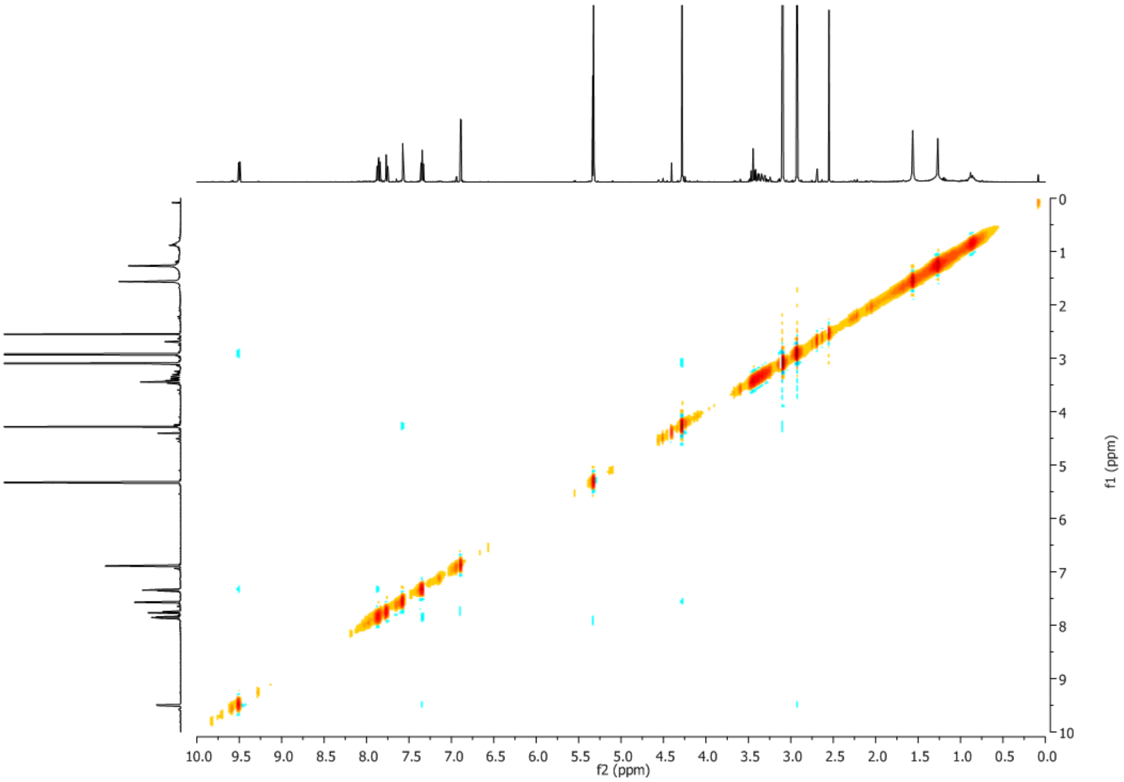
10.0
9.5
9.0
8.5
8.0
7.5
7.0
6.5
6.0
5.5
5.0
4.5
4.0
3.5
3.0
2.5
2.0
1.5
1.0
0.5
0.0
f2 (ppm)
0
1
2
3
4
5
6
7
8
9
10
f1 (ppm)

e)

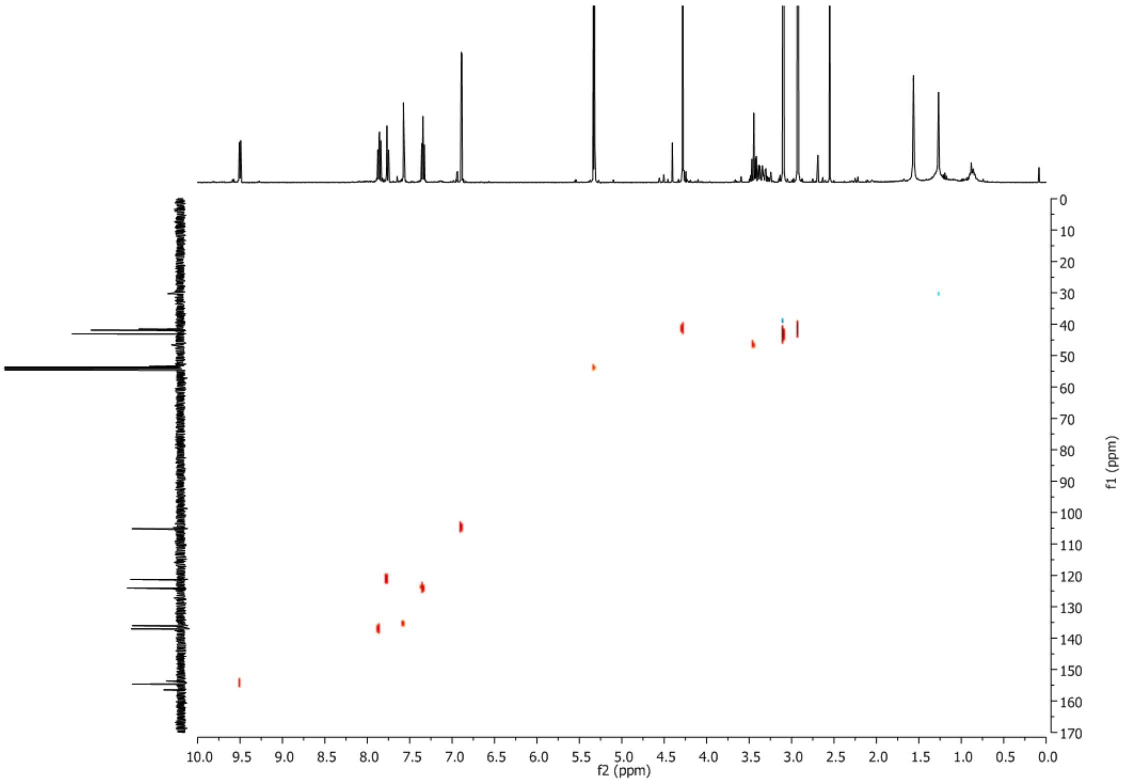

f)

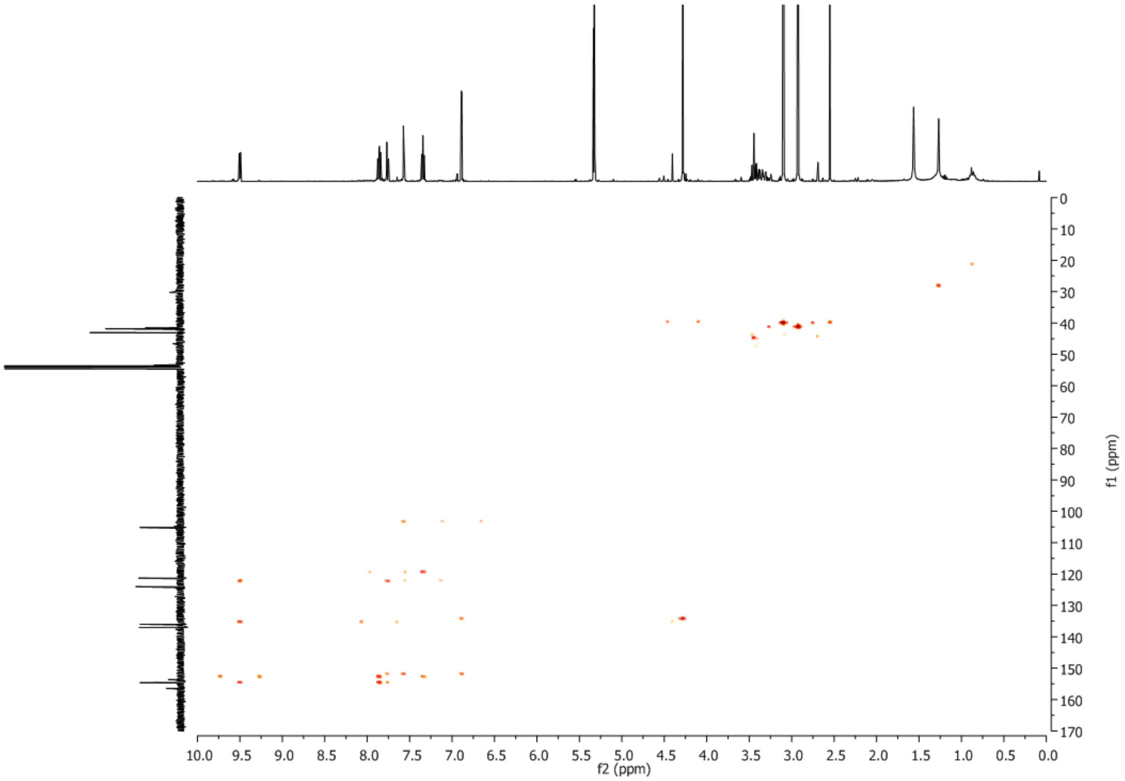

Figure S6.9. NMR spectra of **C6**, 400 MHz, CD_2Cl_2: a) ^{1}H-NMR; b) ^{13}C-NMR; c) COSY; d) NOESY; e) ^{1}H-^{13}C HSQC, f) ^{1}H-^{13}C HMBC.

a)

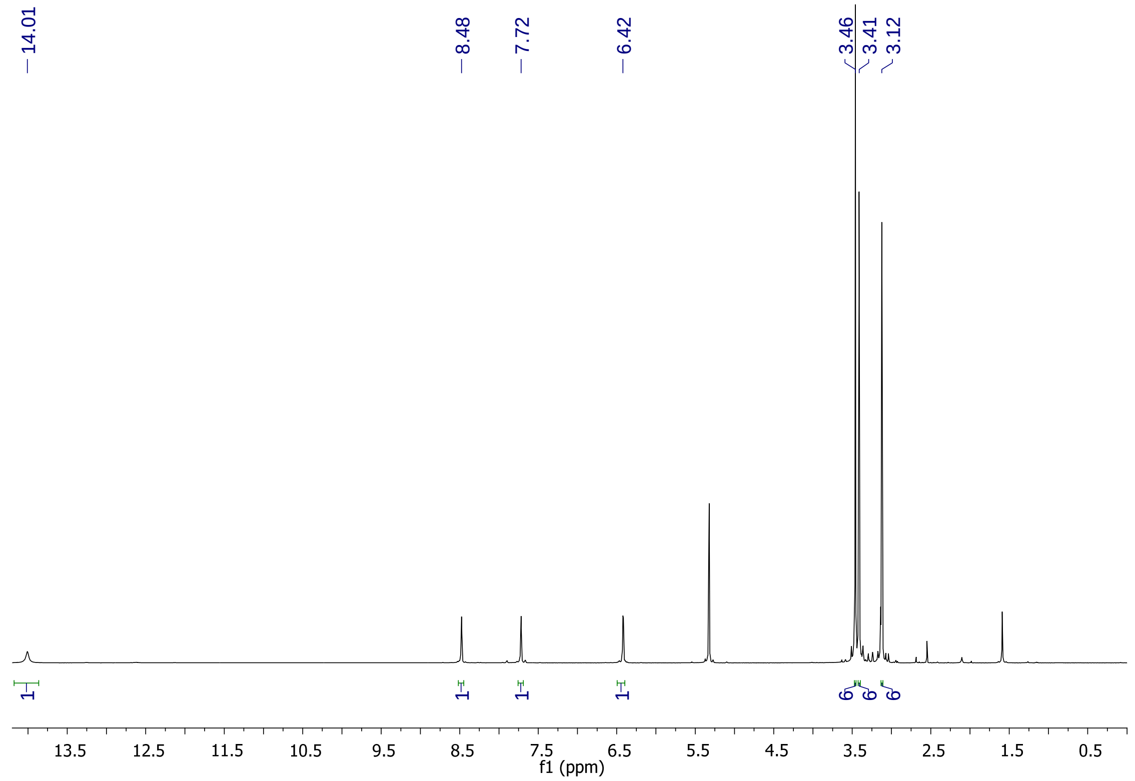
14.01
8.48
7.72
6.42
3.46
3.41
3.12
1
1
1
1
6
6
6
13.5
12.5
11.5
10.5
9.5
8.5
7.5
6.5
5.5
4.5
3.5
2.5
1.5
0.5
f1 (ppm)

b)

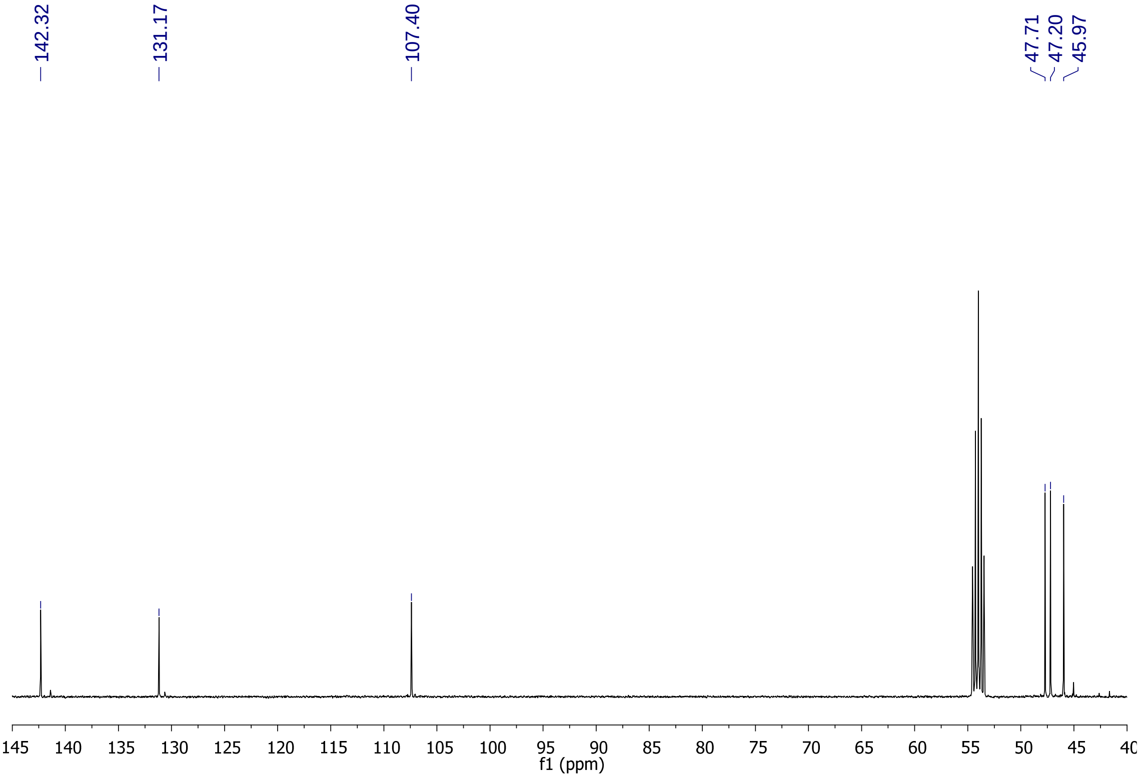
142.32
131.17
107.40
47.71
47.20
45.97
145
140
135
130
125
120
115
110
105
100
95
90
85
80
75
70
65
60
55
50
45
40
f1 (ppm)

c)

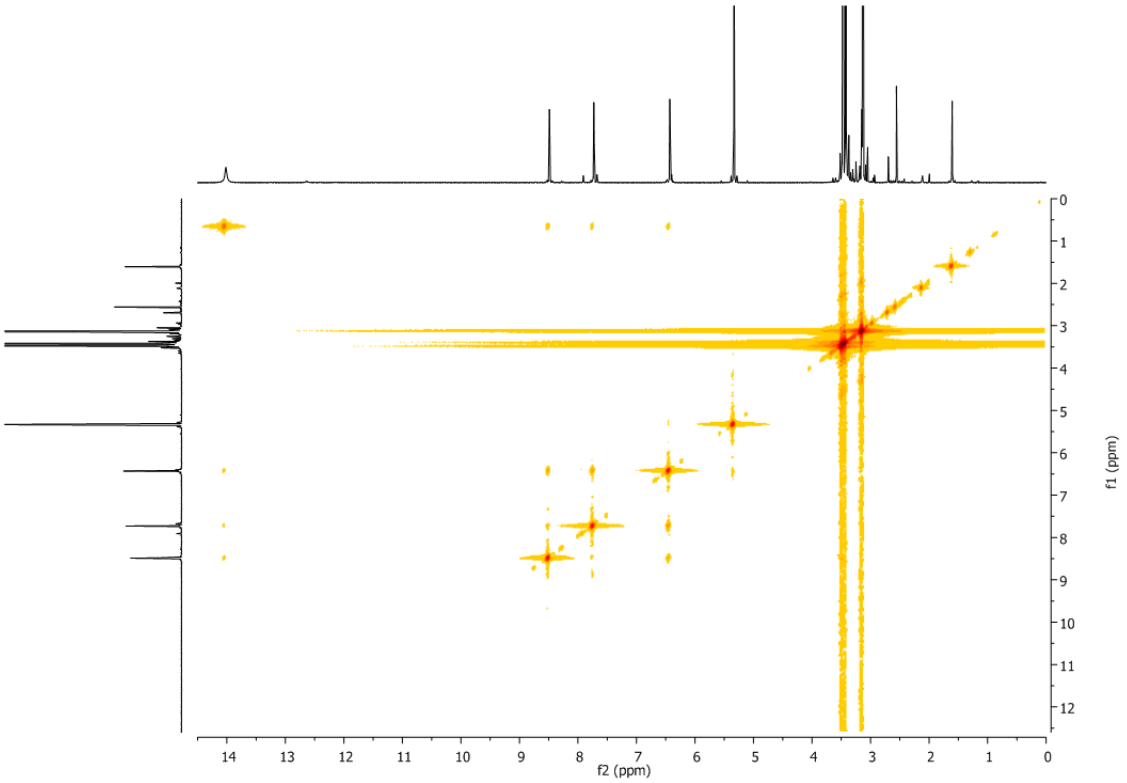
14
13
12
11
10
9
8
7
6
5
4
3
2
1
0
f2 (ppm)
0
1
2
3
4
5
6
7
8
9
10
11
12
f1 (ppm)

d)

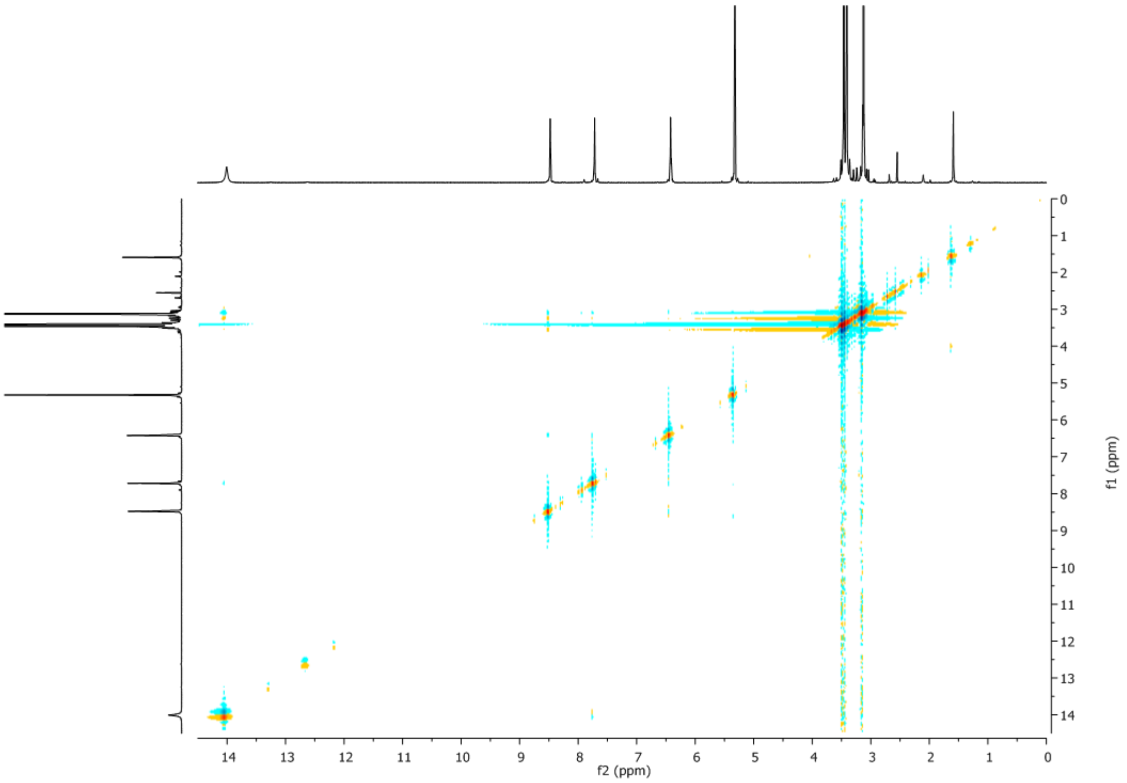
14
13
12
11
10
9
8
7
6
5
4
3
2
1
0
f2 (ppm)
0
1
2
3
4
5
6
7
8
9
10
11
12
13
14
f1 (ppm)

e)

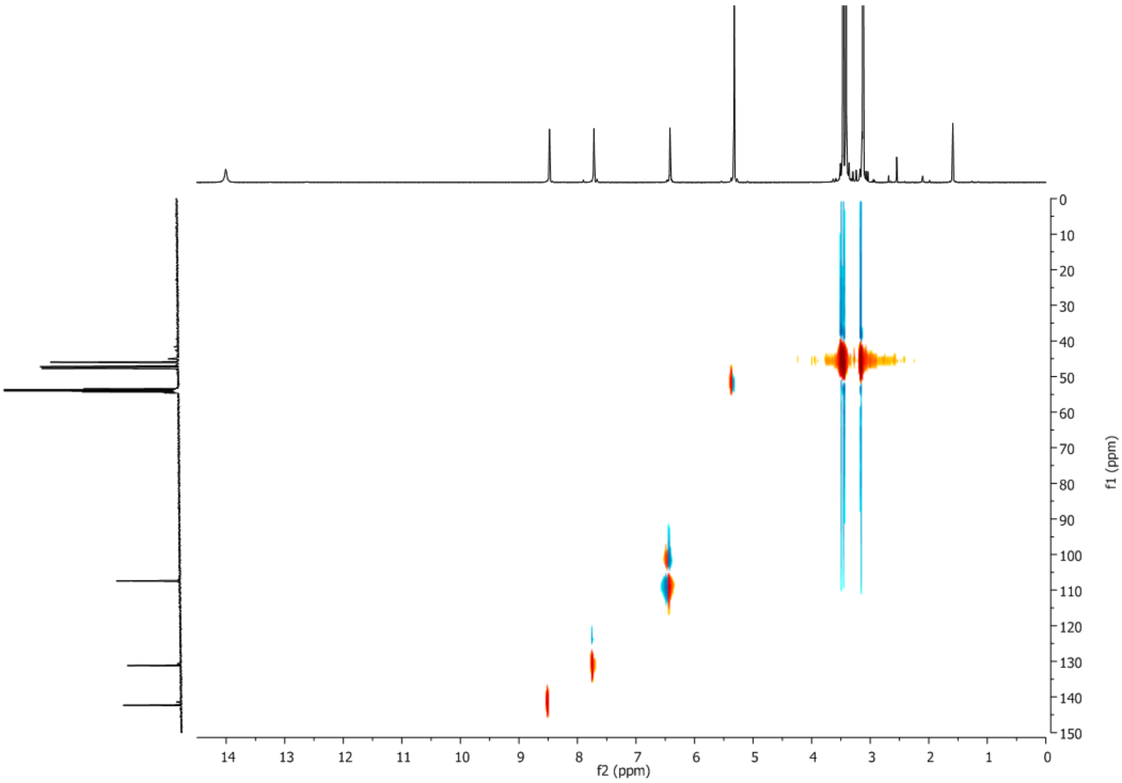

f)

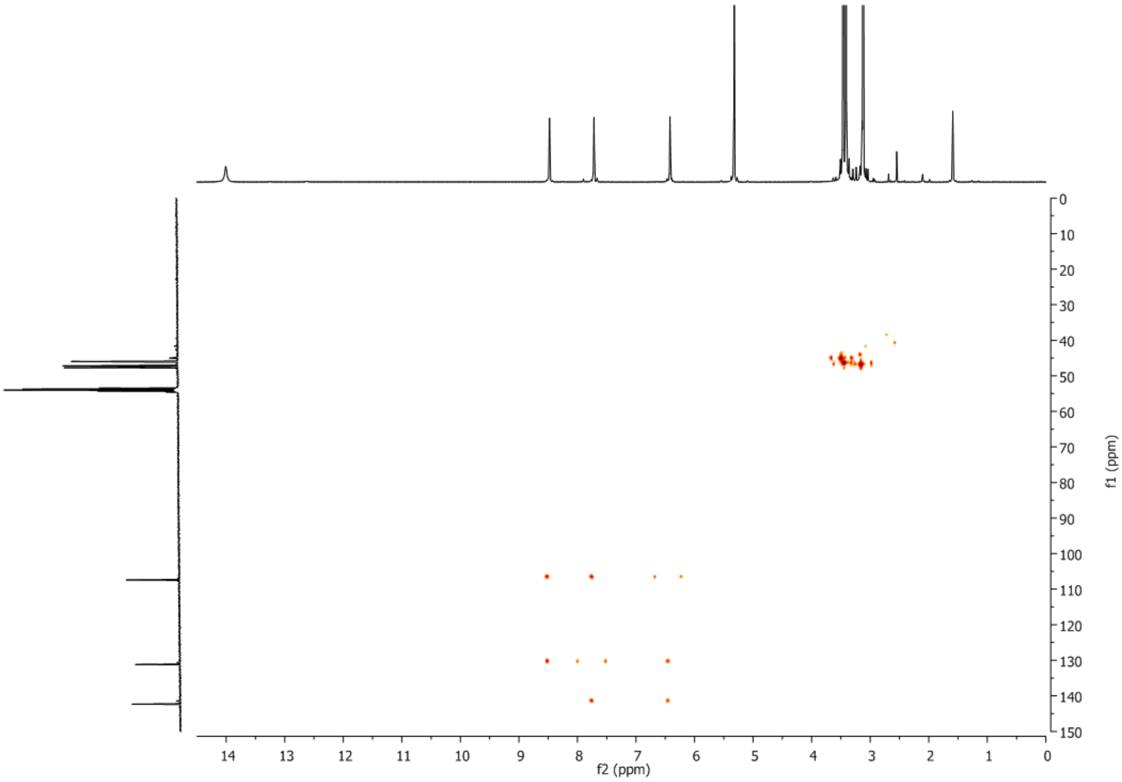

Figure S6.10. NMR spectra of **C7**, 400 MHz, CD_2Cl_2: a) ^{1}H-NMR; b) ^{13}C-NMR; c) COSY; d) NOESY; e) ^{1}H-^{13}C HSQC, f) ^{1}H-^{13}C HMBC.

a)

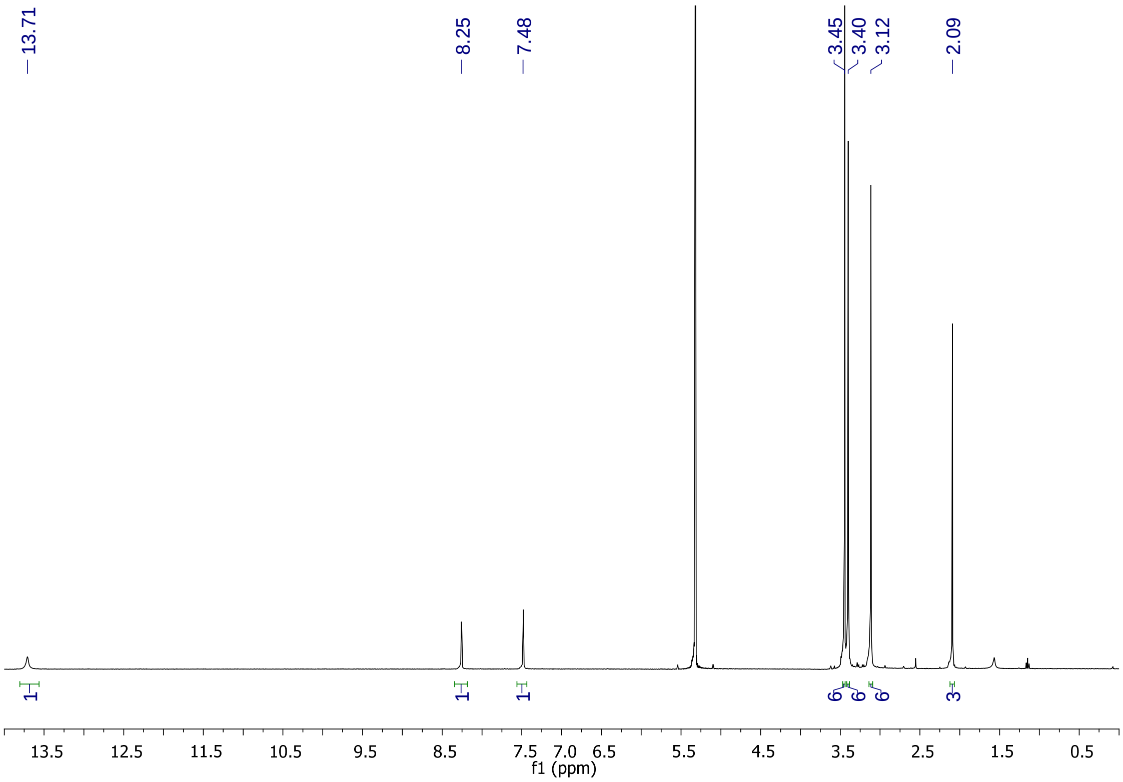
13.71
8.25
7.48
3.45
3.40
3.12
2.09
1
1
1
6
6
6
3
13.5
12.5
11.5
10.5
9.5
8.5
7.5
7.0
6.5
5.5
4.5
3.5
2.5
1.5
0.5
f1 (ppm)

b)

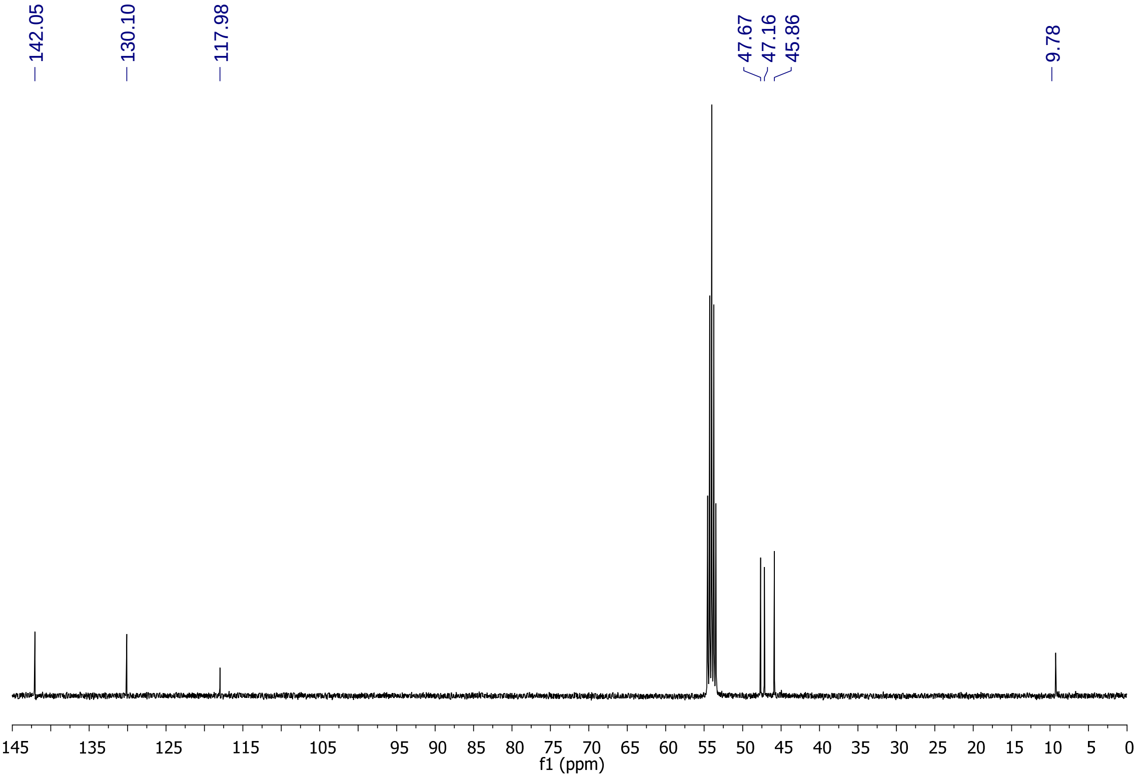
142.05
130.10
117.98
47.67
47.16
45.86
9.78
145
135
125
115
105
95
90
85
80
75
70
65
60
55
50
45
40
35
30
25
20
15
10
5
0
f1 (ppm)

c)

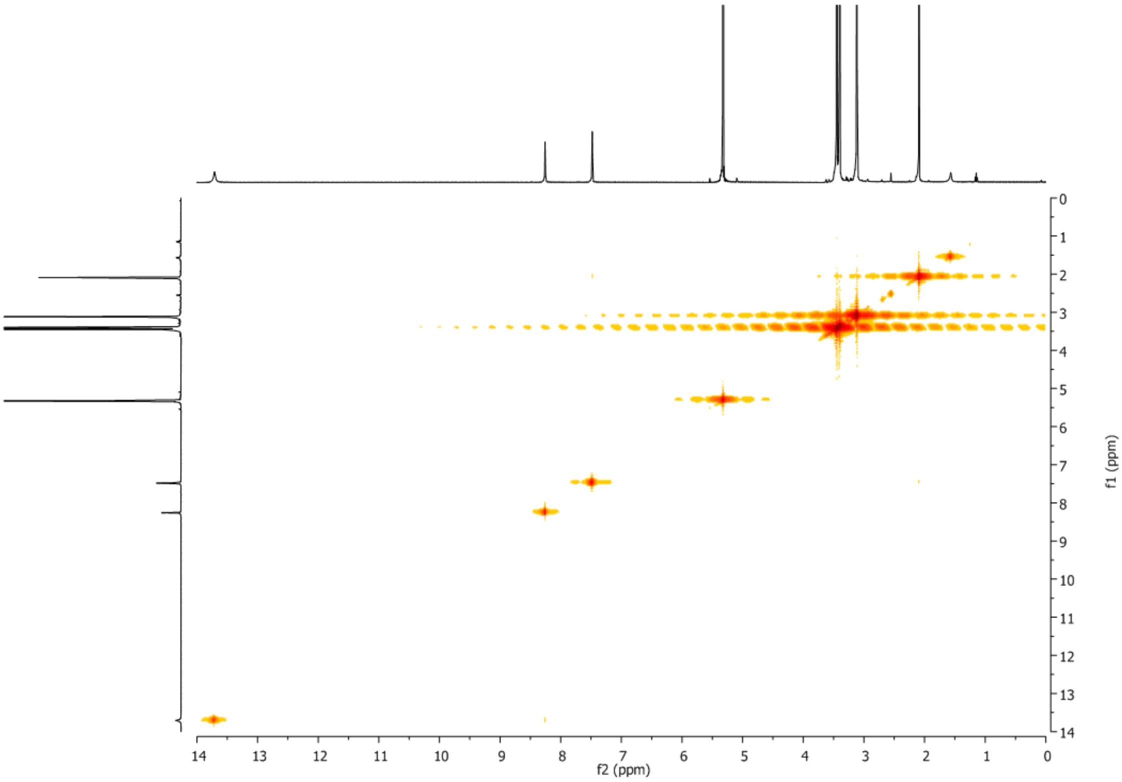
f2 (ppm)
f1 (ppm)
14
13
12
11
10
9
8
7
6
5
4
3
2
1
0

d)

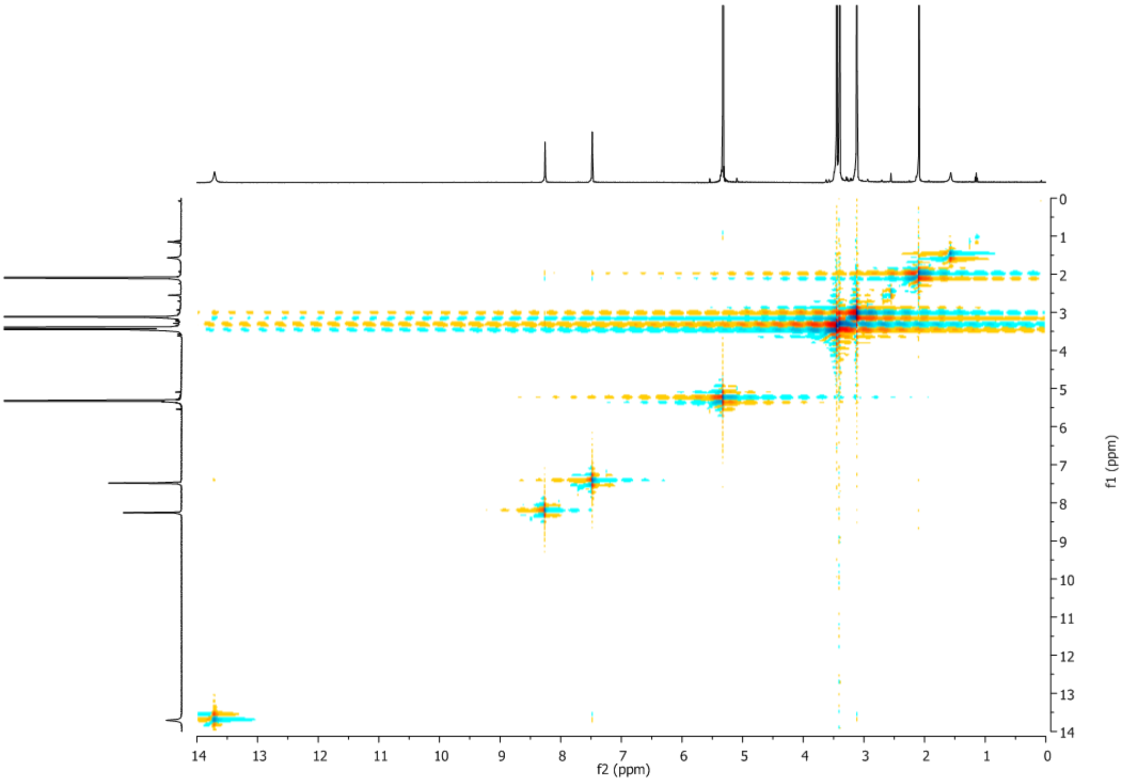
f2 (ppm)
f1 (ppm)
14
13
12
11
10
9
8
7
6
5
4
3
2
1
0

e)

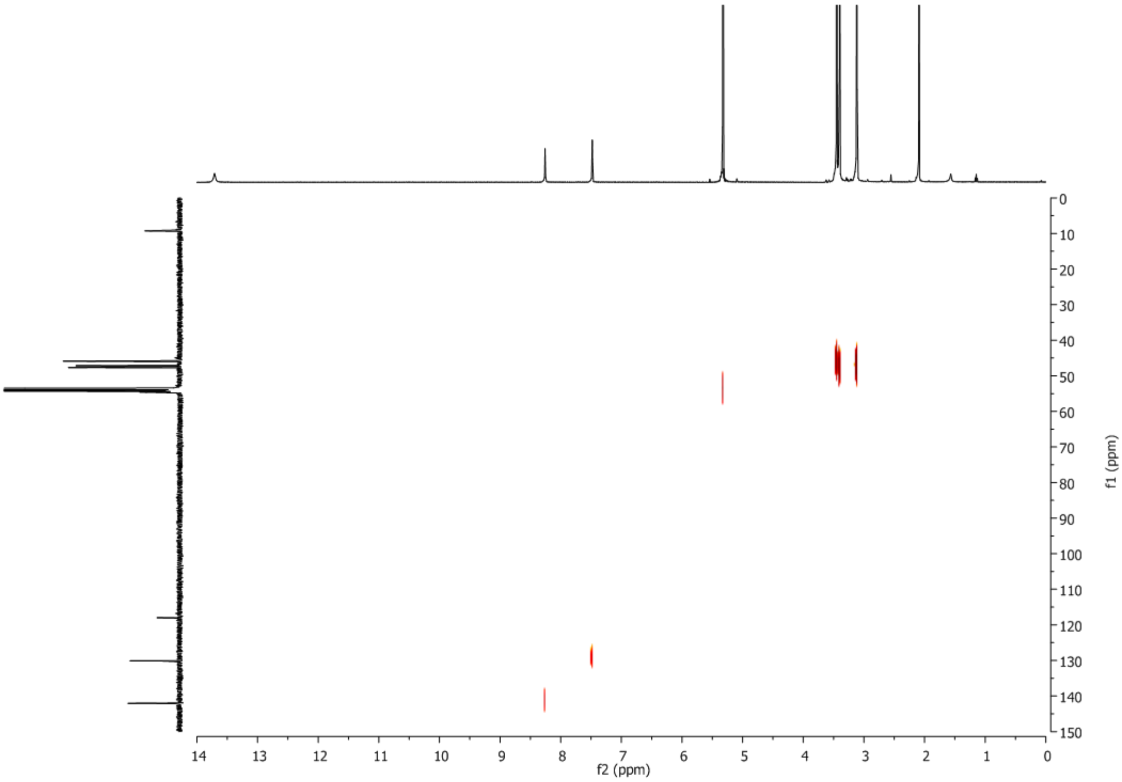

f)

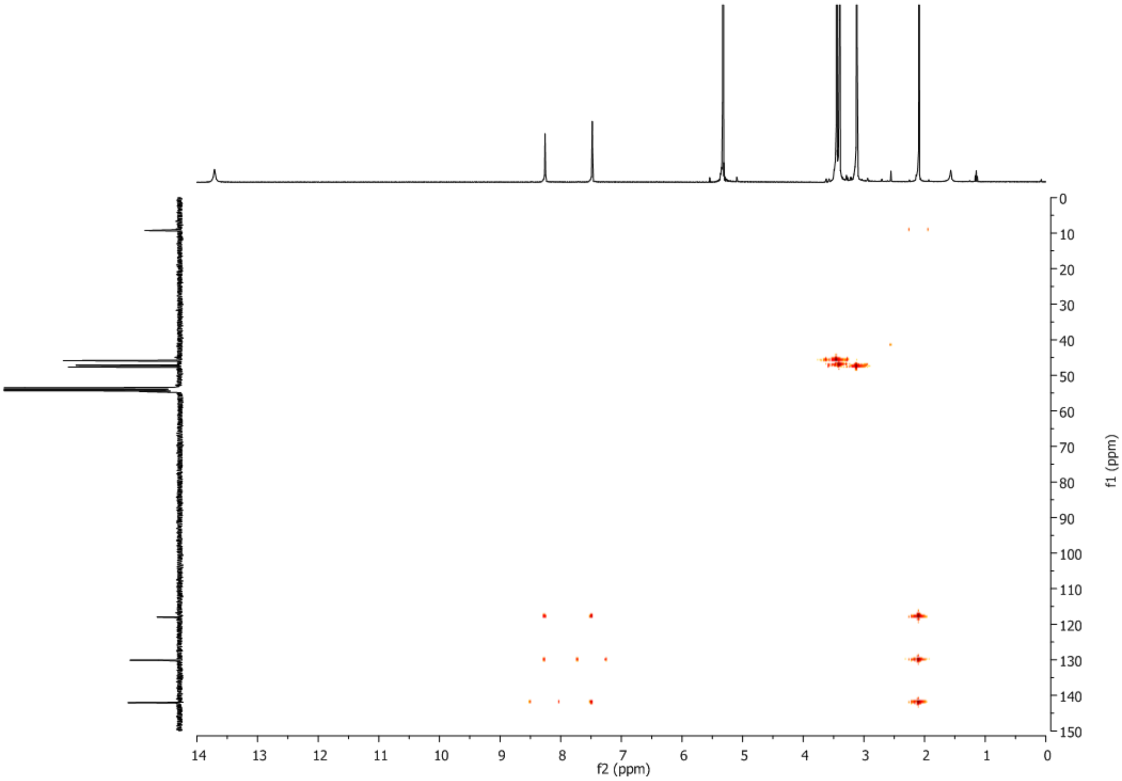

Figure S6.11. NMR spectra of **C8**, 400 MHz, CD_2Cl_2: a) ^{1}H-NMR; b) ^{13}C-NMR; c) COSY; d) NOESY; e) ^{1}H-^{13}C HSQC, f) ^{1}H-^{13}C HMBC.

a)

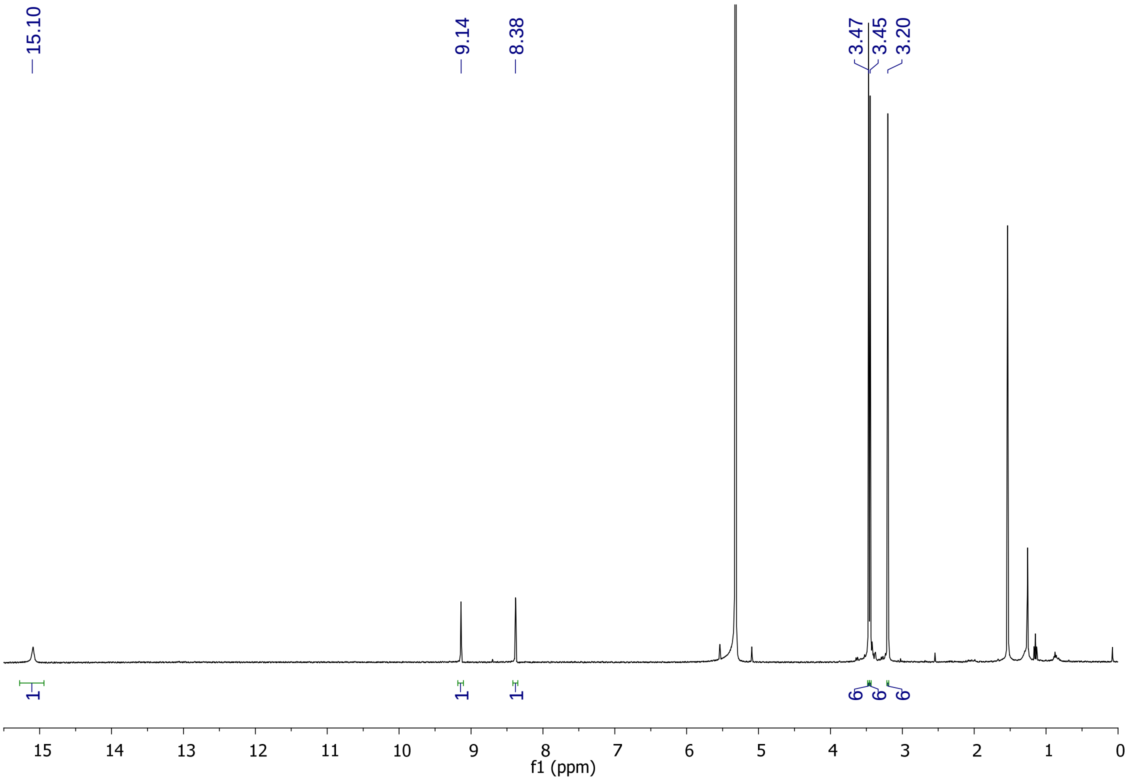
15.10
9.14
8.38
3.47
3.45
3.20
1
1
1
6
6
6
15
14
13
12
11
10
9
8
7
6
5
4
3
2
1
0
f1 (ppm)

b)

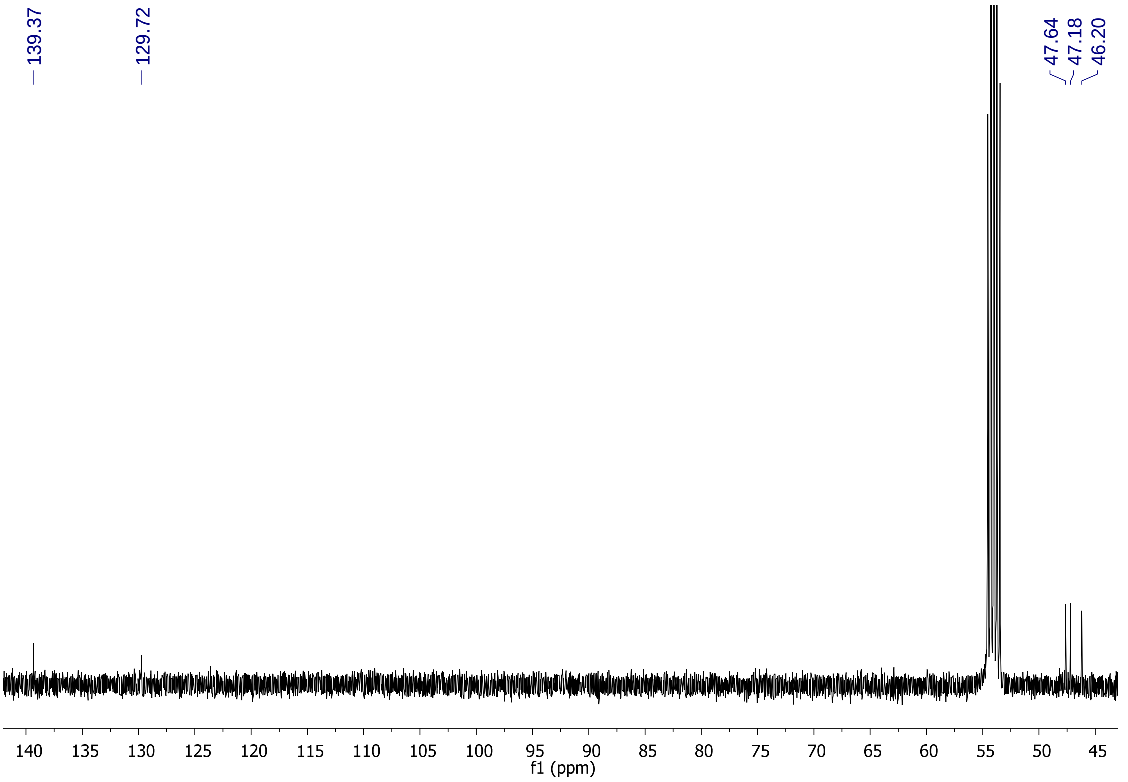
139.37
129.72
47.64
47.18
46.20
140
135
130
125
120
115
110
105
100
95
90
85
80
75
70
65
60
55
50
45
f1 (ppm)

c)

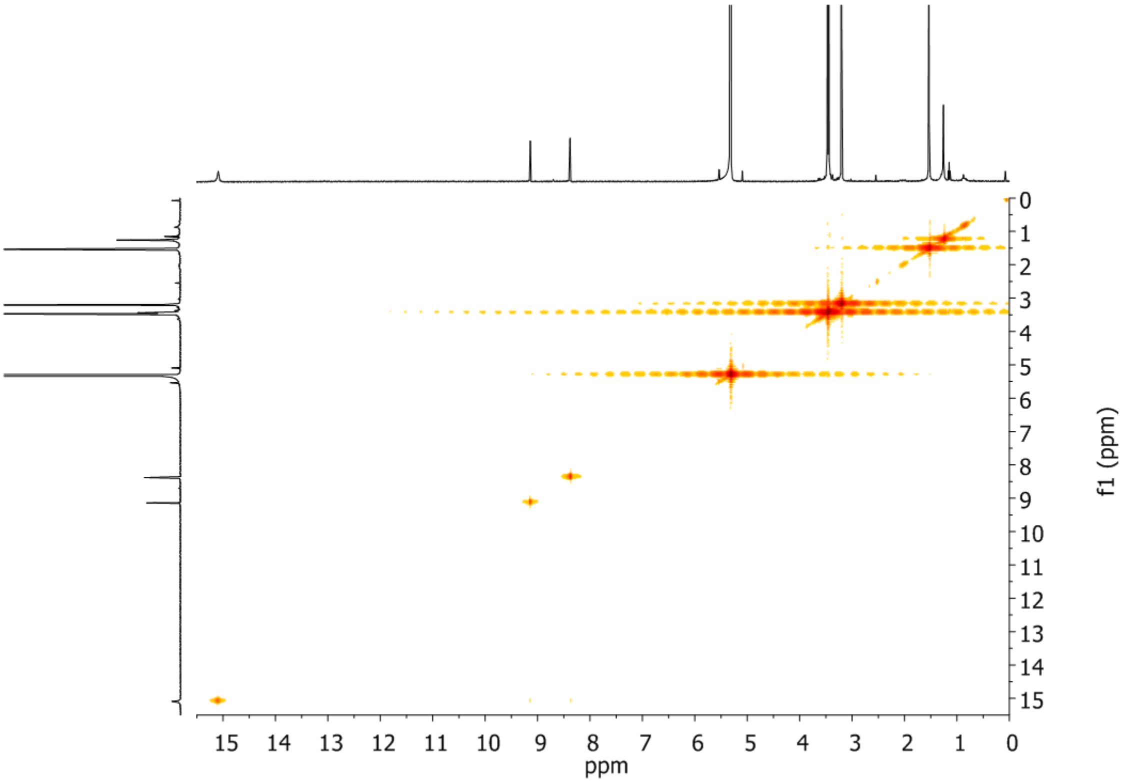
0
1
2
3
4
5
6
7
8
9
10
11
12
13
14
15
f1 (ppm)
15 14 13 12 11 10 9 8 7 6 5 4 3 2 1 0
ppm

d)

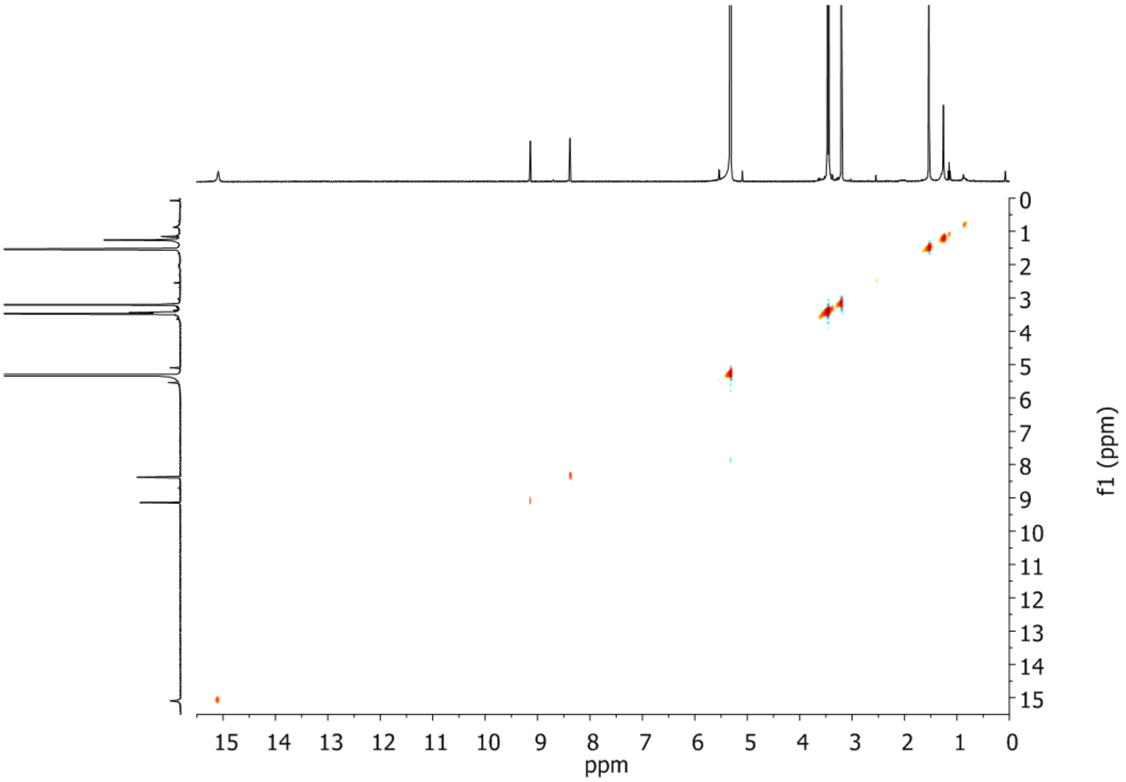
0
1
2
3
4
5
6
7
8
9
10
11
12
13
14
15
f1 (ppm)
15 14 13 12 11 10 9 8 7 6 5 4 3 2 1 0
ppm

e)

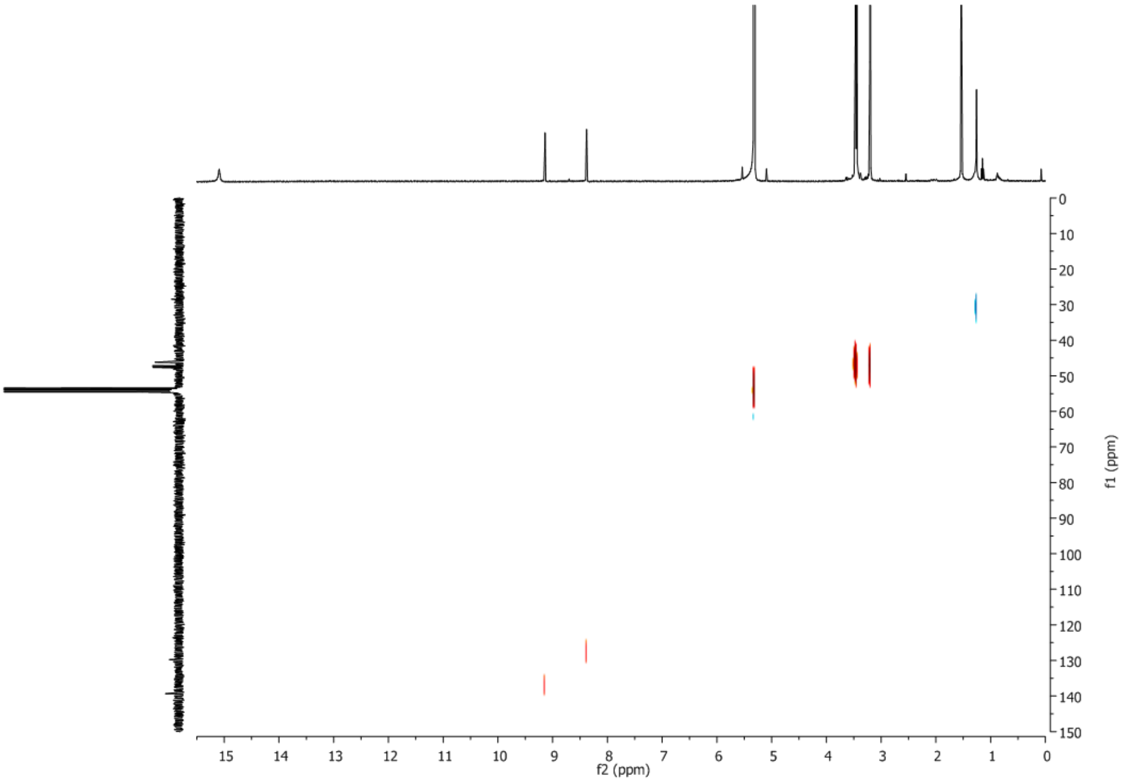

f)

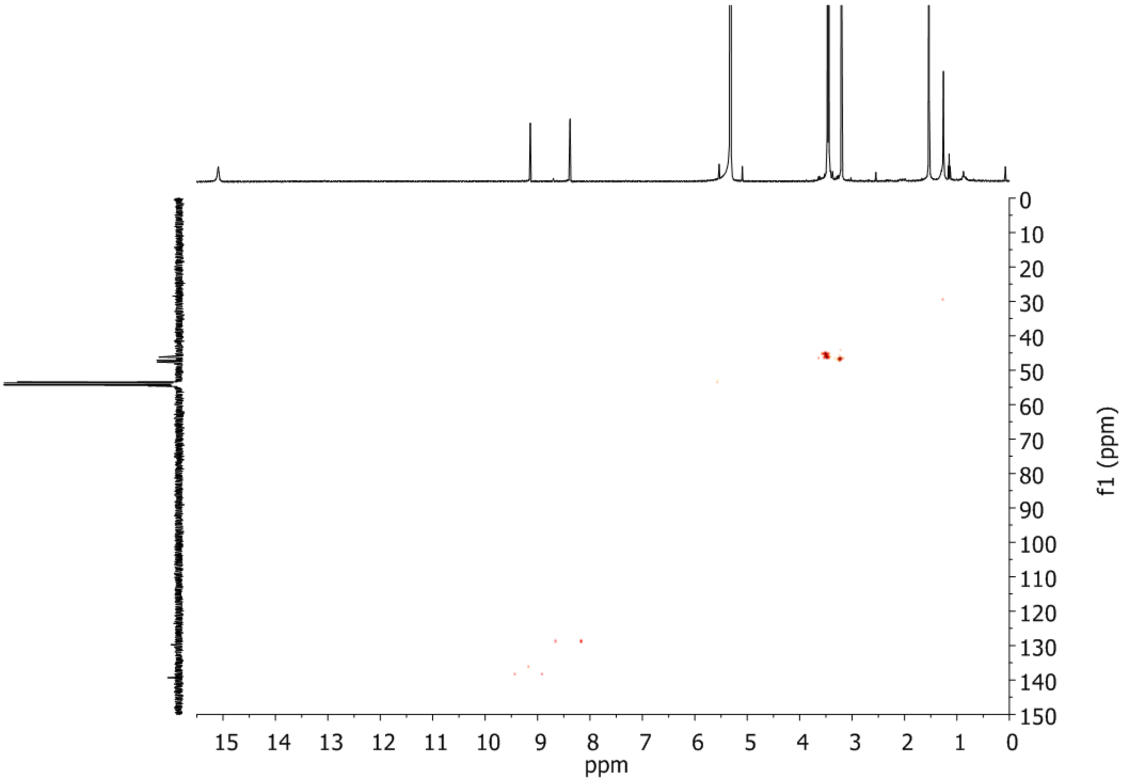

Figure S6.12. NMR spectra of **C9**, 400 MHz, CD_2Cl_2: a) ^{1}H-NMR; b) ^{13}C-NMR; c) COSY; d) NOESY; e) ^{1}H-^{13}C HSQC, f) ^{1}H-^{13}C HMBC.

a)

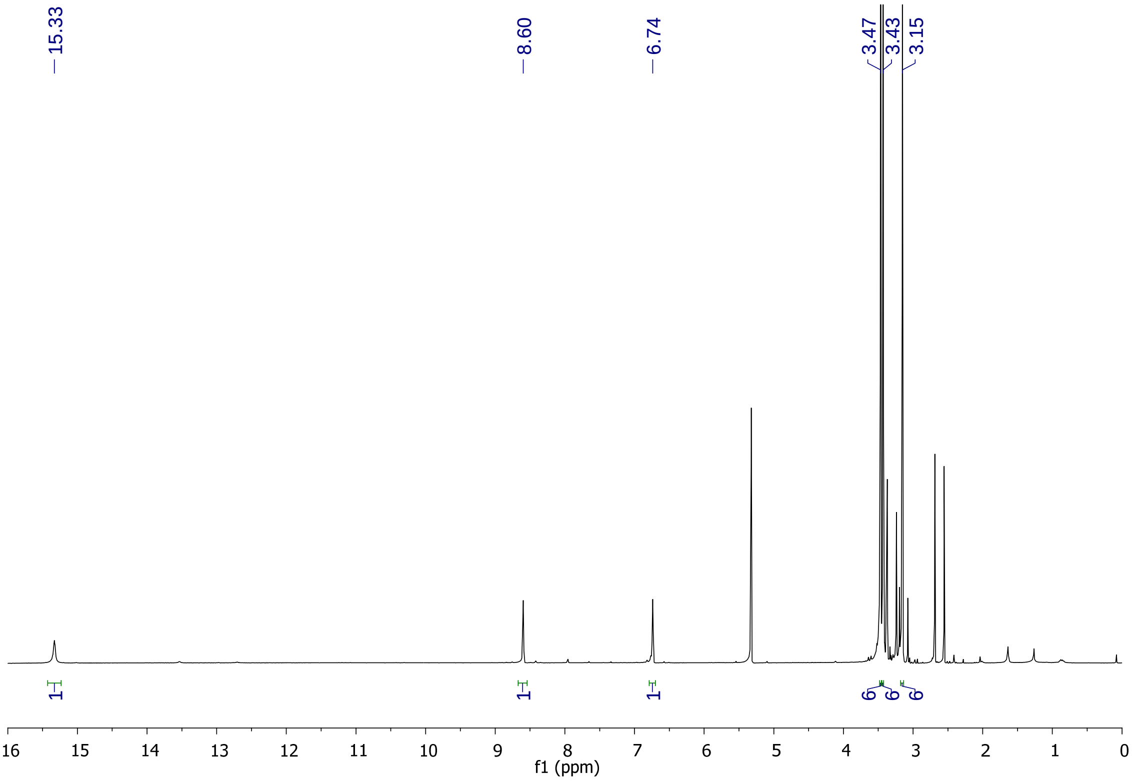
15.33
8.60
6.74
3.47
3.43
3.15
1
1
1
6
6
6
16
15
14
13
12
11
10
9
8
7
6
5
4
3
2
1
0
f1 (ppm)

b)

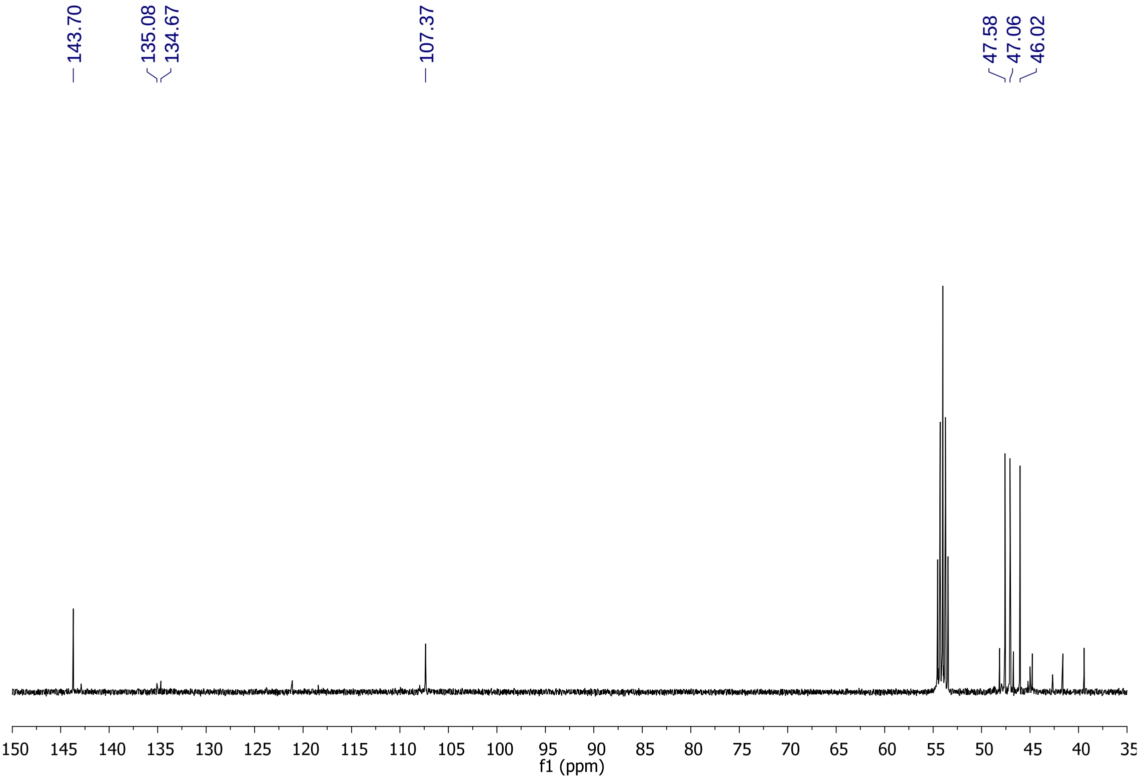
143.70
135.08
134.67
107.37
47.58
47.06
46.02
150
145
140
135
130
125
120
115
110
105
100
95
90
85
80
75
70
65
60
55
50
45
40
35
f1 (ppm)

c)

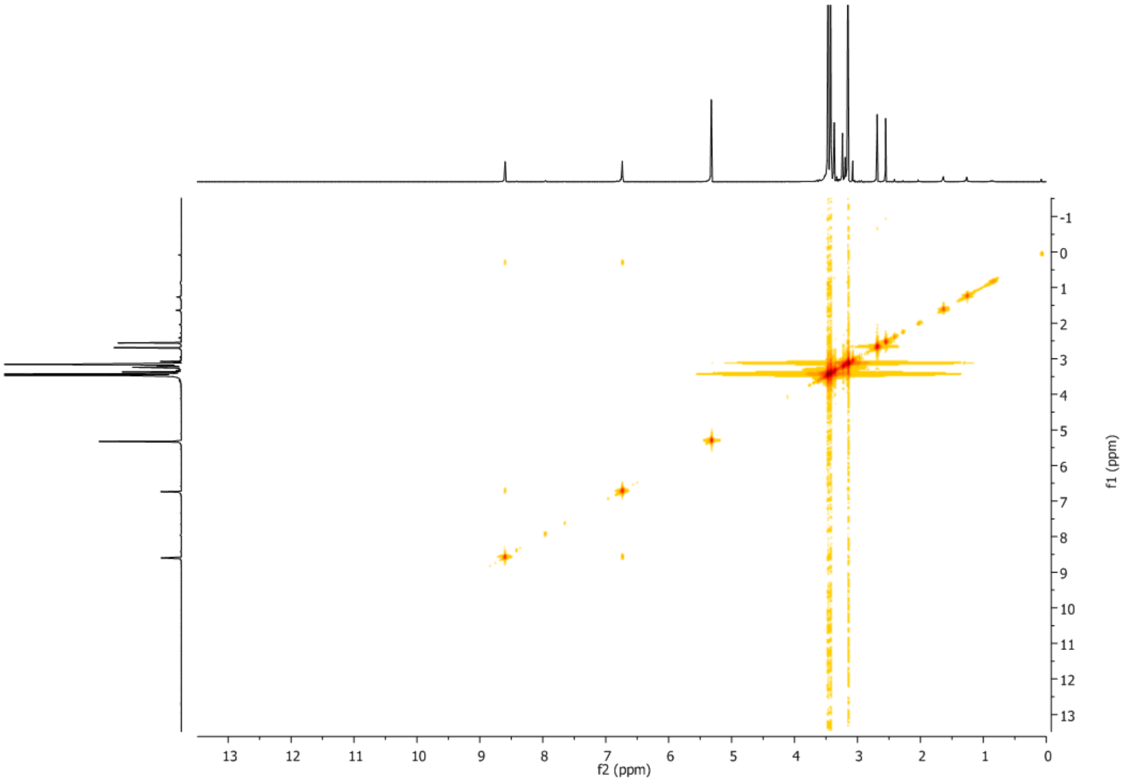
f2 (ppm)
f1 (ppm)
13
12
11
10
9
8
7
6
5
4
3
2
1
0
-1

d)

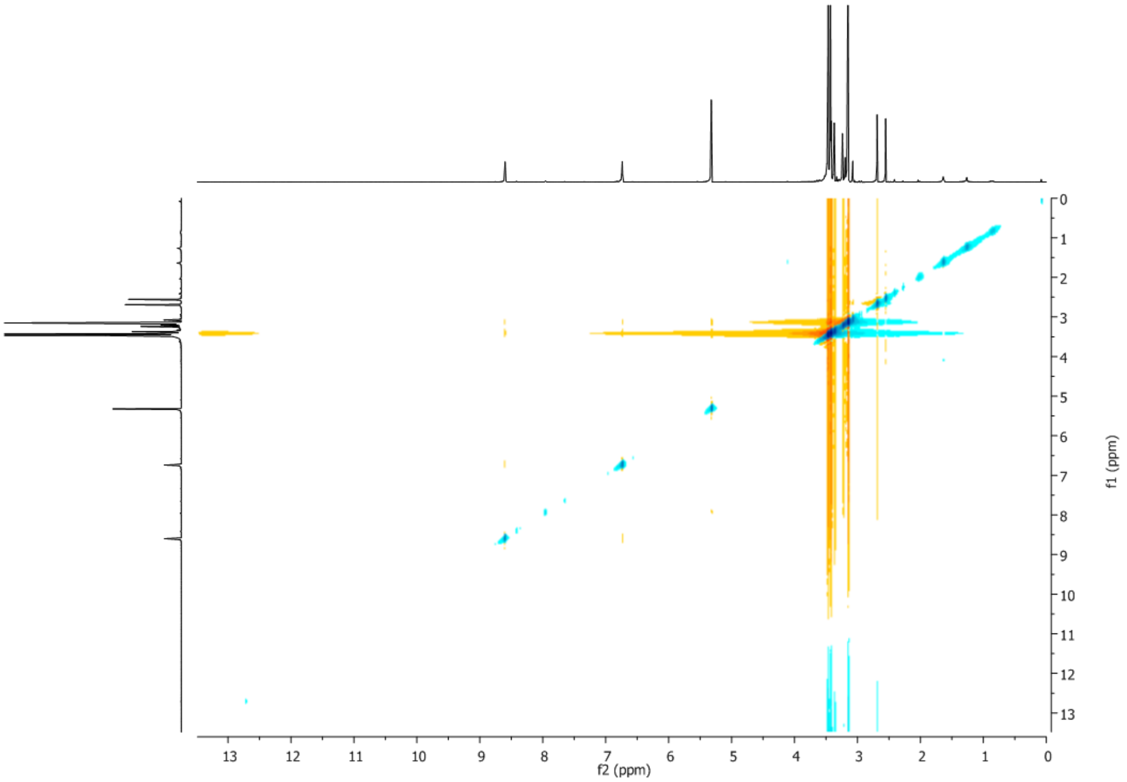
f2 (ppm)
f1 (ppm)
13
12
11
10
9
8
7
6
5
4
3
2
1
0

e)

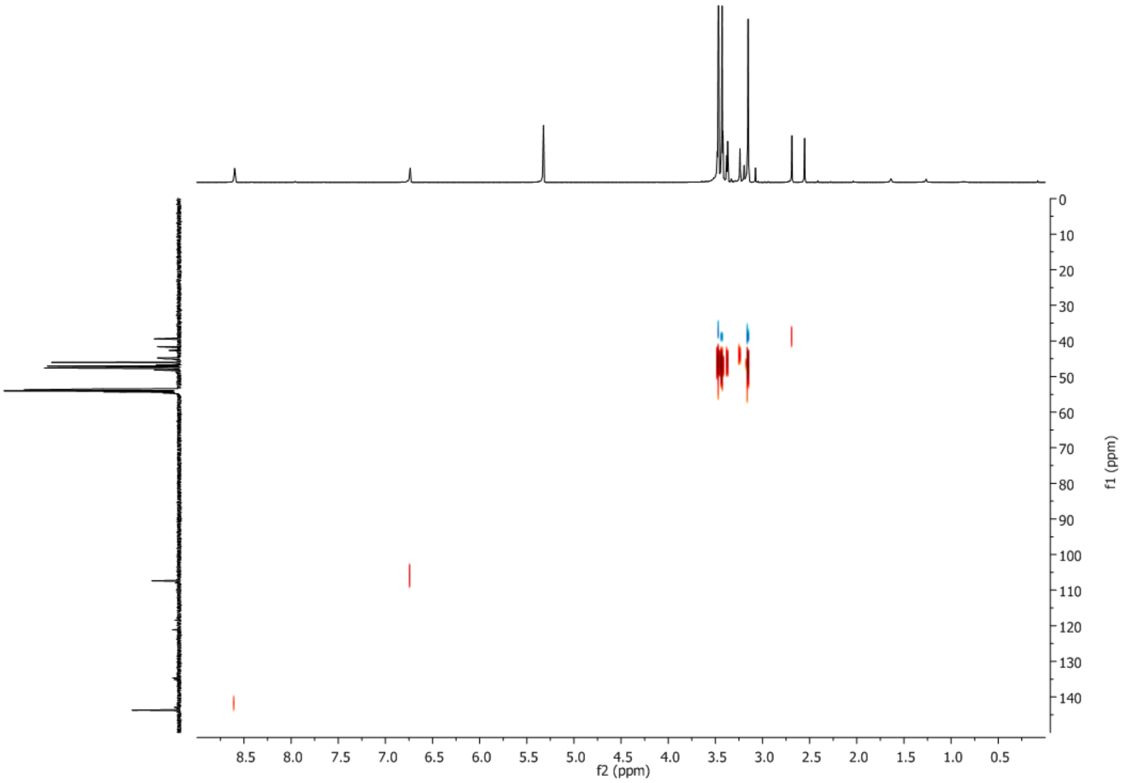

f)

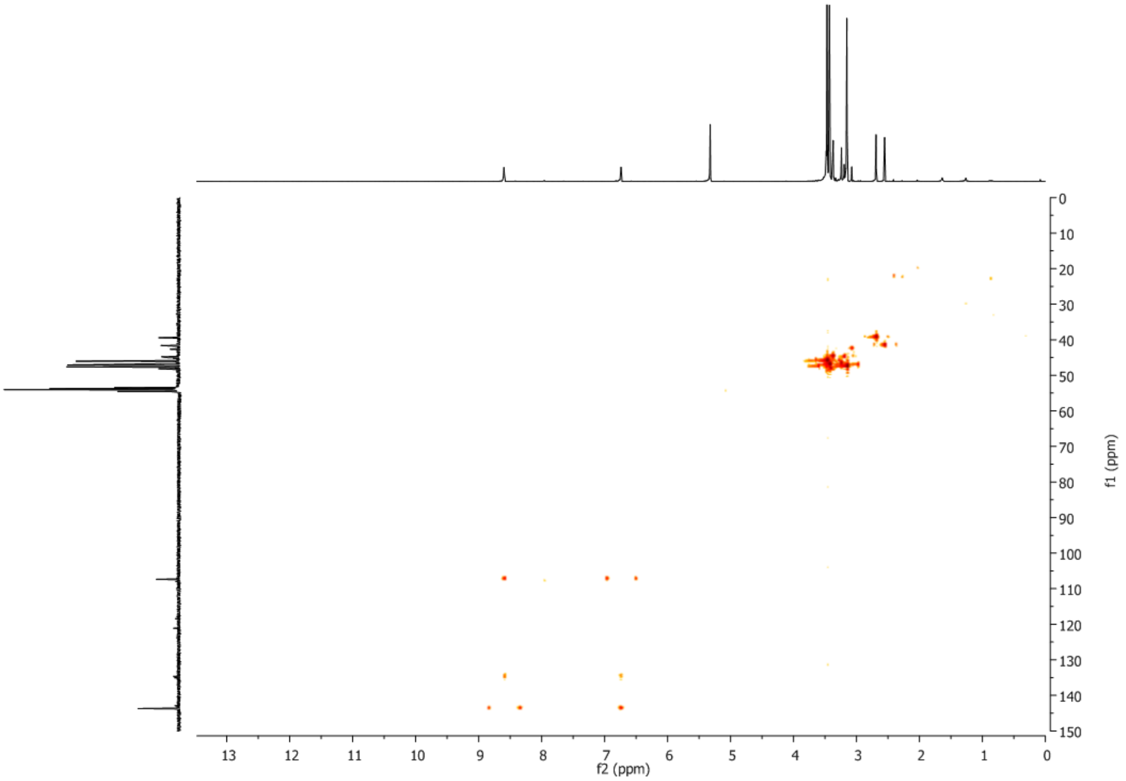

Figure S6.13. NMR spectra of **C10**, 400 MHz, CD_2Cl_2: a) ^{1}H-NMR; b) ^{13}C-NMR; c) COSY; d) NOESY; e) ^{1}H-^{13}C HSQC, f) ^{1}H-^{13}C HMBC.

a)

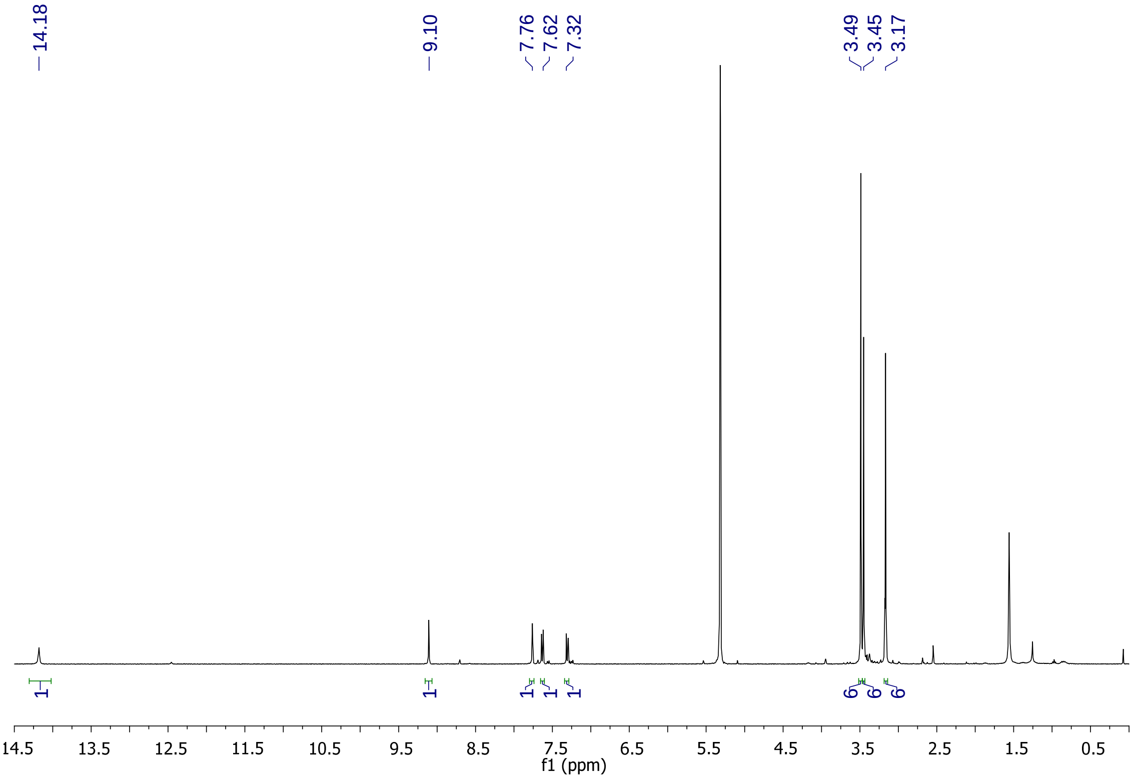
14.18
9.10
7.76
7.62
7.32
3.49
3.45
3.17
1
1
1
1
1
6
6
6
14.5
13.5
12.5
11.5
10.5
9.5
8.5
7.5
6.5
5.5
4.5
3.5
2.5
1.5
0.5
f1 (ppm)

b)

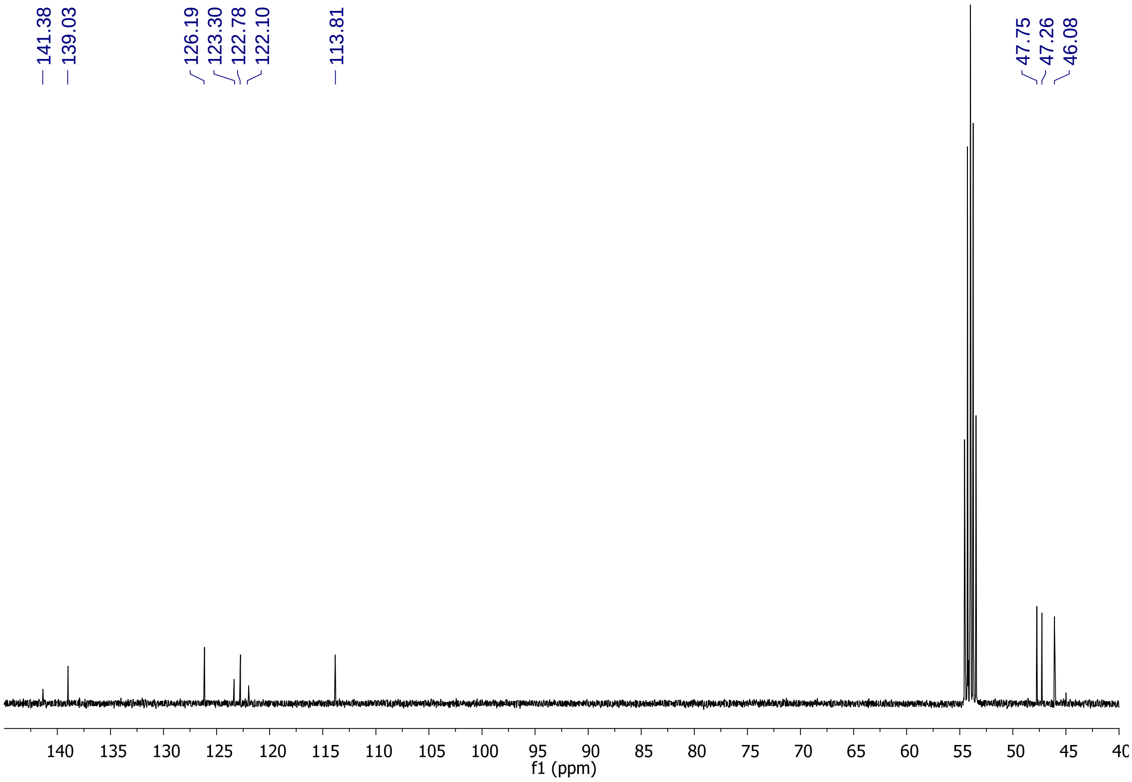
141.38
139.03
126.19
123.30
122.78
122.10
113.81
47.75
47.26
46.08
140
135
130
125
120
115
110
105
100
95
90
85
80
75
70
65
60
55
50
45
40
f1 (ppm)

c)

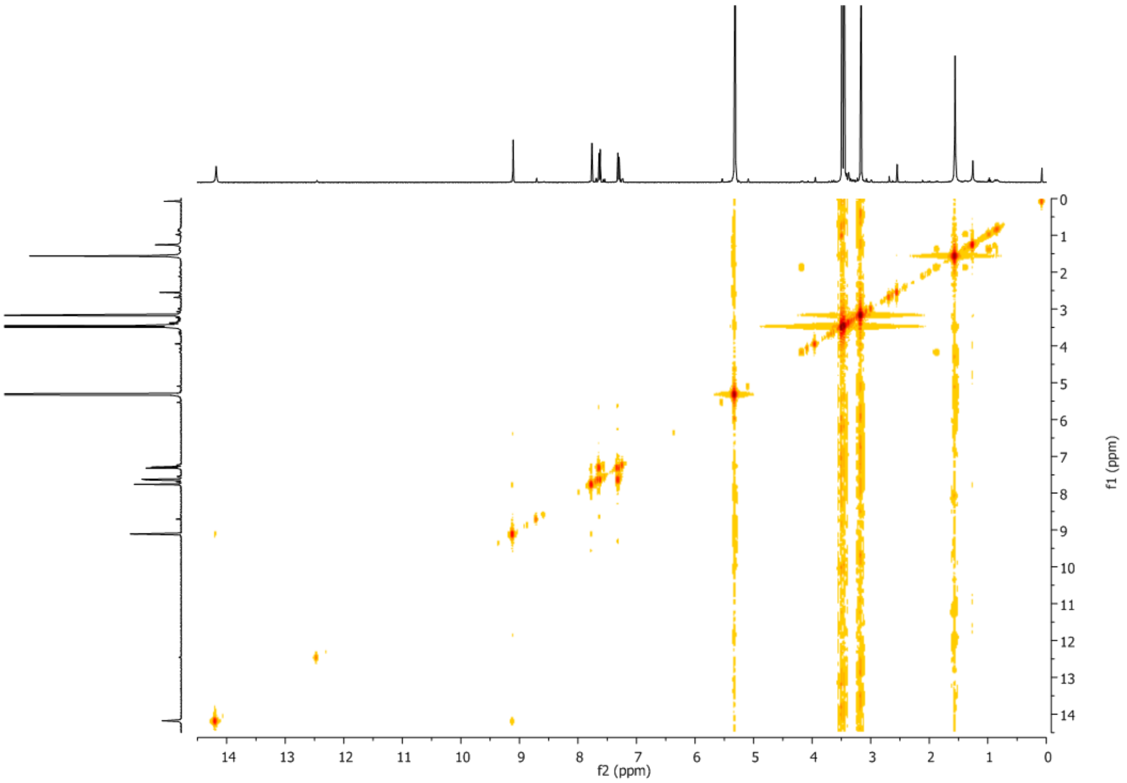
f2 (ppm)
f1 (ppm)
14
13
12
11
10
9
8
7
6
5
4
3
2
1
0

d)

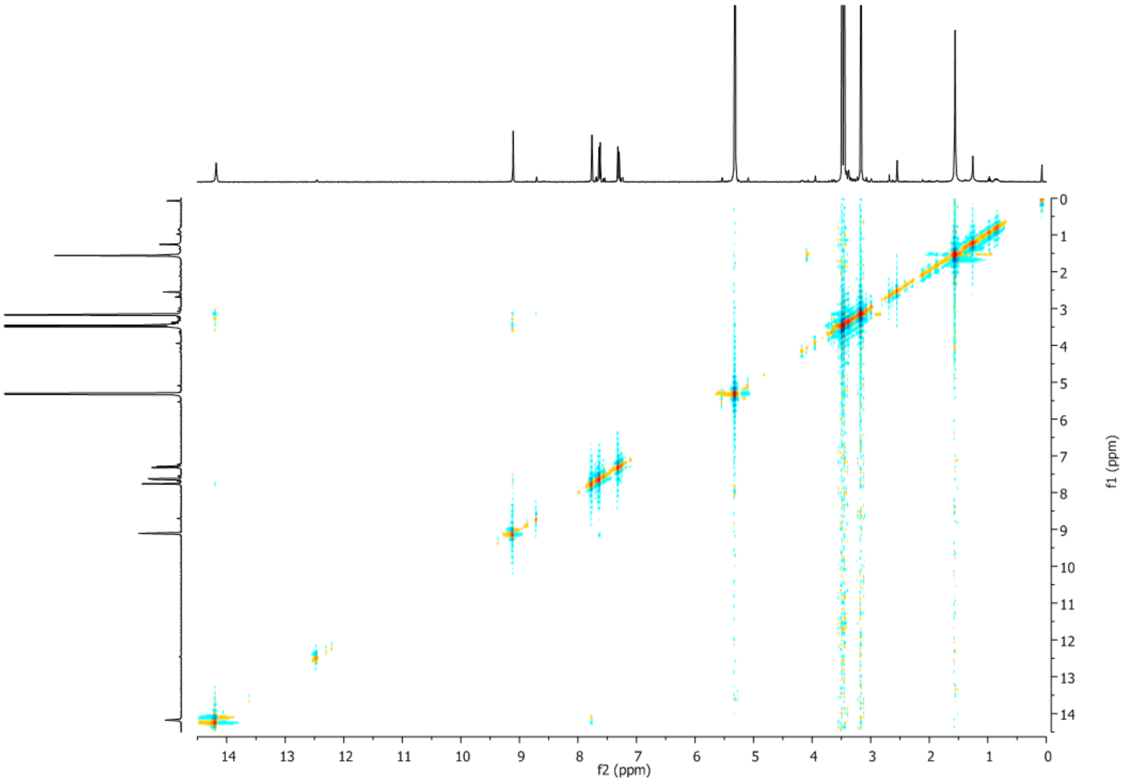
f2 (ppm)
f1 (ppm)
14
13
12
11
10
9
8
7
6
5
4
3
2
1
0

e)

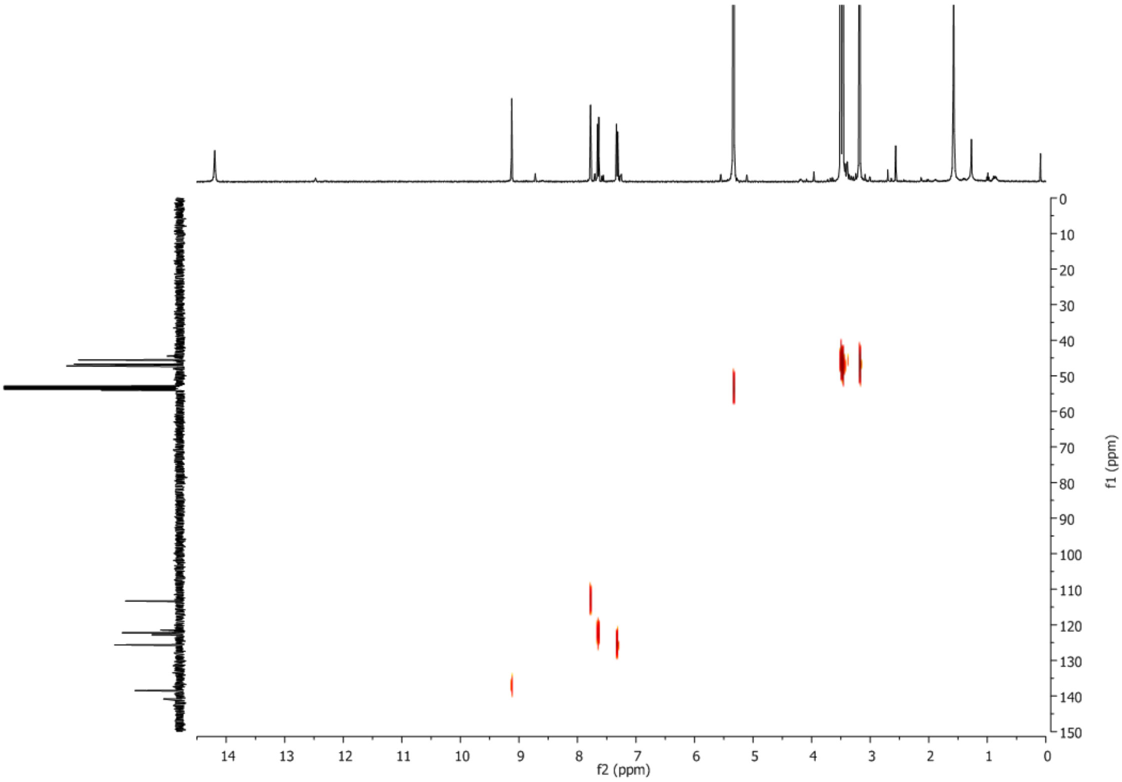

f)

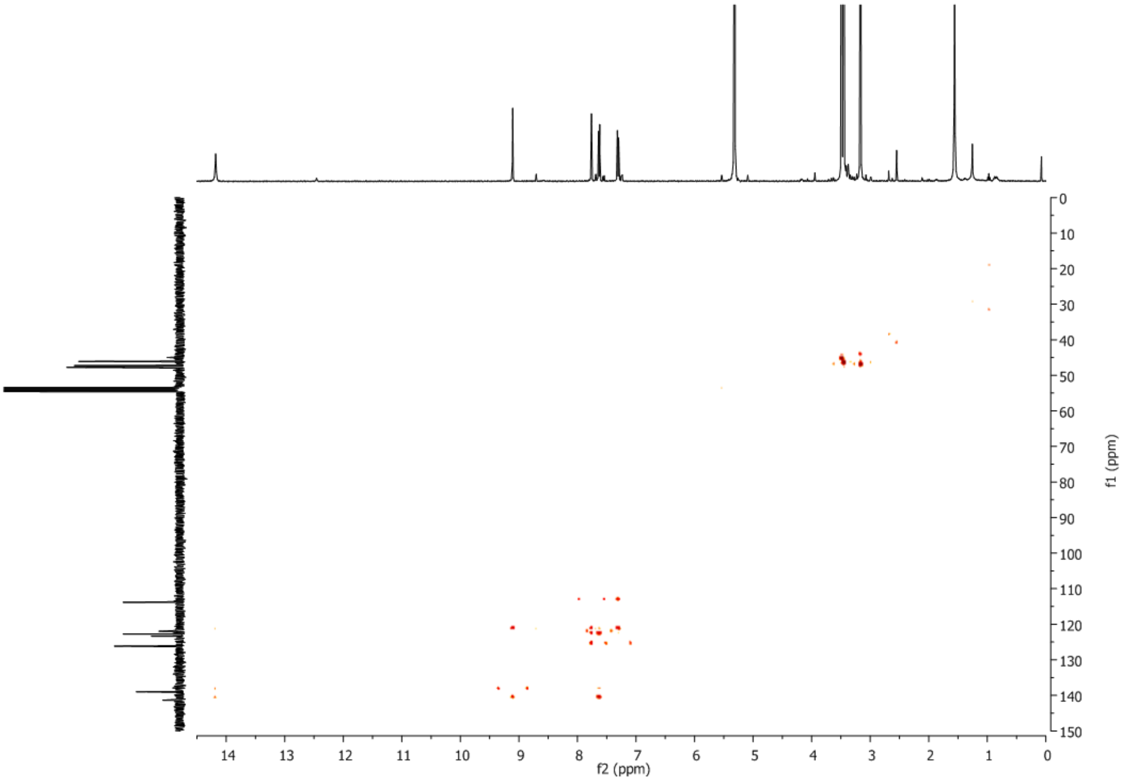

Figure S6.14. NMR spectra of **C11**, 400 MHz, CD_2Cl_2: a) ^{1}H-NMR; b) ^{13}C-NMR; c) COSY; d) NOESY; e) ^{1}H-^{13}C HSQC, f) ^{1}H-^{13}C HMBC.

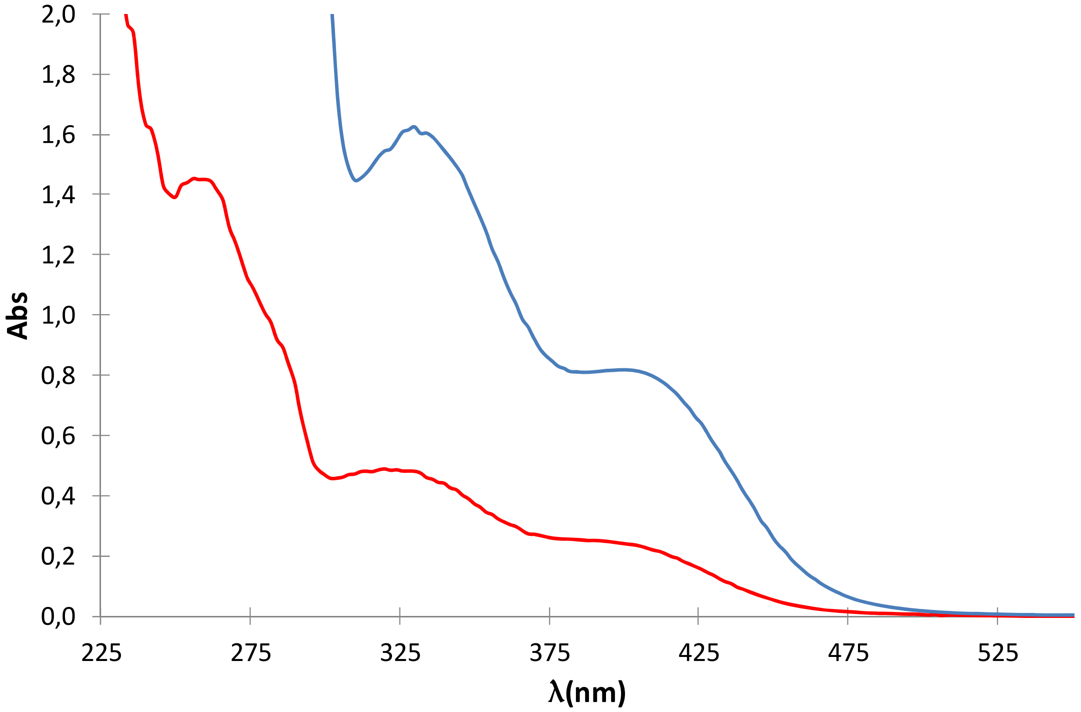

Figure S6.15. UV-visible spectra of 0.12 and 0.7 mM of **C5** in CH_2Cl_2 (red) and CH_3CN (blue), respectively.

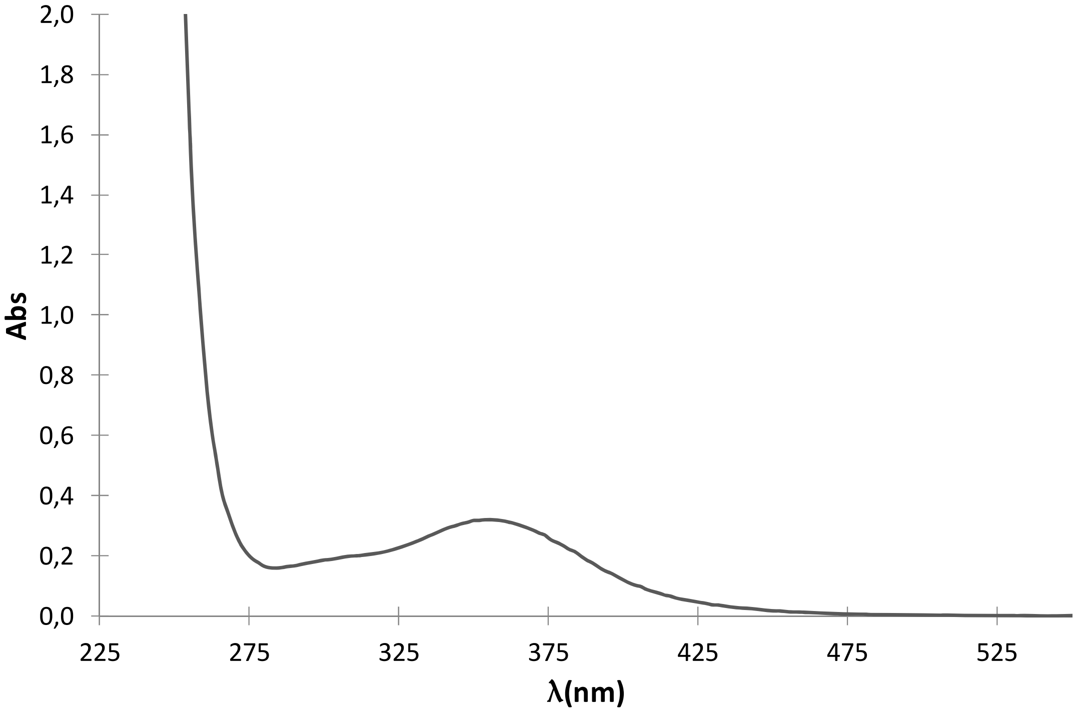

Figure S6.16. UV-visible spectrum of 0.7 mM **C7** in CH_3CN.

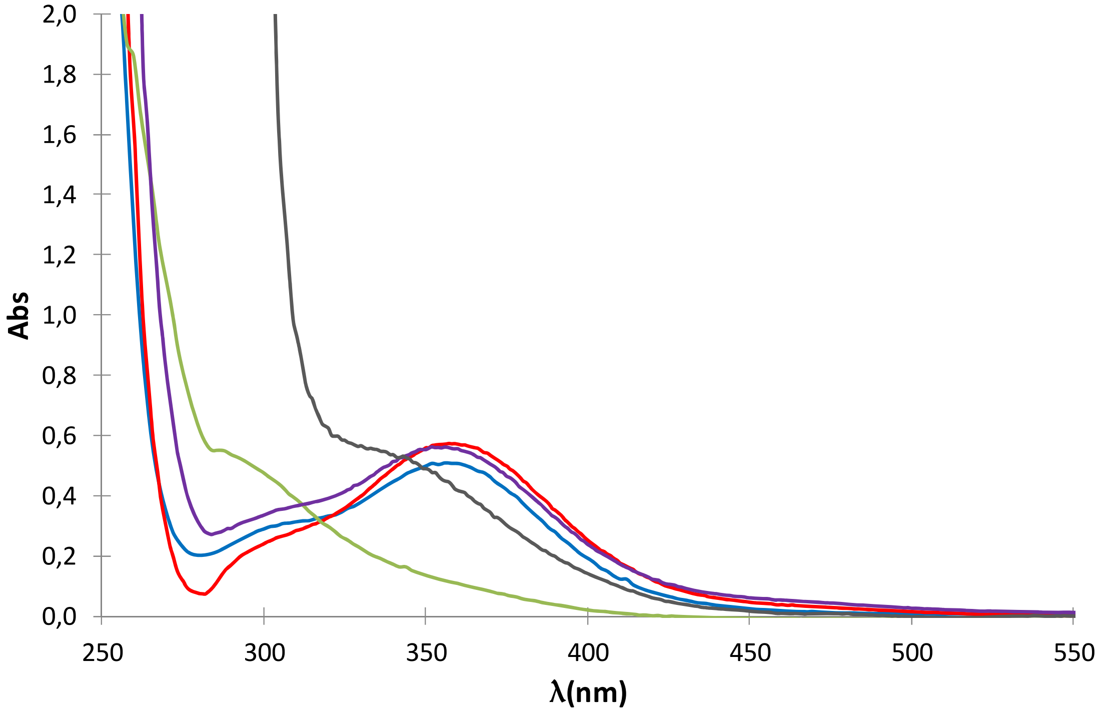

Figure S6.17. UV-visible spectra of 1.1 mM **C7** (blue), **C8** (red), **C9** (green), **C10** (purple) and **C11** (grey) in CH_2Cl_2.

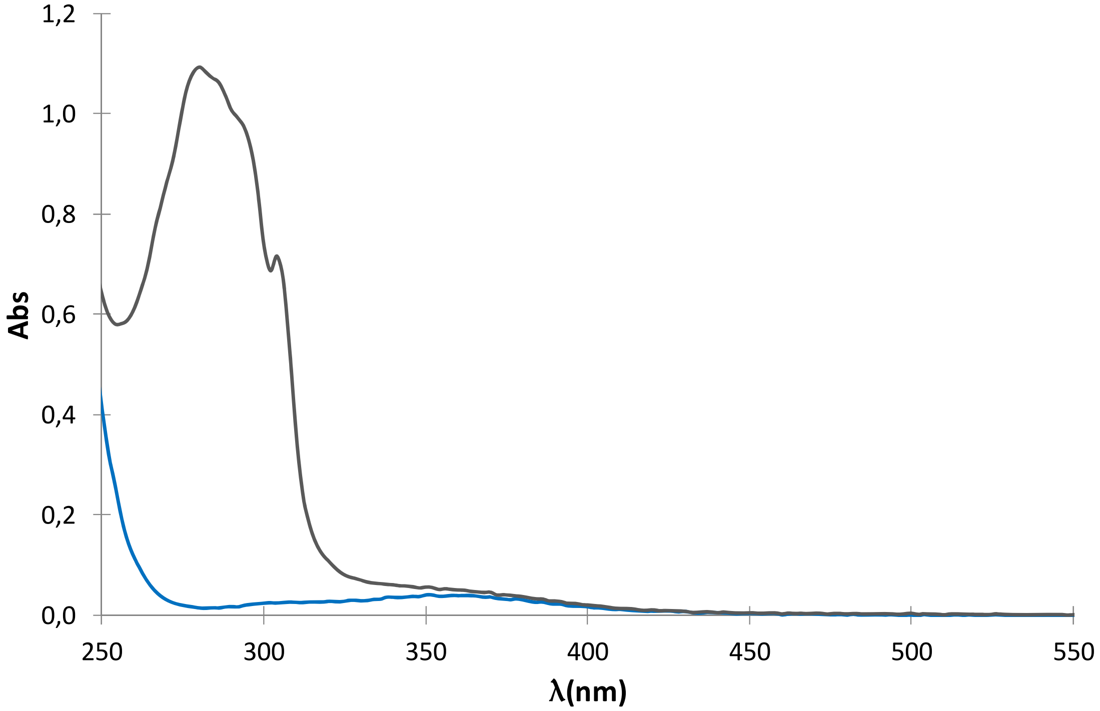

Figure S6.18. UV-visible spectra of 0.1 mM **C7** (blue) and **C11** (grey) in CH_2Cl_2.

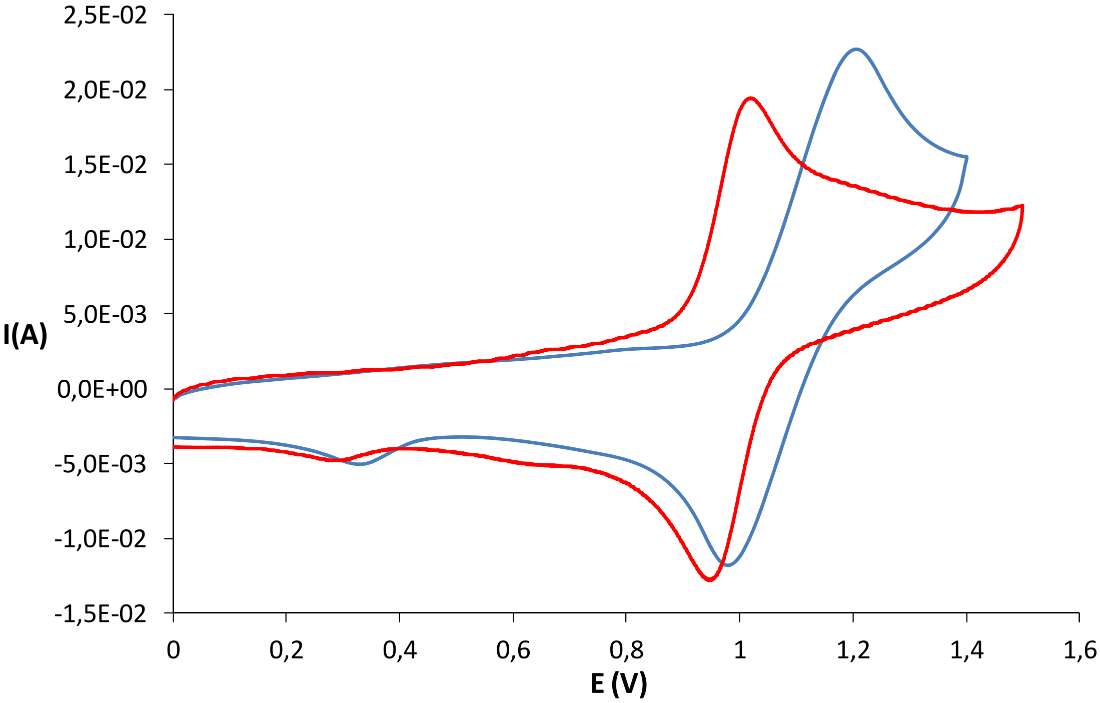

Figure S6.19. Cyclic voltammograms of **C5** in CH_2Cl_2 (blue) and CH_3CN (red).

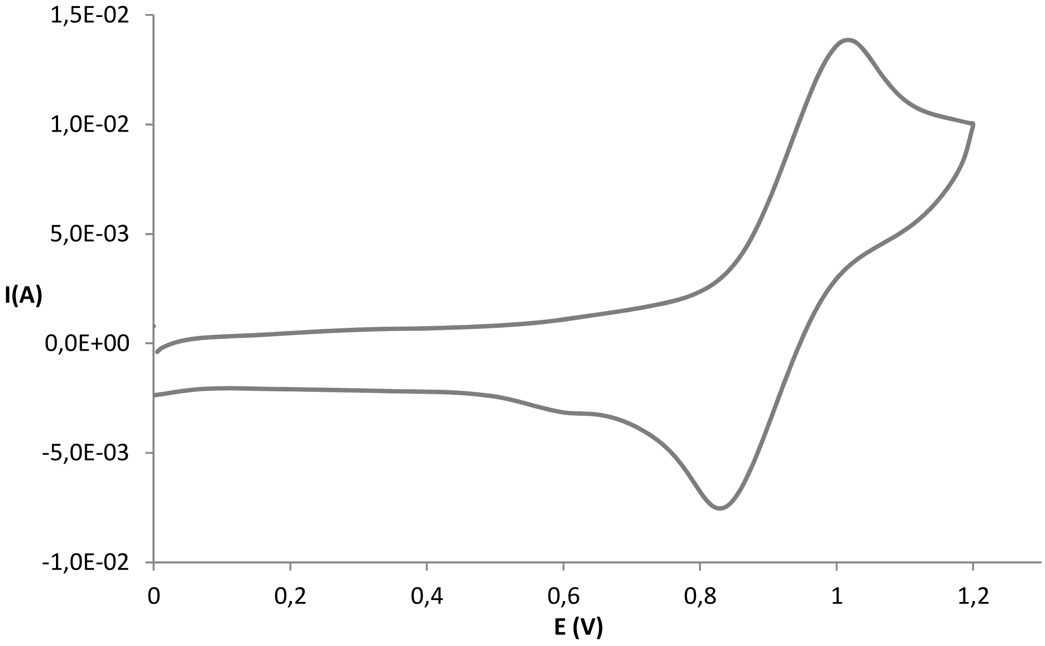

Figure S6.20. Cyclic voltammogram of **C6** in CH_2Cl_2.

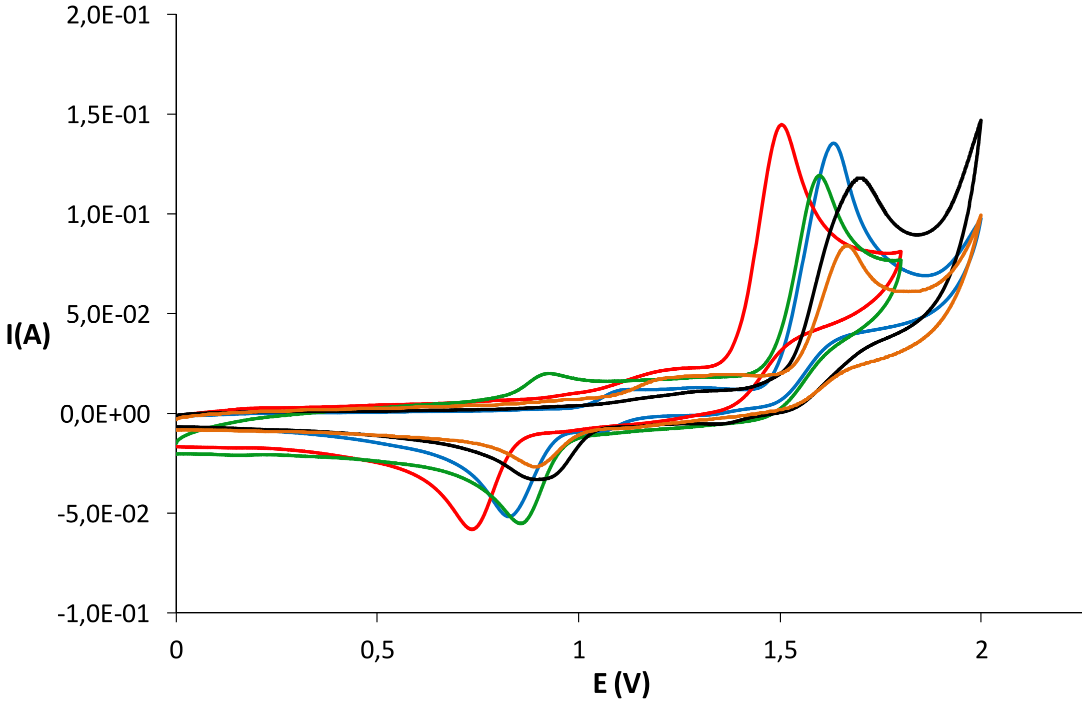

Figure S6.21. Cyclic voltammograms of **C7** (green), **C8** (red), **C9** (blue), **C10** (black) and **C11** (brown) in CH_3CN.

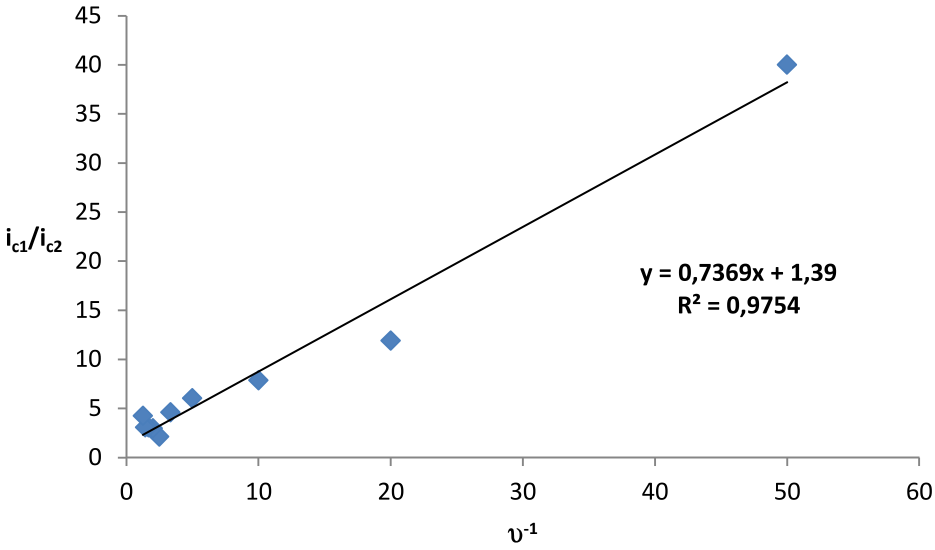

Figure S6.22. Plot of i_{c1}/i_{c2} *vs.* υ^{-1}, plus its linear fitting extrapolating $\upsilon \rightarrow \infty$ to obtain $K^{III}_{(O-S)}$ for complex **C5**.

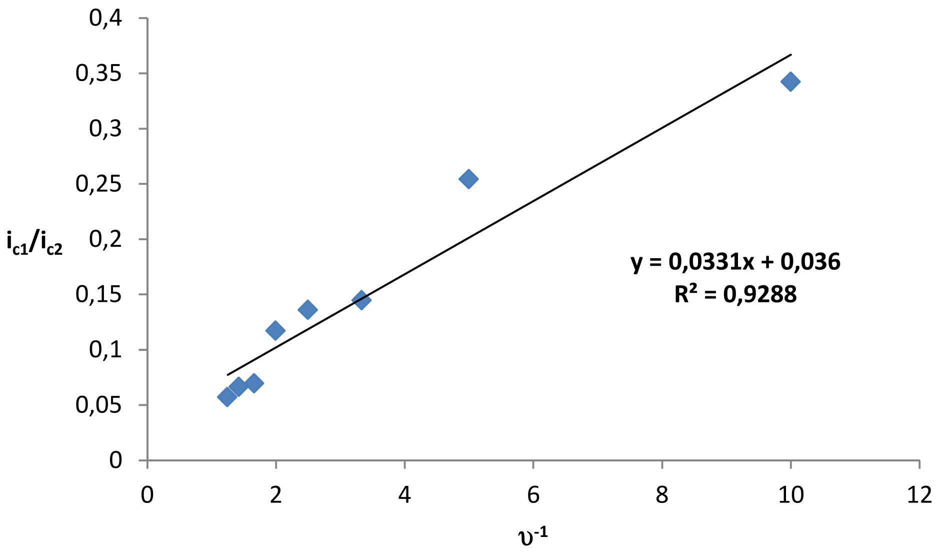

Figure S6.23. Plot of i_{c1}/i_{c2} *vs.* υ^{-1}, plus its linear fitting extrapolating $\upsilon \rightarrow \infty$ to obtain $K^{III}_{(O\text{-}S)}$ for complex **C8**.

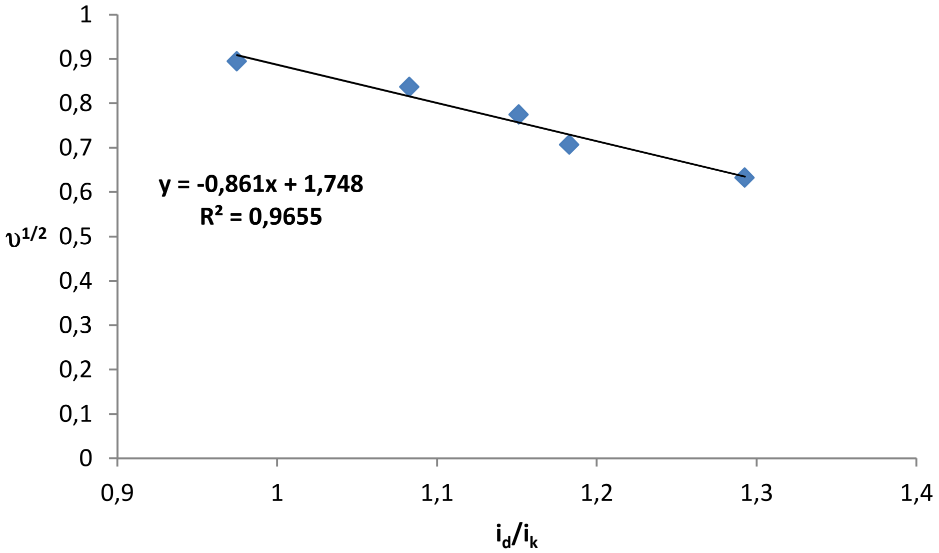

Figure S6.24. Plot of $\upsilon^{1/2}$ *vs.* i_d/i_k to obtain $k^{III}_{(S\text{-}O)}$ and $k^{III}_{(O\text{-}S)}$ for complex **C5**.

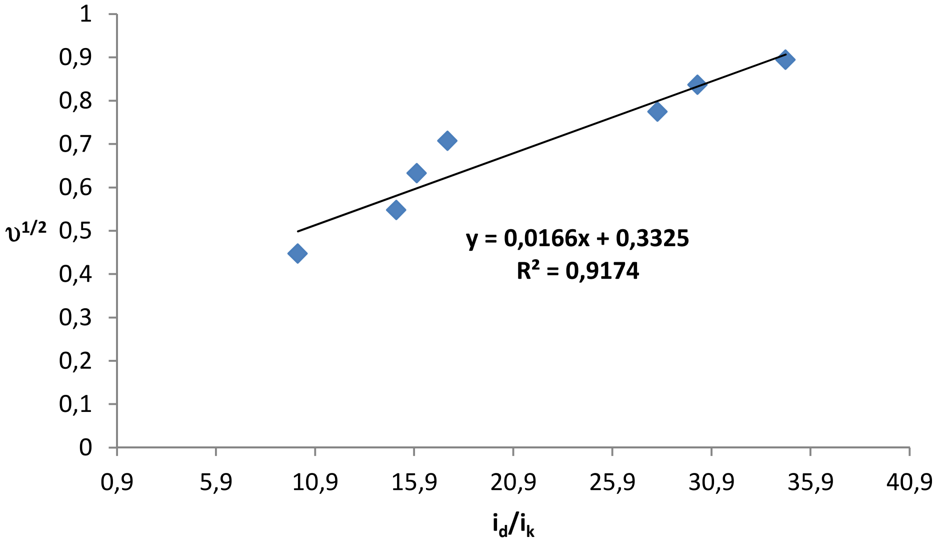

Figure S6.25. Plot of $\upsilon^{1/2}$ *vs.* i_d/i_k to obtain $k^{III}_{(S\text{-}O)}$ and $k^{III}_{(O\text{-}S)}$ for complex **C8**.

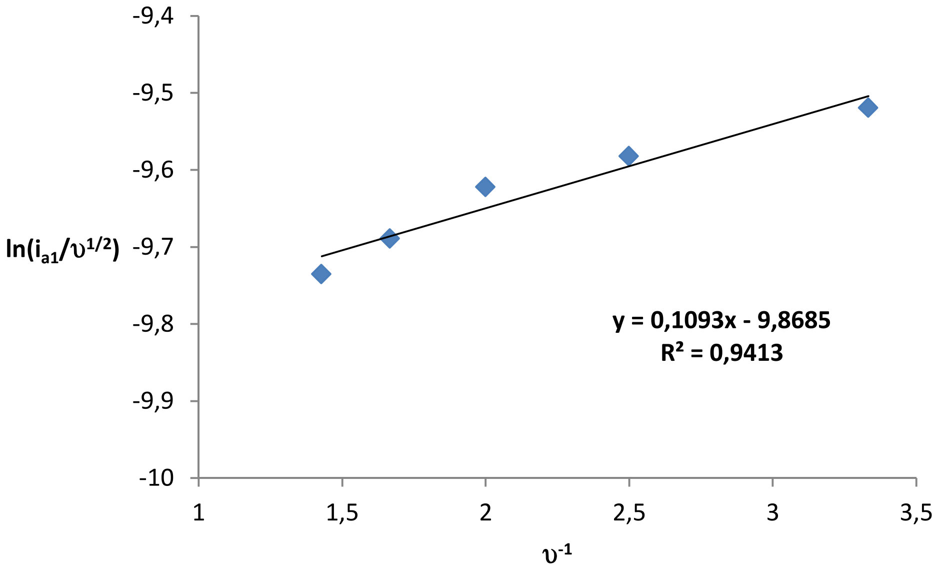

Figure S6.26. Plot of $\ln(i_{a1}/\upsilon^{1/2})$ *vs.* υ^{-1} for complex **C5**.

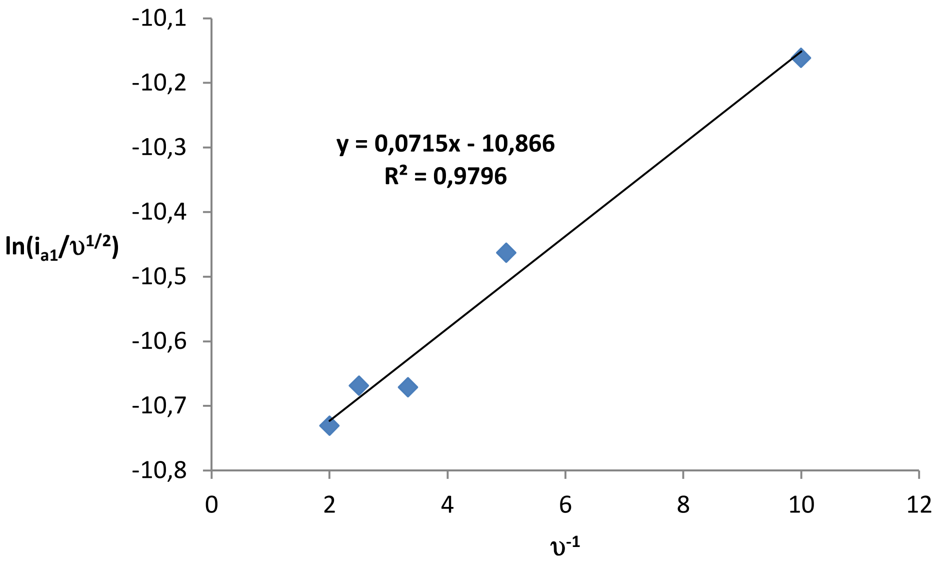

Figure S6.27. Plot of ln(i_{a1}/$\upsilon^{1/2}$) *vs.* υ^{-1} for complex **C8**.

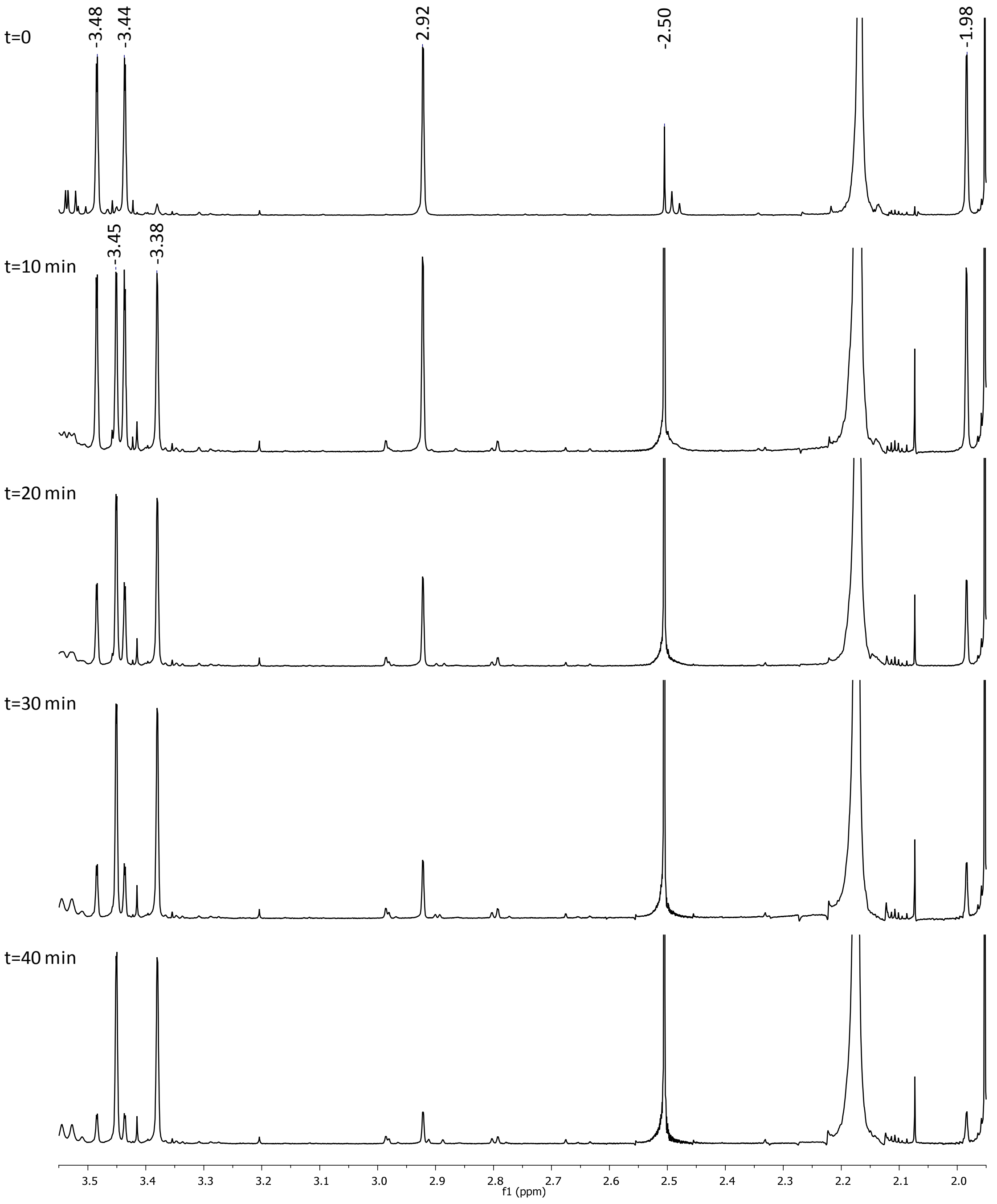

Figure S6.28. ^{1}H-NMR spectra in CD_3CN corresponding to the photochemical conversion of complex **C5** into **C5'**.

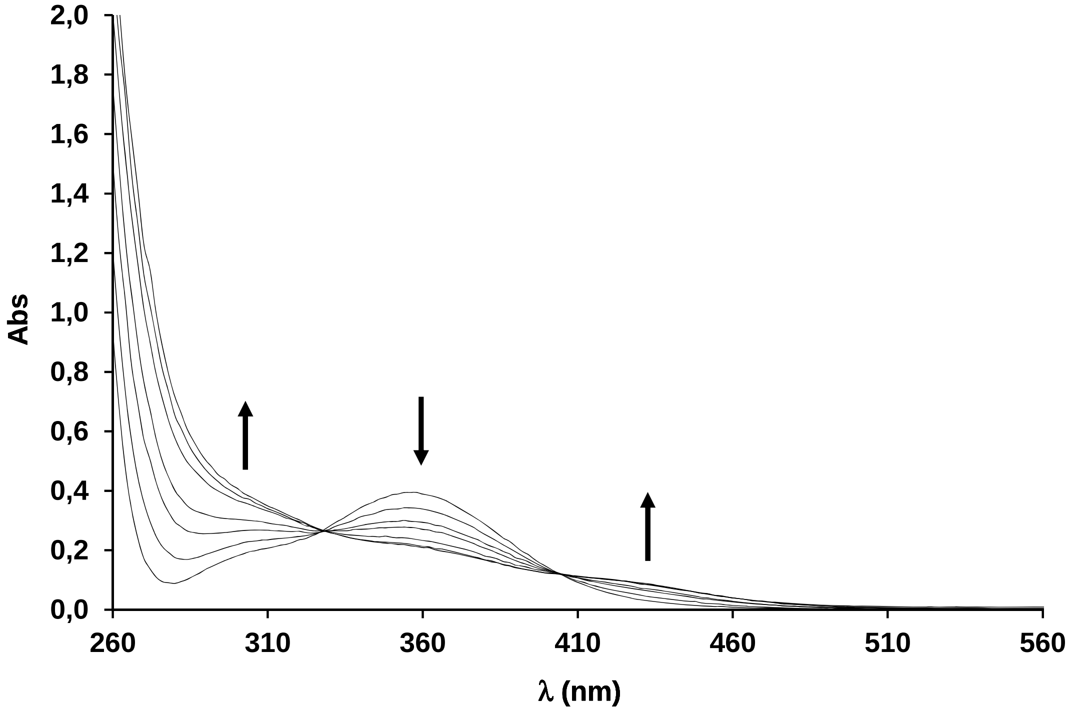

Figure S6.29. UV-visible spectra corresponding to the photochemical transformation of **C8** into **C8’** in acetonitrile.

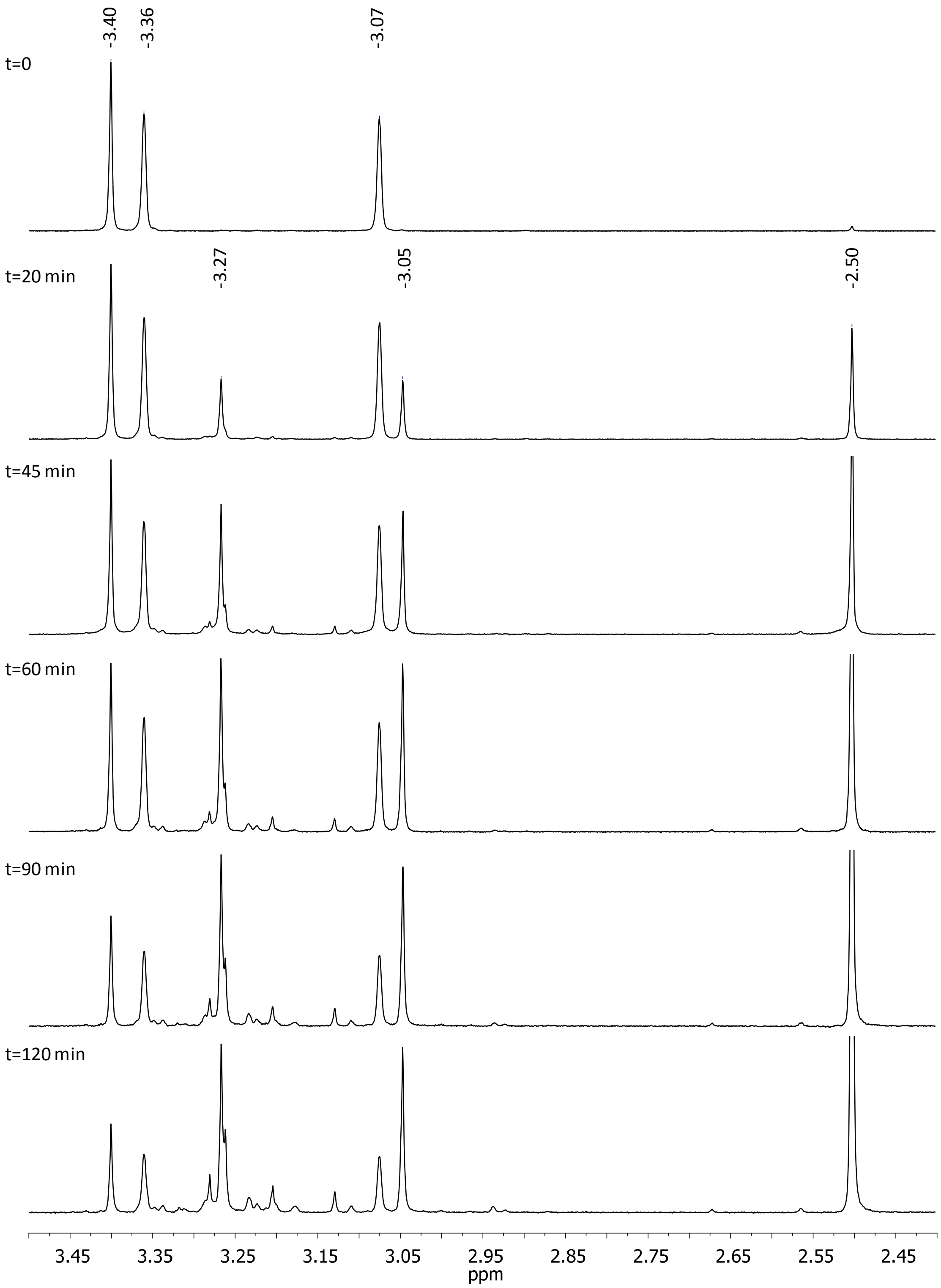

Figure S6.30. ^{1}H-NMR spectra in CD_3CN corresponding to the photochemical conversion of complex **C8** into **C8'**.

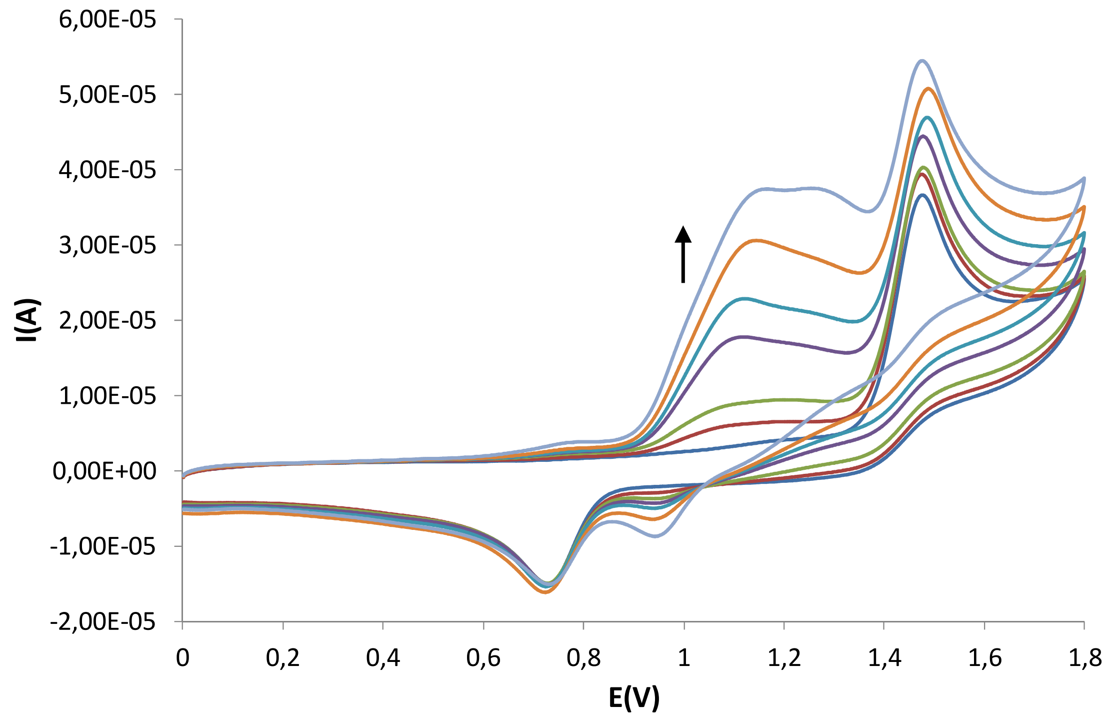

Figure S6.31. Cyclic voltammograms of **C8** (in 0.1M TBAH acetonitrile solution) after irradiation: t = 0, 5, 10, 15, 20, 30 and 60 minutes.

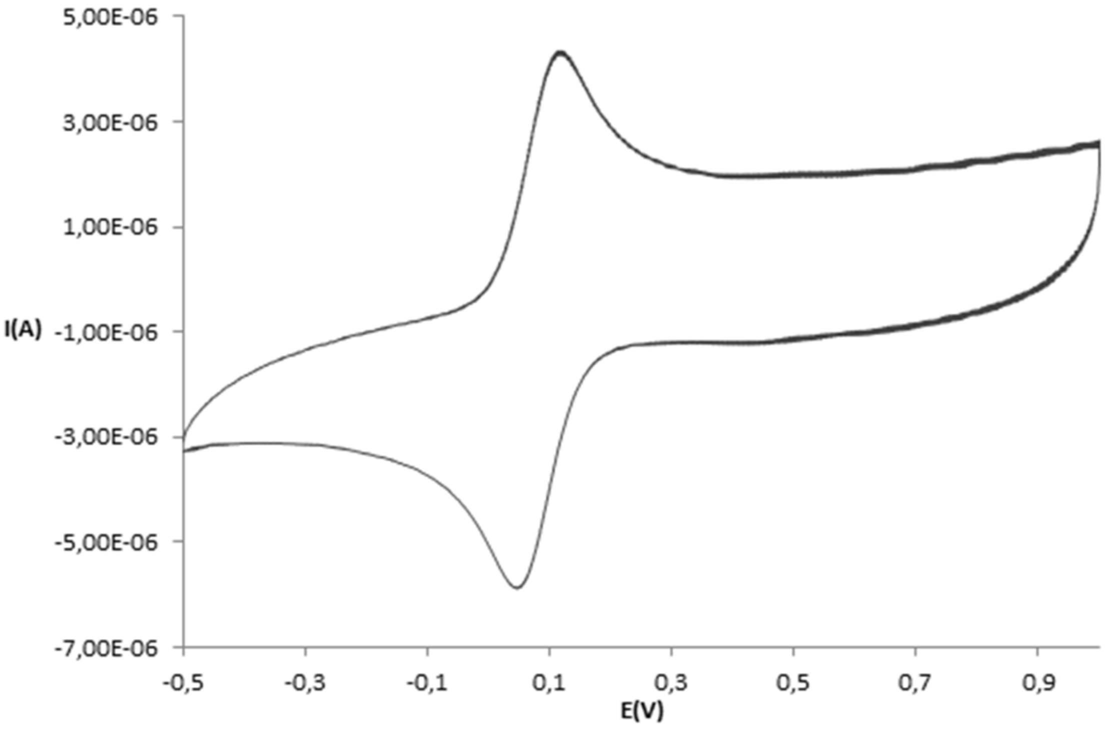

Figure S6.32. Cyclic voltammogram of **C5''** in CH_2Cl_2.

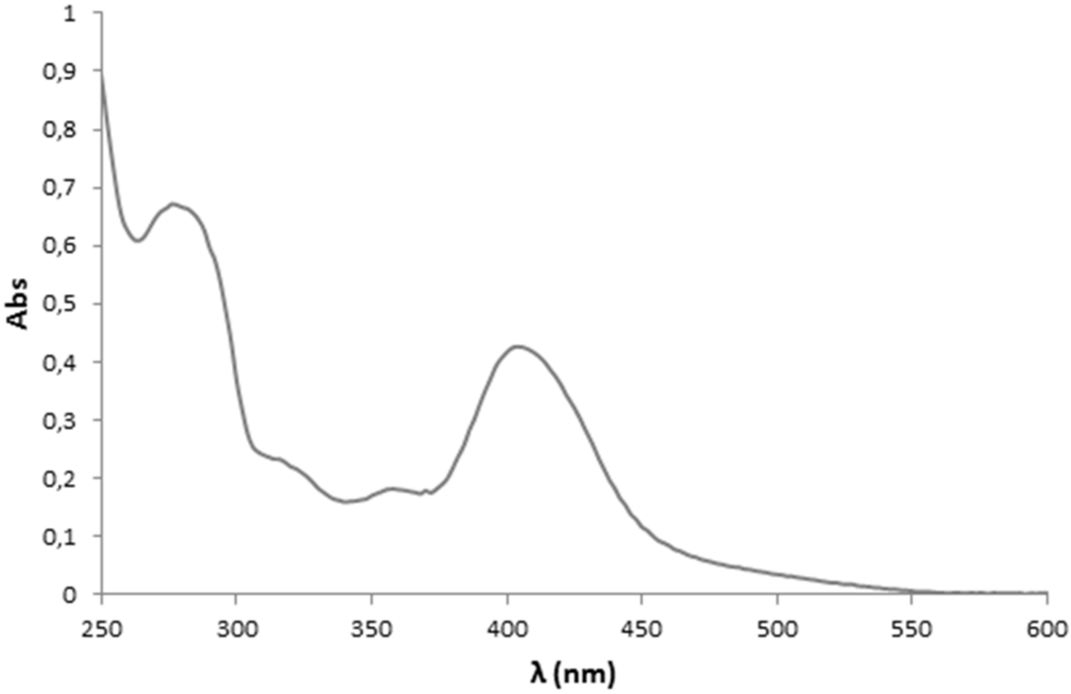

Figure S6.33. UV-visible spectrum of **C5''** in CH_2Cl_2.

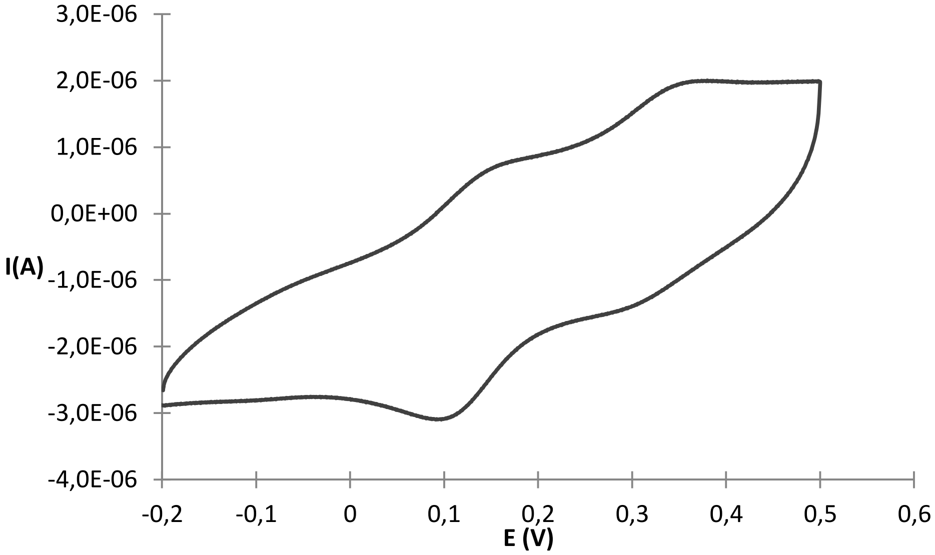

Figure S6.34. Cyclic voltammogram of **C8''** in 0.1 M TBAH CH_2Cl_2 solution.

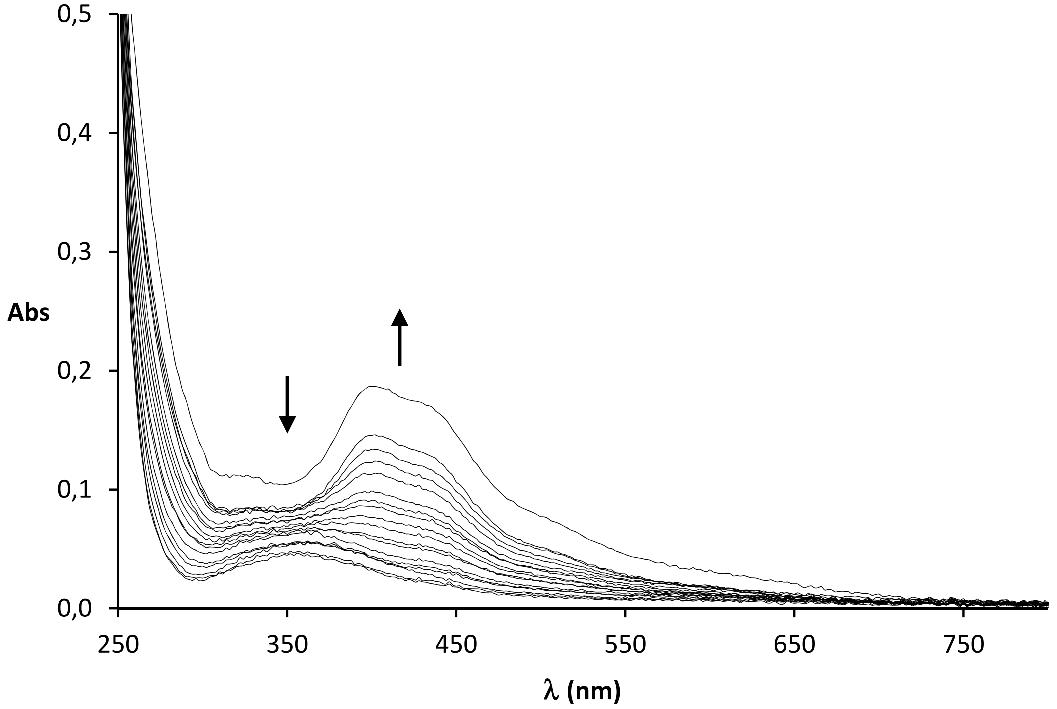

Figure S6.35. UV-visible spectra corresponding to the photochemical transformation of **C8** into **C8''** in chloroform during 24 h.

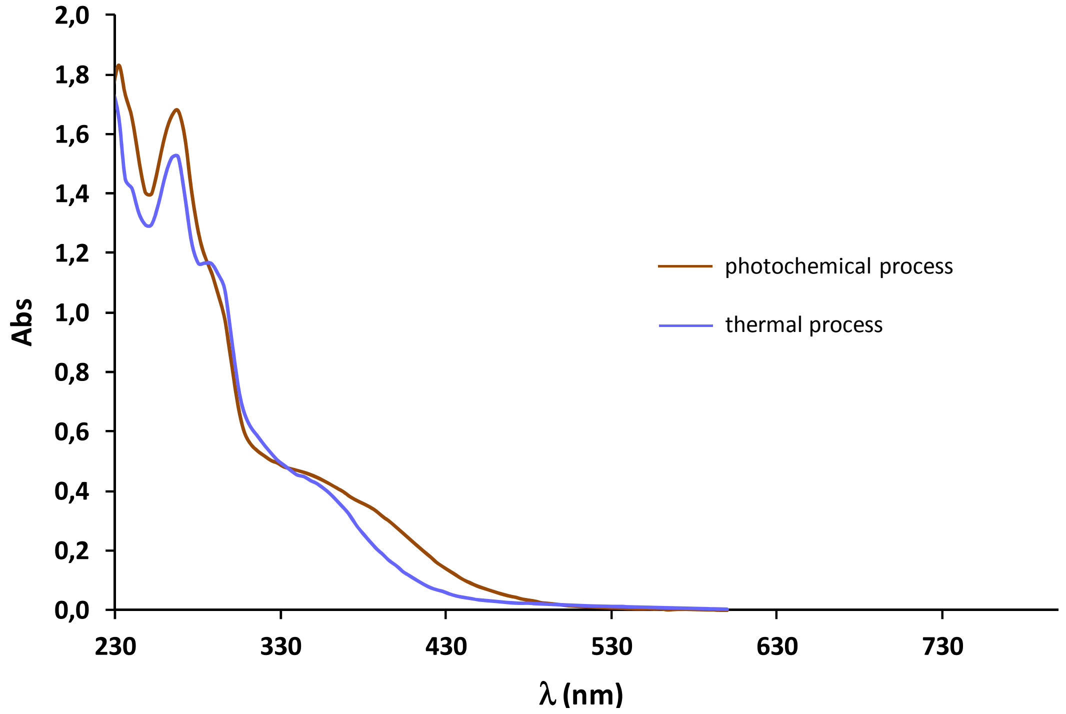

Figure S6.36. Final UV-vis spectra obtained after hydrolysis of complex **C5** under visible light irradiation and upon warming up to 60°C.

Table S6.1. Crystallographic data for complexes **C5**, **C5''** and **C6**.

	C5	**C5''**	**C6**
Empirical formula	$C_{24}H_{40}Cl_4N_6O_5Ru_2S_4$	$C_{11}H_{15}Cl_5N_3ORuS$	$C_{13}H_{21}Cl_2N_3O_2RuS_2$
Formula weight	964.80	515.64	487.42
Crystal system	Monoclinic	Monoclinic	Orthorhombic
Space group	C2/c	P21/c	P b c a
a[Å]	24.7647(10)	9.969(5)	9.1074(10)
b[Å]	11.7498(5)	16.673(8)	14.8633(16)
c[Å]	14.0980(5)	11.326(6)	28.909(3)
α[°]	90	90	90
β[°]	116.3070(10)	96.414 (7)	90
γ[°]	90	90	90
V [$Å^3$]	3677.4(3)	1870.8(16)	3913.3(7)
Formula Units/ cell	4	4	8
Temp. [K]	300(2)	100(2)	293(2)
ρ_{calc}, [Mg/m^{-3}]	1.743	1.831	1.655
μ[mm^{-1}]	1.382	1.665	1.297
Final R indices, [I>2σ(I)]	$R_1 = 0.0224$ $wR_2 = 0.0663$	$R_1 = 0.0400$ $wR_2 = 0.1022$	$R_1 = 0.0747$ $wR_2 = 0.1782$
R indices [all data]	$R_1 = 0.0243$ $wR_2 = 0.0675$	$R_1 = 0.0524$ $wR_2 = 0.1111$	$R_1 = 0.0824$ $wR_2 = 0.1829$

$R_1 = \Sigma||F_o| - |F_c||/\Sigma|F_o|$

$wR_2 = [\Sigma\{w(F_o^2-F_c^2)^2\}/\Sigma\{w(F_o^2)^2\}]^{½}$, where $w = 1/[\sigma^2(Fo^2) + (0.0042P)^2]$ and $P=(F_o^2+2F_c^2)$

Table S6.2. Crystallographic data for complexes **C8** - **C11**.

	C7	**C8**	**C9**	**C10**	**C11**
Empirical formula	$C_9H_{22}Cl_2N_2O_3RuS_3$	$C_{10}H_{24}Cl_2N_2O_3RuS_3$	$C_9H_{21}Cl_2N_3O_5RuS_3$	$C_{10}H_{23}Cl_2F_3N_2O_4RuS_3$	$C_{13}H_{24}BrCl_2N_2O_4RuS_3$
Formula weight	474.44	488.46	519.44	560.45	620.40
Crystal system	Monoclinic	Monoclinic	Monoclinic	Monoclinic	Monoclinic
Space group	P21	P2(1)/c	P21/n	P21/n	P2(1)/c
a[Å]	8.531(7)	8.8684(17)	8.396(7)	8.739(3)	12.493(6)
b[Å]	13.122(11)	14.240(3)	15.783(13)	23.299	13.943(7)
c[Å]	8.953(8)	15.809(3)	14.403(12)	10.690	16.522
α[°]	90	90	90	90	90
β[°]	116.997(13)	102.331(3)	105.773(13)	93.393	130.27(2)
γ[°]	90	90	90	90	90
V [$Å^3$]	893.1(13)	1950.3(6)	1837(3)	2172.9(12)	2195.9(17)
Formula Units/ cell	4	4	4	4	4
Temp. [K]	300(2)	298(2)	298(2)	298(2)	298(2)
ρ_{calc}, [Mg/m^{-3}]	1.764	1.664	1.878	1.713	1.877
μ[mm^{-1}]	1.533	1.407	1.509	1.297	3.083
Final R indices, [I>2σ(I)]	$R_1 = 0.0521$	$R_1 = 0.0256$	$R_1 = 0.0237$	$R_1 = 0.0390$	$R_1 = 0.0387$
	$wR_2 = 0.1475$	$wR_2 = 0.0657$	$wR_2 = 0.0608$	$wR_2 = 0.1193$	$wR_2 = 0.0985$
R indices [all data]	$R_1 = 0.0729$	$R_1 = 0.0298$	$R_1 = 0.0259$	$R_1 = 0.0447$	$R_1 = 0.0523$
	$wR_2 = 0.2150$	$wR_2 = 0.0681$	$wR_2 = 0.0626$	$wR_2 = 0.1229$	$wR_2 = 0.1052$

$R_1 = \Sigma||F_o| - |F_c||/\Sigma|F_o|$ $wR_2 = [\Sigma\{w(F_o^2-F_c^2)^2\}/\Sigma\{w(F_o^2)^2\}]^{½}$, where $w = 1/[\sigma^2(Fo^2) + (0.0042P)^2]$ and $P=(F_o^2+2F_c^2)$

Table S6.3. Selected bond lengths (Å) and angles (°) for **C5** and **C6**.

	C5	**C6**
Ru(1)-N(1)	2.1237(15)	2.064(5)
Ru(1)-N(3)	2.0313(15)	2.058(5)
Ru(1)-S(1)	2.2558(5)	2.2842(15)
Ru(1)-S(2)	2.2432(5)	2.3226(15)
Ru(1)-Cl(1)	2.4103(5)	2.4149(17)
Ru(1)-Cl(2)	2.4277(5)	2.4241(17)
N(1)-Ru(1)-N(3)	76.92(6)	77.7(2)
N(1)-Ru(1)-S(1)	171.61(5)	91.75(14)
N(1)-Ru(1)-S(2)	92.89(4)	87.53(14)
N(1)-Ru(1)-Cl(1)	94.66(4)	94.56(14)
N(1)-Ru(1)-Cl(2)	83.49(4)	174.62(15)
N(3)-Ru(1)-S(1)	96.74(4)	90.50(14)
N(3)-Ru(1)-S(2)	90.03(4)	89.26(14)
N(3)-Ru(1)-Cl(1)	171.27(4)	172.26(15)
N(3)-Ru(1)-Cl(2)	86.95(4)	99.47(15)
S(1)-Ru(1)-S(2)	92.595(19)	179.27(6)
S(1)-Ru(1)-Cl(1)	91.413(19)	89.54(6)
S(1)-Ru(1)-Cl(2)	90.75(2)	92.85(6)
S(2)-Ru(1)-Cl(1)	92.735(19)	90.60(7)
S(2)-Ru(1)-Cl(2)	175.728(18)	87.87(6)
Cl(1)-Ru(1)-Cl(2)	89.83(2)	88.25(7)

Table S6.4. Selected bond lengths (Å) and angles (°) for **C5’’**.

	C5’’
Ru(1)-N(1)	2.118(3)
Ru(1)-N(3)	2.019(3)
Ru(1)-S(1)	2.2639(14)
Ru(1)-Cl(1)	2.3438(13)
Ru(1)-Cl(2)	2.3170(13)
Ru(1)-Cl(3)	2.3464(13)
N(1)-Ru(1)-N(3)	77.91(12)
N(1)-Ru(1)-S(1)	174.81(9)
N(1)-Ru(1)-Cl(1)	92.33(9)
N(1)-Ru(1)-Cl(2)	86.27(9)
N(1)-Ru(1)-Cl(3)	95.14(9)
N(3)-Ru(1)-S(1)	97.44(9)
N(3)-Ru(1)-Cl(1)	86.28(10)
N(3)-Ru(1)-Cl(2)	88.07(10)
N(3)-Ru(1)-Cl(3)	172.46(9)
S(1)-Ru(1)-Cl(1)	89.66(4)
S(1)-Ru(1)-Cl(2)	91.30(4)
S(1)-Ru(1)-Cl(3)	89.62(4)
Cl(1)-Ru(1)-Cl(2)	174.34(4)
Cl(1)-Ru(1)-Cl(3)	91.12(5)
Cl(2)-Ru(1)-Cl(3)	94.46(5)

Table S6.5. Selected bond lengths (Å) and angles (°) for **C8**-**C11**.

	C7	**C8**	**C9**	**C10**	**C11**
Ru(1)-N(1)	2.145(9)	2.1461(18)	2.120(2)	2.145(3)	2.141(3)
Ru(1)-S(1)	2.295(3)	2.2682(7)	2.2455(15)	2.2817(10)	2.2780(15)
Ru(1)-S(2)	2.309(3)	2.3003(6)	2.2690(17)	2.2944(11)	2.2816(13)
Ru(1)-S(3)	2.316(4)	2.2866(6)	2.2760(15)	2.2610(11)	2.2901(11)
Ru(1)-Cl(1)	2.429(4)	2.4267(7)	2.4028(17)	2.3977(11)	2.4211(16)
Ru(1)-Cl(2)	2.447(3)	2.4326(6)	2.3928(16)	2.4187(11)	2.4212(12)
N(1)-Ru(1)-S(1)	94.4(3)	90.52(5)	88.82(5)	94.64(9)	92.63(9)
N(1)-Ru(1)-S(2)	89.8(3)	171.03(5)	173.07(4)	172.82(9)	174.29(8)
N(1)-Ru(1)-S(3)	170.6(3)	94.43(5)	94.80(5)	89.13(9)	88.35(9)
N(1)-Ru(1)-Cl(1)	84.4(3)	84.09(5)	85.69(5)	87.09(9)	85.53(9)
N(1)-Ru(1)-Cl(2)	87.6(3)	88.02(5)	86.46(5)	85.49(9)	85.08(9)
S(1)-Ru(1)-S(2)	91.51(13)	96.14(2)	92.82(4)	91.91(4)	92.46(4)
S(1)-Ru(1)-S(3)	92.16(14)	91.16(2)	93.48(6)	92.74(4)	90.25(5)
S(1)-Ru(1)-Cl(1)	89.39(12)	174.59(2)	174.487(19)	174.64(4)	87.12(5)
S(1)-Ru(1)-Cl(2)	176.63(14)	90.79(2)	92.09(5)	87.35(4)	175.40(4)
S(2)-Ru(1)-S(3)	96.78(14)	91.44(2)	91.83(3)	93.48(4)	94.24(5)
S(2)-Ru(1)-Cl(1)	174.14(14)	89.17(2)	86.76(3)	86.13(4)	92.12(5)
S(2)-Ru(1)-Cl(2)	91.24(12)	85.89(2)	92.69(3)	91.90(4)	89.67(4)
S(3)-Ru(1)-Cl(1)	88.97(13)	89.77(2)	86.52(6)	92.35(5)	173.22(4)
S(3)-Ru(1)-Cl(2)	85.57(14)	176.86(2)	174.31(2)	174.61(4)	93.66(5)
Cl(1)-Ru(1)-Cl(2)	88.08(13)	88.53(2)	88.05(6)	87.73(5)	88.73(5)

Table S6.6. Formulas used for the calculation of rate (*k*) and equilibrium (*K*) constants.

Formula	**Description**
$\frac{i_{c1}}{i_{c2}} = a \cdot \frac{1}{v} + K^{III}_{O-S}$	i_c = cathodic peak intensity (A) a = RT/nF, with: R = Boltzmann constant (J/(K·mol)) T= temperature (K) n = number of exchanged electrons F = Faraday constant (A·s/mol) υ = scan rate (V/s) K = equilibrium constant
$\sqrt{v} = \frac{1}{\frac{0.471}{K^{III}_{O-S}} \cdot \sqrt{\frac{nFl}{RT}}} \cdot \frac{i_d}{i_k} - \frac{1.02}{\frac{0.471}{K^{III}_{O-S}} \cdot \sqrt{\frac{nFl}{RT}}}$	i_d = diffusional current in the absence of a chemical reaction (i_{a1}) i_k = measured peak current (i_{c1}) $l = k^{III}_{O-S} + k^{III}_{S-O}$
$K_{O-S} = \frac{k_{O-S}}{k_{S-O}}$	k_{O-S} and k_{S-O} = kinetic isomerization constants
$K^{II} = K^{III} + e^{\frac{F}{RT}\cdot(E^0_{Ru-S} - E^0_{Ru-O})}$	E^0 = standard potential
$ln\left(\frac{i_{a1}}{\sqrt{v}}\right) = k^{II}_{O-S} \cdot \frac{1}{v} + b$	

Chapter 7

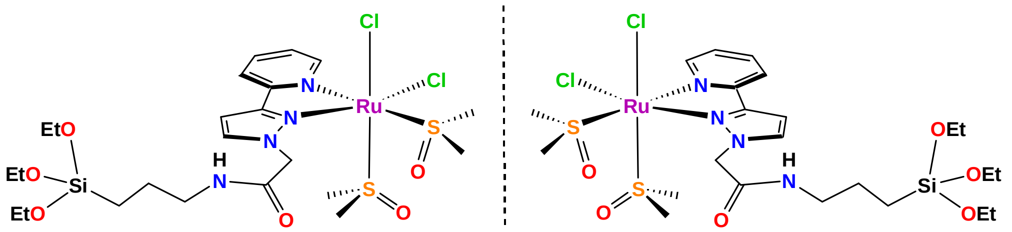

Δ *cis*-Cl, *cis*-dmso **(C12a)** Λ *cis*-Cl *cis*-dmso **(C12a)**

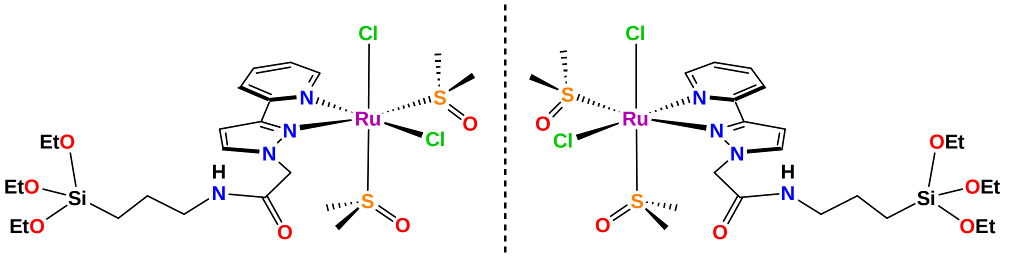

Δ *cis*-Cl *cis*-dmso **(C12b)** Λ *cis*-Cl *cis*-dmso **(C12b)**

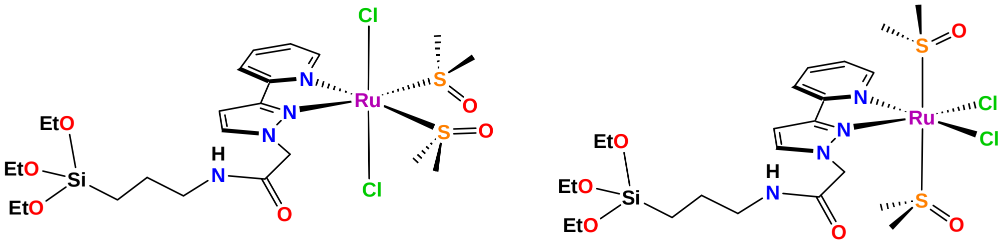

trans-Cl *cis*-dmso **(C12c)** *cis*-Cl *trans*-dmso **(C12d)**

Figure S7.1. Possible isomers for complex **C12**.

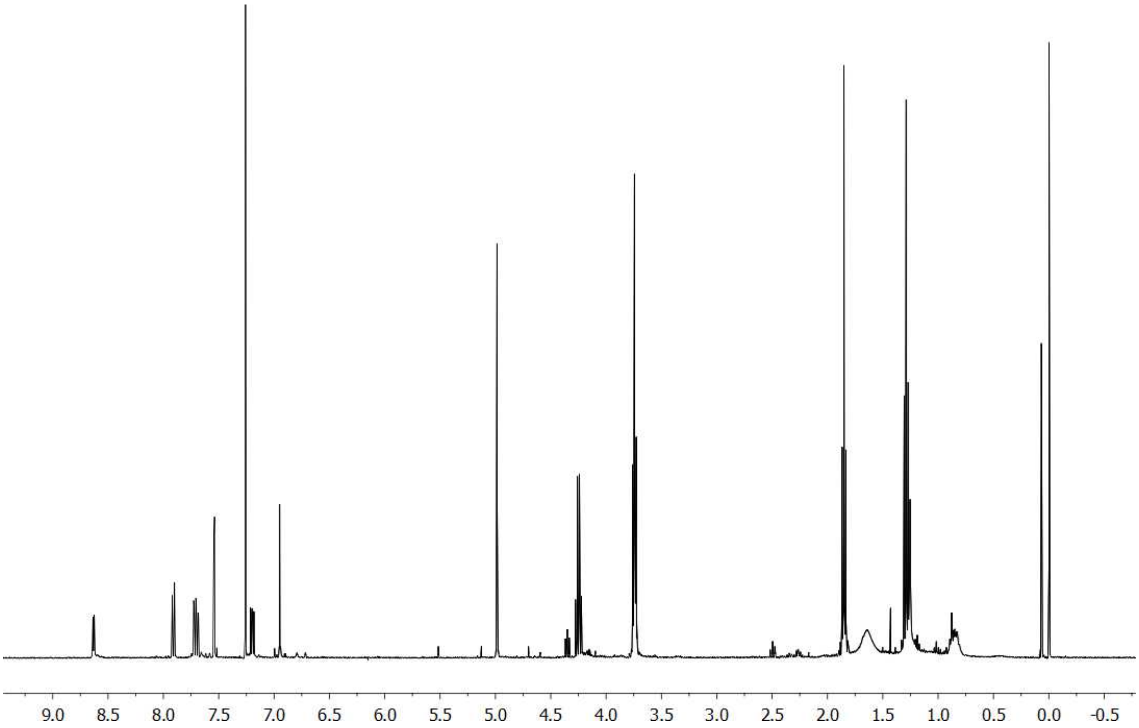

Figure S7.2. ^{1}H-NMR spectrum of ligand **L5**, 400 MHz, $CHCl_3$.

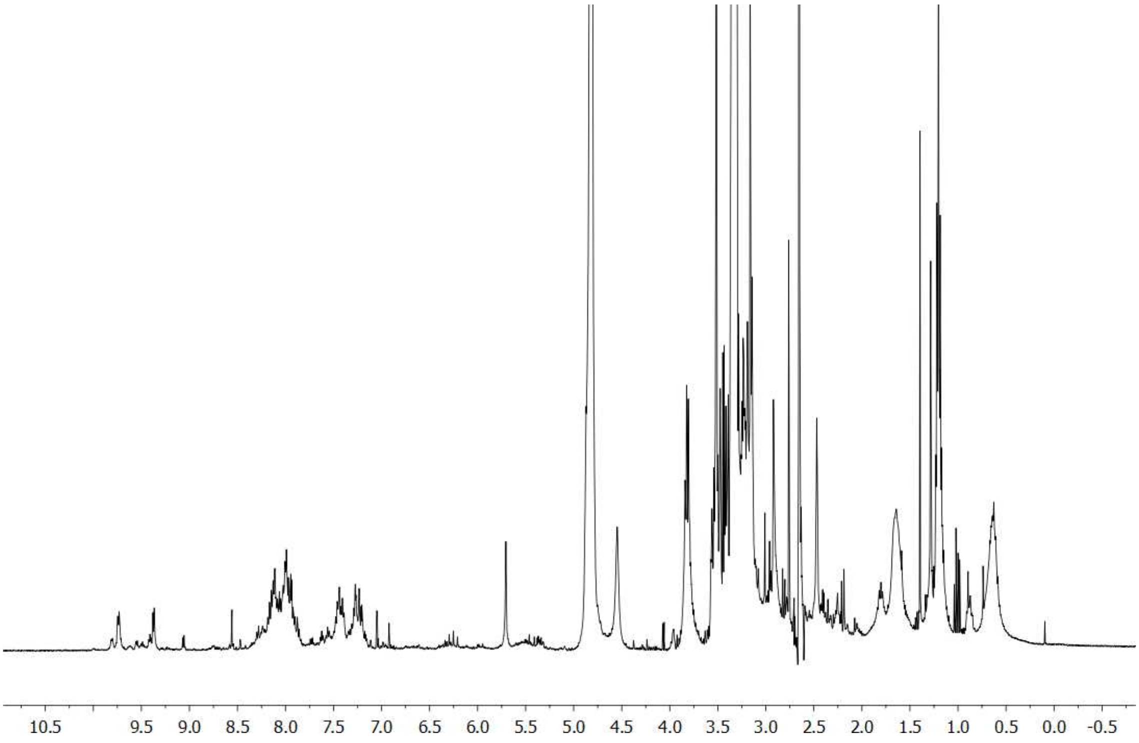

Figure S7.3. ^{1}H-NMR spectrum of complex **C12**, 400 MHz, CH_2Cl_2.